



## Durham E-Theses

---

### *Wiener filter transformations of gravity and magnetic fields and a regional interpretation of the midland valley of Scotland and northern Ireland*

Gunn, Peter J.

#### How to cite:

---

Gunn, Peter J. (1972) *Wiener filter transformations of gravity and magnetic fields and a regional interpretation of the midland valley of Scotland and northern Ireland*, Durham theses, Durham University. Available at Durham E-Theses Online: <http://etheses.dur.ac.uk/8584/>

#### Use policy

---

The full-text may be used and/or reproduced, and given to third parties in any format or medium, without prior permission or charge, for personal research or study, educational, or not-for-profit purposes provided that:

- a full bibliographic reference is made to the original source
- a [link](#) is made to the metadata record in Durham E-Theses
- the full-text is not changed in any way

The full-text must not be sold in any format or medium without the formal permission of the copyright holders.

Please consult the [full Durham E-Theses policy](#) for further details.

WIENER FILTER TRANSFORMATIONS OF GRAVITY AND MAGNETIC  
FIELDS AND A REGIONAL INTERPRETATION OF THE MIDLAND  
VALLEY OF SCOTLAND AND NORTHERN IRELAND

by

PETER J. GUNN

A thesis submitted for the degree of

Doctor of Philosophy

in the

University of Durham

Graduate Society

August 1972



## ABSTRACT

The spectral representation of gravity and magnetic fields shows that the mathematical expressions describing these fields are the result of the convolution of factors which depend on the geometry of the causative body, the physical properties of the body and the type of field being observed. If a field is known then it is possible to remove or alter these factors to map other fields or physical parameters which are linearly related to the observed field. The transformations possible are: continuation, reduction to the pole, converting between gravity and magnetic fields, converting between components of measurement, calculation of derivatives and mapping magnetization and density distributions and relief on interfaces. Digital Wiener filters, designed using a least squares error criterion, provide an accurate method for effecting these transformations. If the field to be transformed is contaminated by noise anomalies, whose average autocorrelation function can be estimated, then the Wiener filter can be optimized to suppress this noise.

The British Isles resulted, in Lower Palaeozoic times, from the collision of two continental masses. Consideration of published geological, aeromagnetic, gravity and crustal seismic data suggests that the Midland Valley of Scotland and Northern Ireland overlies the suture of this ocean closing process. Ophiolite zones on either side of the Midland Valley suggest the location of ancient diverging subduction zones and the Midland Valley graben appears to be down faulted as a result of compression between the two converging continents. It is possible to relate the tectonic, stratigraphic and igneous features of the area to this model and to use the model to predict and to use the geophysics to locate, previously unknown features. The post Carboniferous features in the area appear to be related to continental drifting of Europe from America.

### ACKNOWLEDGEMENTS

I wish to thank Professor M.H.P. Bott for allowing use of the facilities of the Geology Department and for supervising this project.

All computations in this work were carried out using the NUMAC IBM 360/67 computer.

Christina Gunn provided much appreciated moral support and assistance with digitizing and drafting.

A grant from Hunting Geology and Geophysics Ltd., supporting this work, was gratefully received.

## CONTENTS

	Page
CHAPTER 1	1
THEORY OF LINEAR TRANSFORMATIONS OF GRAVITY AND MAGNETIC FIELDS IN TERMS OF FOURIER ANALYSIS	1
1.1 Introduction	1
1.2 Derivation of Expressions for the Spectra of Gravity and Magnetic Fields	2
1.2.1 Gravity Field	2
1.2.2 Magnetic Field	3
1.3 Generalization of the Expressions for the Spectra in Terms of Equivalent Layers	5
1.4 Transformations Possible with Gravity and Magnetic Fields	7
1.5 Inverse Problems in Gravity and Magnetic Interpretation	11
1.5.1 The Linear Inverse Problem	11
1.5.2 The Non Linear Inverse Problem	13
 CHAPTER 2	 17
REVIEW OF METHODS FOR PERFORMING LINEAR TRANS- FORMATIONS OF GRAVITY AND MAGNETIC FIELDS	17
2.1 Introduction	17
2.2 Development of the Analytic Theory of Linear Transformations	17
2.3 Surface Fitting Methods for Numerically Performing Transformations	18
2.4 Linear Transformations as a Filtering Operation	21
2.5 Filtering in the Frequency Domain	25
2.6 Concluding Remarks	27
 CHAPTER 3	 28
PRACTICAL PROBLEMS TO BE CONSIDERED WHEN APPLYING FILTER METHODS	28
3.1 Converting the Data to a Regular Grid	28
3.2 Effects of Digitization	29
3.2.1 Aliasing	29
3.2.2 Gibb's Phenomenon	30
3.3 Truncation Effects	30
3.4 Edge Effects	33
3.5 Smoothing	33
3.6 Characteristics of Coefficients	34
3.6.1 Downward Continuation	35
3.6.2 Upward Continuation	35
3.6.3 Differentiating and Integrating Operators	36
3.6.4 Phase Filters	36
 CHAPTER 4	 37
TRANSFORMATION OF GRAVITY AND MAGNETIC FIELDS USING WIENER FILTERS	37
4.1 General Theory	37
4.2 Applications of One Dimensional Wiener Filters	43

	Page
4.2.1 The Linear Inverse Problem	43
4.2.1.1 Solving for the Magnetization of Vertically Magnetized Vertical Dykes	44
4.2.1.2 Calculation of the Magnetization of a Vertical Infinite Dyke with Inclined Magnetization	46
4.2.1.3 Calculation of the Magnetization of Blocks with a Finite Vertical Thickness	48
4.2.2 Transformations of Gravity and Magnetic Fields	50
4.2.2.1 Reduction to the Pole	50
4.2.2.2 Converting Components of Measurement	51
4.2.2.3 Converting Magnetic Fields into Gravity Fields	51
4.2.2.4 Calculation of Vertical Derivatives	51
4.3 Two Dimensional Wiener Filters	53
4.4 Conclusions	55
CHAPTER 5 APPLICATION OF FILTERS TO INTERPRETATION OF GRAVITY AND MAGNETIC DATA	57
5.1 Direct Interpretation of Gravity and Magnetic Data	57
5.1.1 Test of Linearity	57
5.1.2 Examples of Mapping	59
5.1.3 Conclusions	60
5.2 Automatic Interpretation of Anomalies over Dykes using Matched Filters	60
5.3 Depth Determination using Euler's Relationship	61
CHAPTER 6 OPTIMUM DIGITAL FILTERS	66
6.1 Introduction	66
6.2 Theory of Optimum Wiener Filters in the Presence of Autocorrelated Noise	66
6.3 Estimation of Average Noise Autocorrelation Functions	68
6.3.1 Autocorrelation functions of Fields due to Three dimensional Bodies	69
6.3.1.1 Prisms	69
6.3.1.2 Poles and Dipoles	69
6.3.2 Autocorrelation functions of Fields due to Two Dimensional Bodies	70
6.3.2.1 Dykes	71
6.3.2.1 Lava Flows	72
6.4 Examples of Optimum Wiener Filtering	72
6.5 Other Work on Optimum Filters	73
6.6 Concluding Remarks	74

	Page	
CHAPTER 7	MULTICHANNEL WIENER FILTERS	75
7.1	Introduction to Theory	75
7.2	Detection of Anomalies with a Given Density Magnetization Ratio	76
7.3	Optimum Strike Filtering	78
7.4	Comments	80
CHAPTER 8	EXAMPLES OF THE APPLICATION OF WIENER FILTERS TO REAL DATA	81
8.1	Reduction to the Pole and Magnetization Calculation for an Anomaly in the English Lake District	81
8.2	Basement Mapping for the Southern Uplands and Solway Firth	82
8.3	Density Deconvolution and Mapping of the Weardale Granite	84
8.4	Removal of white noise from a Magnetic Field	86
8.5	Filtering Operations on the Magnetic and Gravity Fields Over a Postulated Tertiary Intrusion in Northern Ireland	87
8.6	Summary and Conclusions concerning the use of Wiener Filters for Transforming Gravity and Magnetic Fields	89
CHAPTER 9	REGIONAL GEOPHYSICAL INTERPRETATION OF THE MIDLAND VALLEY IN SCOTLAND AND NORTHERN IRELAND	91
9.1	Introduction	91
9.1.1	Previous Geological and Geophysical Studies	91
9.1.2	Comments on Interpretation Methods Used	92
9.1.2.1	Qualitative Interpretation	92
9.1.2.2	Quantitative Interpretation	94
9.1.3	Filtered Aeromagnetic Map of the Midland Valley	94
9.2	Lower Palaeozoic Features	95
9.2.1	Southern Uplands	95
9.2.2	Southern Uplands Fault Zone	96
9.2.3	Highland Boundary Fault Zone	100
9.3	Relationship of the Midland Valley to the Proto-Atlantic Ocean	105
9.3.1	Introduction	105
9.3.2	Dewey's Model and its Problems	106
9.3.3	The Midland Valley as an Oceanic Remnant	108
9.3.4	Reinterpretation of Dewey's Evidence	109
9.3.5	Continuation of the Midland Valley into Western Ireland	111
9.3.6	Conclusions	113
9.4	Lower Old Red Sandstone Features	114
9.5	Carboniferous Igneous Activity	118

	Page
9.5.1 Introduction	118
9.5.2 Alkali Dolerite Phase	119
9.5.3 Quartz Dolerite Phase	120
9.5.4 Origins of the Carboniferous Igneous Activity	122
9.6 Post Carboniferous Features	122
9.7 Concluding Comments Concerning the Structure and History of the Midland Valley	127
 APPENDIX 1	
Summary of Previous Geophysical Surveys in the Midland Valley of Scotland and Northern Ireland	128
 APPENDIX 2	
Filtering of Two Dimensional Data and Production of Contour Maps	130
 APPENDIX 3	
Summary of Computer Programs Used	132
 REFERENCES	135
 COMPUTER PROGRAM LISTINGS	
WIEN1D	
WIEN2D	
MULTIW	

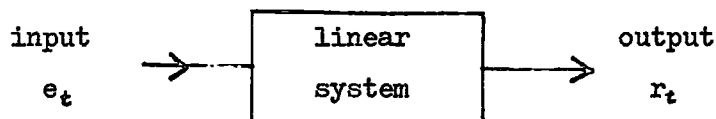
CHAPTER 1

THEORY OF LINEAR TRANSFORMATIONS OF GRAVITY AND MAGNETIC FIELDS IN  
TERMS OF FOURIER ANALYSIS

1.1 Introduction

This study investigates the application of Wiener filters to linear transformations of gravity and magnetic fields.

Linear systems (Hsu, 1970, p.121) are those systems in which linear transformations are performed and such systems obey two basic laws.



(i) If the inputs  $e_1(t)$  and  $e_2(t)$  to the system yield outputs  $r_1(t)$  and  $r_2(t)$  then the Principle of Superposition states that the inputs can be combined or added in any order and they will yield the same output.

i.e. 
$$e_1(t) + e_2(t) = r_1(t) + r_2(t)$$

and 
$$e_2(t) + e_1(t) = r_2(t) + r_1(t)$$

(ii) If  $e_1(t) \rightarrow r_1(t)$  then by the Principle of Homogeneity  $k_1 e_1(t) \rightarrow k_2 r_1(t)$  where  $k_1$  and  $k_2$  are equal constants.

Linear transformations may be accomplished in many ways including electronic processing, matrix transformations and by numerical evaluation of analytical expressions. This study is concerned with the digital filtering approach.

This chapter develops the theory of linear transformations of gravity and magnetic fields in terms of the spectral representation of these fields. This approach allows a unified appreciation of the possible transformations and the frequency response of the necessary operators. Although parts of the theory presented have been published previously the account below is considered more complete and to raise several new points.

Later chapters review how this theory has been applied in the past and demonstrate the applicability of Wiener filters.

## 1.2 Derivation of Expressions for the Spectra of Gravity and Magnetic Fields

Gudmundsson (1966) has derived the expression for the spectrum of a two dimensional (i.e. independent of  $y$ ) magnetic anomaly and has given without proof the generalized expressions for three dimensional gravity and magnetic anomalies. These expressions are derived fully here. The approach differs from that of Gudmundsson (1966) and resembles the method used by Bhattacharyya (1966) in deriving the expression for the magnetic anomaly due to a prism.

### 1.2.1 Gravity Field

The gravitational potential due to a density distribution

$\rho(\alpha, \beta, z)$  at a point  $(x, y, h)$  above the distribution is

$$U_g(x, y, h) = G \int_{-\infty}^{\infty} \int_{-\infty}^{\infty} \int_0^{\infty} \frac{\rho(\alpha, \beta, z)}{[(x-\alpha)^2 + (y-\beta)^2 + (z-h)^2]^{\frac{3}{2}}} d\alpha d\beta dz \quad (1-1)$$

where  $(\alpha, \beta, z)$  are the co-ordinates of an elemental mass unit and  $G$  is the universal gravitational constant.  $Z$  is positive downwards.

The inner part of equation (1-1) is in the form of the convolution integral (Hsu, 1970, p.90) i.e.

$$\int_{-\infty}^{\infty} \int_{-\infty}^{\infty} \frac{\rho(\alpha, \beta, z)}{[(x-\alpha)^2 + (y-\beta)^2 + (z-h)^2]^{\frac{3}{2}}} d\alpha d\beta \equiv \rho(x, y, z) * R(x, y, z-h) \quad (1-2)$$

where  $*$  denotes convolution and

$$R(x, y, z-h) = \frac{1}{[x^2 + y^2 + (z-h)^2]^{\frac{3}{2}}}$$

The convolution theorem (Hsu, 1970, p.90) states that if two terms are convolved in the space domain then they are multiplied in the frequency domain (and vice versa). By taking the Fourier Transform of both sides of (1-1) we obtain

$$U_g(u, v, h) = G \int_0^{\infty} \rho(u, v, z) R(u, v, z-h) dz \quad (1-3)$$

where  $u, v$  are angular frequency co-ordinates.

$$\rho(u, v, z) = \int_{-\infty}^{\infty} \int_{-\infty}^{\infty} \rho(x, y, z) e^{-j(ux+vy)} dx dy$$

and  $U_g(u, v, h)$  and  $R(u, v, z-h)$  are similarly the Fourier transforms of their space domain counterparts.

Bhattacharyya (1966), using an integral expression given by Erdelyi (1954) has shown that

$$\int_{-\infty}^{\infty} \int_{-\infty}^{\infty} \frac{1}{[x^2 + y^2 + (z-h)^2]^{3/2}} \cdot e^{i(ux+vy)} dx dy = \frac{2\pi e^{-(z-h)(u^2+v^2)^{1/2}}}{(u^2+v^2)^{1/2}}$$

This is the expression for the Fourier transform of  $R(x, y, z-h)$

$$\text{So } U_g(u, v, h) = 2\pi G \int_0^{\infty} \rho(u, v, z) \cdot \frac{e^{-(z-h)(u^2+v^2)^{1/2}}}{(u^2+v^2)^{1/2}} \cdot dz \quad (1-4)$$

The vertical component is the normally measured component of gravity and this can be obtained by differentiating the expression for the gravitational potential (equation (1-4)) with respect to  $h$ .

$$G_f(u, v, h) = 2\pi G \int_0^{\infty} \rho(u, v, z) \cdot e^{-(z-h)(u^2+v^2)^{1/2}} dz \quad (1-5)$$

This is the expression given (without proof) by Gudmundsson (1966).

### 1.2.2 Magnetic Field

The magnetic potential due to a magnetization distribution

$m_a(\alpha, \beta, z)$  at  $(x, y, h)$  is

$$U_m = \frac{\partial}{\partial h} \int_0^{\infty} \int_{-\infty}^{\infty} \int_{-\infty}^{\infty} \frac{m_a(\alpha, \beta, z)}{[(x-\alpha)^2 + (y-\beta)^2 + (z-h)^2]^{3/2}} \cdot d\alpha d\beta dz \quad (1-6)$$

where  $\frac{\partial}{\partial h}$  is the directional derivative in the direction of magnetization  $L, M, N$  are the direction cosines of the direction of magnetization (taken as constant), thus

$$\frac{\partial}{\partial h} = L \frac{\partial}{\partial x} + M \frac{\partial}{\partial y} + N \frac{\partial}{\partial z}$$

Equation (1-6) has an identical form to equation (1-1) (except

for the directional derivative) so by the same derivation as was used for the gravity anomaly

$$U_m(u, v, h) = \frac{\partial}{\partial R} \int_0^{\infty} m_d(u, v, z) \frac{e^{-(z-h)(u^2+v^2)^{\frac{1}{2}}}}{(u^2+v^2)^{\frac{1}{2}}} \cdot dz \quad (1-7)$$

It can be shown (Hsu, 1970, p.88) that where  $g$  and  $G$  are Fourier transforms of each other

$$\frac{\partial g}{\partial x} \equiv j u G \quad \frac{\partial g}{\partial y} \equiv j v G$$

So equation (1-7) can be expressed.

$$U_m(u, v, h) = \frac{[Lj u + Mj v + N(u^2+v^2)^{\frac{1}{2}}]}{(u^2+v^2)^{\frac{1}{2}}} \int_0^{\infty} m_d(u, v, z) \cdot e^{-(z-h)(u^2+v^2)^{\frac{1}{2}}} dz$$

To convert the expression for the magnetic potential into the expression for the magnetic field intensity it is necessary to differentiate in the direction of the component of the field that is being measured.

$$\text{i.e.} \quad M_f(u, v, h) = \frac{\partial}{\partial S} U_m(u, v, h)$$

where  $\frac{\partial}{\partial S}$  is the directional derivative in the direction of the component of the field being measured.

$$\text{i.e.} \quad \frac{\partial}{\partial S} = l \frac{\partial}{\partial x} + m \frac{\partial}{\partial y} + n \frac{\partial}{\partial h}$$

where  $l, m, n$  are the direction cosines of the component being measured. So by the same argument as above

$$M_f(u, v, h) = 2\pi [j l u + j m v + N(u^2+v^2)^{\frac{1}{2}}] \cdot \frac{1}{(u^2+v^2)^{\frac{1}{2}}} \int_0^{\infty} m_d(u, v, z) \cdot e^{-(z-h)(u^2+v^2)^{\frac{1}{2}}} dz \quad (1-8)$$

This is equivalent to the expression given (without proof) by Gudmundsson (1966) in the case of a constant direction of magnetization.

### 1.3 Generalization of the Expressions for the Spectra in Terms of Equivalent Layers

It is well established in geophysical literature (for example see Roy (1962)) that a density distribution  $\rho(x, y, z)$  has an equivalent surface density distribution  $\sigma(x, y, d)$  on a surface at depth  $d$ , which gives the same gravity anomaly. This surface distribution of density is called the 'equivalent layer'.

Similarly a magnetization distribution  $m_a(x, y, z)$  may be replaced by a surface distribution of magnetization  $m_s(x, y, d)$

The expression for the gravity and magnetic potentials due to these surface distributions are,

$$U_g(x, y, h) = G \int_{-\infty}^{\infty} \int_{-\infty}^{\infty} \frac{\sigma(\alpha, \beta, d)}{[(x-\alpha)^2 + (y-\beta)^2 + (d-h)^2]^{\frac{3}{2}}} \cdot d\alpha d\beta \quad (1-8)$$

and

$$U_m(x, y, h) = \frac{\partial}{\partial \hat{r}} \int_{-\infty}^{\infty} \int_{-\infty}^{\infty} \frac{m_s(\alpha, \beta, d)}{[(x-\alpha)^2 + (y-\beta)^2 + (d-h)^2]^{\frac{3}{2}}} \cdot d\alpha d\beta \quad (1-9)$$

By using the same mathematical approach as used in determining the generalized expression for the spectra equations (1-8) and (1-9) may be used to develop the expressions for the spectra in terms of equivalent layers. The theory is the same except that it is no longer necessary to integrate with respect to  $z$ .

$$G_f(u, v, h) = 2\pi G \sigma_s(u, v, d) \cdot e^{-(d-h)(u^2+v^2)^{\frac{1}{2}}} \quad (1-10)$$

$$M_f(u, v, h) = 2\pi [jLu + jMv + N(u^2+v^2)^{\frac{1}{2}}] \cdot [jlu + jm v + n(u^2+v^2)^{\frac{1}{2}}] \cdot \frac{m_s(u, v, d) e^{-(d-h)(u^2+v^2)^{\frac{1}{2}}}}{(u^2+v^2)^{\frac{1}{2}}} \quad (1-11)$$

Equations (1-10) and (1-11) are the expressions for the spectra of gravity and magnetic fields in terms of equivalent layers and apply to all gravity and magnetic fields.

If the same bodies cause the gravity and magnetic anomalies and the density and the magnitude and direction of the magnetization are constant throughout the bodies the gravity and magnetic equivalent layers may be related by using Poisson's relationship, which states

$$\underline{m}_a \cdot \nabla U_g = G\rho U_m \quad (1-12)$$

Where  $U_g$  and  $U_m$  are the gravity and magnetic potentials and  $\underline{m}_a$  is the magnetization which can vary in magnitude but not in direction  $G$  is the universal gravitational constant and  $\rho$  is the density of the body which must vary so that  $|\underline{m}_a|/\rho$  is constant everywhere.

Equation (1-12) can be written

$$m_a (iL + jM + kN) \cdot (i \frac{\partial U_g}{\partial x} + j \frac{\partial U_g}{\partial y} + k \frac{\partial U_g}{\partial z}) = G\rho U_m$$

Where L, M, N are the direction cosines of the direction of magnetization.

This reduces to

$$U_m = \frac{m_a}{G\rho} \cdot \frac{\partial U_g}{\partial \hat{r}}$$

$\hat{r}$  is in the direction of magnetization.

This equation has the same form as equation (1-6) used in deriving the magnetic spectra. It relates the magnetic potential to the gravity potential and indicates that we could do the entire calculation using the density distribution (in the case of constant density and magnetization) provided we allow for the constant  $m_a/G\rho$ .

Thus

$$m_s(u, v, d) = \frac{m_a}{G\rho} \cdot \sigma(u, v, d) \quad (1-13)$$

So obviously  $m_s(x, y, d)$  and  $\sigma(x, y, d)$  must be the same functions except for a scaling factor,

$$\text{i.e.} \quad m_s(x, y, d) = m_q \cdot L(x, y, d) \quad (1-14)$$

$$\sigma_s(x, y, d) = \rho \cdot L(x, y, d) \quad (1-15)$$

where  $L(x, y, d)$  is the function defining the spatial distribution.

Equations (1-13), (1-14) and (1-15) relate the gravity and magnetic equivalent layers where the same bodies cause the anomalies and the density and magnetization is the same.

In a general geological situation the densities and magnetizations are not constant for all the bodies present. However, if we can assume the direction of magnetization is constant over the whole area and the densities and magnitudes of magnetization are constant for each individual body, the equivalent layer would be the sum of the individual equivalent layers of each isolated anomaly. Thus the general properties of equations (1-10) and (1-11) are true for any area where the above geological conditions occur.

#### 1.4 Transformations Possible with Gravity and Magnetic Fields

The significance of equations (1-10) and (1-11) lies in the insight they give into transformations on gravity and magnetic fields.

These expressions may be considered as the multiplication of several factors.

i.e.

$$G_f(u, v, o) = 2\pi G \cdot \sigma(u, v, h) \cdot H(u, v, h)$$

$$M_f(u, v, o) = 2\pi D_1(u, v) \cdot D_2(u, v) \cdot I(u, v) \cdot m_s(u, v, h) \cdot H(u, v, h)$$

where

$$\left. \begin{array}{l} 2\pi G \\ 2\pi \end{array} \right\} \text{ scaling factors}$$

$$D_1 = [jLu + jMv + N(u^2 + v^2)^{\frac{1}{2}}] \text{ factor for direction of magnetization.}$$

$$D_2 = [jLu + jMv + n(u^2 + v^2)^{\frac{1}{2}}] \text{ factor for direction of measurement}$$

$$H = e^{-h(u^2 + v^2)^{\frac{1}{2}}} \text{ depth factor}$$

$$\left. \begin{array}{l} \sigma = \sigma(u, v, h) \\ m_s = m_s(u, v, h) \end{array} \right\} \text{ equivalent layer factors}$$

$$I = \frac{1}{(\sigma^2 + \sigma'^2)^{\frac{1}{2}}} \quad \text{an extra factor distinguishing magnetic fields from gravity fields}$$

Now by the convolution theorem multiplication in the frequency domain is equivalent to convolution in the space domain so gravity and magnetic fields are the result of convolution of the above factors. So

$$G_f(x, y, 0) = 2\pi G * H(x, y, h) * \sigma(x, y, h)$$

$$M_f(x, y, 0) = 2\pi * D_1(x, y) * D_2(x, y) * I(x, y) * H(x, y, h) * M_s(x, y, h)$$

where  $*$  denotes convolution.

It is possible to remove the effect of any of these factors from the spectrum by dividing the spectrum by the factor it is desired to remove. This is equivalent to convolving in the space domain by an operator (or filter) whose frequency response is the inverse of that of the factor it is desired to cancel out. Similarly it is possible to add the effect of a factor by multiplying the spectrum by the frequency response of that factor or by convolving in the space domain by a filter with that frequency response.

Hsu (1970) p.133 shows that the convolution of two functions  $h(t)$  and  $f_i(t)$  to give  $f_o(t)$ ,  
 i.e.  $f_o(t) = f_i(t) * h(t)$  (the order of  $f_i(t)$  and  $h(t)$  are interchangeable) is a linear system where  $h(t)$  is the unit impulse response of the system. Thus the convolution of two functions is a linear transformation and, all the following transformations involving convolutions are linear transformation.

The various methods of filtering and their advantages are discussed later. For the present discussion it will be assumed that we have the means to design filters with any desired frequency response and to perform the appropriate convolution operations.

Such filtering operations have relevance in the following transformations:

(i) Continuation of Potential Fields

Dean (1958) was the first to point out that convolving a magnetic or gravity field with a filter whose frequency response is  $e^{h(u^2+v^2)^{\frac{1}{2}}}$  transforms the field into what the field would be at a level  $h$  above or below the level of the original observed field.  $h$  is positive for downward continuation.

(ii) Reduction to the Pole

By convolving the magnetic field with a filter whose frequency response is

$$\frac{(u^2+v^2)^{\frac{1}{2}}}{[j\ell u + jm v + n(u^2+v^2)^{\frac{1}{2}}]} \cdot \frac{(u^2+v^2)^{\frac{1}{2}}}{[j\ell u + jm v + n(u^2+v^2)^{\frac{1}{2}}]}$$

The magnetic field is reduced to what the magnetic field would be at the north magnetic pole. Baranov (1957) was the first to realize that such a 'reduction to the pole' operation is possible. Spector and Grant (1970) report using a frequency domain approach to perform this operation.

(iii) Converting One Component of Measurement into Another

By filtering out the effect of the  $D_z$  factor (the factor for direction of measurement of the magnetic field) and filtering 'in' a factor for a new direction of magnetization, the field will be transformed into the field measured in the new direction of measurement.

The frequency response of such a filter would be:-

$$\frac{[j\ell' u + jm' v + n'(u^2+v^2)^{\frac{1}{2}}]}{[j\ell u + jm v + n(u^2+v^2)^{\frac{1}{2}}]}$$

where  $\ell, m, n$  are the direction cosines of the original direction of measurement;

$\ell', m', n'$  are the direction cosines of the new direction of measurement.

## (iv) Converting Magnetic Fields into Gravity Fields and Vice Versa

By reducing the magnetic field to the pole and filtering with a filter with response the Inverse factor of  $I$ . The magnetic field is transformed into the form of a gravity field. It will differ by the scaling factor  $|M|/G\rho$  for each anomaly with magnetization  $M$  and density  $\rho$ . The frequency response of such a filter will be

$$\frac{(u^2+v^2)^{\frac{1}{2}}}{[jLu + jMv + N(u^2+v^2)^{\frac{1}{2}}] \cdot [jLu + jMv + n(u^2+v^2)^{\frac{1}{2}}]}$$

This transformation can only be done realistically where the direction of magnetization is constant over the area being considered and is known.

Gravity fields may be transformed into the form of magnetic fields. For example, to convert a gravity field into the form of a magnetic field at the north magnetic pole with vertical magnetization the filter would have frequency response.  $(u^2+v^2)^{\frac{1}{2}}$ .

Each anomaly with magnetization  $M$  and density  $\rho$  would have its magnitude scaled by a factor  $G\rho/|M|$ .

## (v) Calculating the Vertical Derivatives of Potential Fields

By differentiating equations (1-9) and (1-10) with respect to  $h$  we introduce a factor into the spectra.

$$\left[ \frac{1}{h} (u^2+v^2)^{\frac{1}{2}} \right]^n$$

where  $n$  is the order of the vertical derivative.

Thus by convolving with filters which have the appropriate response it is possible to calculate the required vertical derivatives of gravity and magnetic fields.

## (vi) Horizontal Derivatives of Potential Fields

Hsu (1970) p.87 shows that if  $F(x)$  has Fourier transform  $F(\omega)$   $F''(x)$  has Fourier transform  $(j\omega)^2 F(\omega)$ .

Thus the required filter to calculate the  $n$ th horizontal derivative in the  $x$  or  $y$  directions has response

$$(ju)^n \quad \text{or} \quad (jv)^n$$

#### (vii) Miscellaneous Filtering Operations

It may be desired to remove certain frequencies from a magnetic or gravity map. In such a situation the frequency response of the filter must be decided and when this is done the filter can be applied. Hall (1968) reports using such a filter to separate deep anomalies (low frequency) from shallow high frequency anomalies.

Fuller (1967) gives the frequency response of a filter capable of enhancing trends in certain directions (a strike filter).

### 1.5 Inverse Problems in Gravity and Magnetic Interpretation

Consideration of the spectral representation of specific situations allows us to devise methods of solving certain inverse problems in gravity and magnetic interpretation.

#### 1.5.1 The Linear Inverse Problem

If the density  $\rho$  and the magnetization  $m_a$  are constant throughout the bodies being considered expressions (1-5) and (1-8) become

$$G_f(u, v, h) = 2\pi G\rho \int_0^\infty S(u, v, z) e^{-(z-h)(u^2+v^2)^{\frac{1}{2}}} dz \quad (1-16)$$

and

$$M_f(u, v, h) = 2\pi m_a [jLu + jMv + N(u^2+v^2)^{\frac{1}{2}}] \cdot [jLu + jMv + N(u^2+v^2)^{\frac{1}{2}}] \int_0^\infty S(u, v, z) e^{-(z-h)(u^2+v^2)^{\frac{1}{2}}} dz \quad (1-17)$$

where  $S(x, y, z)$  is a geometrical factor defining the shape of the body.

$$\text{Let} \quad \int_0^\infty S(u, v, z) e^{-(z-h)(u^2+v^2)^{\frac{1}{2}}} dz = K(u, v, h)$$

The term  $K(u, v, h)$  has been evaluated by Bhattacharyya (1966) for finite prisms with vertical sides. Gudmundsson (1966) gives the solution for a two dimensional dipping prism.

It will now be shown how it is possible to solve directly for the magnetization of a prism using filtering methods. In the following argument only a magnetized rectangular prism is considered. The reasoning is equally valid for other geometrical shapes and for gravity anomalies although in these situations some of the factors will be different.

Using Bhattacharyya's (1966) results the expression for the spectrum of the magnetic field due to a finite prism, widths  $2a$  and  $2b$ , depth  $h$  and thickness  $t$  is:-

$$M_f(u, v, h) = 2\pi m_a \cdot D_1(u, v) \cdot D_2(u, v) \cdot I \cdot I \cdot H(u, v, h) \cdot S_1(u, a) \cdot S_2(u, b) \cdot T(u, v, t) \quad (1-18)$$

the factors  $D_1, D_2, I, H$  have the same definitions as previously.

$$\begin{aligned} m_a &= \text{magnetization of the prism} \\ S_1 &= \frac{\sin(ua)}{u} = \text{factor for width in } u \text{ direction} \\ S_2 &= \frac{\sin(vb)}{v} = \text{factor for width in } v \text{ direction} \\ T &= (1 - e^{-t(u^2+v^2)^{\frac{1}{2}}}) = \text{thickness factor} \end{aligned}$$

Written in the space domain equation (1-18) is

$$M_f(x, y, h) = 2\pi m_a * D_1(x, y) * D_2(x, y) * I(x, y) * I(x, y) * H(x, y, h) * S_1(x, a) * S_2(y, b) * T(x, y, t)$$

As in the case with the equivalent layers the magnetic field of a prism is the result of convolving several factors.

As previously convolving with specific filters allows us to remove factors. If the angle of magnetization and the depth and thickness of the prism are known it is possible to design a filter with frequency response

$$\frac{1}{I(u, v)} \cdot \frac{1}{I(u, v)} \cdot \frac{1}{D_1(u, v)} \cdot \frac{1}{D_2(u, v)} \cdot \frac{1}{H(u, v, h)} \cdot \frac{1}{T(u, v, t)} \quad (1-19)$$

If these terms are removed from the spectrum we are left with:-

$$M'_f(u, v, h) = 2\pi m_a \frac{\sin(ua)}{u} \cdot \frac{\sin(vb)}{v}$$

where  $M'_f$  is the filtered spectrum.

The space domain equivalent of equation (1-20) (i.e. the result of convolving a filter whose frequency response is defined by equation (1-19) with the original magnetic anomaly) would be a rectangular box car function whose height is directly proportional to the magnetization of the prism and whose sides exactly define the edges of the prism. This is so because the space domain equivalent of a  $\frac{\sin(x)}{x}$  function is a rectangular pulse function (Hsu, 1970, p.112).

Thus it is possible to solve directly for the magnetization and position of the prism.

If the magnetic field is the result of several magnetic prisms, all with the same depth, thickness and direction of magnetization the output after convolving the field with the filter described above will be a series of rectangular box car functions defining the positions of the prisms and the height of each box car will be proportional to the magnetization of the prism it corresponds to. This is true because we are dealing with a linear system (Hsu, 1970, p.121) and with linear systems and inputs and outputs are additive. This is the principle of super-position.

#### 1.5.2 The Non Linear Inverse Problem

##### Direct Solution for the Shape of a Body causing a Gravity or Magnetic Anomaly

In theory it is not possible to use a linear method to solve directly for the shape of a body causing a gravity or magnetic anomaly.

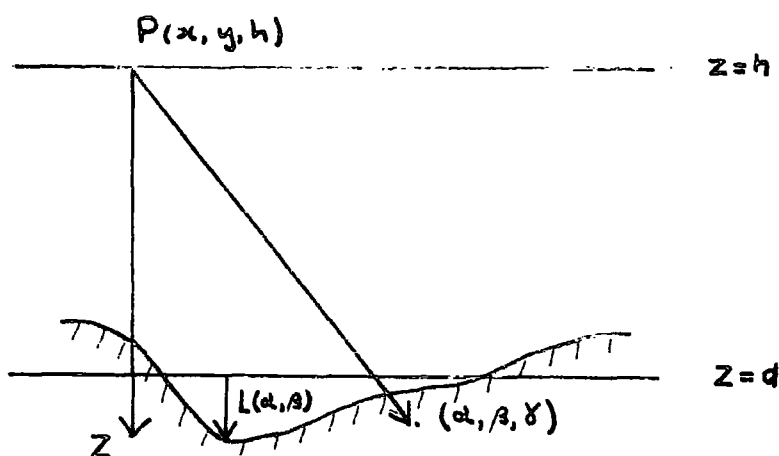
This can be demonstrated by considering the case of a magnetized prism. Ideally by specifying all the variables except one we would hope for a unique specification of the remaining variable. When solving for the shape of a prism we wish to calculate either the depth  $h$  or the thickness  $t$ . In the expression for the spectrum of the prism (equation (1-18)) both the depth and thickness factors

contain an expression of the form  $e^{a\omega}$  where  $a$  is a constant and  $\omega$  is the frequency variable. Although it may be possible to remove all factors except the depth factor, the remaining expression in the space domain is of the form  $\frac{2a}{a^2+x^2}$  (this is the Fourier transform of  $e^{a\omega}$ ). This is not a linear expression for the constant  $a$ .

As any body may be considered as a summation of prisms of infinitely small width this argument for the non-linearity of the solution of the shape is general.

However, it is possible to solve for the shape using linear methods if we make an approximation. Peters (1949) was first to describe this method. It is developed here in spectral terms for the magnetic case. The mathematics is analogous for the gravity case.

Fig. 1-1



The magnetic potential at point  $P(x, y, h)$  due to the distribution of magnetized rocks shown in Fig. 1-1 is:-

$$U_m(x, y, h) = 2\pi m \left[ \frac{\partial}{\partial K} \int_{-\infty}^{\infty} \int_{-\infty}^{\infty} \int_d^{d+L(\alpha, \beta)} \frac{d\alpha d\beta d\gamma}{[(x-\alpha)^2 + (y-\beta)^2 + (z-\gamma)^2]^{\frac{3}{2}}} \right]_{z=h} \quad (1-21)$$

The important approximation for the next step is the condition  $|L| \ll d$ . From examples later it will be shown that this approximation is not as critical as it may appear.

If this approximation holds then equation (1-21) becomes:-

$$U(x, y, h) = 2\pi m \left[ \frac{\partial}{\partial R} \iint_{-\infty}^{\infty} \frac{L(\alpha, \beta) d\alpha d\beta}{[(x-\alpha)^2 + (y-\beta)^2 + (z-d)^2]^{\frac{1}{2}}} \right]_{z=h} \quad (1-22)$$

This expression for the magnetic potential has exactly the same form as the potential due to a surface distribution of magnetization and in fact

$$m_s(x, y, h) = m \cdot L(x, y)$$

Similarly for the gravity case

$$\sigma(x, y, h) = \rho \cdot L(x, y)$$

Thus the equivalent layer is a direct reflection of an approximation to the undulations on an interface.

The problem thus becomes a linear one as the gravity and magnetic fields have a convolution factor directly related to the shape.

$$G_f(x, y, h) = 2\pi G \rho * L(x, y) * H(x, y, h) \quad (1-23)$$

$$M_f(x, y, h) = 2\pi m * D_1(x, y) * D_2(x, y) * I(x, y) * L(x, y) * H(x, y, h) \quad (1-24)$$

Equations (1-23) and (1-24) can be solved by deconvolving the appropriate factors (as in solving for the magnetization) so that only the  $L(x, y)$  term remains.

There are two additional applications of equations (1-23) and (1-24).

If the anomaly is caused by a layer of constant vertical thickness the spectrum of the layer is effectively the difference in the spectra of the two interfaces where one has a depth  $t$  ( $t$  is the vertical thickness of the layer) below the other. This introduces an extra factor;

$$T(u, v, t) = (1 - e^{-t(u^2 + v^2)^{\frac{1}{2}}})$$

into the spectrum.

This factor must also be deconvolved when such layers are being mapped.

Where the body causing a gravity or magnetic anomaly is finite in all directions it can be regarded as the field of the difference in the fields of two interfaces. In this situation  $L(x, y)$  will represent an approximation to the vertical thickness of the body.

## CHAPTER 2

### REVIEW OF METHODS FOR PERFORMING LINEAR TRANSFORMATIONS OF GRAVITY AND MAGNETIC FIELDS

#### 2.1 Introduction

The methods for linear transformations of gravity and magnetic fields have shown a steady evolution since the first realization that such transformations are analytically possible. Early work consisted of numerical attempts to evaluate integral expressions and was restricted in pre-computer days by the need to keep calculations to a minimum. The advent of computers and the knowledge that the transformations are a filtering operation allowed direct design of filters both in the space and frequency domains. Recent work has concentrated on methods of filtering designed for optimum speed and accuracy. This chapter reviews this development.

#### 2.2 Development of the Analytic Theory of Linear Transformations

Much of the theory and many of the ideas for the transformations of gravity and magnetic data can be traced to Evjen (1936). Evjen determined potential fields at lower levels by a Taylor (or Maclaurin) expansion which expressed the continued field in terms of the original field and its derivatives. He gives relationships expressing all the higher derivatives in terms of the second horizontal derivatives and the vertical gradient of the original field. Evjen quotes the analytical expression for upward continuation and by differentiating it he obtains an analytical expression for the vertical gradient of the field.

Peters (1949), in what is basically an extension of Evjen's (1936) work, gives analytical expressions for upward and downward continuation, vertical gradient and the components of the field expressed in terms of the original observed field.

Henderson and Zeitz (1949) perform upward continuation with total fields. The formula they use has the same form as the one used by Peters (1949) for vertical fields. It has been suggested by Grant and West (1967) p.220 and p.314 that total field can not be used in continuation processes, however Henderson (1970) has published a detailed vindication of his theory including a proof of the often quoted upward continuation formula.

Bullard and Cooper (1949) derive the analytic expression for downward continuation.

Hughes and Pondrom (1947), Affleck (1948) and Skeels and Watson (1949) give expressions relating the various components of gravity and magnetic fields.

Baranov (1957) has used Poisson's relationship between gravity and magnetic fields to produce the relationship between the magnetic field for inclined magnetization and what the magnetic field would be for vertical magnetization. This process has become known as 'reduction to the pole'.

Bott, Smith and Stacey (1966) give the analytic expression to convert a two dimensional magnetic anomaly into a gravity anomaly. Their method can be extended to three dimensions and does not require that the anomaly be magnetized in the direction of measurement as Baranov's (1957) method does. This type of transformation has become known as a 'pseudo gravity' transformation.

Grant and West (1967) give a summary of the mathematics presented by many of these workers.

### 2.3 Surface Fitting Methods for Numerically Performing Transformations

The formulae given by the authors listed in the previous section can all be evaluated by conventional numerical techniques. The method used by many authors was to numerically fit a surface defined

by a mathematical function to a finite area of the observed data. The mathematical functions were chosen to simplify numerical evaluation of the analytic expressions approximated by these functions. Many workers have extended this idea to produce numerical sets of coefficients which, when convolved with the field data, effectively combine the surface fitting and numerical evaluation of the relevant expressions to produce an approximation to the transformed field.

This section reviews these methods.

Peter's (1949) fitted least squares polynomials through his observed data which allowed evaluation of the derivatives necessary for his transformations.

Henderson and Zeitz (1949) approximated the field by a Fourier Bessel series which allowed the second vertical derivative to be calculated.

Elkins (1951) and Rosenbach (1954) approximate the field by a power series and calculate orthogonal second horizontal derivatives of this power series. The second vertical derivative can then be obtained from Laplace's equation. In a similar application, Bhattacharyya (1969) uses bicubic spline functions to obtain the horizontal derivatives.

Henderson (1960) continues the field upwards to several different levels by a method similar to Peters (1949). He then fits a polynomial through the field at different levels and extrapolates it to get the downward continued field. By differentiation of the polynomial he obtains the vertical derivatives of the field.

Tomoda and Aki (1955) and Tsuboi and Tomoda (1958) have approximated the field by a function of the type

$$b_{ij} \frac{\sin(x)}{x} \cdot \frac{\sin(y)}{y}$$

and have shown that this allows a simple analytic formula representation of the upward and downward continued fields. Tsuboi, Oldham and Waithman (1958) and Oldham (1967) publish coefficient sets to evaluate these formulae.

Ring residual methods, such as described by Griffin (1949) consist of removing the average field surrounding a point from the field at the point. This is effectively fitting a plane surface to what is considered to be the regional anomaly. A method of fitting a least squares polynomial to the observed field in order to estimate the regional has been described by Grant (1957).

The density or magnetization distribution causing gravity and magnetic fields is not unique and for any observed field a distribution may be calculated on any horizontal surface below the level of observations which gives the same field as the observed. Roy (1962) gives a proof of this. Some workers have used computed equivalent layer distributions to recompute fields with different characteristics.

Talwani (1964) considers the contours of a gravity map as representing the density distribution of an equivalent layer and he computes the field at a higher level by calculating the effect, at the higher level, of laminae with the density distribution given by the contours.

Bott (1967a) computes an equivalent layer of differently magnetized blocks by solving a set of simultaneous equations relating the magnetization of the blocks to the observed magnetic field. Bott's method can be used to calculate sets of coefficients. Ingles (1971) has extended Bott's matrix method to gravity fields and has used it to convert between gravity and magnetic fields as well as to perform continuation operations.

Tsuboi and Fuchida (1958) have expressed the equivalent layer for a gravity field in terms of a double Fourier series and they show that

the gravity field at different levels may be calculated by multiplying each term by  $e^{h(u^2+v^2)^{\frac{1}{2}}}$  where  $h$  is the continuation distance ( $+ve$  downwards) and  $u$  and  $v$  are the frequencies in the  $x$  and  $y$  directions.

Danes (1962) also uses the Fourier series method for continuation. Danes has worked out factors by which the terms of the Fourier series must be multiplied to convert it to the Fourier series of the derivatives of the field.

Bhattacharyya (1965) has performed reduction to the pole transformations by multiplying Fourier series by appropriate factors.

The Fourier series method is a filter method in principle because different frequency components are multiplied by different factors to perform the transformation. This is what happens in a filtering operation in which a set of filter coefficients with a known frequency response are convolved with a signal. The filter method for performing transformations, which has superseded the Fourier series method, is reviewed in the following section.

#### 2.4 Linear Transformations as a Filtering Operation

Swartz (1954) appears to have been the first to realize that calculation of residuals and derivatives using grids of coefficients are convolution operations in which the output can be predicted from a knowledge of the frequency response of the filter being applied.

Dean (1958) gives a clearer and more detailed account of the transformations of gravity and magnetic fields as filter operations.

Byerly (1965) has added some details to Dean's (1958) discussion.

Various workers such as Mesko (1965), (1966) and Dampney (1966) have studied the coefficient sets published by previous workers by comparing the computed frequency response of these coefficients with the analytic frequency response of the operation. Mesko (1965) and

Dampney (1966) have used the property that residual, derivative and continuation coefficients have circular symmetry and they have only considered it necessary to compute the radial frequency response. Much more meaningful studies have been done by Darby and Davies (1967) and Fuller (1967) who have computed the two dimensional frequency responses of various published coefficient sets. From their results it can be seen that some of the published methods deviate markedly from the theoretical response both in radial variations and by being non-symmetric.

As an improved method of calculating coefficient sets Dean (1958), Dampney (1966), Fuller (1967), Darby and Davies (1967), Zurflueh (1967) and Agarwal and Lal (1971) have used the direct design method of computing filter coefficients which have known frequency responses.

A full development of the theory is given below because none of these authors has considered every aspect.

Fuller (1967) has given the following mathematics for symmetric filters. The theory developed here is completely general.

The two dimensional convolution integral is

$$c(x,y) = \int_{-\infty}^{\infty} \int_{-\infty}^{\infty} f(\alpha,\beta) \cdot b(x-\alpha,y-\beta) d\alpha d\beta \quad (2-1)$$

where  $b(x,y)$  is the input data

$c(x,y)$  is the output data

$f(x,y)$  is the filtering function

To evaluate (2-1) numerically it is necessary for  $f(x,y)$  to exist over a finite range of  $x$  and  $y$ ; i.e. it is necessary for  $f(x,y)$  to be zero for  $|x| \gg X$  and  $|y| \gg Y$ . Generally this is not so in gravity and magnetic filtering operations and  $f(x,y)$  must be truncated. The problem of truncation is considered in a later section and for this development we shall assume that the above limits hold.

Thus

$$C(x, y) = \int_{-y}^y \int_{-x}^x f(\alpha, \beta) \cdot b(x-\alpha, y-\beta) d\alpha d\beta \quad (2-2)$$

If  $f(x, y)$  and  $b(x, y)$  are sampled at discrete constant intervals (2-2) can be expressed numerically.

$$C(x, y) \cong \sum_{n=-\frac{y}{\Delta y}}^{\frac{y}{\Delta y}} \sum_{k=-\frac{x}{\Delta x}}^{\frac{x}{\Delta x}} f(k\Delta x, n\Delta y) \cdot b(x-k\Delta x, y-n\Delta y) \Delta x \Delta y$$

where  $\Delta x$  and  $\Delta y$  are the sample intervals in the  $x$  and  $y$  directions.

By letting  $\Delta x = \Delta y = 1$  we have

$$C(x, y) = \sum_{n=-y}^y \sum_{k=-x}^x f(k, n) \cdot b(x-k, y-n) \quad (2-3)$$

where  $f(k, n)$  are the filter coefficients.

Equation (2-3) is the general space domain expression relating the input of a two dimensional digital filter to its output. If the input and desired output are known then a set of simultaneous equations is established and they can be solved to give the filter coefficients. If the number of equations is greater than the number of filter coefficients then a least squares solution can be obtained. A variation of this approach is fully investigated in Chapter 4 which studies the application of Wiener filters.

Alternatively the filter coefficients may be calculated using Fourier transforms. The convolution theorem shows that convolution in the space domain is equivalent to multiplication in the frequency domain so the frequency domain equivalent of (2-1) is

$$C(u, v) = F(u, v) \cdot B(u, v) \quad (2-4)$$

The capitals denote the Fourier transforms have been taken; for example  $f(x, y)$  and  $F(u, v)$  are related by the Fourier transform pair.

$$F(u, v) = \int_{-\infty}^{\infty} \int_{-\infty}^{\infty} f(x, y) \cdot e^{-i(u x + v y)} dx dy \quad (2-5)$$

$$f(x, y) = \int_{-\infty}^{\infty} \int_{-\infty}^{\infty} F(u, v) \cdot e^{i(ux + vy)} du dv \quad (2-6)$$

Thus if the frequency response of a filter  $F(u, v)$  is known equation (2-6) can be evaluated to give  $f(x, y)$  the space domain filtering function.

To evaluate (2-6) numerically the maximum frequency we may consider is the Nyquist frequency defined by the sample interval  $\Delta x$ . The Nyquist frequency  $N_f = \frac{1}{2\Delta x} = 0.5$  cycles per data interval.

The Nyquist frequency is explained more fully later. With digitized data we have to consider

$$u = 2\pi f_x$$

$$v = 2\pi f_y$$

where  $f_x$  and  $f_y$  are in units of cycles per data interval.

The expression for equation (2-6) in digital form is

$$f(k, n) = \sum_{\ell=-\frac{0.5}{\Delta f_x}}^{\frac{0.5}{\Delta f_x}} \sum_{m=-\frac{0.5}{\Delta f_y}}^{\frac{0.5}{\Delta f_y}} 4\pi^2 F(\ell \Delta f_x, m \Delta f_y) \cdot [\cos(2\pi \ell \Delta f_x k) \cdot \cos(2\pi m \Delta f_y n) - \sin(2\pi \ell \Delta f_x k) \cdot \sin(2\pi m \Delta f_y n) + j \cos(2\pi \ell \Delta f_x k) \cdot \sin(2\pi m \Delta f_y n) + j \sin(2\pi \ell \Delta f_x k) \cdot \cos(2\pi m \Delta f_y n)] \Delta f_x \Delta f_y \quad (2-7)$$

where  $F(\ell \Delta f_x, m \Delta f_y)$  is the digitized frequency response of the filter

Equation (2-7) is the general expression to calculate a filter with a desired frequency response.

Because of the radial symmetry of coefficients whose frequency response is real it is only necessary to calculate the coefficients in half a quadrant of the grid of coefficients. The rest can be determined by symmetry.

No worker appears to have used the direct Fourier method to design filter coefficients whose response includes complex terms. Equation (2-7) shows that this is possible and the theory in Chapter 1 shows that there are several transformations where this could be desirable.

As both equation (2-3) and equation (2-7) are numerical attempts to evaluate the convolution integral the accuracy of the filter is improved by keeping  $\Delta x$  and  $\Delta y$  as small as possible while keeping the number of coefficients and their areal spread as large as possible. The coefficients designed by this method may not be the optimum for the transformation. The problem of optimum filter design is considered in Chapter 4.

As pointed out by Dean (1958) and Darby and Davies (1967) the radial symmetry of some transform operations allows these transformations to be considered in terms of zero order Hankel transformations (the cylindrical polar co-ordinate/of Fourier Transforms). Although Darby and Davis (1967) and Lavin and Devane (1970) have managed to use Hankel transformations for some problems the method lacks generality because they are difficult to evaluate except for simple cases and the theory is difficult to adapt to data on a rectangular grid.

## 2.5 Filtering in the Frequency Domain

Since convolution in the space domain is equivalent to multiplication in the frequency domain (see Chapter 1) it is possible to convolve two functions by taking the Fourier transformations of both functions (their transfer functions), multiplying the resultant transforms and then performing an inverse transformation of the result to give the convolved output in the space domain. Until the advent of the Fast Fourier Transform (FFT) technique (Cooley and Tukey, 1965) this method was considerably more time consuming than conventional convolution. Cochran et al. (1967) have shown for two dimensional real data with  $N^2$  points that the number of multiplications involved in using the FFT method to filter in the frequency domain is of the order  $(4N^2 \log_2 N + \frac{1}{2}N^2)$  whereas filtering in the space domain with an

operator with  $M^2$  coefficients requires  $M^2N^2$  multiplications. Thus with very large numbers of coefficients the FFT method will be considerably faster. In cases where the coefficient array is relatively small the advantage is less spectacular. For example when convolving a  $128 \times 128$  array with an  $11 \times 11$  filter the FFT method is 4 times faster than the convolution method which takes about 60 seconds CPU time for this operation on an IBM360/67 computer.

The FFT method also has the advantage that extremely complicated filters may be designed directly and accurately from their known frequency response.

Black and Scollar (1969) give a discussion of the application of the method to two dimensional geophysical filtering and Spector (1968) and Kanasewich and Agarwal (1970) report using the method for reduction to the pole transformations.

However, transforming a finite function into the frequency domain using the FFT assumes that the space domain function is periodically repeated and if there is a step at the boundary of the original function (i.e. the starting and finishing levels of the function are different) then oscillations are produced in the computed spectrum. To eliminate these, regional trends must be removed from the data before the transformation. Even this may not completely eliminate a step at the edge and in any case the apparent regional may vary with the length of the data. For these reasons, adjacent areas of data processed with the FFT method may not match at the boundaries.

A practical problem is that published computer algorithms for the FFT (Robinson, 1967, IBM, 1968) require data with dimensions which are a power of 2. Black and Scollar (1969) have developed a method where the dimensions of the data may be highly composite (the product of many small prime factors) but even this is not always convenient.

Because of the theoretical and practical difficulties which have to be faced when using the frequency domain method of filtering, in order to achieve a modest reduction in computer time, the author prefers the space domain method of filtering. As shown in Chapter 4 the space domain method produces accurate results.

## 2.6 Concluding Remarks

It must be realized that all the methods reviewed in this chapter constitute numerical attempts to evaluate infinite integrals using finite amounts of data. Consequently even though excellent results may be obtained the output can never be as the theoretical output would be. For this reason, if curve matching interpretive techniques are to be used on transformed data, it is best to apply the same transformation to the model data so that the distortion will be the same.

## CHAPTER 3

### PRACTICAL PROBLEMS TO BE CONSIDERED WHEN APPLYING FILTER METHODS

Digital filtering is effectively an attempt to numerically evaluate infinite integrals and as with all numerical methods it is important to understand the limitations and problems.

#### 3.1 Converting the Data to a Regular Grid

Digital filter methods require the signal to be sampled on a equispaced grid (generally, but not necessarily cartesian). This process is called digitizing.

The straightforward method of superimposing a grid over a contour map and mentally interpolating the values at the corners of the grid can cause errors because:

- (i) the contouring may not be exact
- (ii) the mental interpolation may not be exact

Such errors are a problem when a form of high pass filtering is applied which emphasizes small irregularities.

Recently various attempts have been made to apply computers to convert irregularly spaced field data to regularly spaced data. Most of these methods (which have been reviewed by Walters, 1969 ) consist of fitting mathematical surfaces through groups of points. Visually satisfactory results are generally obtained when the results are contoured.

Methods more relevant to aeromagnetic surveys have been developed by Bhattacharyya (1969) and Naudy (1970). They use all the information along parallel flight lines and fit curves perpendicular to the flight lines to grid the data.

Cubic spline interpolation (Bhattacharyya, 1969) has been used in this thesis to convert irregularly spaced data along profiles to regularly spaced data.

However, even with computer gridding of the data it may still be necessary to apply some smoothing to the data (see below).

### 3.2 Effects of Digitization

#### 3.2.1 Aliasing

Blackman and Tukey (1958) p.31 and Jenkins and Watts (1968) p.51 have considered the effects of sampling continuous signals at uniform intervals and have shown that the maximum frequency which can be uniquely defined by a sampled signal is the Nyquist frequency.

$$N_f = \frac{1}{2\Delta t}$$

where  $\Delta t$  is the sample interval. This frequency is also called the folding frequency because if the spectrum of such a sampled series is calculated it is symmetric about  $N_f$ . Frequencies equispaced on either side of  $N_f$  are indistinguishable from each other. This effect is known as aliasing. Thus in any analysis with digitized data either the frequencies above the Nyquist frequency must be removed or their effects must be insignificant. In the analysis of gravity and magnetic fields the spectrum is dominated by the  $e^{-h(\omega^2 + \nu^2)^{\frac{1}{2}}}$  term where  $h$  is the depth. This in general makes the higher frequencies insignificant relative to the lower frequencies, thus the aliasing problem is not critical although it should not be completely disregarded. The phenomenon of aliasing also determines the minimum grid spacing practical for a set of data. Obviously this interval can not be less than the interval of measurement of the original data.

It is difficult to decide how to apply such a criterion to an aeromagnetic survey with continuous data along parallel lines. Strictly, the minimum grid interval allowable is equal to the line spacing. If the lines are flown perpendicular to the strike of the anomalies so that the high frequency trends perpendicular to the flight

lines are negligible then a grid spacing closer than the flight line interval should sample the field adequately and without aliasing errors.

### 3.2.2 Gibbs Phenomenon

Another effect of having the data in digital form, so that the higher frequencies are not specified, is that it is never possible to exactly obtain as output a function which in theory we would expect. This effect is called Gibb's phenomenon (Hsu, 1970, p.253). It is most noticeable where the output should be a step function. In this case the actual output is a step function with ripples before and after the step. The ripples can be decreased by making the sample interval smaller but they can never be completely eliminated.

### 3.3 Truncation Effects

The spectral effects of truncating infinite functions were first considered by Blackman and Tukey (1958). Jenkins and Watts (1968) give a clearer and more detailed account of the theory.

The effects can be considered thus:

If  $S(t)$  is an infinite function and is only known in the interval we consider the signal to be multiplied by  $w(t)$  where  $w(t)$  is a data window (also called a lag window).

$$S_T(t) = S(t) \cdot w(t)$$

where  $S_T(t)$  is the truncated signal and

$$\begin{aligned} w(t) &\neq 0 & |t| \leq T/2 \\ &= 0 & |t| > T/2 \end{aligned}$$

From the convolution theorem we know that multiplication in the time domain is equivalent to convolution in the frequency domain so

$$S_T(f) = \int_{-\infty}^{\infty} S(g) \cdot w(f-g) dg$$

where  $S_T(f)$ ,  $S(f)$  and  $w(f)$  are the Fourier transforms of  $S_T(t)$ ,  $S(t)$  and  $w(t)$ .  $w(f)$  is called a spectral window.

This means that truncating a signal results in its spectrum being filtered by  $\omega(f)$ . Ideally this filtering effect should be a minimum i.e.  $\omega(f)$  should be a spike (corresponding to  $\omega(t)$  being infinite and always equal to 1. i.e. an infinite length of  $s(t)$ ).

The figures shown on p.246 of Jenkins and Watts (1968) and p.15 of Blackman and Tukey (1958) show some common spectral windows. It can be seen that the windows with the narrowest central peak (i.e. the closest to the ideal unit spike) have the largest side lobes. These side lobes cause what is called 'leakage'. This is because these side lobes are convolved with the true spectrum to cause oscillations in the estimated spectrum (this is called a loss in stability).

Windows with a broader central peak have smaller side lobes and cause less oscillation on the estimated spectrum but the spectral estimates in this case have the finer detail smoothed out (this is called a loss in fidelity).

The design and choice of a perfect window must allow for these two conflicting effects as well as the nature of the true spectrum.

Both Blackman and Tukey (1958) and Jenkins and Watts (1968) admit that the best window for a particular situation has to be chosen by an empirical approach.

The windows which have had the most general use in gravity and magnetic applications (see Gudmundsson (1966), Fuller (1967), Kanasewich and Agarwal (1970)) and which have been used successfully by the author are, in their two dimensional digital form:

Rectangular Window

$$\begin{aligned} \omega(k,n) &= 1 \quad \text{for } |k| \leq x \\ &\quad |n| \leq y \\ &= 0 \quad \text{otherwise} \end{aligned}$$

Hamming Window

$$w(k,n) = 0.54 + 0.46 \cos \left[ \frac{\pi (k^2 + n^2)}{(X^2 + Y^2)} \right] \quad \text{for } |k| \leq X \\ |n| \leq Y \\ = 0 \quad \text{otherwise}$$

Hanning Window

$$w(k,n) := 0.5 \left( 1 + \cos \left[ \frac{\pi (k^2 + n^2)}{(X^2 + Y^2)} \right] \right) \quad \text{for } |k| \leq X \\ |n| \leq Y \\ = 0 \quad \text{otherwise}$$

It does not seem possible to give an exact criteria for choosing when to use a particular window. As a general rule the rectangular window is best for very long records, the Hamming window is best for intermediate length records and the Hanning window is best for short records. 'Short' and 'Long' are used here in a purely relative sense.

Obviously  $S(t)$  should be as long as possible.

In this thesis truncation has relevance in the calculation of filter coefficients. There are two distinct situations.

a) Calculation of Filter Coefficients by the Fourier Transform Method:

The coefficients calculated by the Fourier transform method will be exact but there may be too many of them. If it is desired to shorten the spread of the coefficients it will have to be done by applying a data window. The window will have to be chosen to give the least distortion of the frequency response of the coefficients away from the ideal frequency response of the filter.

An example of the effects of truncation on the frequency response of an operator is given by Fuller (1967) Fig. 32. Fuller truncates a set of ideal downward continuation coefficients using the Hanning window. He truncates to an unrealistically short spread and causes severe distortion in the spectrum.

#### b) Calculating Coefficients in the Space Domain:

In the case where we calculate a set of coefficients to transform a known input into a desired output we are calculating a filter whose frequency response is the frequency response of the transformation. If either the input or the desired output are infinite then they must be truncated with a data window. They must be truncated so that their spectra are not distorted otherwise the problem will be incorrectly specified and the calculated coefficients will not be correct.

It is important to note the subtle difference in truncating the coefficients after they have been calculated (Case (a)) and truncating the signal and output before calculation of the coefficients (Case (b)).

#### 3.4 Edge Effects

When applying sets of coefficients to data there is always a loss of coverage because the centre coefficient and hence the last output point can not be at the edge of the map without the surrounding coefficients being off the edge of the data. This effect can be reduced by using smaller (and hence less accurate) sets of coefficients near the edge of the data or by extrapolating the data so that it is possible to calculate filtered values up to the edges.

The author has used an inverted mirror image (i.e. treated the data as a repeated odd function) for extrapolation purposes. This gives a smooth function with the same trend as the original data at the edges of the map.

#### 3.5 Smoothing

Because downward continuation and derivative filters are high pass filters it is often necessary to apply some form of smoothing to remove high frequency noise from the data as this noise may be excessively exaggerated by the transformation. Noise in magnetic and gravity fields may be caused by geological structures shallower

than the structures of interest or by errors in the original measurements or compilation.

Bullard and Cooper (1948) suggest convolving the data by a function with frequency response  $e^{-\gamma u^2}$  where  $\gamma$  is an arbitrary factor which specifies the degree of smoothing. This is effectively an application of the error function.

Dampney (1966) suggests using a low pass filter to cut out frequencies for which the noise level exceeds the signal level.

The process of digitizing is a form of filtering and some of the high frequencies may be suppressed by increasing the grid size.

Linear methods such as these generally distort part of the signal anomalies because there is always spectral overlap between the signal and the noise.

A non-linear method, described by Naudy (1967) has been used effectively by the author to remove spike type errors from profiles. Naudy's method detects the spikes using a width criterion and removes them by fitting a curve through them. The method is frequency independent and removes all the spike or none of it. A computer program NLFILT has been written to do this.

Clarke (1969) gives a method for calculating optimum downward continuation and derivative filters when the statistical characteristics of the signal and noise are known. An investigation of this approach and other methods of noise removal are given in Chapter 6.

### 3.6 Characteristics of Coefficients

A computer program COEFF has been written to evaluate equation 1-7 and has been used to calculate sets of coefficients for several important transformations whose frequency responses were derived in Chapter 1. The numerical behaviour of these coefficients allows certain limits to be anticipated in the performance of these filtering operations.

Although only the coefficients for profiles are considered the same general comments apply to two dimensional coefficients.

### 3.6.1 Downward continuation

Sets of downward continuation coefficients were calculated for continuation intervals of  $h = 1, 2, 3, 4, 5$  grid units. For this example 211 coefficients were calculated. The behaviour is similar for other numbers of coefficients, the only difference being the greater the number of coefficients, the more accurately the continued field is calculated. Each set of coefficients consists of an alternating set of positive and negative coefficients which have a hyperbolic decay in amplitude. Fig. 3-1a shows a plot of these amplitudes. Only half the coefficients are shown because they are symmetric about the centre.

A critical factor is that the numerical value of the coefficients become impractically large for continuation distances greater than 2 grid intervals. These large values of the coefficients enormously magnify small data errors. This is a direct result of the fact that the frequency response of a downward continuation filter increases exponentially with the continuation distance. The maximum continuation distance appears, for practical purposes, to be 2 grid intervals.

The general shape of the decay envelope of the coefficients suggests that the values in the immediate vicinity of the point at which the filtered value is being calculated are the most important.

### 3.6.2 Upward Continuation

Fig. 3-1b shows a plot of the amplitudes of a set of upward continuation coefficients for continuation distances  $h = 1, 2, 3, 4, 5$  grid units. There is no problem about the magnitude of the coefficients because upward continuation is a stable low pass operation. The coefficients are broad and slowly varying and this suggests the areal extent of the operators may be important.

### 3.6.3 Differentiating and Integrating Operators

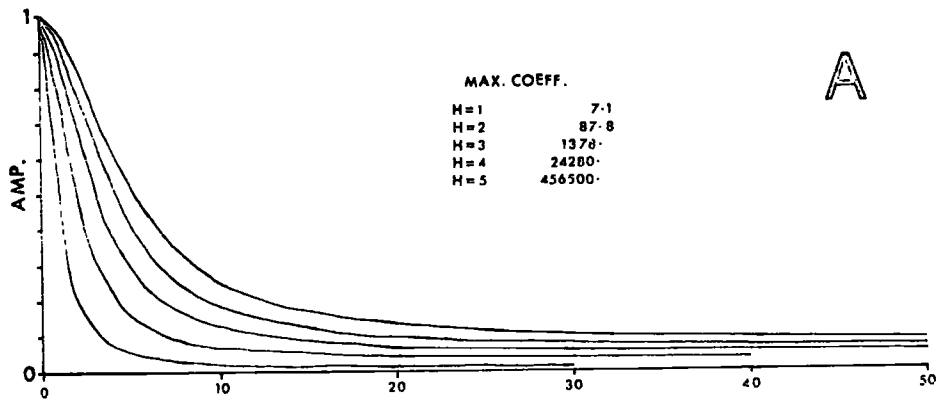
In 1.4 it is shown that vertical derivatives introduce a factor  $\frac{1}{h} [(\omega^2 + \sigma^2)^{\frac{1}{2}}]^n$  into the spectrum of the field. ( $n$  is the order of the derivative).

Vertical derivatives are high pass filters and their coefficients have a similar behaviour to downward continuation coefficients.

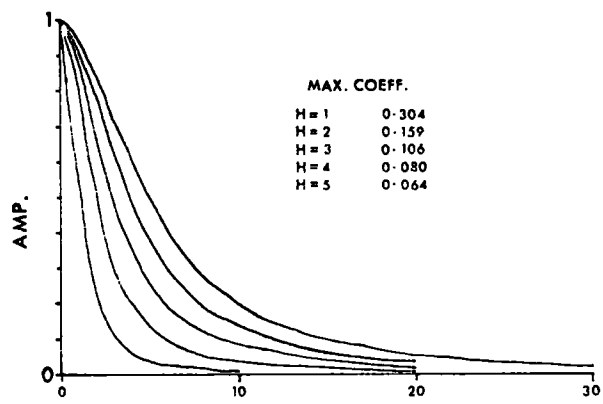
Vertical integration introduces a factor the inverse of the factor above into the spectrum. Coefficient sets to perform vertical integration are low pass filters and have the same numerical behaviour as upward continuation filters.

### 3.6.4 Phase Filters

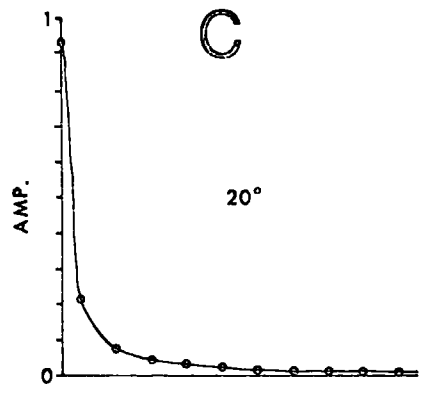
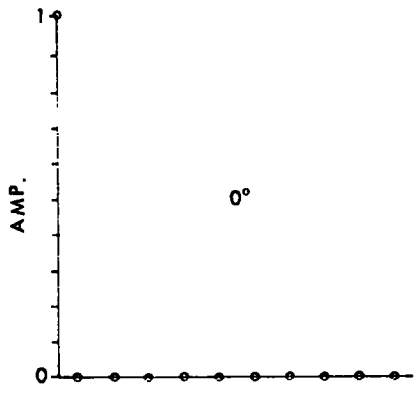
Filters whose frequency response involves complex terms of the type  $(a + jb)^n$ , such as reduction to the pole filters, cause a phase shift in the data. Fig. 3-1c shows a plot of the amplitudes of a set of phase filters. The increasing asymmetry of the coefficients for increasing phase shifts suggests an increase in the difficulty of the transformation.



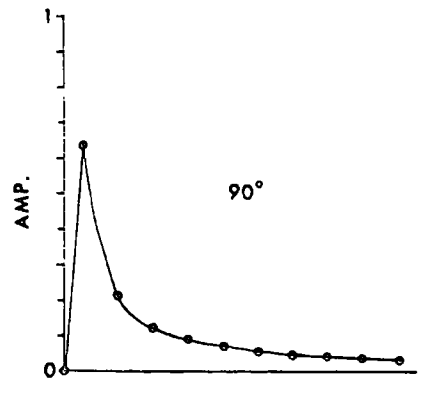
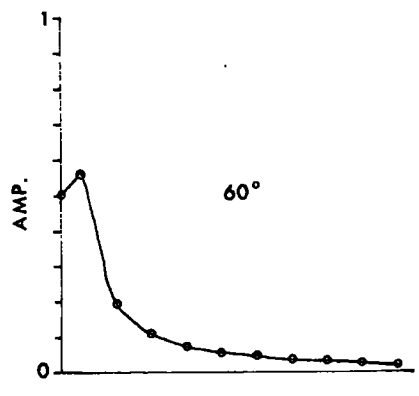
A



B



C



CHAPTER 4

TRANSFORMATIONS OF GRAVITY AND MAGNETIC FIELDS USING WIENER FILTERS

4.1 General Theory

A Wiener filter is a filter which converts a given input into a desired output such that the sum of the squares of the differences between the desired output and the actual output is a minimum.

The theory of such filters was originally developed in terms of integral calculus by Wiener (1949). Clarke (1969) gives an outline of Wiener's theory applied to two dimensional signals.

Suppose the input to a linear system is denoted  $b(x,y)$  and a weighting function  $f(x,y)$  is sought for which

$$c(x,y) = \int_{-\infty}^{\infty} \int_{-\infty}^{\infty} f(x',y') \cdot b(x-x', y-y') dx' dy'$$

will closely approximate some desired output function  $d(x,y)$ .

We wish to find  $f(x,y)$  which minimizes the mean square error between the desired system output and the actual output i.e. minimizes

$$\overline{e^2(x,y)} = \overline{[d(x,y) - c(x,y)]^2}$$

The bar denotes that averages are taken.

By defining the autocorrelation

$$\Phi_{II}(x_0, y_0) = \overline{b(x,y) \cdot b(x-x_0, y-y_0)}$$

and the crosscorrelation

$$\Phi_{DI}(x_0, y_0) = \overline{d(x,y) \cdot b(x-x_0, y-y_0)}$$

then

$$e^2(x,y) = \Phi_{DI}(0,0) - 2 \int_{-\infty}^{\infty} \int_{-\infty}^{\infty} f(x',y') \Phi_{DI}(x',y') dx' dy' \\ + \int_{-\infty}^{\infty} \int_{-\infty}^{\infty} \int_{-\infty}^{\infty} \int_{-\infty}^{\infty} f(x',y') \cdot f(x'',y'') \cdot \Phi_{II}(x-x', y-y'') dx' dy' dx'' dy''$$

By variational methods it can be shown that the  $f(x,y)$  which minimizes  $e^2(x,y)$  must satisfy the equation

$$\Phi_{DI}(x,y) = \int_{-\infty}^{\infty} \int_{-\infty}^{\infty} f(x',y') \Phi_{II}(x-x', y-y') dx' dy'$$

This is known as the Wiener Hopf equation.

The work of Robinson and Treitel (1967) and Robinson (1967) has been largely responsible for Wiener's theory being adapted to data in digital form and for its application to the computer processing of seismic data.

The mathematics given below follows the method developed by Treitel and Robinson (1966) who presented it in the context of single channels of data being filtered by one sided operators (considering only past values of the signal). The theory given here has been extended to two dimensional data where the filter considers the signal surrounding the point at which the signal is being transformed.

The Problem:

To convert the digital signal  $b(x,y)$  with dimensions  $2j+1, 2k+1$  where  $-j \leq x \leq j$  and  $-k \leq y \leq k$  into the desired digital output  $d(x,y)$  with dimensions  $2j+2m+1, 2k+2n+1$  where  $-(j+m) \leq x \leq (j+m)$  and  $-(k+n) \leq y \leq (k+n)$ .

with digital filter coefficients  $f(x,y)$  with dimensions  $2m+1, 2n+1$  where  $-m \leq x \leq m$  and  $-n \leq y \leq n$ . Such that the Error Energy is a minimum

where

$$\text{Error Energy } I = \sum_{x=-m-j}^{m+j} \sum_{y=-n-k}^{n+k} (d(x,y) - C(x,y))^2 \quad (4-1)$$

where  $C(x,y)$  is the result of the two dimensional convolution

$$C(x,y) = \sum_{s=-m}^m \sum_{t=-n}^n f(s,t) \cdot b(x-s, y-t) \quad (4-2)$$

To determine the filter coefficients which give the minimum error energy we take partial derivatives of (4-1) with respect to the filter coefficients and equate to zero i.e.

$$\frac{\partial I}{\partial f(i,j)} = \sum_{x=-m-j}^{m+j} \sum_{y=-n-k}^{n+k} \left[ d(x,y) - \left( \sum_{s=-m}^m \sum_{t=-n}^n f(s,t) \cdot b(x-s, y-t) \right) \right]. \quad (4-3)$$

$$(b(x-i, y-j)) = 0$$

This gives

$$\sum_{x=-m-j}^{m+j} \sum_{y=-n-k}^{n+k} d(x,y) \cdot b(x-i, y-j) + \sum_{x=-m-j}^{m+j} \sum_{y=-n-k}^{n+k} \quad (4-4)$$

Now 
$$\left( \sum_{s=-m}^m \sum_{t=-n}^n f(s,t) \cdot b(x-s, y-t) \right) \cdot b(x-i, y-j) = 0$$

$$\phi_{II}(i-s, j-k) = \sum_{x=-m-j}^{m+j} \sum_{y=-n-k}^{n+k} b(x-s, y-t) \cdot b(x-s, y-t) \quad (4-5)$$

is the autocorrelation of the input.

$$\phi_{DI}(i, j) = \sum_{x=-m-j}^{m+j} \sum_{y=-n-k}^{n+k} d(x-s, y-t) \cdot b(x-i, y-j) \quad (4-6)$$

is the cross correlation of the desired output and the input.

Substituting (4-5) and (4-6) into (4-4) we obtain

$$\phi_{DI}(i, j) = \sum_{s=-m}^m \sum_{t=-n}^n f(s,t) \cdot \phi_{II}(i-s, j-t) \quad (4-7)$$

This is the digital equivalent of the Wiener Hopf equation.

The set of simultaneous equations given by (4-7) can be solved to give the filter coefficients.

Clarke (1969) who has used Wiener theory to design downward continuation and derivative filters performs his filtering operations in the frequency domain. Clarke shows that the transfer function of a Wiener filter is

$$F(u, v) = \frac{P_{DI}(u, v)}{P_{II}(u, v)}$$

where

$P_{DI}$  is the Fourier transform of the crosscorrelation of the desired output and the input;

$P_{II}$  is the Fourier transform of the autocorrelation of the input.

This study is concerned with the space domain application of Wiener filters. The frequency domain approach suffers from the disadvantages discussed in 2-5 and the problems of finding Fourier transforms of the relevant autocorrelation functions.

The solution of (4-7) will be considered separately for profiles and maps.

(i) One Dimensional Data

For one dimensional data equation (4-7) reduces to

$$\phi_{DI}(i) = \sum_{s=-m}^m f_s \phi_{II}(i-s) \quad (4-8)$$

$$\phi_{DI}(i) = \sum_{x=-m-j}^{m+j} d(x) \cdot b(x-i)$$

is the crosscorrelation between the desired output and the input and

$$\phi_{II}(i-s) = \sum_{x=-m-j}^{m+j} b(x-s) \cdot b(x-i)$$

is the autocorrelation of the input

Equation (4-8) can be written out fully

$$\begin{aligned} f_{(-m)} \phi_{II}(-m) + f_{(-m+1)} \phi_{II}(-m+1) + f_{(-m+2)} \phi_{II}(-m+2) + \dots + f_{(m)} \phi_{II}(m) &= \phi_{DI}(-m) \\ f_{(-m)} \phi_{II}(-m+1) + f_{(-m+1)} \phi_{II}(-m) + f_{(-m+2)} \phi_{II}(-m+1) + \dots + f_{(m)} \phi_{II}(m-1) &= \phi_{DI}(-m+1) \\ f_{(-m)} \phi_{II}(-m+2) + f_{(-m+1)} \phi_{II}(-m+1) + f_{(-m+2)} \phi_{II}(-m) + \dots + f_{(m)} \phi_{II}(m-2) &= \phi_{DI}(-m+2) \quad (4-9) \\ \dots & \dots \\ f_{(-m)} \phi_{II}(m-1) + f_{(-m+1)} \phi_{II}(m-2) + f_{(-m+2)} \phi_{II}(m-3) + \dots + f_{(m)} \phi_{II}(-m+1) &= \phi_{DI}(m-1) \\ f_{(-m)} \phi_{II}(m) + f_{(-m+1)} \phi_{II}(m-1) + f_{(-m+2)} \phi_{II}(m-2) + \dots + f_{(m)} \phi_{II}(-m) &= \phi_{DI}(m) \end{aligned}$$

Now the autocorrelation function is even i.e.  $\phi_{II}(-i) = \phi_{II}(i)$

so equation (4-9) can be written in matrix form

$$\begin{bmatrix} \phi_{II}(-m) & \phi_{II}(-m+1) & \phi_{II}(-m+2) & \dots & \phi_{II}(m) \\ \phi_{II}(-m+1) & \phi_{II}(-m) & \phi_{II}(-m+1) & \dots & \phi_{II}(m-1) \\ \phi_{II}(-m+2) & \phi_{II}(-m+1) & \phi_{II}(-m) & \dots & \phi_{II}(m-2) \\ \dots & \dots & \dots & \dots & \dots \\ \phi_{II}(m-1) & \phi_{II}(m-2) & \phi_{II}(m-3) & \dots & \phi_{II}(-m+1) \\ \phi_{II}(m) & \phi_{II}(m-1) & \phi_{II}(m-2) & \dots & \phi_{II}(-m) \end{bmatrix} \begin{bmatrix} f_{(m)} \\ f_{(m-1)} \\ f_{(m-2)} \\ \dots \\ f_{(-m+1)} \\ f_{(-m)} \end{bmatrix} = \begin{bmatrix} \phi_{DI}(-m) \\ \phi_{DI}(-m+1) \\ \phi_{DI}(-m+2) \\ \dots \\ \phi_{DI}(m-1) \\ \phi_{DI}(m) \end{bmatrix} \quad (4-10)$$

The high degree of symmetry of the autocorrelation matrix (called a Toeplitz structure) has been used by Levinson (1947) to devise an efficient recursive technique for solving the set of simultaneous equations defined by (4-10). The Levinson routine allows over 200

coefficients to be calculated in less than 10 seconds on an IBM 360/67 computer and only requires  $m^2$  storage locations (where  $m$  is the number of unknowns) compared with  $m^3$  storage locations required by conventional algorithms for solving simultaneous equations.

A computer routine EUREKA which solves simultaneous equations using the Levinson method has been published by Robinson (1967). This subroutine has been incorporated by the author into a computer program WIEN1D which calculates one dimensional sets of Wiener filter coefficients.

(ii) Two Dimensional Data

Consideration of the symmetry conditions of equation (4.7) simplifies its solution. Fig. 4-1 shows the autocorrelation matrix

a) General Case

The two dimensional autocorrelation function displays the symmetry

$$\phi_{II}(j,k) = \phi_{II}(-j,-k)$$

Thus the matrix of the autocorrelation function is symmetric about a principal diagonal. A subroutine GELS has been published by IBM (1968) to solve simultaneous equations with this property.

b) Symmetric Case

In cases where the input has an axis of symmetry the autocorrelation function becomes symmetric.

i.e. 
$$\phi_{II}(|j|, |k|) = \phi_{II}(|j|, |k|)$$

In this situation the autocorrelation matrix can be partitioned into submatrices and the matrix of submatrices has Toeplitz symmetry. A recursive solution to this problem has been developed by Wiggins and Robinson (1965) and a subroutine NORME has been published by Robinson (1967) to apply this method.

$$\begin{array}{c}
\emptyset_{II}(i,j) \\
\begin{array}{l}
(0,0)(0,-1)(0,-2) \quad (-1,0)(-1,-1)(-1,-2) \quad (-2,0)(-2,-1)(-2,-2) \\
(0,1)(0,0)(0,-1) \quad (-1,1)(-1,0)(-1,-1) \quad (-2,1)(-2,0)(-2,-1) \\
(0,2)(0,1)(0,0) \quad (-1,2)(-1,1)(-1,0) \quad (-2,2)(-2,1)(-2,0) \\
(1,0)(1,-1)(1,-2) \quad (0,0)(0,-1)(0,-2) \quad (-1,0)(-1,-1)(-1,-2) \\
(1,1)(1,0)(1,-1) \quad (0,1)(0,0)(0,-1) \quad (-1,1)(-1,0)(-1,-1) \\
(1,2)(1,1)(1,0) \quad (0,2)(0,1)(0,0) \quad (-1,2)(-1,1)(-1,0) \\
(2,0)(2,-1)(2,-2) \quad (1,0)(1,-1)(1,-2) \quad (0,0)(0,-1)(0,-2) \\
(2,1)(2,0)(2,-1) \quad (1,1)(1,0)(1,-1) \quad (0,1)(0,0)(0,-1) \\
(2,2)(2,1)(2,0) \quad (1,2)(1,1)(1,0) \quad (0,2)(0,1)(0,0)
\end{array} \\
\emptyset_{DI}(i,j) \\
\begin{array}{l}
(-1,-1) \\
(-1,0) \\
(-1,1) \\
(0,-1) \\
(0,0) \\
(0,1) \\
(1,-1) \\
(1,0) \\
(1,1)
\end{array} \\
= \\
\begin{array}{l}
(-1,-1) \\
(-1,0) \\
(-1,1) \\
(0,-1) \\
(0,0) \\
(0,1) \\
(1,-1) \\
(1,0) \\
(1,1)
\end{array}
\end{array}$$

Fig. 4-1 Normal equations, in matrix notation for the solution of a  $3 \times 3$  two dimensional Wiener filter. Figures in brackets give the subscripts of the parameters.

A computer routine WIEN2D has been written by the author to calculate two dimensional Wiener filter coefficients for the general case.

It is important to realize that the Wiener filter does not guarantee a perfect output but only the optimum, according to the least error energy criteria, for a fixed number of coefficients.

In general the performance of a Wiener filter improves as the number of coefficients increases. This characteristic has been investigated by Treitel and Robinson (1966) for one dimensional data and confirmed by the author for two dimensional data. A feature of this improvement is that it tends to become insignificant after a certain size of filter has been reached. This optimum size varies with the problem.

The original theory of Wiener was developed for the statistical processing of infinite signals and hence the Wiener Hopf equation involves averages of the correlation functions. For the digital processing of gravity and magnetic data it is necessary to make two important assumptions to compensate for the fact that infinite signals are not being processed and that it may not be possible to determine average correlation functions.

The first approximation is to assume that if coefficients are calculated using fields due to model bodies which have the approximate average dimensions of the bodies causing the field to be transformed then these coefficients can be applied to such data.

The second approximation involves the truncation of the model fields used for calculating the coefficients. Gravity and magnetic fields normally decay slowly away from the centre of the causative body and it is impractical to perform the model transformation on very long signals. Rather than simply to cut off the model fields

at their edges it has been found better to truncate the input signal and the desired output signal by multiplying by a data window (see 3.3). The Hamming window, as discussed below, has been found to give good results.

Extensive tests by the author, including the examples given later in this thesis, indicate that these approximations are justified.

#### 4.2 Applications of One Dimensional Wiener Filters

The theoretical magnetic profiles used on this section and in various other examples throughout this thesis were calculated using a computer program MAG2D which is based on the method of Talwani (1964).

A similar computer program GRAV2D based on the method of Talwani, Worzel and Landisman (1959) has been used to calculate synthetic gravity data.

Both MAG2D and GRAV2D were originally written as part of the author's M.Sc. project (Gunn, 1967).

##### 4.2.1 The Linear Inverse Problem

Digital Wiener filters were originally written to remove reverberations from seismic records (Robinson, 1967). After a seismic explosion, the sharp impulse of energy travels through the earth and may be multiply reflected in such a way that the signal arriving at the geophone is of little value to the seismic interpreter. Seismologists are able to define the filtering properties of a given set of layers with reasonable precision and their problem has been to design a finite length inverse filter to remove these effects. Robinson gives the theory to calculate an exact inverse filter to a known impulse response but the method is mainly of theoretical interest because the resultant inverse filter may have an infinite length. A more practical solution to the problem has been found by calculating the Wiener filter to convert the impulse response of the earth's filtering effect as closely as possible into a unit spike. The

resultant filter, called a deconvolution filter, is the optimum least squares finite length inverse filter.

This method of designing inverse filters has a direct application on the solution of the linear inverse problem in gravity and magnetic interpretation. The theory in 1.5.1 showed that the gravity or magnetic field of a prism is the result of the convolution of several factors and that convolution of the field by the appropriate inverse factors will give as output a square wave whose amplitude is directly proportional to the density or magnetization of the prism and whose edges outline the edges of the prism.

Several applications of Wiener filters to solving the linear inverse problem will now be demonstrated and discussed.

#### 4.2.1.1 Solving for the Magnetization of Vertically Magnetized Vertical Dykes

The Problem: to calculate, using a magnetic profile, the magnetizations of a series of infinite, vertically magnetized, vertical dykes all at depth 4 units and with different widths.

The solution of this problem involves a downward continuation of 4 units (see equation 1-18). As such a large continuation is extremely sensitive to data errors, coefficients were calculated for a continuation distance of 2 units and when they were applied to the profile being filtered a zero was inserted between each coefficient. This effectively made the continuation distance 4 units but still gave an output value for each input value.

The computer program WIEN1D was used to calculate and apply the appropriate filter coefficients.

The input to WIEN1D was specified thus:

input signal - the magnetic field over a vertically magnetized infinite vertical prism, depth 2 units, width 9 units, magnetization 0.001 emu.

$$B_x = B_{-j}, B_{-j+1}, B_{-j+2} \dots B_0 \dots B_{j-2}, B_{j-1}, B_j$$

desired output - scaled magnetization of the model prism

$$D_x = D_{-j}, D_{-j+1}, D_{-j+2}, \dots, D_0, \dots, D_{j-2}, D_{j-1}, D_j \\ = 0, 0, 0, \dots, 1, 1, 1, 1, 1, 1, 1, \dots, 0, 0, 0$$

LD = length of desired output = LB

LA = number of filter coefficients to be calculated = 211

(it is not necessary for LA to equal LB)

The 1's in the desired output indicate that the magnetization of the model prism used to calculate the coefficients is to be regarded as a standard of unity. The 9 values of 1 represent a square wave with the width of the model prism.

The set of Wiener filter coefficients calculated to shape the input signal into the desired output are the optimum coefficients (in the least square sense) to deconvolve all factors except the width factor and the magnetization factor from the input magnetic profile. These coefficients will deconvolve the same factors from any other profile and the results of such an operation are shown in Fig.4-2. The magnetic profile over four vertically magnetized infinite vertical prisms has been converted into a set of square waves where, as expected, the width of the square wave outlines the positions of the prisms and the amplitudes of the square waves are directly proportional to the magnetizations of the prisms.

The small ripples at the corners of the square waves are due to Gibb's phenomenon. They could be reduced but not eliminated by reducing the sample interval to 1 unit. This would require a continuation distance of 4 units and for the reasons given above this is not desirable.

The dimensions of the model body used for calculating the coefficients were chosen to be an approximate average of the dimensions of the bodies causing the profile to be filtered. This ensured that

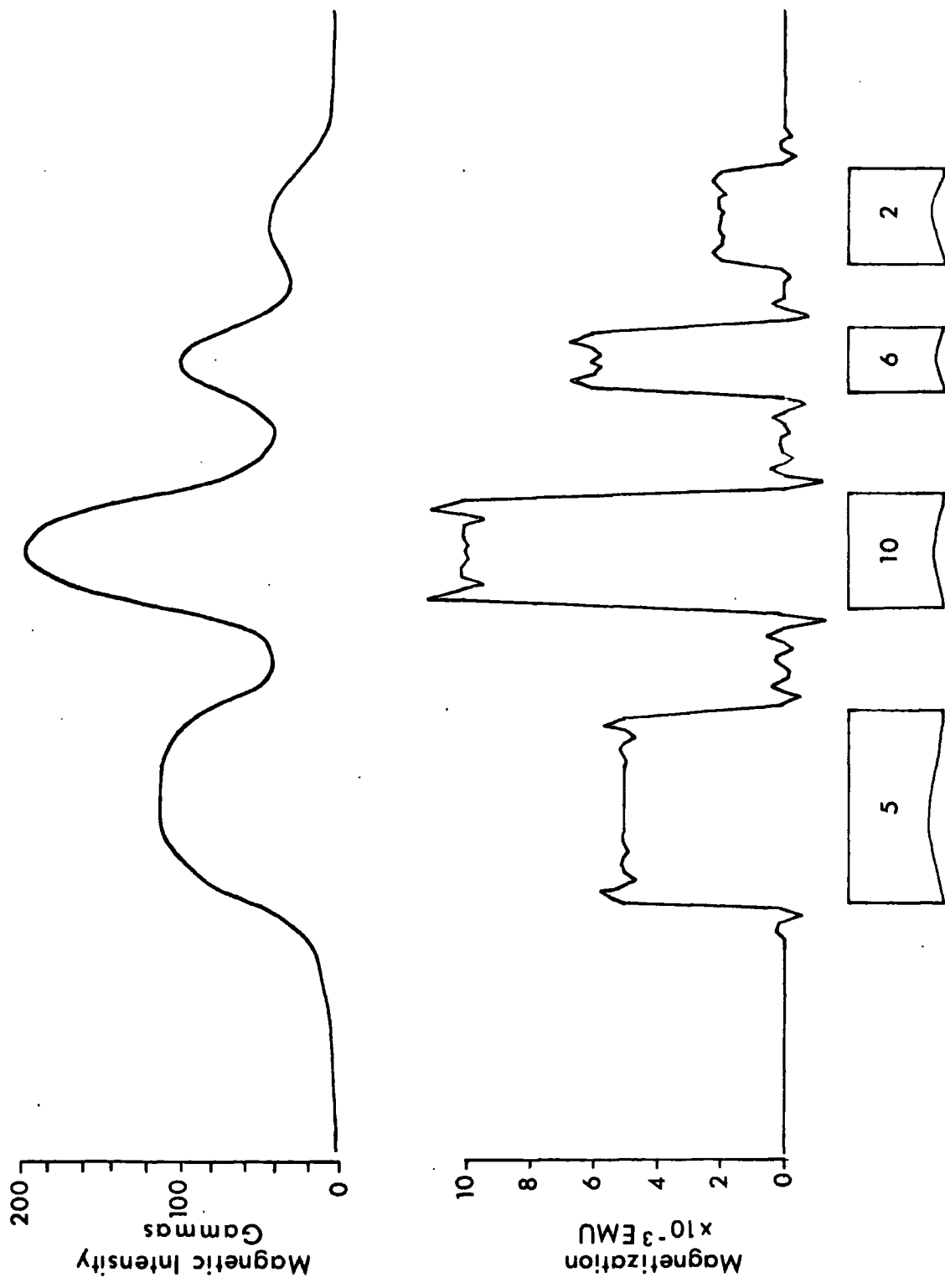


Fig. 4-2 Output of an inverse convolution filter designed to calculate the magnetization distribution of a series of vertically magnetized vertical infinite dykes. The numbers shown in the dykes give the magnetizations of the dykes x 10<sup>-3</sup> emu.

the filter was to some extent designed for the particular problem.

In seismology a finite length wavelet is being deconvolved but in gravity and magnetic applications the areal extent of the anomaly that is the input signal may cause problems. As gravity and magnetic anomalies decay slowly away from the central peak it may be necessary to truncate the anomaly. If the truncation is done at points before the field has decayed to an insignificant level a step is left at the ends of the input signal and the filter designed will be the inverse of the input signal complete with steps. This will give spurious ripples in data processed with this filter. It has been found that truncation of the data using a Hamming window provides the smoothing necessary to preserve the spectral characteristics of the input signal so that the designed filters produce good results.

In the example of Fig. 4-2 a Hamming window was used to truncate the input signal. In this application it was found that an application of a rectangular window gave almost identical results. This was because the field on the flanks of the input signal had decreased to a very small level (0.1% of the maximum). Truncation does however become important where the rate of decay is slower. The effects of truncation are discussed more fully in 4.3.

#### 4.2.1.2 Calculation of the Magnetization of a Vertical Infinite Dyke with Inclined Magnetization

To calculate the magnetization of a non vertically magnetized dyke the method of specifying the input and desired output to `WIEN1D` are the same as for the vertically magnetized case except that the input signal must be the magnetic field of a prism whose direction of magnetization is the same as that of the dykes to be filtered.

Fig. 4-3 shows the results of applying a set of coefficients calculated in this manner.

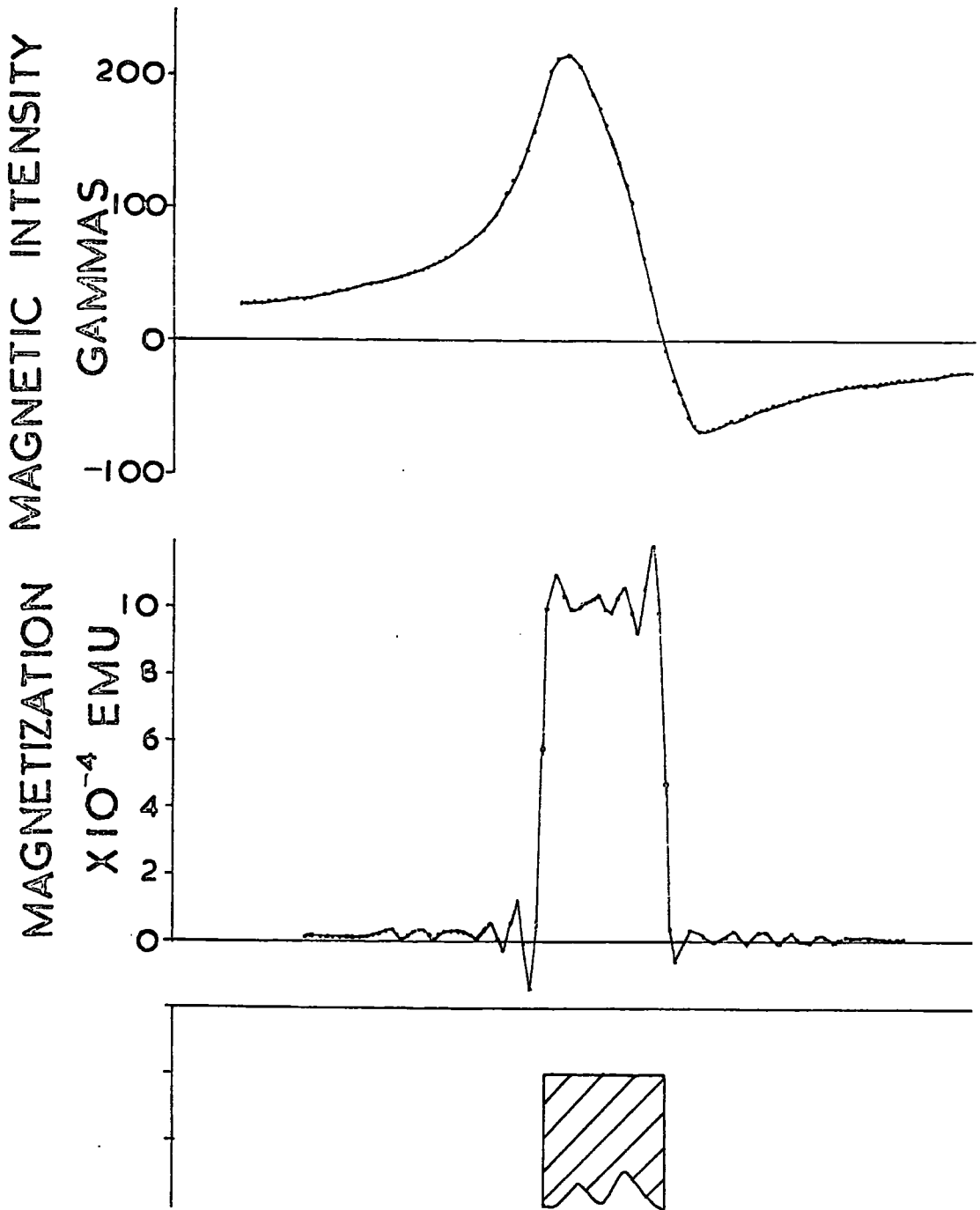


Fig. 4-3 Calculation of the magnetization of a vertical infinite dyke magnetized in a field dipping 65° in the direction of the magnetic profile.

The oscillations due to Gibb's phenomenon are again noticeable and in this example they are antisymmetric with respect to the square waves.

A low amplitude long wavelength regional slope can be noticed in the output. This is the result of the inability of the finite length filter, operating on a finite length of data, to correctly phase shift and integrate all the frequency components of the signal necessary to give an exact output. It has been found in practice that this discrepancy increases as the dip angle of the field diverges from  $90^\circ$ .

Truncation of the input signal is important for non vertical magnetization because the field decays more slowly than for vertical magnetization and it approaches the zero level from different sides of the zero line.

Robinson and Treitel (1966) show that the performance of a one dimensional Wiener filter may be improved by lagging the output relative to the input. This corresponds to a filter in which the point at which the filtered value is being calculated is not at the centre of the operator. It is obvious that the optimum Wiener filter for a transformation involving no phase shift (i.e. transformations whose frequency response have no complex terms), must be symmetric about the central point because only such coefficients have zero phase shift. The calculations in 3.6.4 show that the theoretical coefficients for a transformation involving a complex term of the type  $(a+jb)u$  are antisymmetric about the central coefficient and it would appear that the optimum Wiener filter for such a transformation should have the same type of symmetry.

To test this reasoning the optimum lag position was calculated for the set of coefficients to perform the transformation of Fig.4-3.

Wiggins and Robinson (1965) describe a technique which they call 'Simpson sideways recursion' which allows a rapid determination of the optimum lag position for the output of a Wiener filter. Robinson (1967) has published a subroutine (SIDE) which performs the Simpson recursion method and this has been incorporated by the author into a computer program (SHIFTY).

Fig. 4-4 shows a plot of the normalized error energy for different output lags. The normalized error energy  $E$  is the value of the average squared error divided by the zeroth lag of the desired output's autocorrelation function. For a perfect filter  $E = 0$ , and  $E = 1$  for the worst case.

Fig. 4-4 shows that for the example considered the optimum lag position is almost immaterial because of the large flat minimum of normalized error energies. The fact that the optimum lag position is slightly different from the position corresponding to a centred operator is thought due to the effects of truncating the input signal.

Fig. 4-4 is considered to verify that centred operators are the optimum (or very close to it) for all filter transformations using profiles of gravity and magnetic data.

#### 4.2.1.3 Calculation of the Magnetization of Blocks with a Finite Vertical Thickness

To use WIEN1D to calculate coefficients to solve for the magnetizations of finite blocks of known depth, thickness and direction of magnetization the input signal  $B_x$  must be the magnetic field over such a block. The resultant coefficients will deconvolve the same factors as in the two previous examples but will also deconvolve the thickness factor.

Fig. 4-5 shows the magnetic field due to a series of vertically magnetized blocks and the magnetization profile obtained by applying a Wiener filter. The differences in the levels of the plateaus of

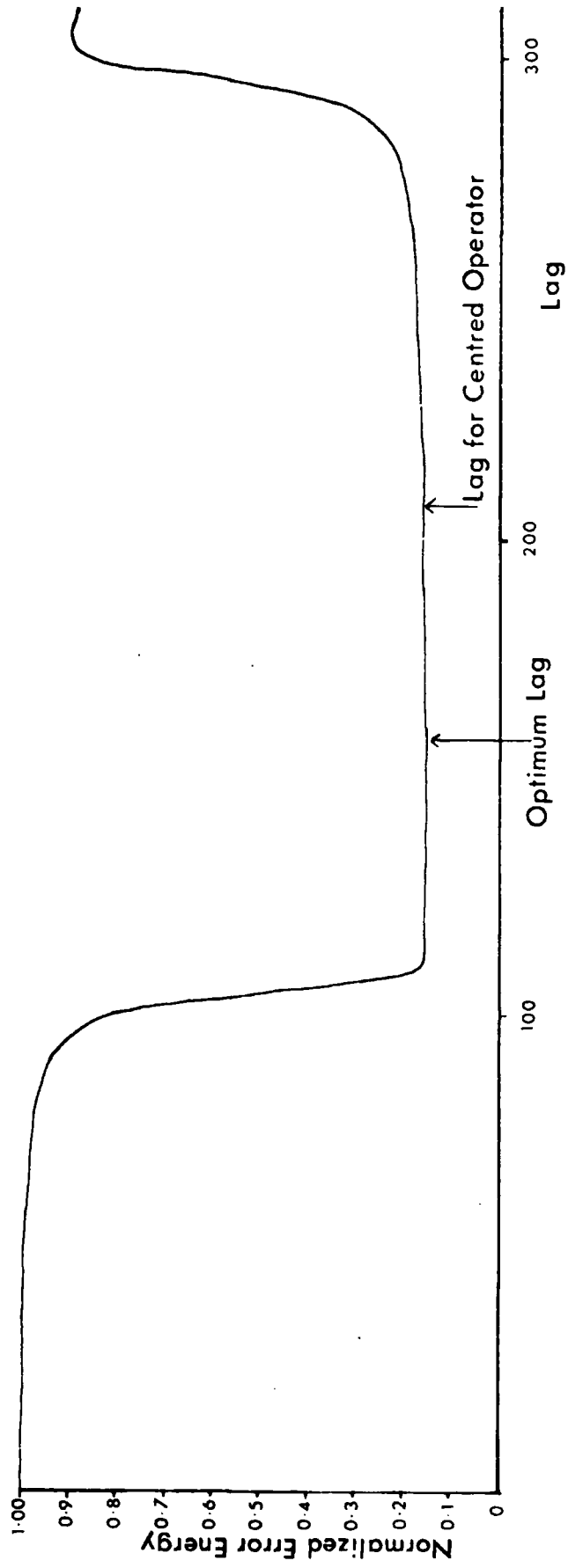


FIG. 4-4 Variation of the error energy of an inverted filter with the lag of the desired output.

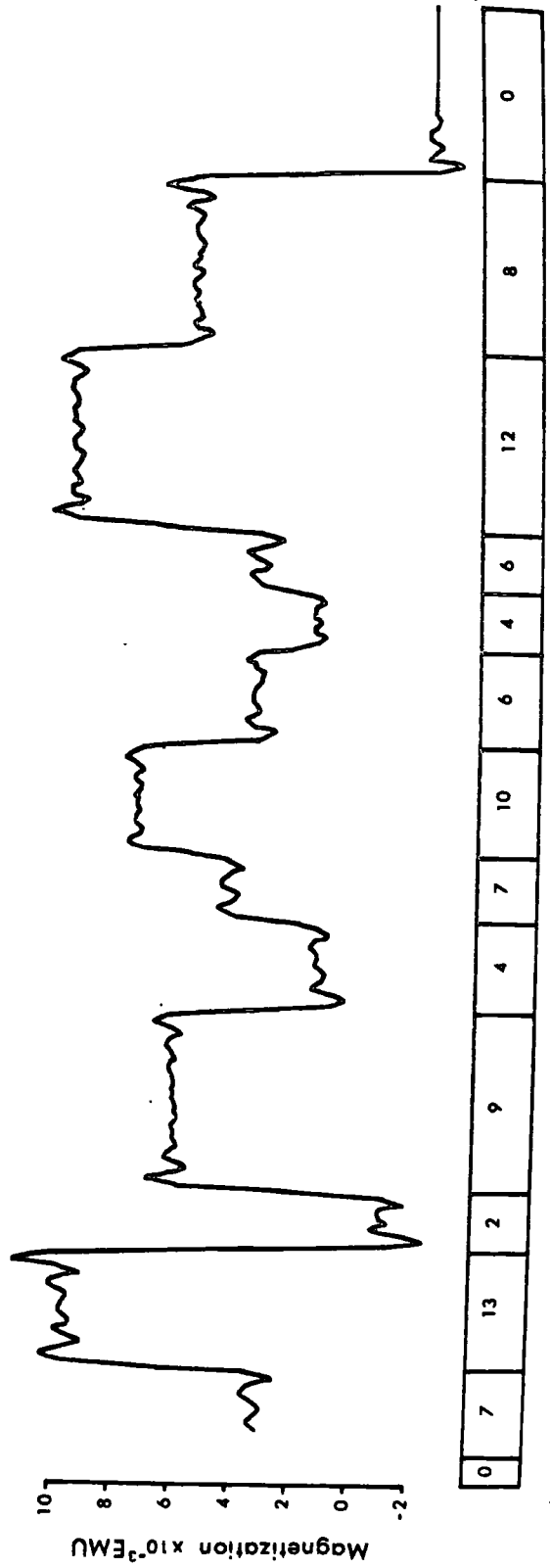
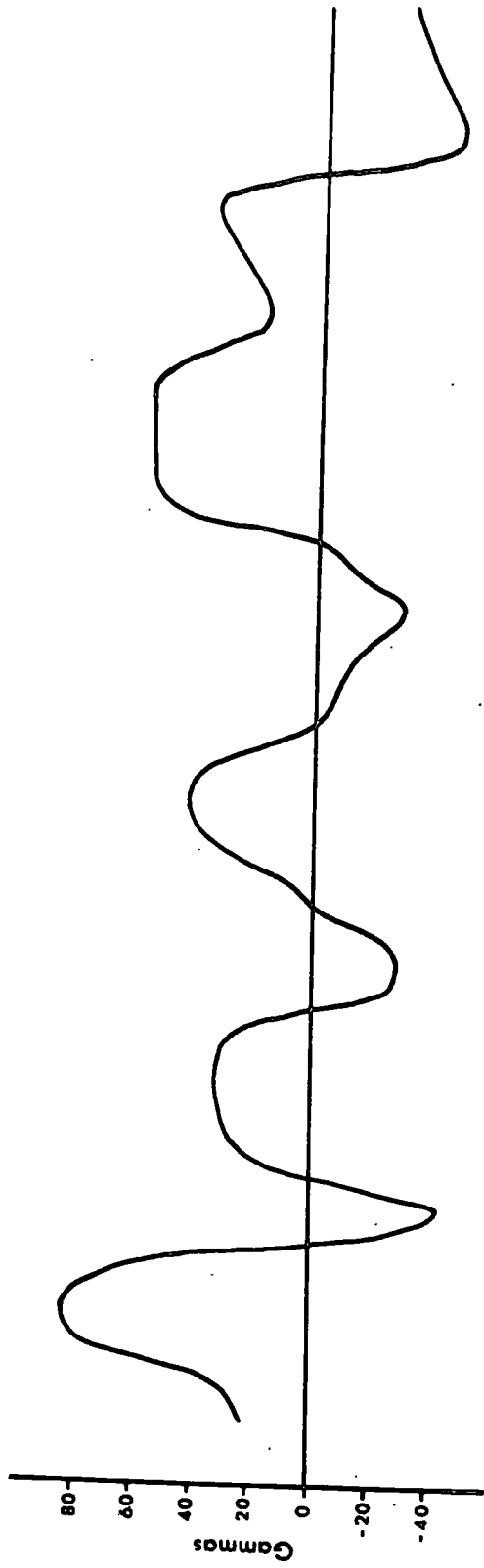


FIG. 4-5 Calculation of the magnetization of a layer of vertically magnetized blocks. The number in the block gives the block position  $\times 10^{-5}$  cm.

the output correspond to changes of magnetization in adjacent blocks. The oscillations in the output are due to Gibb's phenomenon.

The absolute values of the calculated magnetizations are not correct although the relative changes between the levels of the plateaus still accurately reflect the changes of magnetization between adjacent blocks. This discrepancy is caused by the inability of the finite length filter to exactly numerically evaluate the infinite convolution integral and by the method of extrapolation used at the ends of the data. WIEN1D automatically extrapolates the signal to be filtered by taking inverted mirror images about the end points.

$$\begin{aligned} & B(-m-t) = 2 \cdot B(-m) - B(-m-t) \\ \text{i.e.} \quad & B(m+t) = 2 \cdot B(m) - B(m-t) \end{aligned}$$

Although this allows filtered values to be calculated for all points of the original profile the accuracy naturally decreases towards the ends.

The filter applied to the signal in Fig. 4-5 has a spread of 210 points on either side of the point where the operator was applied and thus the filtered output was effected by the extrapolated data. It is considered preferable to suffer a loss in accuracy than to have no output at all.

The filtering operations described in this section could be used to determine magnetizations of rocks in areas where the geometry of the rocks is well known. For example in shield areas, where most rocks outcrop at the surface, magnetization profiles could be produced to outline the rock masses and to allow an approximate identification of rock types.

Bott (1967a) has used the matrix method to study the magnetizations of layers of lava causing sea floor magnetic anomalies. Wiener filters could also be applied to this problem.

#### 4.2.2 Transformations of Gravity and Magnetic Fields

In 1.4 the transformations possible with gravity and magnetic fields were discussed in terms of the convolution operations necessary to perform such transformations. In 2.4 it was shown that filter coefficients for the transformations may be calculated by solving a set of simultaneous equations in which the input and output of the transformation are related by the filter coefficients. In this section the Wiener filter variation of this method is investigated. By using an original field and a transformed field as the known input and the desired output to WIEN1D a set of generally applicable coefficients for the transformation can be calculated. In the previous section the Wiener filter was used to deconvolve certain factors from the profile. In this section it is used to add convolution factors as well as remove them.

The following examples demonstrate how effective this method is.

##### 4.2.2.1 Reduction to the Pole

Fig. 4-6 shows an example where the magnetic field due to a non vertically magnetized body has been converted to what the field would be if the body were vertically magnetized. This is an example of a reduction of the magnetic field to the magnetic pole. The coefficients to effect this transformation were calculated using WIEN1D with the following specifications:

input signal: a profile of the magnetic field over a vertical prism depth to the top of 2 units, width 9 units and an infinite depth to the bottom. The strike of the magnetic profile was  $65^{\circ}$ E of magnetic north and the dip of the Earth's field was  $65^{\circ}$  downwards.

desired output: the magnetic field over the same body as in the input signal but with the inclination of the earth's field at  $90^{\circ}$ . The magnetization of the body was the same as the body in the input signal.

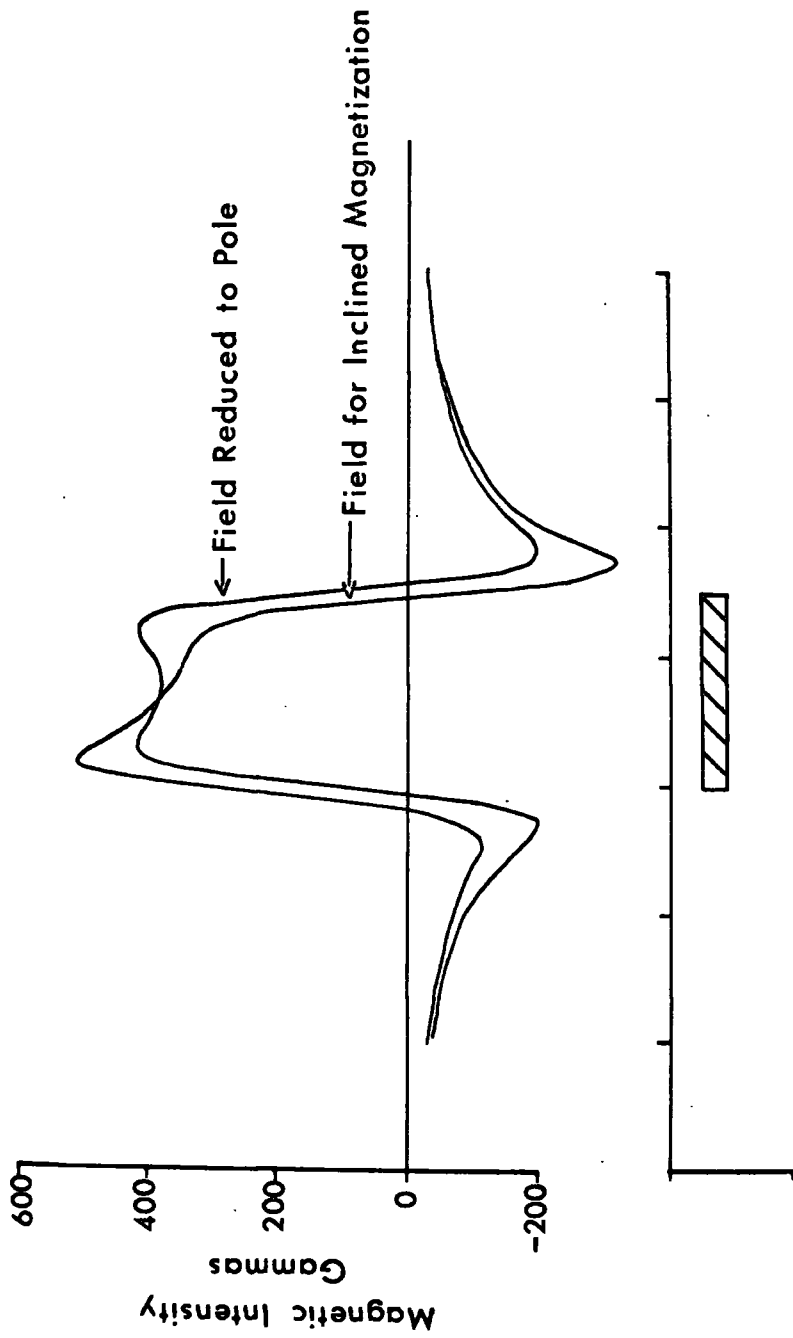


Fig. 4-6 Example of reduction to the pole for profiles. Strike of the profile is  $65^{\circ}$ E. of magnetic north. The dip of the earth's field is  $65^{\circ}$  downwards. Magnetization is by induction only.

The length and sample interval parameters were the same as used in the examples of the magnetization calculations.

Both the known input and the desired output were tapered by a Hamming window.

It should be noted that, because the profile over the body is not towards magnetic north, the dip of magnetization in the body is not  $65^\circ$  but the resolved component of the earth's field in the direction of the profile. This factor is automatically compensated for in the evaluation of the coefficients.

#### 4.2.2.2 Converting Components of Measurement

Fig. 4-7 shows an example where the horizontal magnetic field due to a body has been converted by filtering into the total field due to the body (which in this case is the same as the vertical field since the body is vertically magnetized). Again the coefficients were calculated by using WIEN1D to perform a similar transformation on model data. Any other conversion between components of measurement may be done similarly.

#### 4.2.2.3 Converting Magnetic Fields into Gravity Fields

Fig. 4-8 shows an example where a magnetic field has been converted into a gravity field. The transformation gives the true shape of the anomaly but numerically underestimates the field by a constant amount. This happens because the operation is effectively an integration of the long wavelength components of the magnetic field and the finite set of filter coefficients underestimates their effect.

#### 4.2.2.4 Calculation of Vertical Derivatives

From 1.4 it can be seen that the magnetic field of a vertically magnetized body is equivalent to the first vertical derivative of the gravity anomaly of the same body multiplied by a scaling factor.

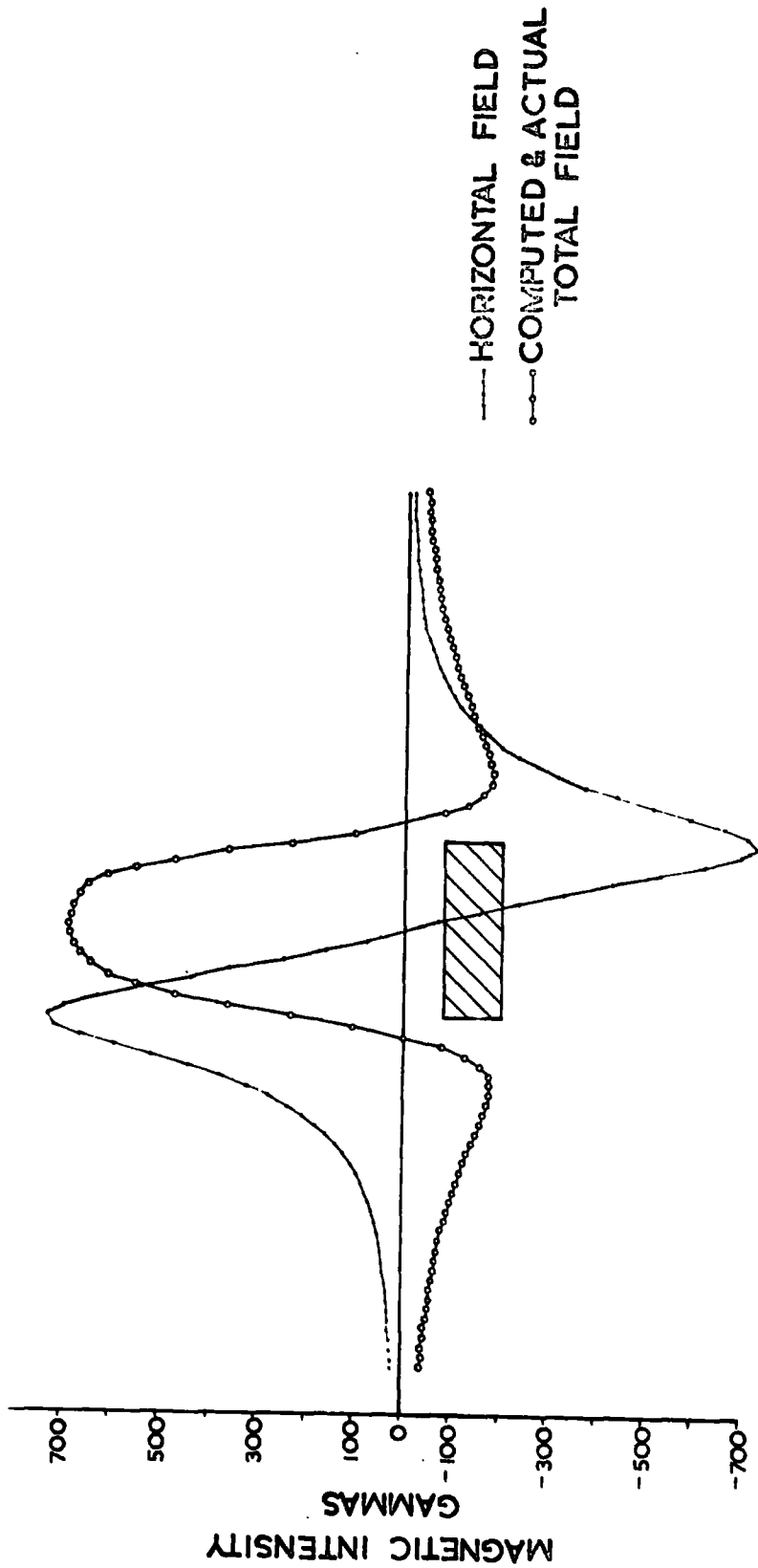


FIG. 4-7 Example where the horizontal magnetic field of a vertically magnetized body has been converted into the total magnetic field due to the same body. The coefficients for this transformation were calculated using an infinite vertical cylinder with the same depth and width as the block type body used in the example.

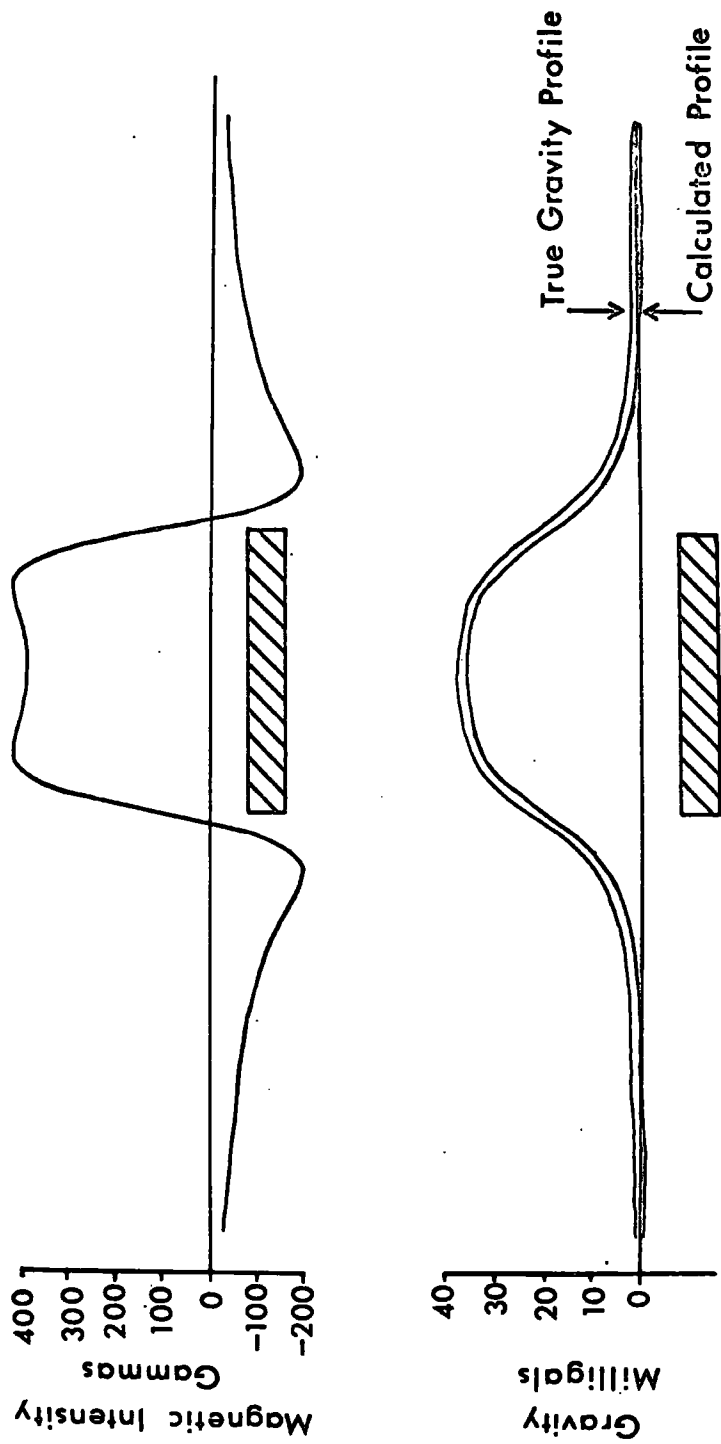


Fig. 4-8 Converting a magnetic profile over a vertically magnetized body into a gravity profile.

The frequency response of the appropriate one dimensional gravity to magnetic transformation is

$$\frac{M_u}{G\rho}$$

The coefficients for such a transformation can be used to calculate the vertical gradient of profile data.

There are several ways of extending this principle to calculate the second vertical derivative. Convolving the vertical gradient coefficients with themselves gives a set of second derivative coefficients. The vertical gradient coefficients can be used to calculate the vertical gradient of the magnetic anomaly and a set of Wiener filter coefficients to convert the gravity anomaly into the vertical gradient of the magnetic anomaly will be a set of second derivative coefficients. Simply applying a set of vertical gradient coefficients twice to the same data gives the second vertical derivative of the data.

The outputs of vertical derivative operations performed by the methods described must be corrected for the scaling factor and converted to the correct units by dividing by the data grid interval.

Fig. 4-9 shows an example of how vertical gradient and second derivative filters may be used to resolve two interfering anomalies by suppressing the long wavelengths. The second derivative in this example was calculated by applying the vertical gradient coefficients twice.

A computer program SPECTM has been used to calculate the amplitude spectrum of the vertical gradient coefficients used in the example of Fig. 4-9. The resultant spectrum, shown in Fig. 4-10 consists of a straight line with gradient  $M/G\rho$ . Thus in this example the Wiener method produces a filter whose frequency response closely approximates the theoretical response.

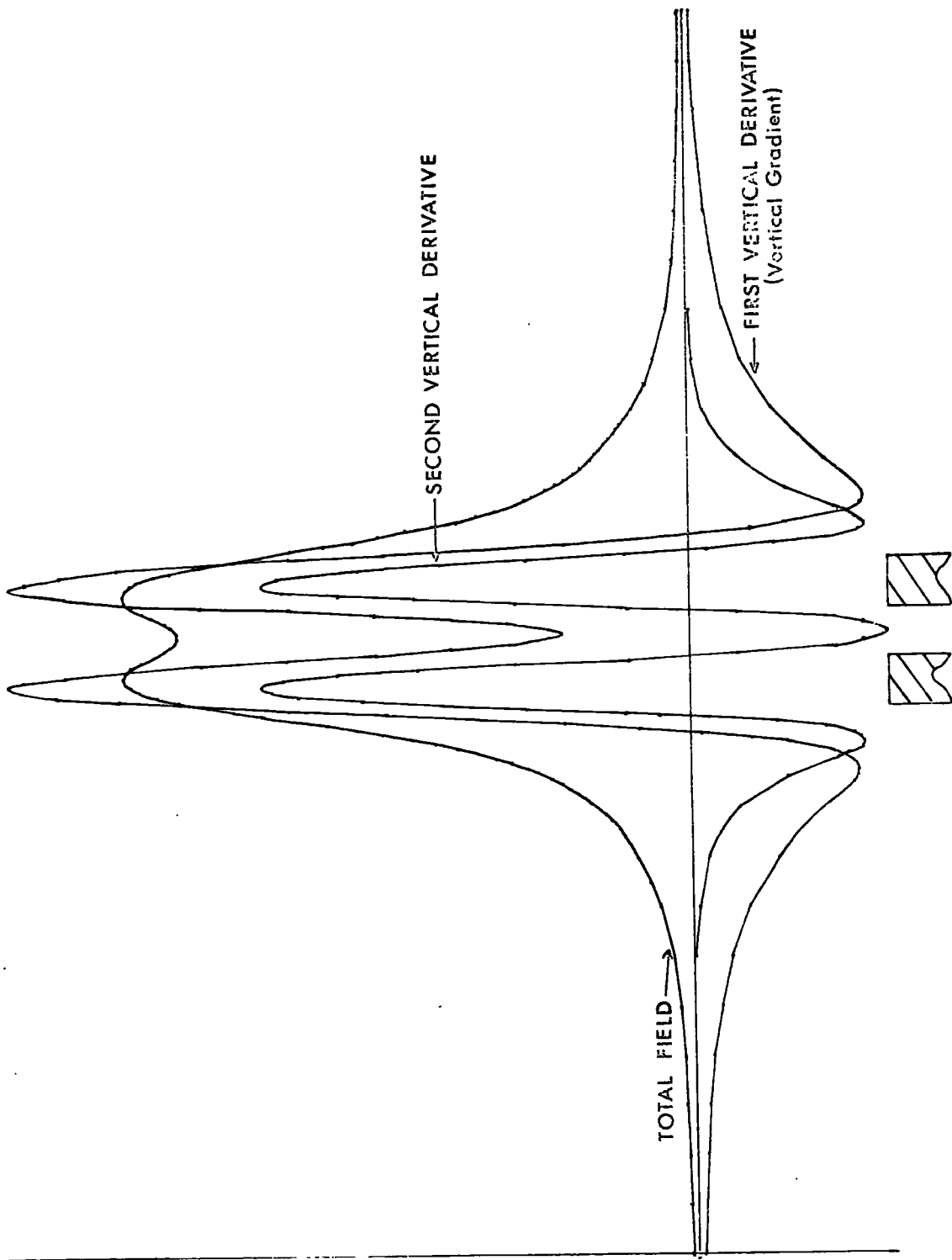


FIG. 4-9 Example demonstrating the ability of vertical gradient and second vertical gradient filters to resolve the magnetic fields of two closely spaced bodies. The units of distance in the diagram are arbitrary and the amplitudes of the profiles have been scaled to allow direct visual comparisons to be made.

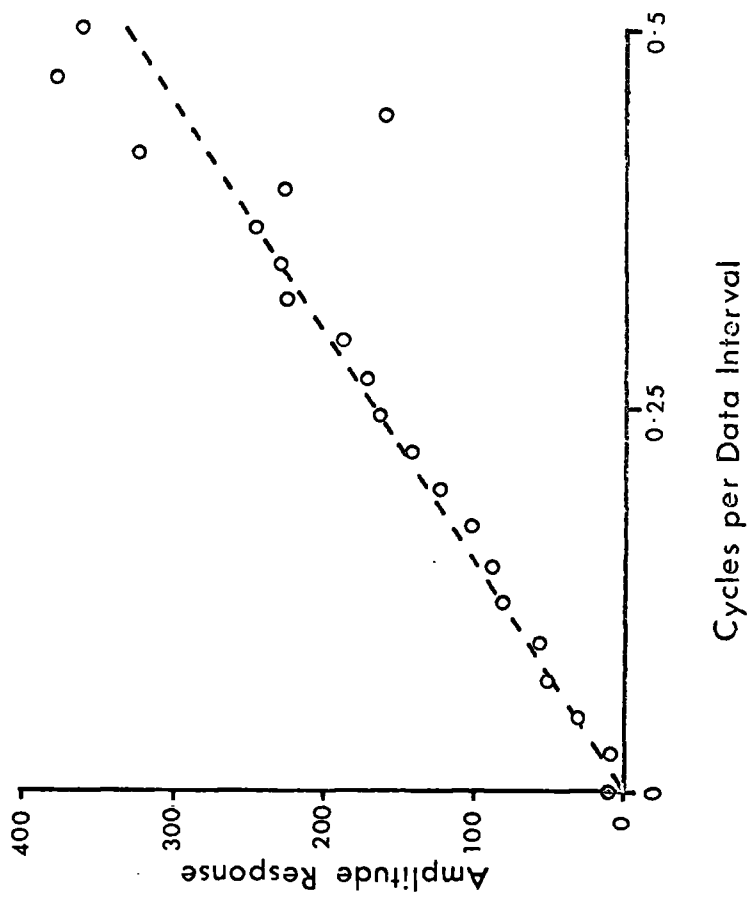


Fig. 4-10 Amplitude response of a calculated vertical gradient filter. The gradient of the straight line in this example is  $\frac{M u}{G}$  where  $\rho$  is the density and  $M$  is the magnetization of the model bodies used to calculate the coefficients.  $G$  is the universal gravitational constant and  $u$  is frequency in cycles/data interval.

This method could be used to calculate the  $m/\rho$  ratio for real anomalies although it should be remembered that for one dimensional data  $m$  will be the component in the plane of the profile.

The same general comments apply to two dimensional data but the radial frequency  $(u^2 + v^2)^{\frac{1}{2}}$  must be considered instead of  $u$ .

#### 4.3 Two Dimensional Wiener Filters

The gravity and magnetic fields of prismatic bodies which have been used in this section were calculated using the computer programs GRAVPR and MAGPR. The basic subroutines for these programs were written by Mr. A. Goodacre of the Geology Department, University of Durham (see Goodacre, 1972).

The calculation of two dimensional Wiener filters involves an extra problem because a rectangular grid of coefficients is being designed to convert a rectangular grid of input points into a rectangular grid of output points. As the theoretical impulse responses of most coefficient sets involved in gravity and magnetic transformations have some form of radial symmetry this rectangular effect causes a distortion of the output. The discussion below illustrates this effect and shows how it may be reduced by applying a two-dimensional truncation window with radial symmetry.

The computer program WIEN2D was used to calculate a 13x13 filter to deconvolve the gravity field of a prism with top at 0.4 km and bottom at 10 km to obtain the density distribution. The gravity field over a 5x5 prism with depth to the top of 0.4km and depth to the bottom of 10 km was used as the model field for the calculations. This filter was applied to the gravity field over a 7x5 prism which had its top and bottom at the same depths as the original model body.

Fig. 4-11b shows the output where an unaltered square grid of field values has been used as the input in the filter calculations.

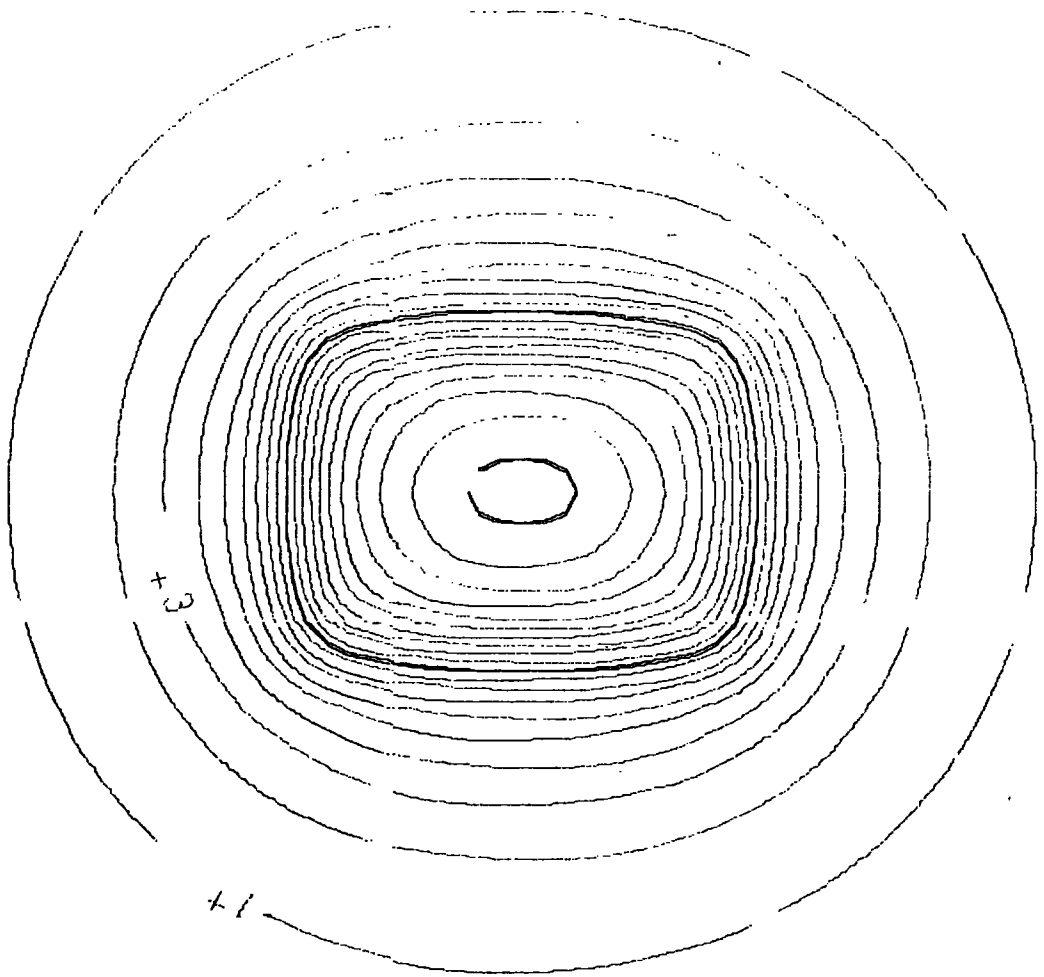


Fig. 4-11a Gravity field over a 5x7 km. prism, depth to top 0.4 km., depth to bottom 10.0 km., with density contrast 0.1 gm./cc.

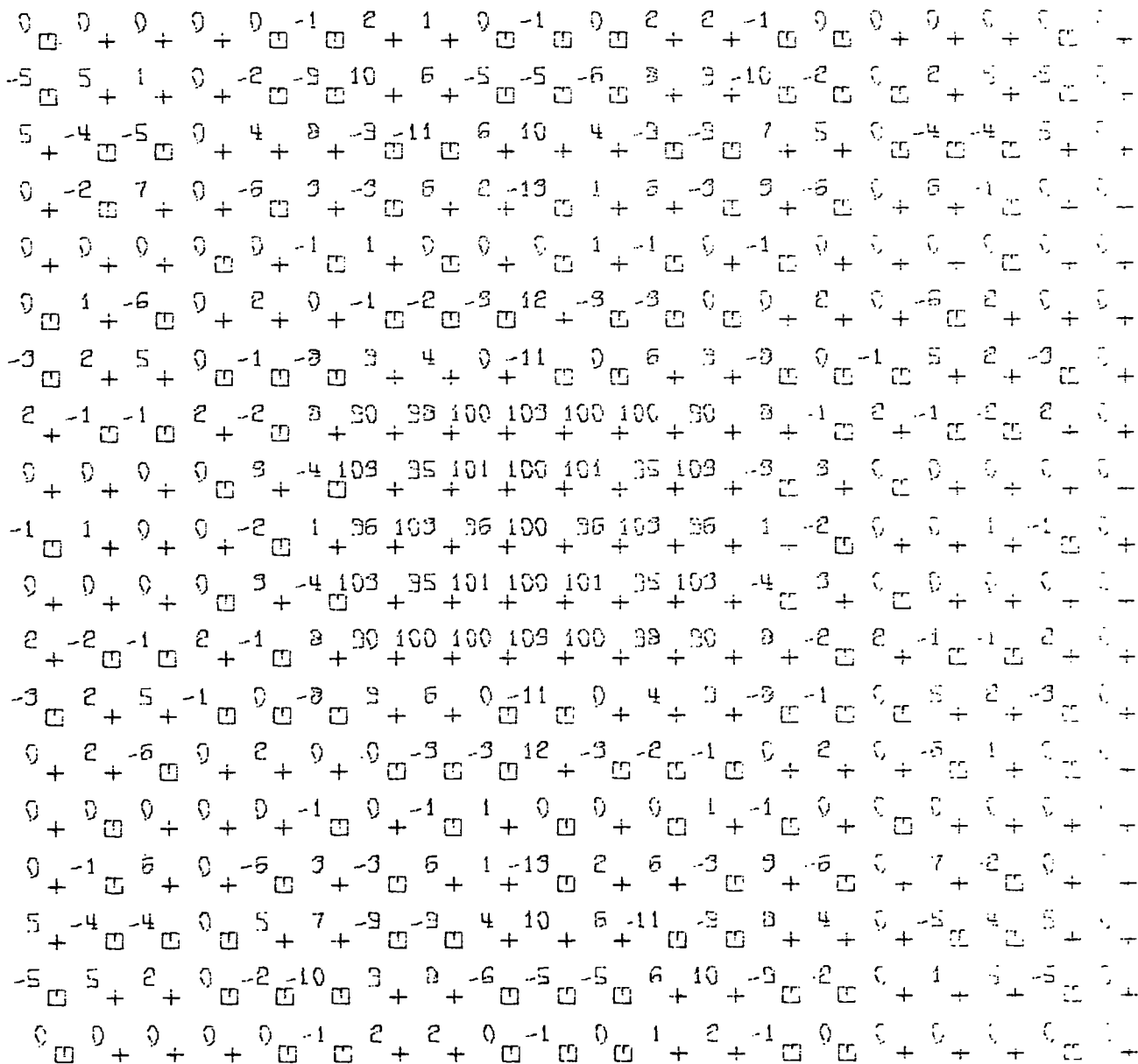


Fig. 4-11b Result of applying a deconvolution filter to the field shown in Fig. 4-11a. Output shows the density distribution between 0.4 and 10.0 km. in gm./cc. $\times 10^{-3}$ . No tapering was used during the calculation of the filter coefficients.

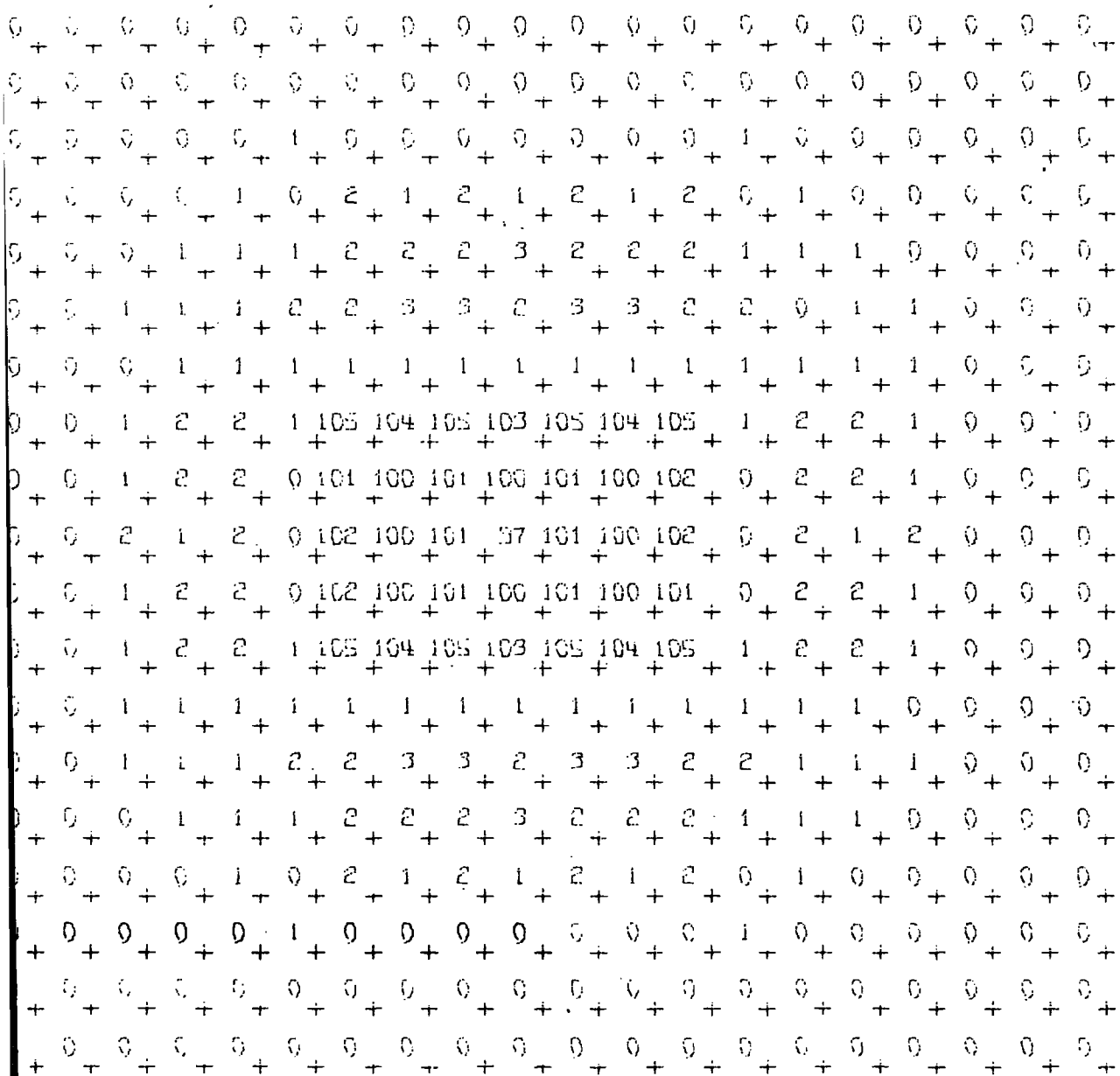


Fig. 4-11c Result of applying a deconvolution filter to the field shown in Fig. 4-11a. Output shows the density distribution between 0.4 and 10.0 km. in  $gn/cc \cdot x 10^{-3}$ . Hamming window tapering was used during the calculation of the filter coefficients.

Fig. 4-11c shows the output where a two dimensional Hamming window has been applied to the input. Although both outputs give a good representation of the density distribution, the output in the un-tapered case is markedly more oscillatory and asymmetric than in the tapered case. This is due to both the effect of a step at the edge of the data and the effect of the input signal being square. The output from the tapered case does not suffer from these effects but a low amplitude long wavelength seems to be superimposed over the entire output. This is apparently a result of the fact that the Hamming window smooths the spectrum of the function it is applied to. This low amplitude effect is noticeable in the examples of one dimensional filtering in which the Hamming window was used.

Fuller (1967) has studied the properties of two dimensional sets of filter coefficients by computing their Fourier transforms and comparing them with the ideal frequency responses of the operations. A computer program SPECT2, based on the theory published by Fuller, has been written to compute the Fourier transform of two dimensional digital data and has been used to calculate the amplitude spectra of the two Wiener filters discussed above. The results are shown in Fig. 4-12.

These spectra are basically similar but differ slightly in the region of the higher frequencies. They also tend to lose their radial symmetry in the region of the higher frequencies.

Although both spectra have similar numerical values to the theoretical frequency response of the transformation they become markedly different in the region of the higher frequencies. These deviations are not serious because, as the example presented show, the filters give good results.

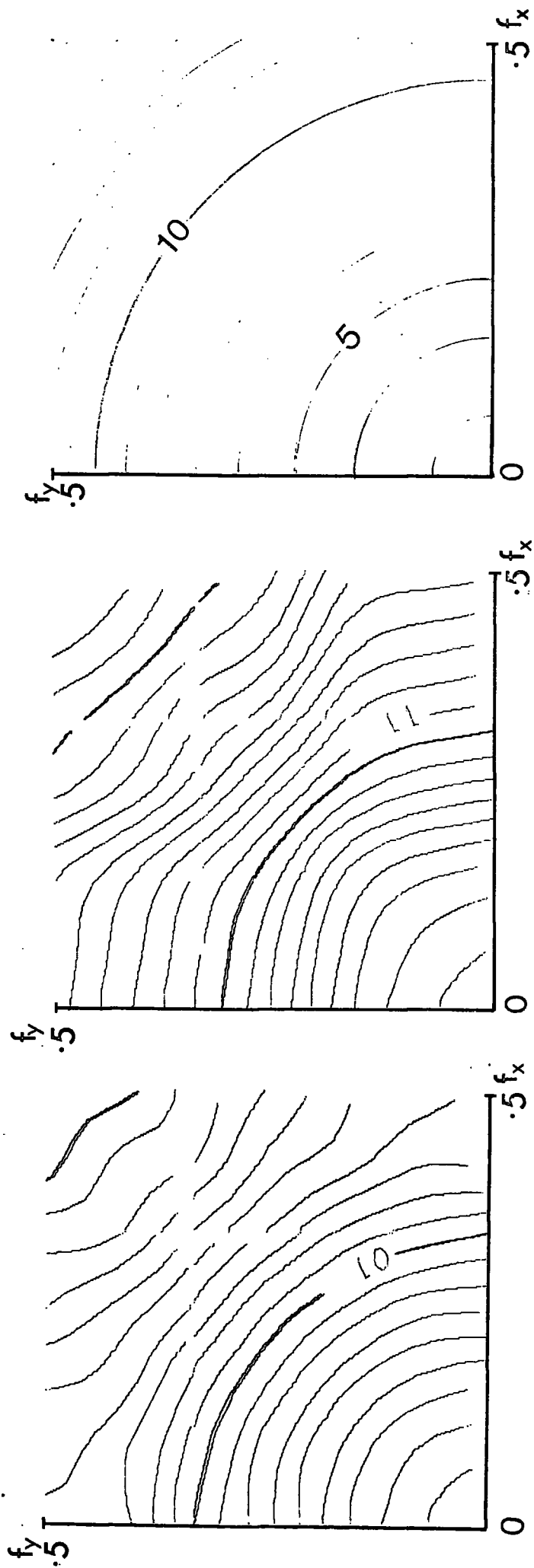


Fig. 4-12 Computed and theoretical spectra of coefficients to effect the transformation to give the density distribution of prismatic type bodies, top 0.4 km, and depth to bottom 10.0 km. The filter is designed to give an output of 1.00 for a density of 0.1 g/cc uniformly distributed between these depths.

- A. No tapering used in filter design.
  - B. Bearing window tapering used in filter design.
  - C. Non-uniformly distributed density.
- Contours give  $\rho = 10^{-2}$ .

Fuller (1967) has derived amplitude spectra for coefficient sets derived by Peters (1949), Henderson and Zeitz (1949), Elkins (1950), Rosenbach (1953) and Henderson (1960) all these exhibit the same defects, often in a more severe form. Even the filter coefficients derived by Fuller (1967) using the Fourier transform method deviate from the ideal frequency response and show an asymmetry for the higher frequencies. These effects seem characteristic of two dimensional grid coefficient sets.

Fig. 4-13 shows an example where the magnetization of a prism, magnetized in a non vertical direction with a declination and inclination different from the earth's field, has been calculated by Wiener filtering. Fig. 4-14 shows an example of a reduction to the pole transformation.

In both these examples the low amplitude long wavelength discrepancy, noticed in the study of profile transformations, is present. Examples of reduction to the pole transformations given by Baranov (1957) who used a filter method, Bhattacharyya (1965) who has used a Fourier analysis method and Spector (1968) who has used the Fourier transform method all show this effect.

#### 4.4 Conclusions

The examples shown in this chapter have shown that Wiener filtering is a straightforward and accurate method for effecting transformations of gravity and magnetic fields. In several instances the output of the filter deviated from the true output by small amounts. This is not to be unexpected when attempting to perform an infinite integral type transformation with finite sets of filter coefficients and would probably happen in a worse form when using other methods which are not designed for the situation as the Wiener filters are.

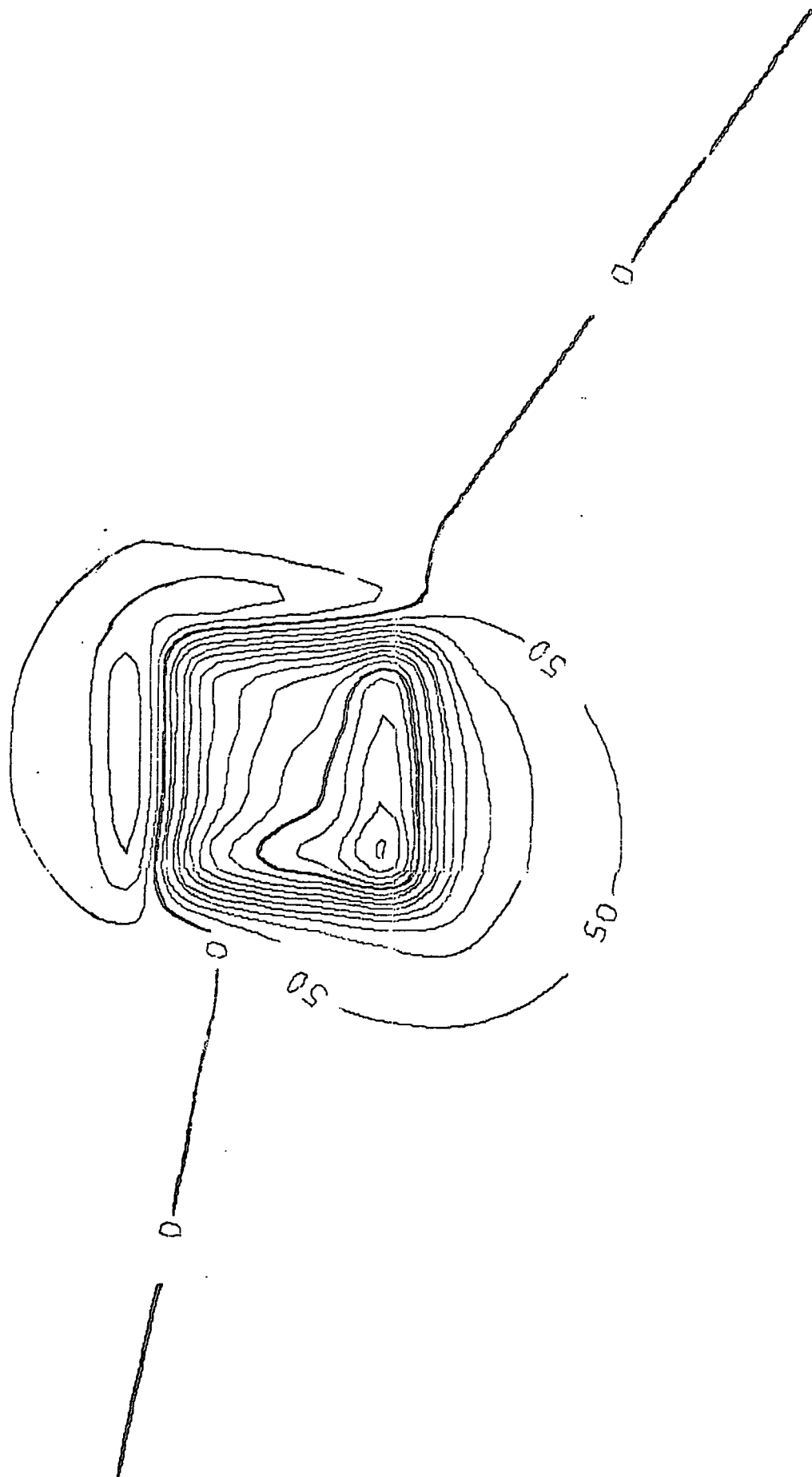


Fig. 4-13a Magnetic field over a 5x5 meter, magnetization 0.001 emu. in direction 70° towards 40° east of magnetic north in a field directed 65° towards 40° east of magnetic north. Top of plot is 0.5 units below level of 50. field strength. Bottom is at 9.5 units below level of 50. The lines are at the top of the diagram and at the sides of the plot. The top and bottom are not marked.



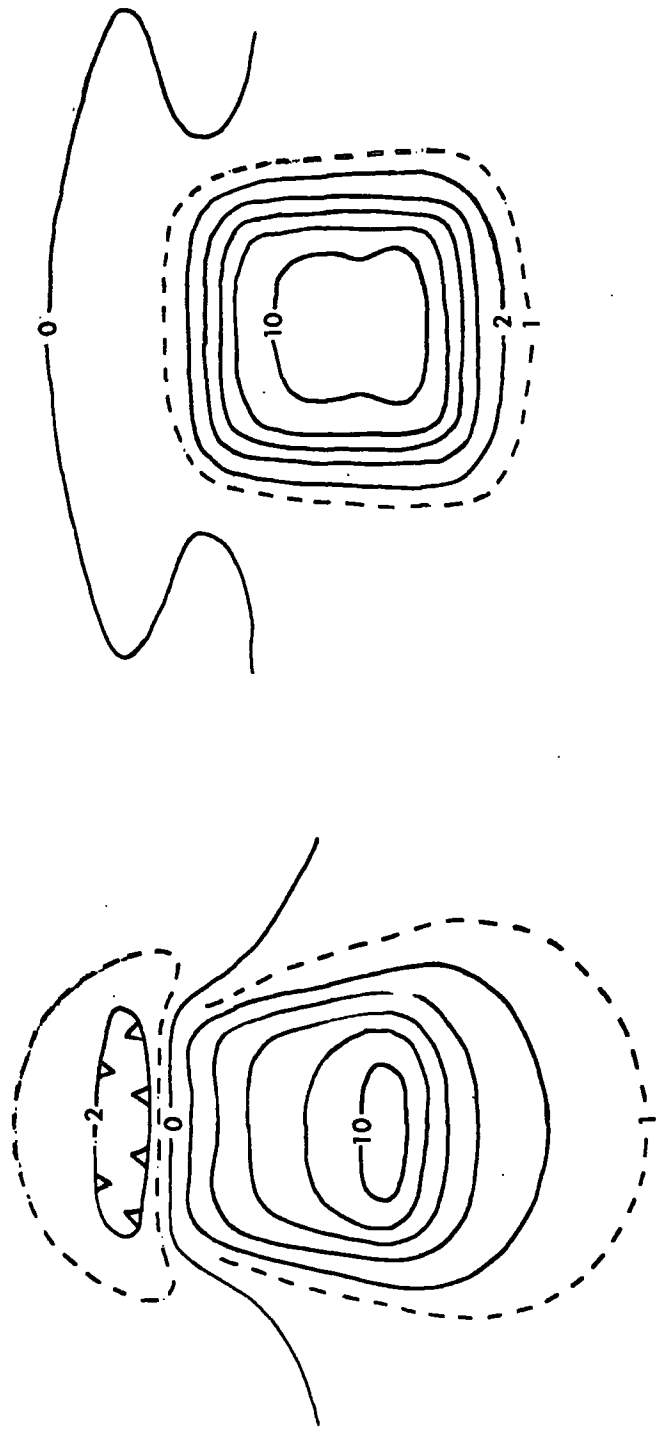


Fig. 4-14 Example of reduction to the pole for map data. Figure on left is the magnetic field over a  $5 \times 5$  infinite prism which has a depth to its top of 0.5 units. Magnetization is by induction in a field dipping  $65^\circ$  downwards. The figure on the right shows the field reduced to the pole.

The greatest errors occur when the integration of long wavelength effects are concerned i.e. when compensating for dip in the direction of magnetization or converting magnetic anomalies to gravity anomalies. In none of these examples has the distortion been serious and the long wavelength effects become part of the regional background.

## CHAPTER 5

### APPLICATION OF FILTERS TO INTERPRETATION OF GRAVITY AND MAGNETIC DATA

#### 5.1 Direct Interpretation of Gravity and Magnetic Data

The theory showing that the undulations of a contact surface or layer or the vertical thickness of a layer may be approximately mapped by convolution methods was derived in 1.5.2. The studies described in this section demonstrate that accurate results may be obtained by the application of Wiener filters to these problems.

Serbulenko (1965) has realized the possibility of using Wiener filters to map an interface using a gravity profile. He assigns a mathematical expression to represent theoretical probability model of the relief of the boundary and obtains a series expression for the impulse response of the required filter. The success of Serbulenko's method depends on assigning correct values to the statistical parameters. It is not known if the method works because no examples are given.

##### 5.1.1 Test of Linearity

Because the mapping problem is approximately linear, Wiener filter coefficients for the transformation may be calculated using the same approach as in Chapter 4, i.e. using a model transformation in which a given input is related to a known desired output.

To test the linearity of the response, a Wiener filter was applied to the problem of calculating the depths to the bottoms of magnetic prisms where the depths to the tops were known.

To calculate the filter coefficients the known input  $B_x$  to WIEN1D was specified as the magnetic field over a vertically magnetized prism with a depth to the top of 2 units, a vertical thickness of 4 units and a width of 9 units. The desired output  $D_x$  was specified as a

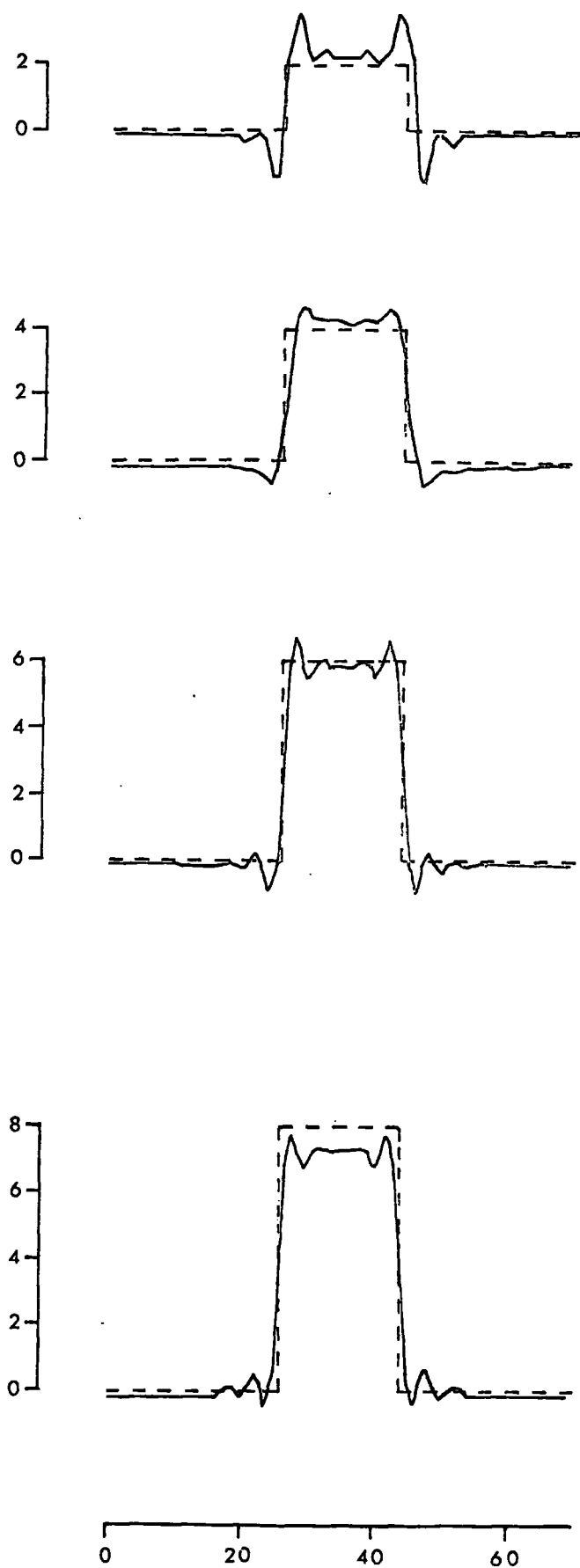
series of 9 values of 4 flanked by zeros. The desired output represents the vertical thickness of the prism and the calculated coefficients thus transform the field into a representation of this thickness.

Fig. 5-1 shows the results of applying these coefficients to a set of vertically magnetized prisms which have the same depth to the top as the model prism. It can be seen that the calculated thickness is almost exactly correct for the prism with a vertical thickness of 4 units. This prism has the same thickness as the model prism and this agreement is to be expected. For prisms thinner than 4 units the calculated thicknesses over estimate the true thickness but never by more than 10%. Gibb's phenomenon becomes very noticeable for very small thicknesses because the higher frequencies become more important and digitization prevents them being adequately defined. For the prism of thickness 6 units the thickness is underestimated by 10% of the true thickness.

Qualitatively it appears that the errors increase more rapidly when the true thickness exceeds that of the model used for calculating the coefficients. It should be noted that these errors are a relatively small percentage when expressed in terms of the depth from the plane of observation to the bottom of the prism.

Thus it may be concluded that Wiener filtering can give good estimates of the vertical thicknesses of the bodies causing anomalies when the coefficients are designed with a knowledge of the approximate dimensions of the bodies. An analysis of percentage errors, such as has been done with the examples of Fig. 5.1 would allow correction factors to be calculated to refine the output.

The following section demonstrates the accuracy of Wiener filters for mapping in more general applications.



--- True Depth  
 —— Computed Depth

Units of Distance are Arbitrary

Fig. 5-1 Test of the linearity of the output of a Wiener filter. The diagram shows the exact and computed distance between the top and bottom of a set of vertically magnetized prisms which all have their top surface 2 units below the level of observations but have different depths to their bottom surface.

### 5.1.2 Examples of Mapping

Figs. 5-2 and 5-3 show examples where Wiener filters have been used to map interfaces causing gravity and magnetic anomalies. To correctly scale the calculated profiles it has been necessary to know the density and magnetization contrasts and the depth at one point on the interface. In practice this information would have to be obtained from a drill hole or by a detailed interpretation of part of the profile by another method. One such method is demonstrated in 7.2.

The results of these mappings give very good agreement with the true shape of the body. The small oscillations near the ends of the body are probably due to Gibb's phenomenon.

Fig. 5-4 shows an example where the Wiener filter method has given a good estimate of the vertical thickness of a body of constant vertical thickness but varying depth, by transforming the magnetic profile over such a body.

Two dimensional interfaces may also be mapped. Fig. 5-5 illustrates an example where the gravity anomaly over a hemispherical shaped body has been used to map the bottom surface of the hemisphere. The gravity field over the hemisphere was calculated using a computer program THIRDM, written by Folkman (1969) and based on the method of Talwani and Ewing (1960).

During the preparation of the examples presented above it was found that the accuracy of the output varied slightly with the model used to calculate the coefficients. As to be expected, it was found that for the best results the model used should have the same approximate vertical thickness and position of top and bottom as the body to be mapped. This allows better averages of the correlation functions to be obtained for calculating the filter coefficients.

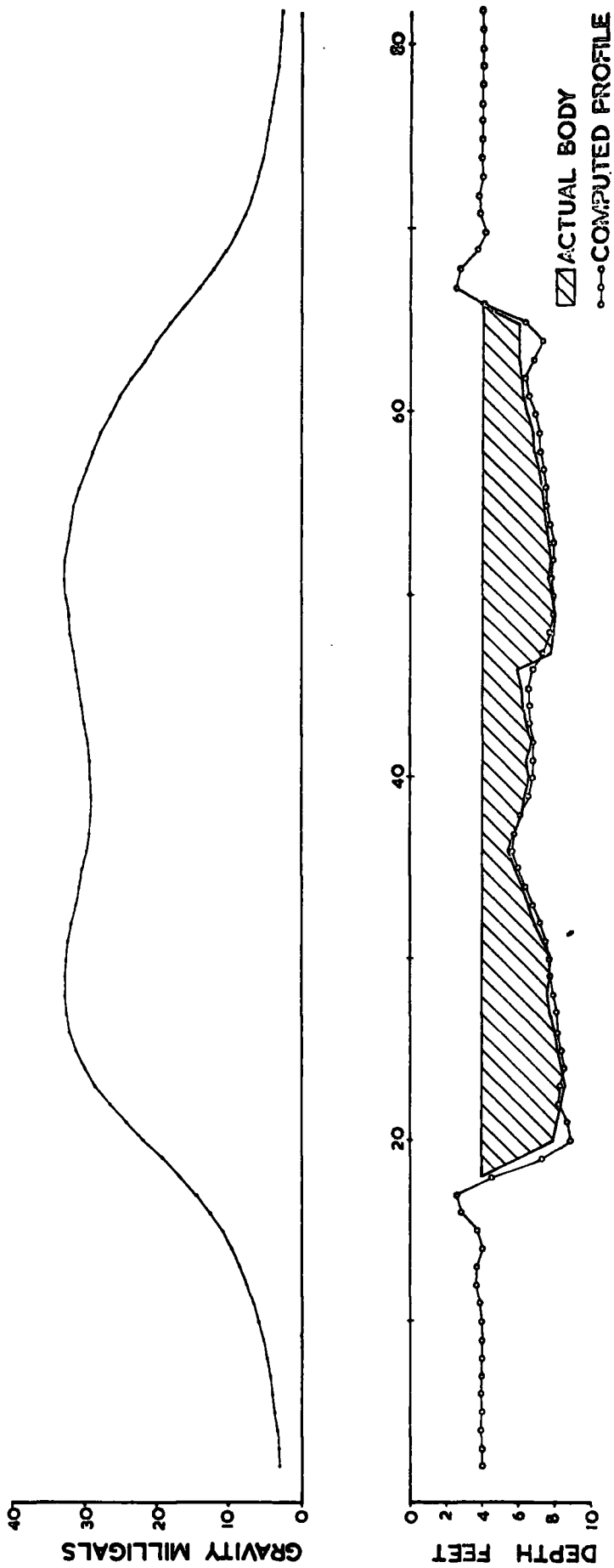


Fig. 5-2 An example of applying a Wiener filter to map an interface causing a gravity anomaly. The model body used to calculate the filter coefficients had a depth of 4 units, a width of 9 units and a vertical thickness of 4 units.

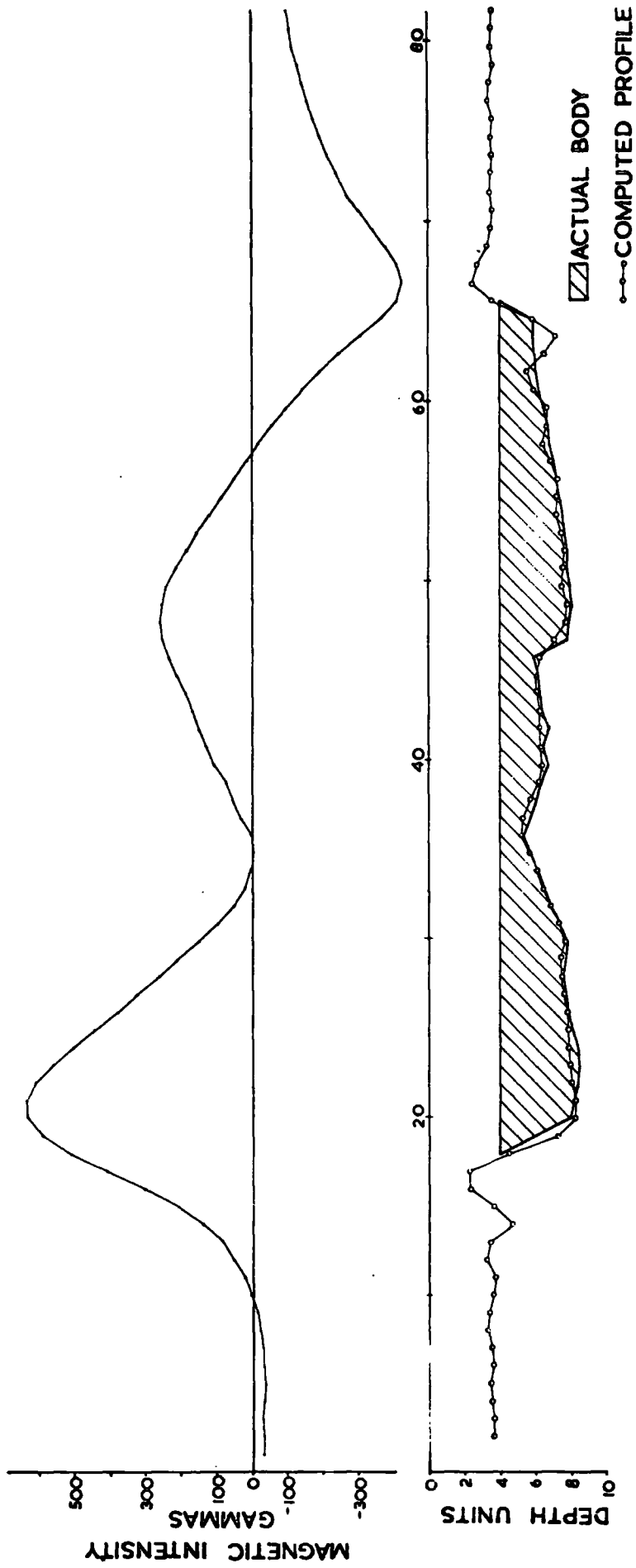


Fig. 5-3 An example of applying a Wiener filter to map an interface causing a magnetic anomaly. The model body used to calculate the filter coefficients had a depth of 4 units, a width of 9 units and a vertical thickness of 4 units. The magnetization of both the model body and the body shown in the diagram was by induction in a field dipping  $65^\circ$  in the direction of the profile.

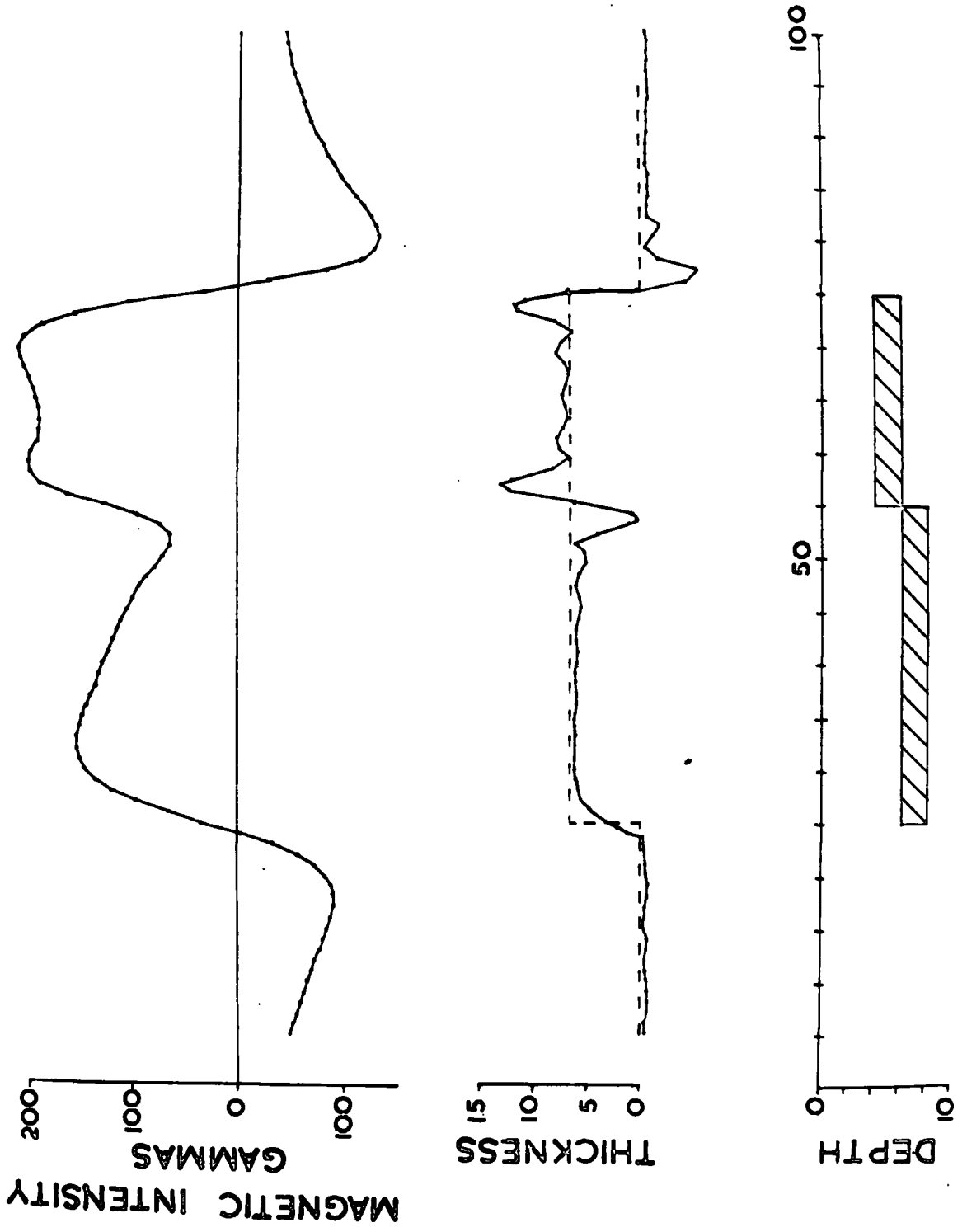


FIG. 5-4 Wiener filter mapping of the vertical thickness of a body using a magnetic profile.

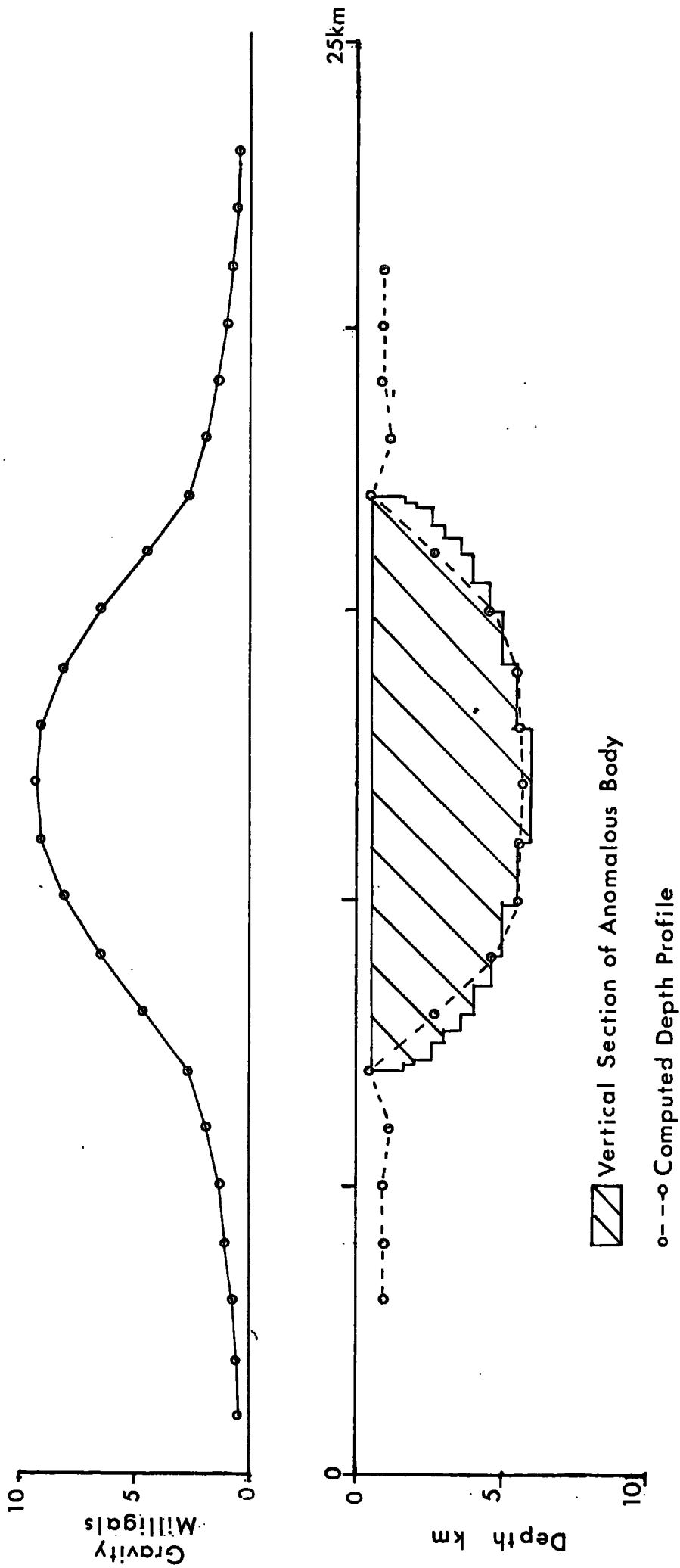


Fig. 5-5 Application of a two dimensional Wiener filter to mapping the bottom surface of a hemisphere. Although only a profile across the centre of the hemisphere is shown in the diagram the filter was applied to two dimensional data. Density contrast of hemisphere is 0.1 gm./cc.

### 5.1.3 Conclusions

The accuracy of the output of the Wiener filter direct interpretation method as demonstrated above is sufficient for most interpretation purposes. The results could be improved by an iterative technique. The results of the first output could be used to compute a profile to be compared with the original profile and the residual errors could be reprocessed with the filter coefficients to calculate corrections to the previous results. This process could be repeated until a suitable level of agreement is reached between the observed and calculated profile.

Such iterative techniques, but based on different principles, have been developed by Bott (1960), Tanner (1967) and Laving (1971).

## 5.2 Automatic Interpretation of Anomalies over Dykes using Matched Filters

For a given digital waveform, the digital filter, (subject to the constraint that the energy of its coefficients is unity), which gives the maximum output amplitude possible, has an impulse response which is the reverse of the waveform being filtered. Such filters, discussed by Treitel and Robinson (1969), are called matched (or cross-correlation) filters and the maximum output amplitude property allows an automatic method for interpreting the anomalies due to dyke like bodies.

A computer program MATCH has been written to crosscorrelate the anomaly profile due to an infinite vertically magnetized vertical dyke with the anomaly profiles due to other infinite vertically magnetized vertical dykes with different depth width ratios. Fig.5-6 shows a plot of the maximum outputs obtained for each correlation. As expected the maximum maximum output (or maximum correlation) occurred with the dyke with the same depth and width as the dyke

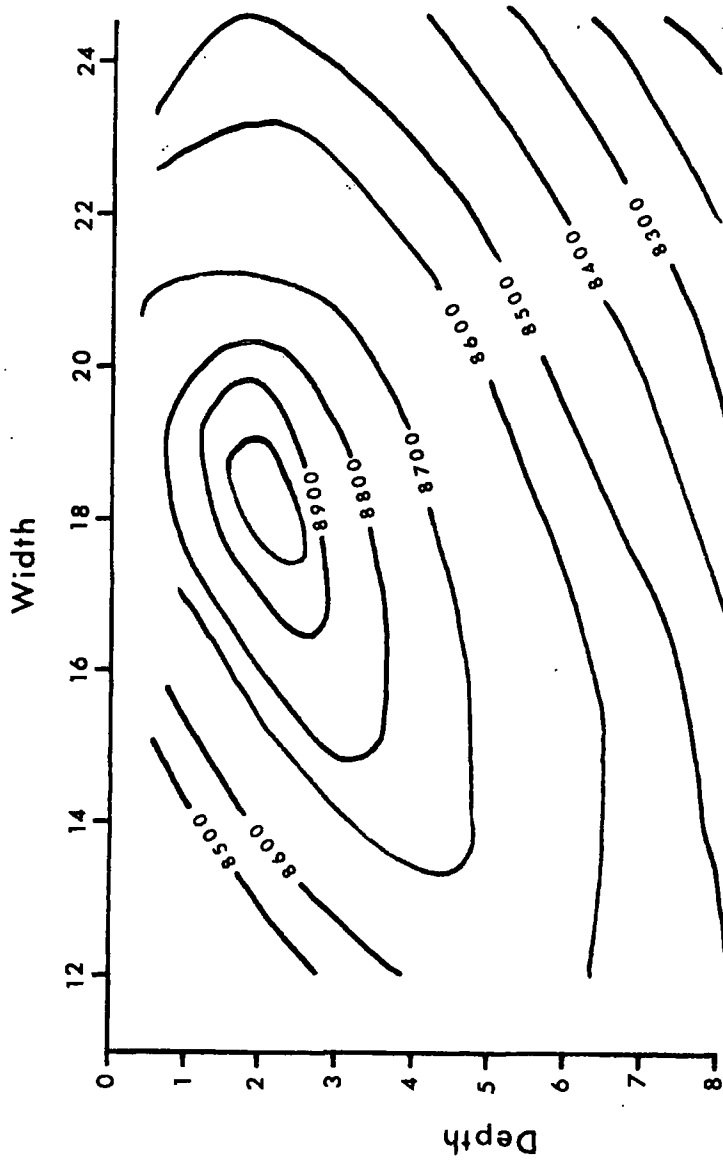


Fig. 5-6 Plot of the matched filter outputs obtained by convolving the magnetic field of a vertically magnetized vertical infinite dyke, depth 2 units and width 18 units with the magnetic profiles of other vertically magnetized vertical infinite dykes with varying depths and widths.

being interpreted. The point of maximum match also gives the centre of the dyke.

To interpret infinite dykes with a dip or non vertical magnetization the process would have to be performed using autocorrelation functions instead of anomaly profiles because as shown in 6.3.2.1 the autocorrelation function of an infinite dyke depends only on its depth and width. Also for the method to be applied to real data linear regional trends would have to be removed from the profiles. This could be achieved by calculating derivatives and performing the interpretation using the derivatives.

Although the method works (at least in the noise free case) the development was not pursued further because of its excessive computer time requirements. The example shown required 14 minutes CPU time on an IBM 360/67 computer. This time could be reduced by using less frequently sampled curves for the crosscorrelations but it is felt that alternative automatic interpretive methods (e.g. Butler, 1970) provide more practical ways for interpreting the anomalies due to dykes.

### 5.3 Depth Determinations using Euler's Relationship

Slack et al. (1967) describe a method which they claim can identify the type of body causing an anomaly and calculate its depth by using combined measurements of total field and vertical gradient.

The basis of their method is as follows:

Many structures produce magnetic anomalies which can be mathematically expressed in the form

$$F = K/r^n \quad (5-1)$$

where  $F$  = magnitude of the magnetic anomaly

$K$  = a constant which depends on geometry, magnetization and the direction of the earth's field.

$r$  = distance from detecting element to centre of body

$n$  = an exponent depending on geometry

For such fields it can be proved

$$x \frac{\partial F}{\partial x} + y \frac{\partial F}{\partial y} + z \frac{\partial F}{\partial z} = -n F \quad (5-2)$$

$x$  and  $y$  are distances measured horizontally along the  $x$  and  $y$  axes from the centre of the anomalous structure.  $z$  is the vertical distance from the centre of the structure to the point at which the anomaly is measured. Equation 5.2 is known as Euler's relationship.

If the field and the vertical gradient are measured, and the horizontal derivatives are calculated at different points, sets of linear equations are obtained which allow the calculation of  $z$  and  $n$ .

Slack et al. state that  $n = 2$  for a horizontal cylinder,  $n = 3$  for a sphere and that  $n$  is independent of  $z$  and diagnostic for the depth-width ratio of prismatic bodies. They combine this anomaly identification with the depths determined using  $z$  to produce geological interpretations of aeromagnetic data.

The theoretical basis of this interpretation has been seriously questioned by La Fehr (in Steenland, 1968) who has shown that  $n$  is in fact depth dependent for many shapes and  $z$  is the depth to the centres of the causative bodies and not the tops as Slack et al. have taken for their interpretations.

The principles of the method however do have applications provided that its limitations are realized. From the formulae published by Heiland (1963) and Jacobs (1963) it can be seen that:

For magnetic anomalies:

- $n = 1$  for lines of magnetic poles
- $n = 2$  for isolated magnetic poles
- $n = 3$  for dipoles and spheres

It should be noted that  $n$  is not equal to 2 for horizontal magnetic cylinders as stated by Slack et al. This can be confirmed using the formula for the field over a horizontal cylinder published by Parker Gay (1963).

For gravity anomalies

$$n = 1 \text{ for point source}$$

$$n = 2 \text{ for infinite horizontal line source}$$

In cases where these configurations of poles approximate geological shapes Euler's relationship can be useful.

If the vertical gradient and field are known at two levels over the maximum of an anomaly (the point where its horizontal derivatives are zero) then

$$Z = \frac{\Delta Z \frac{\partial F_1}{\partial Z}}{\left[ \frac{\partial F_2}{\partial Z} - \frac{F_2}{F_1} \frac{\partial F_1}{\partial Z} \right]} \quad (5-3)$$

and

$$n = \frac{Z}{F_1} \cdot \frac{\partial F_1}{\partial Z} \quad (5-4)$$

where

$Z$  = depth to centre of body

$n$  = decay exponent

$F_1$  = field at first level

$\frac{\partial F_1}{\partial Z}$  = vertical gradient of field at first level

$F_2$  = field at second level

$\frac{\partial F_2}{\partial Z}$  = vertical gradient of field at second level

$\Delta Z$  = vertical distance between two levels of the field being used

If a field is known on one level then the other field and vertical gradient values necessary to solve equations 5.3 and 5.4 may be calculated by filtering methods (see Chapter 4).

An application of this method will now be demonstrated.

For two dimensional dyke like bodies with an elongation in the direction of magnetization and a depth width ratio greater than 1 a line of poles approximation may be used. As a test example a magnetic profile striking  $342^\circ$  was calculated across an infinite vertical dyke depth 30 units, width 10 units in a field with declination  $350^\circ$  and dip  $70^\circ$  downwards. As the strike of a profile diverges from the plane of the azimuth the apparent dip of the field in the plane of the profile approaches  $90^\circ$  and in fact becomes  $90^\circ$  when the profiles are perpendicular to the plane of the azimuth. Thus in the example being considered the dip of the field in the plane of the profile is close to  $90^\circ$  and only the magnetic poles induced on the top of the body should have any effect. The line of poles model should be valid in this situation.

To numerically interpret the anomaly the field 4 units higher was calculated by modelling and the vertical gradients of the fields at the upper and lower levels were calculated by filtering.

The values obtained were

$$\begin{array}{ll}
 F_1 = 24.3 \text{ gammas} & F_2 = 20.6 \text{ gammas} \\
 \frac{\partial F_1}{\partial z} = 0.752 \text{ gammas/unit} & \frac{\partial F_2}{\partial z} = 0.590 \text{ gammas/unit} \\
 \Delta z = 4 \text{ units} &
 \end{array}$$

$$\begin{array}{lll}
 Z = \frac{4 \times 0.590}{0.590 - \frac{20.6}{23.4} \times 0.752} & = \frac{2.36}{0.590 - 0.662} & = 32.8 \text{ units}
 \end{array}$$

$$\eta = \frac{32.8 \times 0.752}{23.4} = 1.05$$

The  $\eta$  parameter estimated (1.05) gives almost exact agreement with the theoretical value for a line of poles. The depth of 32.8 units is reasonable because the magnetic pole approximating the top

of the body would be expected to be below the top of the body causing the anomaly.

From the figures in the calculation however it can be seen that small inaccuracies in the estimated vertical gradients would cause large errors in the estimated depth. It must be concluded that for real data incorporating regional effects and noise it may be impractical to apply the method.

## CHAPTER 6

### OPTIMUM DIGITAL FILTERS

#### 6.1 Introduction

Gravity and magnetic interpretation is often hindered by the presence of anomalies caused by bodies other than those of interest. It is not possible to completely eliminate these noise anomalies by linear filtering without distorting the signal anomalies because there is always spectral overlap between the signal and noise. If the autocorrelation of the noise can be estimated it is possible to design, according to a least squares criteria, an optimum Wiener filter such that the signal suffers minimum distortion while the noise is reduced by as much as possible.

#### 6.2 Theory of Optimum Wiener Filters in the Presence of Autocorrelated Noise

The following theory, for the design of two dimensional Wiener filters in the presence of autocorrelated noise, has been adapted from the treatment given by Treitel and Robinson (1966) for one dimensional seismic applications.

We assume that the two dimensional digital signal  $b_{(x,y)}$  is embedded in stationary noise  $U_{(x,y)}$  which has a known autocorrelation function  $\phi_{UU}$ . The digital signal to be processed  $S_{(x,y)}$  is the sum of the signal and noise (which are assumed to be uncorrelated).

i.e. 
$$S_{(x,y)} = b_{(x,y)} + U_{(x,y)}$$

We wish to design a digital filter according to two criteria:

(i) Shape the digital signal  $b_{(x,y)}$  (with dimensions  $2j+1, 2k+1$  where  $-j \leq x \leq j$  and  $-k \leq y \leq k$ ) into the desired digital output  $d_{(x,y)}$  with (dimensions  $2j+2m+1, 2k+2n+1$  where  $-(j+m) \leq x \leq (j+m)$  and  $-(k+n) \leq y \leq (k+n)$ ) such that the Error Energy is a minimum.

(ii) Produce as little output power as possible when the stationary noise is the only input. The power of a signal is the sum of the squares of its amplitudes.

The quantity to be minimized is:

$I$  = (sum of squared errors between the desired output and the filtered signal wavelet)

+  $\gamma$  (Power of filtered noise)

$\gamma$  is a weighting parameter whose magnitude depends on the problem.

Written mathematically

$$I = \sum_{x=-m-j}^{m+j} \sum_{y=-n-k}^{n+k} (d(x,y) - C(x,y))^2 + \gamma E\{h(x,y)^2\} \quad (6-1)$$

where  $E\{ \}$  denotes the ensemble average

and

$$h(x,y) = \sum_{s=-m}^m \sum_{t=-n}^n f(s,t) \cdot U(x-s, y-t)$$

$C(x,y)$  and  $f(s,t)$  have the same meaning as in 4.1.

Using the same approach as in 4.1, i.e. taking the partial derivatives of  $I$  with respect to the filter coefficients and equating to zero, the following set of simultaneous equations is obtained.

$$\phi_{Dz}(i,j) = \sum_{s=-m}^m \sum_{t=-n}^n f(s,t) \cdot [\phi_{II}(i-s, j-k) + \phi_{UU}(i-s, j-k)] \quad (6-2)$$

The matrix of the right hand side of this equation has the same symmetry properties as the matrix of equation (4-7) and may be solved by the same methods.

The computer programs WIEN1D and WIEN2D have been generalized to be capable of calculating Wiener filter coefficients in the presence of autocorrelated noise.

Clarke (1969) has published the theory for the calculation of optimum Wiener filters to be applied in the frequency domain. The transfer function of an optimum Wiener filter is:

$$H_{opt}(u, \nu) = \frac{P_{DI}(u, \nu)}{P_{II}(u, \nu) + \nu P_{NN}(u, \nu)}$$

where

$P_{II}$  is the power spectrum of the autocorrelation of the input

$P_{DI}$  is the power spectrum of the crosscorrelation of the input and desired output

$P_{NN}$  is the power spectrum of the autocorrelation of the noise

As remarked in 4.1 the frequency method can be difficult to apply.

This chapter demonstrates the generality and relative simplicity of the space domain approach and also emphasizes the importance of the weighting parameter  $\nu$ , a factor which Clarke (1969) has ignored.

### 6.3 Estimation of Average Noise Autocorrelation Functions

For the theory derived in the previous section to be correct in the statistical sense the correlation functions used for solving equation (6-2) should be averages.

In Chapters 4 and 5 it was demonstrated that the average correlation functions involving the input and the desired output can be approximated using the fields over bodies which have the approximate average dimensions of the bodies causing the field to be transformed.

Noise anomalies in magnetic data are most often caused by intrusions and lava flows which can be approximated by prism type bodies and layers of poles and dipoles. In such situations it is possible to obtain realistic estimates of the noise autocorrelation. Although the following discussion is mainly concerned with magnetic examples, the theory is equally valid, in fact simpler, for gravity applications.

### 6.3.1 Autocorrelation Function of Fields due to Three Dimensional Bodies

#### 6.3.1.1 Prisms

Spector and Grant (1970) have studied the power spectra of ensembles of prism type bodies (with a known direction of magnetization) and they use the assumption that the expected power density function is equal to the ensemble average of the power spectrum. (The power spectrum is the square of the Fourier amplitude spectrum). By reducing the magnetic field to the pole and by assuming that the parameters in the expression for the spectrum have rectangular frequency distributions they obtain an analytic expression for the power spectrum in terms of the mean values of the parameters causing the field. Although the assumption of rectangular frequency distributions for the variables appears an oversimplification, tests by Spector and Grant (1970) on the power spectra of real data confirm the validity of their approximations.

Because the autocorrelation function  $\phi_{II}$  is related to the power spectrum  $|A(u)|^2$  by the Wiener Khintchine theorem (Hsu, 1970, p.98)

i.e. 
$$\phi_{II} = \frac{1}{2\pi} \int_{-\infty}^{\infty} |A(u)|^2 e^{ju} du$$

the average autocorrelation of the noise can be determined from a power spectrum calculated using estimated averages. Spector and Grant (1970) demonstrate that logarithmic power spectra may be used to estimate average signal and noise parameters for survey data.

#### 6.3.1.2 Poles and Dipoles

The average autocorrelation function of the field is not equal to the autocorrelation function of the field caused by a body whose parameters are the average of those of the bodies causing the field

except in the limiting case where all the bodies are identical (this property can be seen in the formula published by Spector and Grant (1970)). This condition, however, is closely approximated when the dimensions of the bodies causing the noise are such that they can be approximated by poles and dipoles i.e. when the depth is large and the block size is small.

Clarke (1969) has derived the autocorrelation function for a random distribution of point masses on a plane. It is the same as the autocorrelation function of a single point source multiplied by a scaling factor. Similarly it can be shown that the autocorrelation functions of random distributions of poles and dipoles (with constant direction of magnetization) on a plane are the same as those of single poles and dipoles multiplied by scaling factors. Spector and Bhattacharyya (1966) derive the expressions for the autocorrelation functions of point poles and dipoles and these could be used to calculate the form of model noise autocorrelations. The amplitudes of the autocorrelation functions estimated in this way would not be correct but this is not important because, as is shown below, the weighting function  $\psi$  in equation (6-2) is the critical factor.

No published method is known to the author for calculating an autocorrelation function of a field caused by an assemblage of three dimensional bodies with random directions of magnetization. It could possibly be estimated by calculating the autocorrelation function of an assemblage of randomly distributed model bodies with random directions of magnetization. It could also be estimated by autocorrelating data known to be caused by such noise.

### 6.3.2 Autocorrelation Functions of Fields due to Two Dimensional Bodies

An important property of the autocorrelation functions of fields due to two dimensional bodies is that they are independent of the direction of the component of measurement and the direction of

magnetization. This can be shown by considering the generalized spectral representation of these fields (equations (1-8) and (1-9)). The power spectrum is the square of the Fourier amplitude spectrum and is independent of any directional term in the two dimensional case. As the autocorrelation is related to the power spectrum through the Wiener Khintchine equation the autocorrelation must also be independent of the direction terms. This fact greatly simplifies noise modelling for the two dimensional case as only the geometry of the noise bodies needs to be considered.

#### 6.3.2.1 Dykes

Bruckshaw and Kunaratnum (1963) have shown that for any infinite dipping dyke with a horizontal top there is a vertical infinite dyke with the same depth and width, but not necessarily the same direction of magnetization, which gives the same magnetic field. Thus the autocorrelation function of infinite dykes must be independent of the dip of the dyke and depend only on the depth, width and the effect of the magnetization as a scaling factor.

As the depth width ratio of the dyke increases the anomaly due to the dyke becomes similar to the anomaly due to a thin sheet at the same depth. This approximation becomes valid when the depth width ratio is greater than 1, and in such cases the autocorrelation function depends only on the depth of the dyke and a scaling factor.

Usually the dykes in a dyke swarm causing noise on a magnetic profile all occur at the same depth and have widths which are small with respect to the survey height. In such situations the autocorrelation of the anomaly due to a vertically magnetized, vertical, infinite, thin dyke, with its top at the same depth as the dyke swarm, would give a good estimate of the shape of the noise autocorrelation.

### 6.3.2.2. Lava Flows

A lava flow causing an irregular magnetic field can be approximated by a layer of differently magnetized blocks or dipoles. If the lateral magnetization variation in the lava flow is random and rapid then the form of the noise autocorrelation may be estimated by calculating the autocorrelation of the field due to a single vertically magnetized block or dipole with the same depth and vertical thickness parameters as the lava flow.

Naidu (1967) has derived the expression for the autocorrelation of the potential field due to a random distribution of sources in a vertical plane.

### 6.4 Examples of Optimum Wiener Filtering

Fig. 6-1 shows an example where an optimum Wiener filter has been applied to remove the effects of a small shallow block from the magnetic profile over a deeper, relatively large vertical dyke.

To calculate the filter coefficients, the input signal was taken as the anomaly over the dyke and the noise was taken as the anomaly over the block. The desired output was specified as the anomaly over the dyke. The filter was thus designed specifically to suppress the effects of the block relative to the effects of the dyke.

Fig. 6-1 shows how critically the appearance of the filtered output depends on the weighting factor  $\nu$  which determines the relative reduction of the noise power. To determine the optimum  $\nu$  a compromise choice must be made between noise reduction and signal distortion. This choice is best made by visual inspection of different outputs.

From the theory given in 6.3.2 the coefficients calculated for this example are generally applicable to situations where random distributions of similar blocks overly random distributions of infinite dykes with the same depths and widths as the model dyke

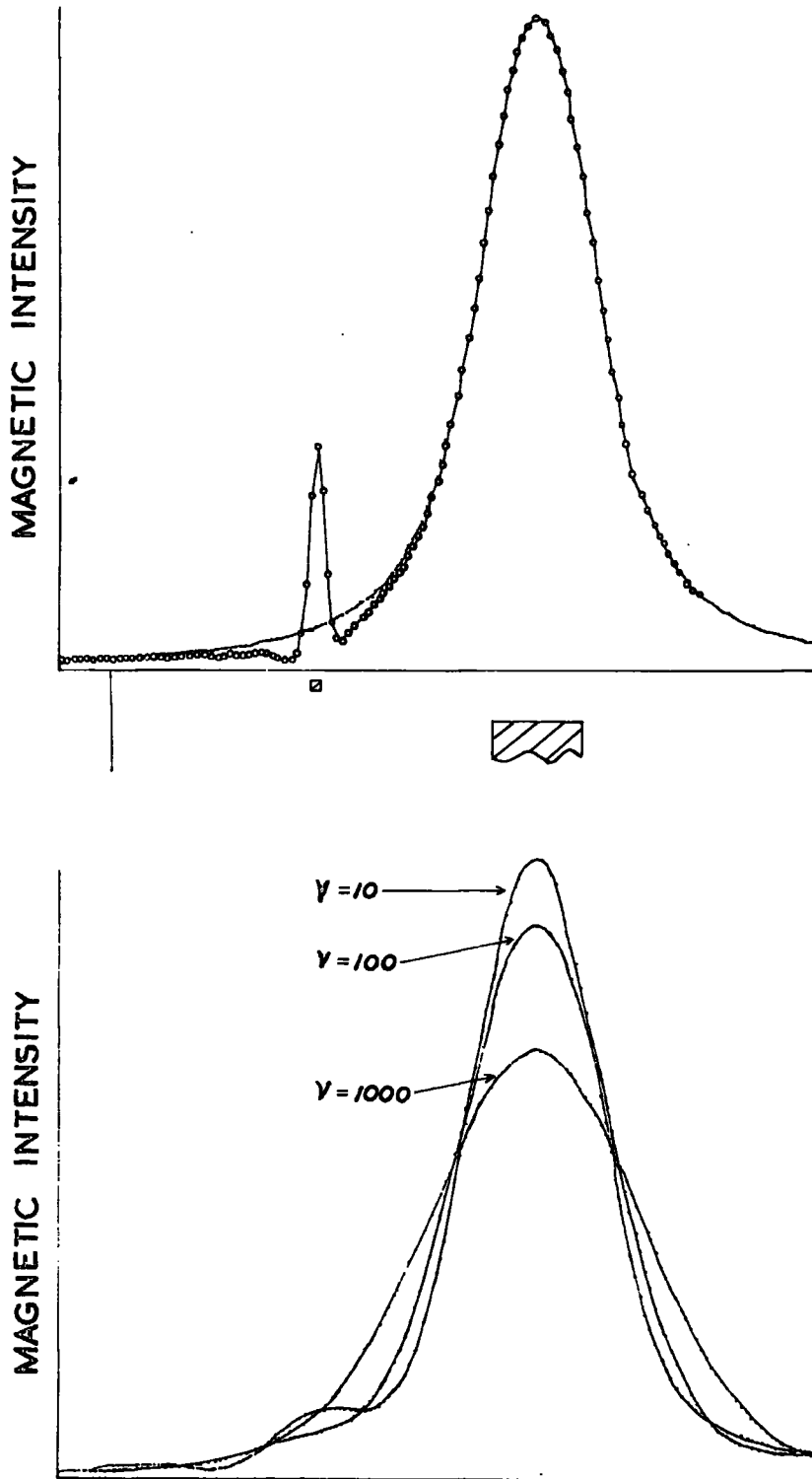


Fig. 6-1 Application of an optimum Wiener filter to separate the magnetic effects of a block type body and a vertical dyke. Top diagram shows original combined effects of the bodies. Bottom diagram shows the results of applying Wiener filters calculated using different values of  $\gamma$ , the noise reduction factor.

of Fig. 6-1. This is verified by the example shown in Fig. 6-2 where these coefficients have been successfully applied to suppress the noise due to such a random distribution of blocks overlying a dipping dyke which has the same depth and width as the vertical dyke used to calculate the coefficients.

#### 6.5 Other Work on Optimum Filters

Clarke (1969) has designed optimum downward continuation and derivative filters using the frequency domain alternative for Wiener filtering. Clarke in practice only deals with an example where the noise is white (i.e. the noise power is equal at all frequencies) and his method is difficult to extend to more general applications.

Strakhov (1966a,b) has developed a filtering scheme in which the filter coefficients are designed under two constraints:

- a) the distortion of the signal is a minimum
- b) the variance of the noise is reduced by a given factor

Strakhov's filter is thus designed on similar principles to the Wiener filter. Naidu (1966), (1968) has successfully applied Strakhov's method.

Spector (1968) estimates the noise component of the logarithmic power spectrum of magnetic fields visually. By subtracting this component from the spectrum and transforming the field back into the space domain a form of optimum filtering is achieved. It is difficult to estimate the amount of signal distortion with this method.

Matched filters, discussed by Treitel and Robinson (1969) in a seismic context, are a form of optimum filter which are designed to give the largest possible output value for a given input. The matched filter for a waveform is the reverse waveform of itself and the output is thus its autocorrelation function. If autocorrelated noise is present the matched filter may be designed to allow for it.

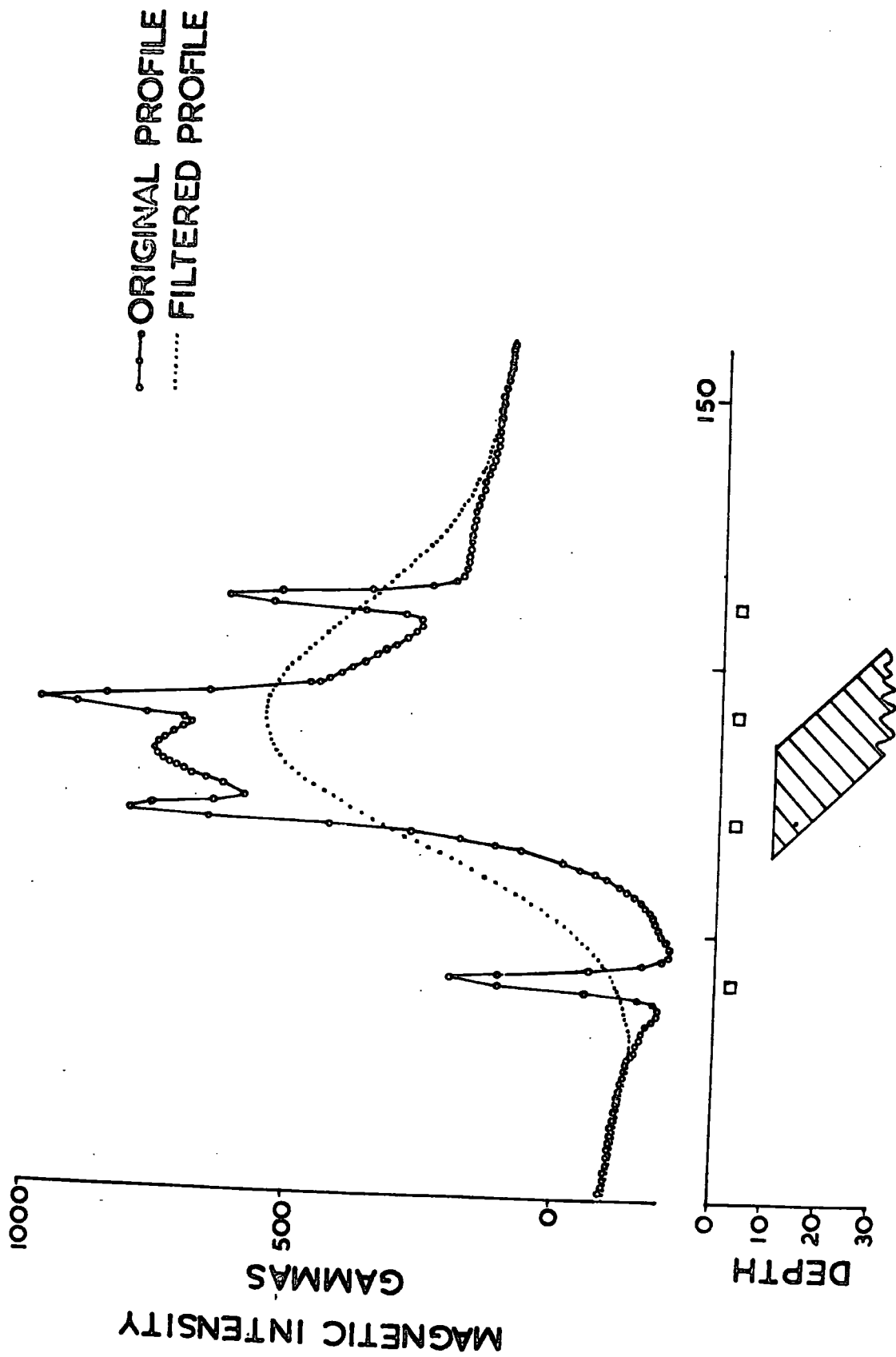


Fig. 6-2 Application of an optimum Wiener filter to remove the magnetic effects of a random distribution of block type bodies from the magnetic effects of an infinite dyke.  $\gamma = 1000$ .

Tests by the author have shown that in practice the matched filter provides a good method of noise suppression but the output waveform becomes very broad and this significantly reduces its usefulness.

#### 6.6 Concluding Remarks

The theory and examples presented have demonstrated the use of space domain Wiener filters in providing an optimum separation between the effects of two different types of bodies. The same principles can be extended to apply this method to any field transformation; for example to suppress noise during a gravity to magnetics transformation or when an interface is being mapped directly from gravity or magnetic data.

The discussion above was concerned with geologic noise. If the noise is caused by measurement and compilation inaccuracies and can be regarded as white the method can still be applied. In such a situation the noise waveform must be represented by a unit spike (a unit spike contains equal amounts of all frequencies (Hsu, 1970, p.102) and is thus spectrally identical to white noise except for a scaling factor). It would be necessary to conduct tests to determine the optimum weighting factor  $\nu$  for the white noise suppression.

CHAPTER 7MULTICHANNEL WIENER FILTERS7.1 Introduction to Theory

Many linear systems have multiple inputs and outputs, all of which are interrelated. Such systems are called multichannel systems and as with single channel systems appropriate filtering operations on the input channels can yield output data which presents the distribution of parameters in a manner not obvious in the input data.

The design of digital multichannel Wiener filters has been described by Robinson (1967), Galbraith and Wiggins (1968), Davies and Mercado (1968) and Treitel (1970) and is a straightforward extension of the theory for single channel Wiener filters.

An outline of this theory is presented below.

We wish to operate on a set of digital inputs  $b(i,s)$  ( $i$  is the input channel index,  $s$  is space coordinate), with a digital filter  $f(i,j,s)$  to produce a set of desired digital outputs  $d(j,s)$  such that the average squared difference between the actual output  $y(j,s)$  and the desired output is a minimum. Fig. 7.1 shows a block diagram of the input output relationships in the case where there are three input and three output channels.

$b(i,s)$  = input on  $i^{\text{th}}$  channel

$f(i,j,s)$  = filter for  $i^{\text{th}}$  input and  $j^{\text{th}}$  output channel

$y(j,s)$  = output on  $j^{\text{th}}$  channel

$$y(j,s) = \sum_i \sum_k f(i,j,k) \cdot b(i,s-k)$$

$d(j,s)$  = desired output on  $j^{\text{th}}$  channel

$e_s^2$  = squared error

$$e_s^2 = \sum_{j=1}^n (y(j,s) - d(j,s))^2$$

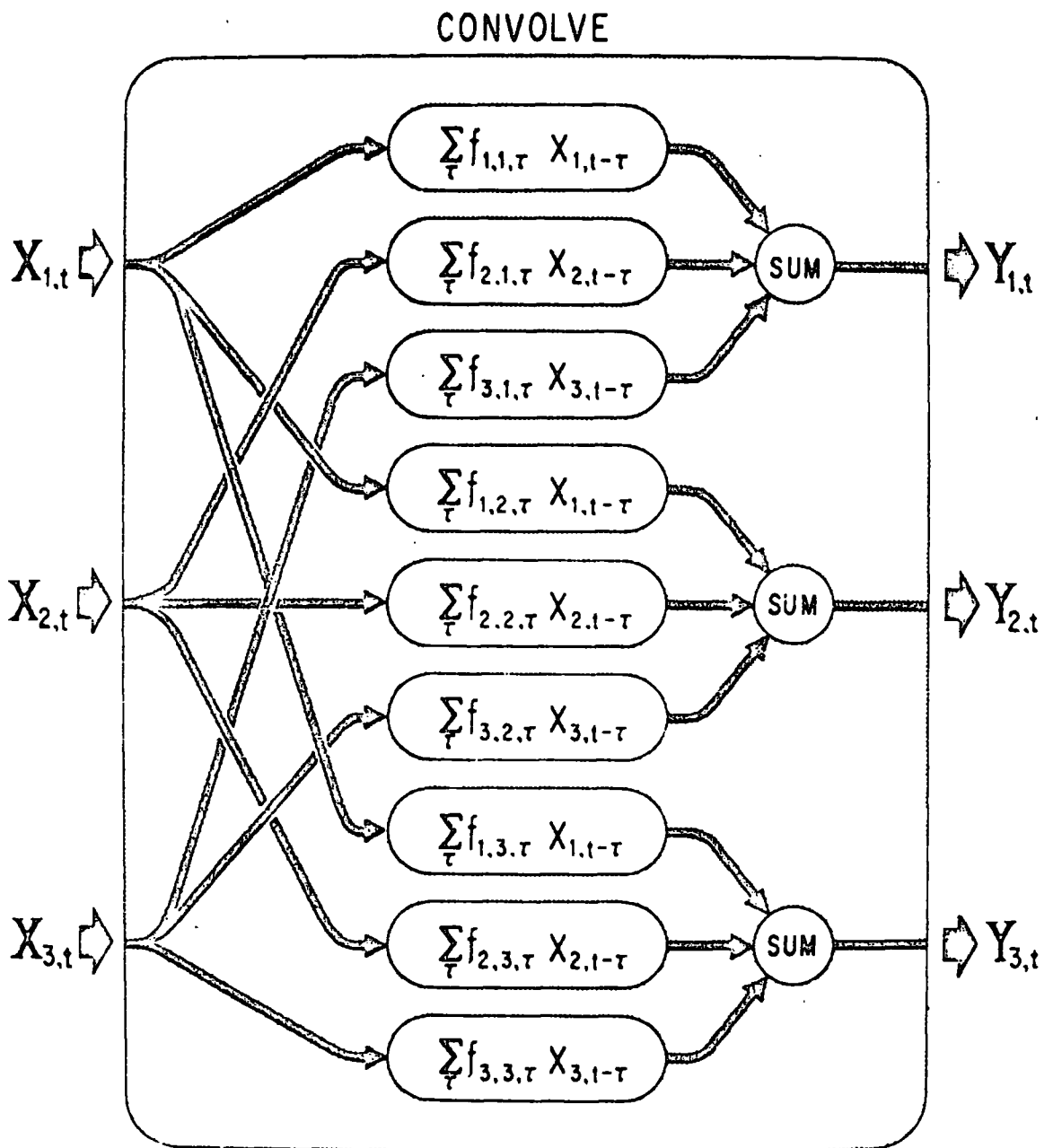


Fig. 7-1 Block diagram illustrating a multichannel filtering system with three input and three output channels. (Diagram reproduced from Galbraith and Wiggins (1968)).

By taking partial derivatives of the equation for the squared error with respect to each filter coefficient and equating each of these equations to zero the system of multichannel normal equations which allow calculation of the filter coefficients is obtained.

For the case with  $r$  input channels of length  $\ell$ , and  $n$  output channels where the filters for each channel are to consist of  $m+1$  coefficients, the normal equations are

$$\sum_{i=1}^n \sum_{k=0}^m f(i, q, k) \cdot R(i, p, s-k) = G(q, p, s) \quad (7-1)$$

where the autocorrelation

$$R(i, p, s-k) = \sum_t b(i, t-k) \cdot b(p, t-s)$$

and the crosscorrelation

$$G(q, p, s) = \sum_t d(q, t) \cdot b(p, t-s)$$

The symmetry properties of the normal equations, when expressed in matrix form, have been used by Wiggins and Robinson (1965) to devise a recursive method for their solution. Robinson (1967) has published subroutine **WIENER** which incorporates this method and can calculate multichannel Wiener filter coefficients. The author has written a computer program **MULTIW** based on **WIENER**, which as well as calculating the filter coefficients, applies them to multichannel data.

## 7.2 Detection of Anomalies with a given Magnetization-Density Ratio

If a random distribution of block type bodies of known depth, thickness and direction of magnetization occurs and gravity and magnetic profiles are available over the bodies then it is possible to design a multichannel filter to detect the bodies with a given magnetization-density ratio.

To calculate such a filter the input to MULTIW must be specified as the gravity and magnetic fields over such a block and the desired output must be specified as a square wave whose width is equal to the width of the block. The resultant filter will thus deconvolve the appropriate factors from the two input channels and add the outputs in such a way that the desired square wave occurs as the output.

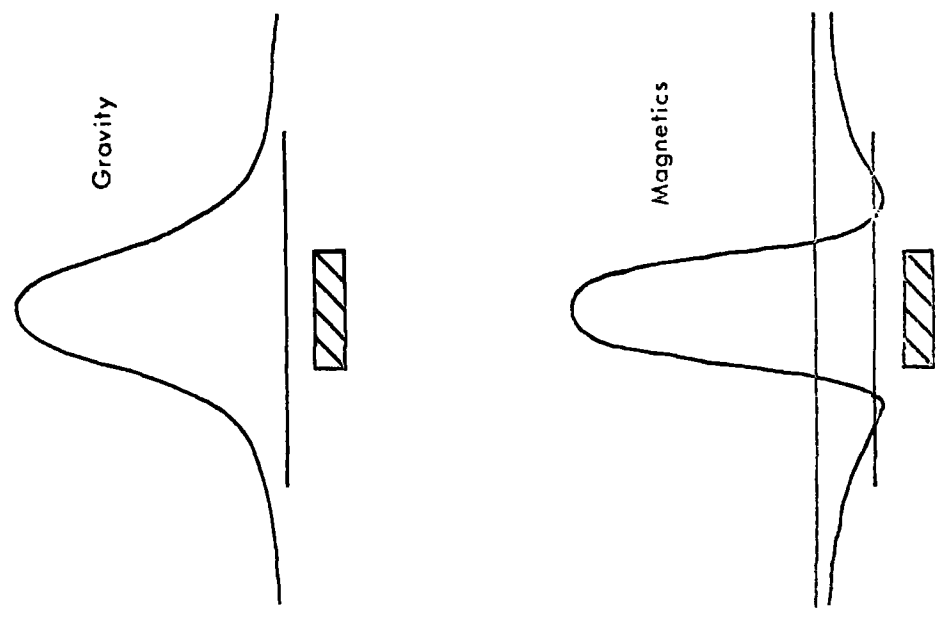
Fig. 7.2 demonstrates applications of such a filter which when applied to test data generates the desired square wave when a particular magnetization-density ratio is detected. It should be noted that the square wave outlines the causative body regardless of its width. In cases where coincident gravity and magnetic anomalies occur and the magnetization density ratio differs from the target ratio, the output deviates from a square wave.

The amplitude of the square wave output is scaled relative to the amplitude of the model square wave used in the calculation of the coefficients by the proportion that the magnetization and density of the detected bodies are different from the magnetization and density of the model bodies being used for the coefficient calculation.

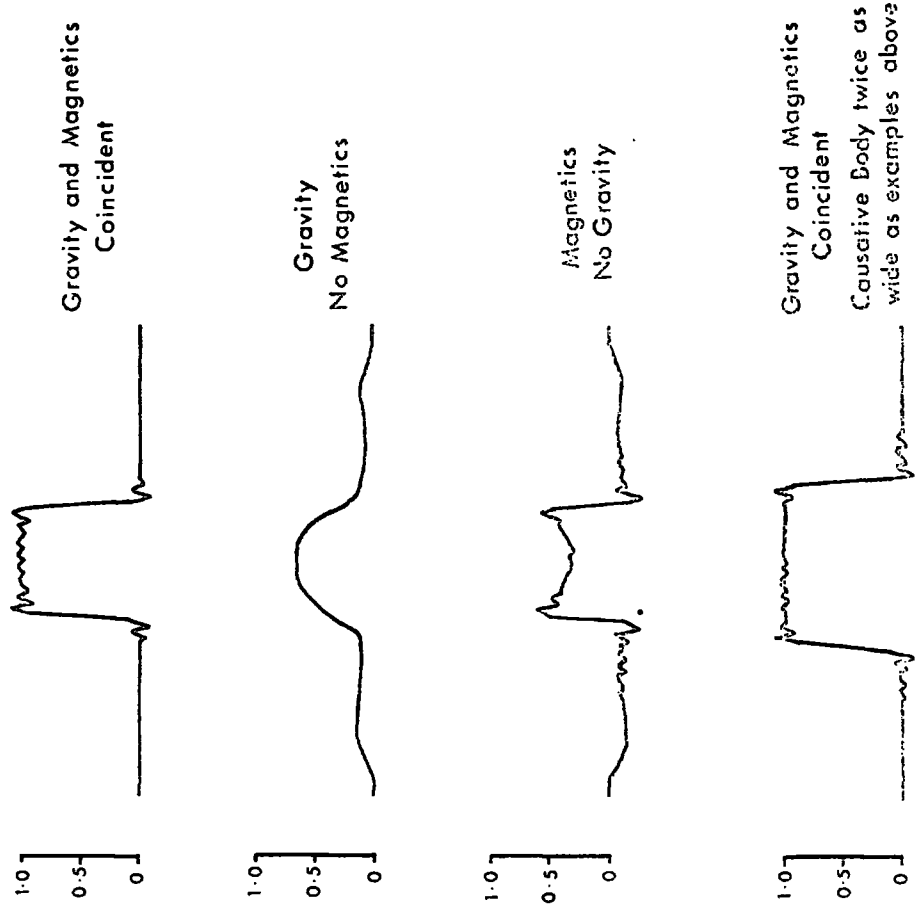
Such a filter method, as the one demonstrated in this section, could be applied in an area where numerous dykes occur but only those with a particular magnetization density ratio are of economic interest.

It is thought that this method using multichannel filtering to detect predetermined ratios of physical properties could probably be extended to include combined analysis of gravity, magnetic and electromagnetic results. Such an approach could identify the type of rock causing the anomalies. The application of the method to processing multichannel electromagnetic results is beyond the scope of this thesis but it would be well worth a separate study.

Multichannel INPUT



Single Channel OUTPUT



▨ Causative Body

Fig. 7-2 Results of the application of a filter to extract block type bodies with a specified density and vibrational ratio. Inputs to the multichannel filter are the gravity and magnetics signals over a block type body. The hatched rectangular pulse is a causative body. The output signals are the results of the filter's operation. The filter's response is shown in the hatched rectangular pulse.

### 7.3 Optimum Strike Filtering

Chapter 6 discussed the adaption of the Wiener filter method to provide an optimum separation between two types of anomalies. Multi-channel Wiener theory allows filters to be designed which provide an optimum resolution between anomalies with different strikes. General purpose strike filters have been designed by Fuller (1967), however the filters described in this section are optimum (in the least squares sense) and the design incorporates information about the type of anomalies to be separated as well as their strikes.

Galbraith and Wiggins (1968) discuss the application of multi-channel Wiener filters to filtering events with different moveout on seismic records. Their theory can be adapted to gravity and magnetic applications.

We consider the multichannel input  $b(i,s)$  to consist of two parts, the signal  $S(i,s)$  and the noise  $N(i,s)$

i.e. 
$$b(i,s) = S(i,s) + N(i,s)$$

We wish to design a filter such that the signal is distorted by the least possible amount according to the least squares criterion and that the noise power is reduced by as much as possible. Assuming that the signal is not correlated with the noise we have

$$R(i,j,t) = R^{SIG}(i,j,t) + \nu R^{NOISE}(i,j,t)$$

and

$$G(i,j,t) = R^{SIG}(i,j,t)$$

$\nu$  is the weight of the noise reduction

These relations can be substituted in the multichannel normal equations (7-1) to give a set of simultaneous equations for the calculation of multichannel Wiener filters in the presence of auto-correlated noise. The computer program MULTIW has been generalized to include this case.

Multichannel correlation functions consist of series of cross-correlations and autocorrelations between the various input and output channels. If these channels consist of gravity or magnetic profiles over two dimensional bodies, then, providing that all the bodies have the same dip and direction of magnetization the same properties will apply for multichannel correlation functions as deduced in Chapter 6 for single channel correlation functions of fields over two dimensional bodies. This means that model correlation functions may be calculated using vertical magnetization instead of inclined magnetization and for the calculation of correlation functions of fields over infinite dykes the fields over vertically magnetized vertical dykes may be used.

An application of multichannel strike filtering will now be demonstrated.

The problem is to resolve the effects of two sets of dykes striking in different directions. The dykes of interest have depth 4 units, width 1 unit and strike at right angles to the direction of the profiles. The dykes to be filtered have depth 4 units, width 0.7 units and strike at  $45^\circ$  with respect to the profiles. Both sets of dykes have vertical dips and are magnetized by induction in a field dipping  $65^\circ$  in the plane of the profiles.

To calculate coefficients to perform this separation the input signal was specified as a set of three profiles over a dyke with the same dimensions as the dykes of interest. The position of the dyke was the same for all three profiles thus modelling a situation where the strike of the dyke is at right angles to the profile. The desired output was specified as a single profile over the dyke. The noise was specified similarly to the signal except that the positions of the dykes were offset relative to each other to simulate a strike at  $45^\circ$  relative

to the profiles. Because the correlation functions are independent of the dip of the field it has been possible to use the fields over vertically magnetized bodies for the model fields.

Fig. 7-3 illustrates an example where the filter coefficients calculated in the manner described above have been successfully applied to separate non-vertically magnetized dykes with different strikes. It has been found by testing that the optimum visual resolution of the two types of anomalies can be improved by empirical variation of the noise reduction weighting factor  $V$  .

As with other methods of optimum filtering the applicability of this method depends on how well the average correlation functions of the signal and noise are estimated. In well defined situations, such as in the example presented above, the correlation functions can be realistically estimated from model fields and useful sets of filter coefficients can be obtained.

#### 7.4 Comments

One possible application of multichannel filtering which has not been investigated is the combined analysis of gravity and magnetic profiles to map interfaces. Because the gravity and magnetic profiles contain the same information about the interface it is concluded that no significant improvement would be gained over results obtained by averaging separate mappings using gravity and magnetic profiles. A similar conclusion has been reached by Davies and Mercado (1968) who have compared multichannel seismic deconvolution results with those obtained from the averages of single channel deconvolutions.

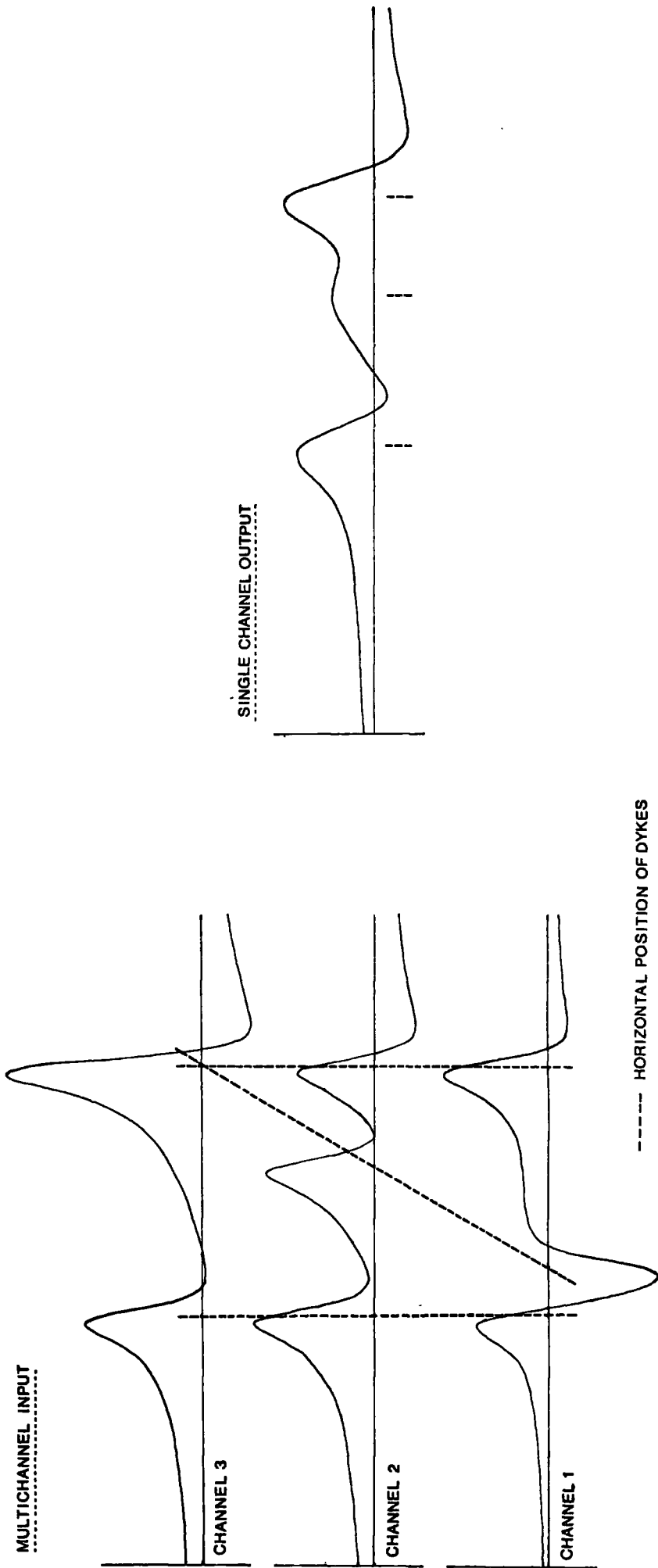


Fig. 7-3 An example of optimum multichannel strike filtering. The input to the filter is three parallel magnetic profiles across a series of vertically magnetized vertical thin dykes, all at the same depth but having different strikes. The filtered output corresponds to Channel 2 and shows that the effects of the dyke striking obliquely to the profile have been reduced relative to the effects of the dykes striking perpendicularly to the profile. The noise reduction factor  $\gamma = 1.0$ .

CHAPTER 8EXAMPLES OF THE APPLICATION OF WIENER FILTERS TO REAL DATA8.1 Reduction to the Pole and Magnetization Calculation for an Anomaly in the English Lake District

An aeromagnetic anomaly from the northern end of the English Lake District was chosen to test the Wiener filter method for reduction to the pole and magnetization calculation. A profile, digitized from the Aeromagnetic Map of Great Britain (1964), is shown in Fig. 8-1a. The data of this profile was converted to the regular spacing necessary for filtering using the computer program SPLINE, which applies the cubic spline method of interpolation (Bhattacharyya, 1969).

The anomaly was assumed to be magnetized solely by induction in the earth's field and the symmetry of the anomaly obtained by the reduction to the pole process tends to confirm this (Fig. 8-1b).

The form of the anomaly suggests that it is caused by a vertical prism type body with a finite depth extent and Fig. 3c shows a magnetization profile assuming that the top of the body is 100 metres below ground surface and its bottom is 10 km. below ground surface. The depth estimate for the top of the body is based on geological conditions outcropping in the area (Eastwood et al., 1968) which suggest the anomaly may be due to Ordovician Borrowdale Volcanic rocks masked by a thin cover of Carboniferous and Triassic sediments. The study of the magnetic basement in the area, described in the next section, indicates that 10 km. is a reasonable limit to the bottom of the body.

Tests on model bodies show the accuracy of the depth to the bottom is not very critical for magnetization determinations in situations with the dimensions being considered. The magnetization profile has the square wave form expected although it has high frequency effects caused by data noise.

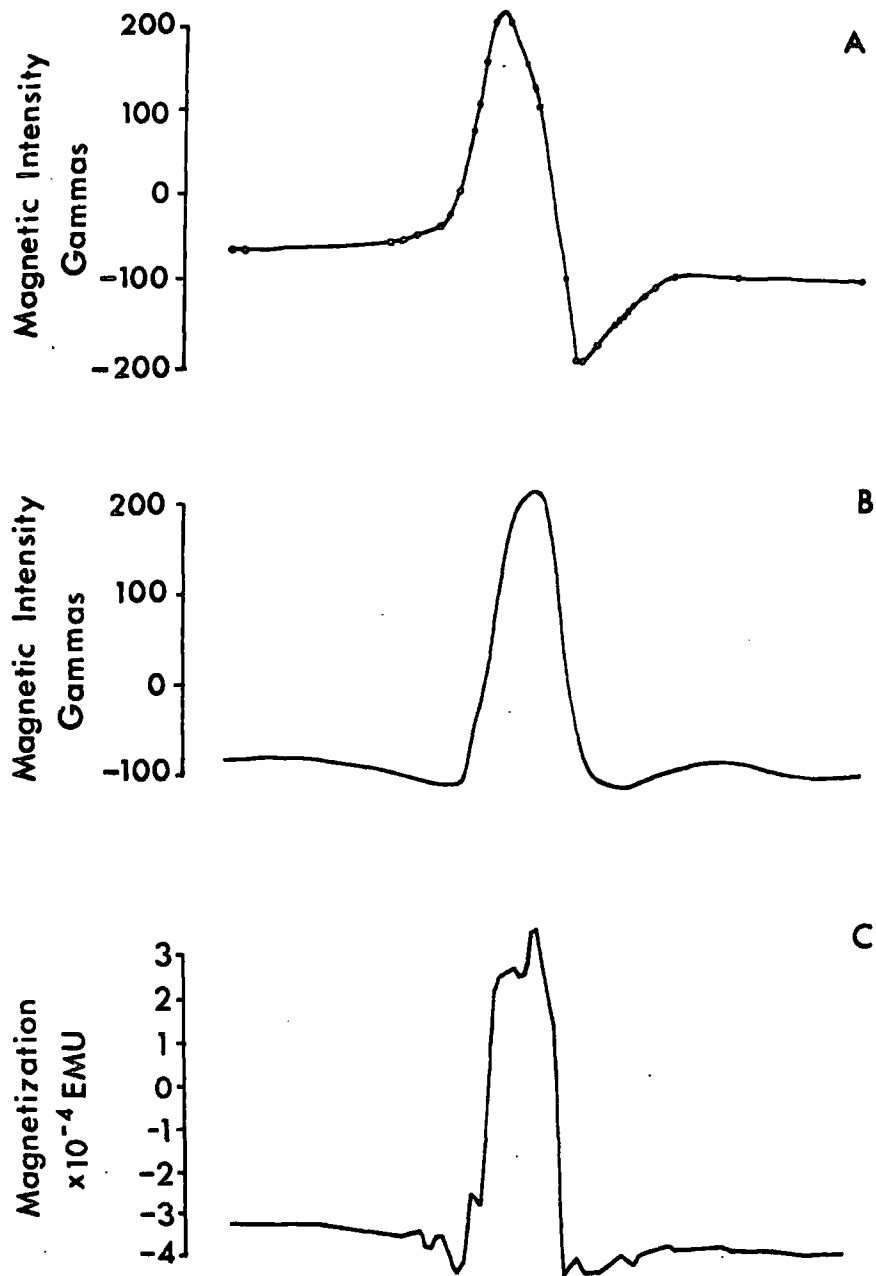


Fig. 8-1 A. Magnetic profile regenerated from contour map data using spline interpolation. Heavy dots correspond to positions of contour lines.

B. Magnetic profile reduced to pole.

C. Magnetization profile  
National Grid co-ordinates of the ends of the profile are NY121119 and NY114153.

Bush (1971) conducted ground magnetometer surveys over the anomaly and has performed a detailed analysis of his results. Bush concluded that the anomaly is caused by rocks of the Borrowdale Volcanic Series in a steeply dipping limb of an eroded anticline. Bush used several methods of interpretation and decided that the magnetization is induced with a magnitude of 0.0009 emu and that the body has a depth of burial of 200-300 metres below ground level and its depth extent is approximately 6 km.

Nesbitt (1965) studied the magnetic properties of the Borrowdale Volcanic Series and has shown that the magnetization is predominantly induced with a magnitude of 0.0008 emu.

The slightly lower estimate of 0.0007 emu obtained by the Wiener filter method is probably the result of assuming a depth extent larger than it really is.

## 8.2 Basement Mapping for the Southern Uplands and Solway Firth

A striking feature of the aeromagnetic map for the south of Scotland and the north of England (published by the Geological Survey of Great Britain, 1964) are the alternating belts of high and low values of the magnetic field. These zones, approximately 40 km. wide and striking with a Caledonoid trend are particularly noticeable in the region of the Southern Uplands between the Midland Valley and the Solway Firth.

The geology of the Southern Uplands has been described by Greig (1971) and consists of tightly folded Lower Palaeozoic sedimentary rocks.

Walton (1965), from palaeogeographic studies, has deduced the position of an axial rise influencing sedimentation in Ordovician times. This rise corresponds in position with the magnetic high over the Southern Uplands.

The existence of this rise is confirmed by seismic evidence published by Agger and Carpenter (1964) which shows a rise in the non

sedimentary crust beneath the Southern Uplands.

The gravity studies of Bott (1965) indicate a sedimentary basin corresponding to a magnetic low positioned over the Solway Firth.

Thus the regional magnetic anomalies over the Southern Uplands appear to reflect undulations on a magnetic basement.

Walton (1963) has reinterpreted the structure of the sedimentary rocks of the Southern Uplands and disagrees with the ideas of Peach and Horne (1899) that they consist largely of isoclinal folds. Walton considers the dominant structural features to be a series of faulted monoclines. There is no magnetic evidence relating to these monoclines and this suggests that the magnetic basement and the overlying sediments may have reacted differently to the compression which has obviously occurred within the Southern Uplands. The magnetic basement appears to have merely buckled as a result of crustal shortening whereas the Lower Palaeozoic sediments have undergone both thrusting and folding.

This section demonstrates the application of the Wiener filter method to the mapping of the magnetic basement.

For the interpretation the basement was assumed to be uniformly magnetized in the direction of the earth's field.

The profile shown in Fig. 8-2 was digitized at points where the contour lines crossed the line of the profile and the spline interpolation routine was used to convert the data to a regular spacing. The computer program WIEN1D was used to produce a depth profile assuming that the magnitude of the magnetization was 0.001 emu. To convert this result into a true depth profile it is necessary to know the depth at one point on the profile and the magnetization of the basement. In this situation these parameters were unknown so a non-linear optimization routine was written to solve for the three unknowns i.e. the constant regional background, the magnetization and the depth to one point. The computer program written, MINIM, incorporated the non-linear optimization

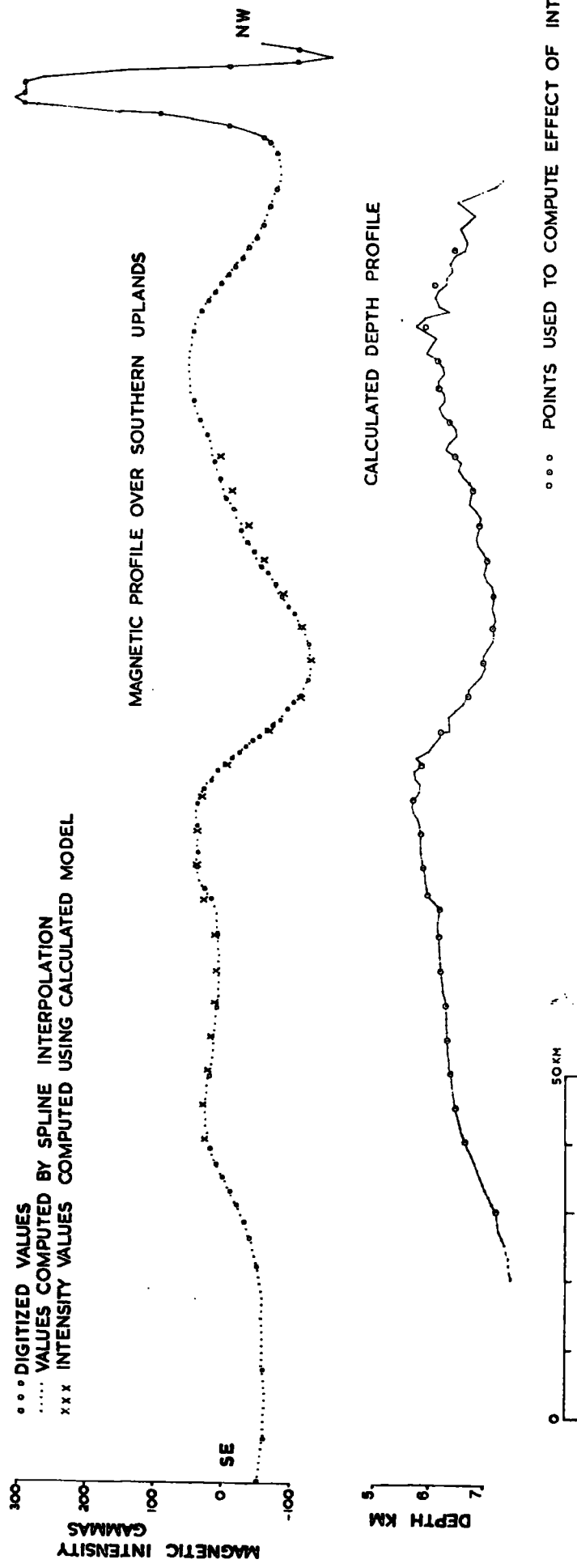


Fig. 8-2 Magnetic profile across the Southern Uplands and the relief of a magnetic interface which may cause the anomaly. The relative relief of the calculated using, Wener's theory. The absolute depth and magnetization (0.001 c.g.s.) were calculated using an optimization routine. N. Brown's 1971 co-ordinates of ends of profile are 60° 12' 00" and 15° 52' 00".

routine MINUIT published by CERN (1970) and used the relative depths calculated by WIEN1D. WIEN1D took 20 seconds to perform the filtering operating and MINIM took 40 seconds to calculate the three unknowns.

Fig. 8-2 shows the calculated depth profile. Al-Chalabi (1970) has interpreted part of the same area using a non-linear optimization routine in which the magnetization (direction and magnitude), regional background, and all the depth points were treated as variables. Al-Chalabi obtained a direction of magnetization closely corresponding with that of the earth's field but the magnetization value he obtained (0.001 emu) differs from the value obtained in the example above.

As was shown in Chapter 1, the thickness of a layer and its magnetization are both scaling factors of the equivalent layer for a magnetic field and it must be expected that for thin layers their product is the important factor and not their individual values. This means that a large broad minimum would be expected in any least squares attempt to optimize these factors. This effect could cause the discrepancy.

Laving (1971) has interpreted the Solway Firth anomaly using different set values of magnetization. The profiles determined by Laving (1971), Al-Chalabi (1970) and in Fig. 8-2 are all basically the same in shape but differ in amplitude due to the different values of magnetization used.

### 8.3 Density Deconvolution and Mapping of the Weardale Granite

Gravity surveys of the Northern Pennines of England, summarized by Bott (1967b), revealed a gravity low which suggested the presence of a granitic intrusion (the Weardale Granite). Subsequent drilling at Rookhope encountered granite at a depth of 380 metres below the ground surface.

Bott (1967b) has interpreted gravity profiles across the Weardale granite using end corrections and has shown that it approximates a prism with its bottom at approximately 10 km.

The gravity field over the Weardale Granite has been used to test the density deconvolution method developed in 4.3.

The gravity map of the Weardale Granite (Fig. 8-3) was digitized on a 2.5 km grid and Fig. 8-4 shows the result of applying a filter designed to calculate the density distribution assuming that the top of the body is at 0.4 km. and the bottom is at 10 km.. If the granite was caused by a prism type body with these dimensions then the output of the filter operation would be a plateau of constant density values outlining the areal position of the prism. The calculated output only approximates this and this is thought to be the result of relief on the top of the granite.

It was shown in Chapter 5 that the output of a deconvolution process in an application such as described above gives a very good approximation to the shape of a body. To convert from the density contours of Fig. 8-4 into contours of relative relief the following relationship applies:

$$\text{depth} = \frac{\text{Thickness of Prism used to calculate coefficients}}{\text{density contrast of body}}$$

X difference in computed density between two points

Bott (1967b), from a consideration of density data and his quantitative interpretation considers a possible density contrast of the Weardale Granite to be 0.13 gm./cc.. In the example shown in Fig. 8-4 this is very close to the computed density difference between the level in density over the Weardale Granite and the background level. However, when attempting to calculate a depth contour map of the Weardale Granite using a density contrast of 0.13 gm./cc. and tying all

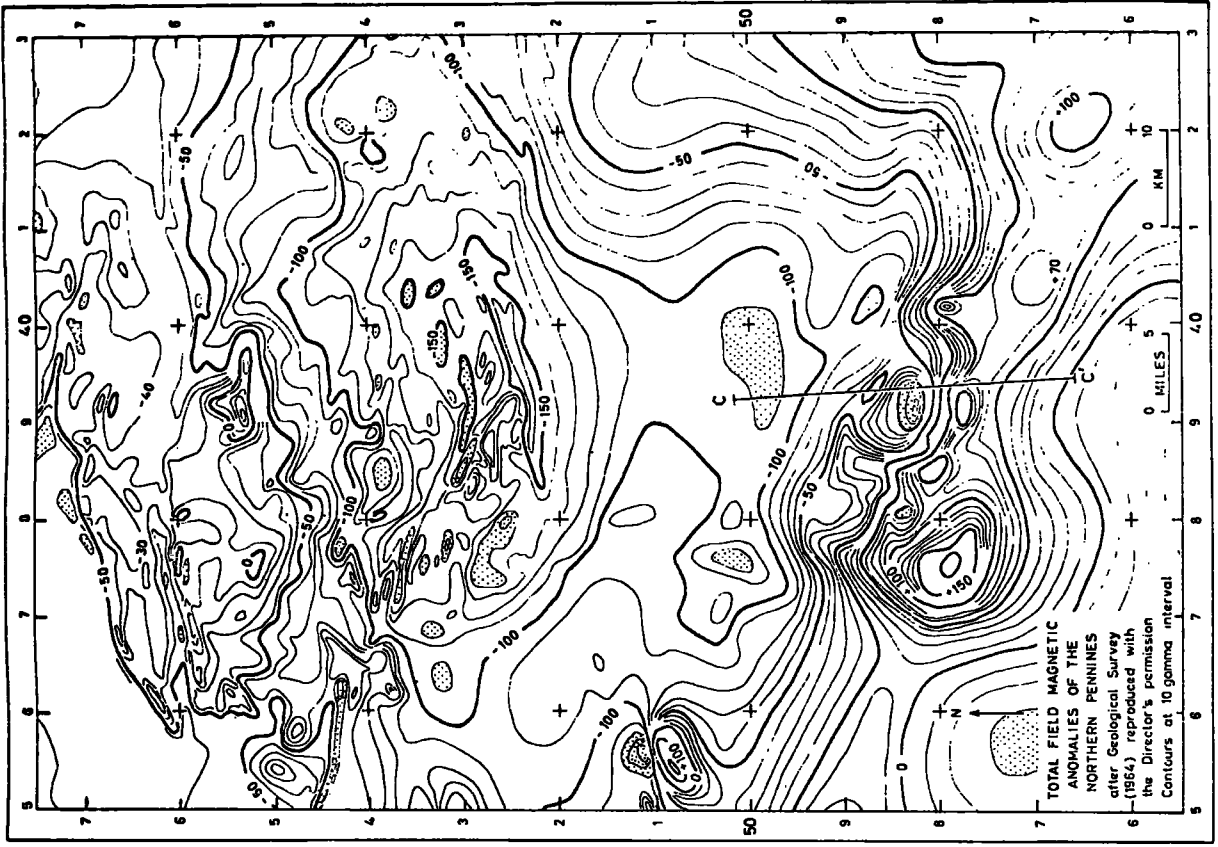
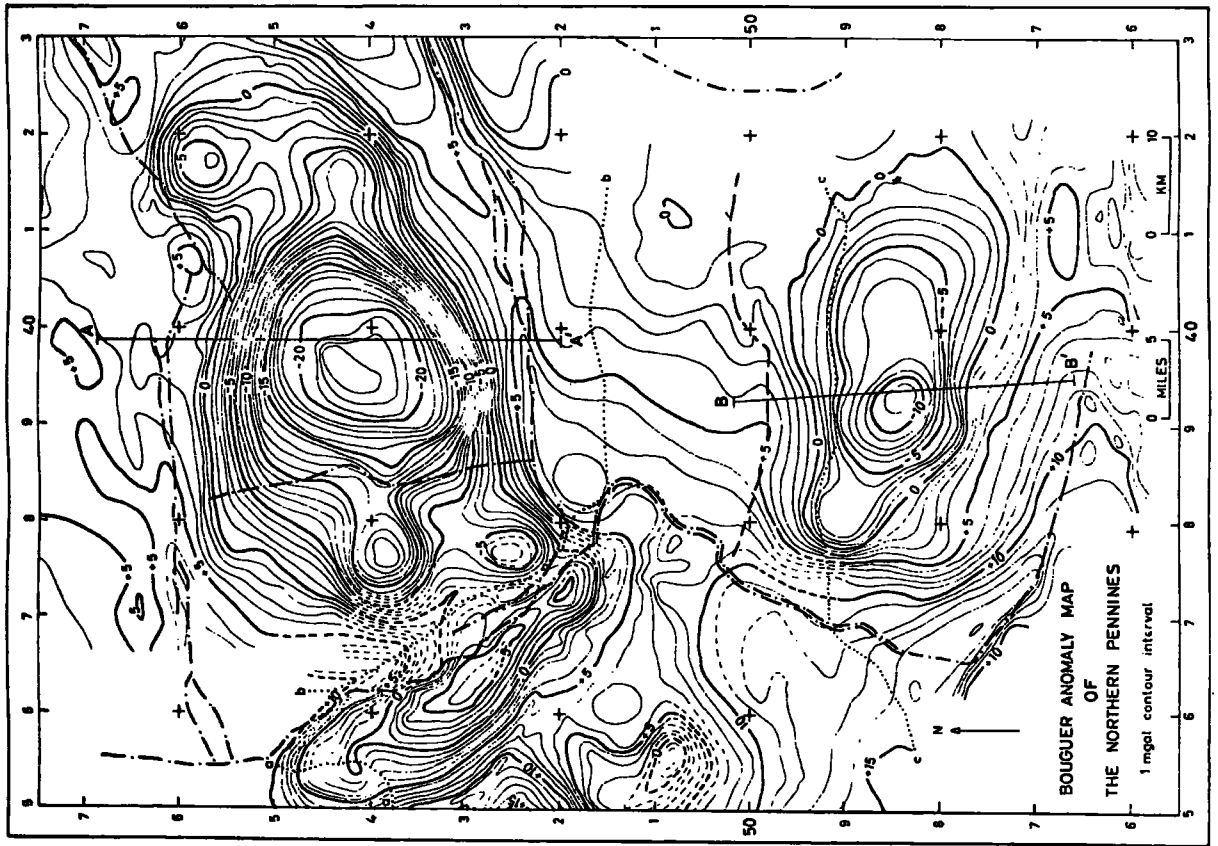


Fig. C-3 Gravity and magnetic fields over the Moorhale Granite. Diagrams reproduced from Dott (1976) with author's permission.

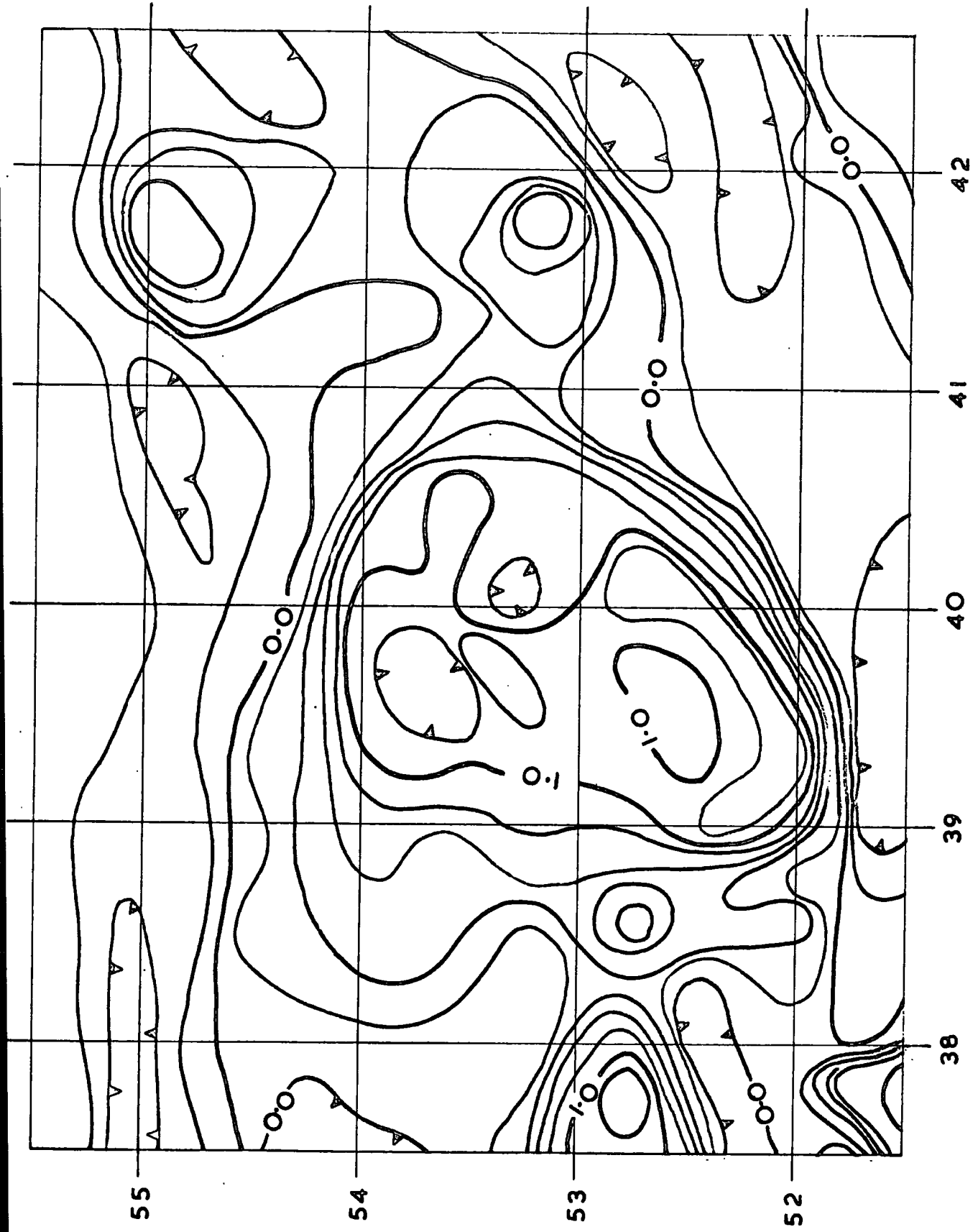


Fig. 2-4 Output of a deconvolution filter applied to the gravity field over the Weardale Granite. Contours (in  $\text{gm/cc.}$ ) show the density distribution between depths of 0.4 km. and 10.0 km.

calculations to the known depth of the granite in the Rookhope borehole, some of the depths came out above the ground surface. This is probably due to regional effects being superimposed on the gravity field. It could also be due to the fact that the topography is irregular in the area of the survey. The free air gravity correction does not alter the level of the observation point so the observed field is effected by varying distances from the top of the body. It is also possible that there are density inhomogeneities in the granite and surrounding sediments.

Gibb's phenomenon may account for some irregularities in the mapped surface.

Nevertheless it is considered that the density deconvolution method provides a better detailing of the Weardale Granite than the original gravity map.

#### 8.4 Removal of White Noise from a Magnetic Field

Fig. 8-3 shows the part of the Aeromagnetic Map of Great Britain (published by the Geological Survey of Great Britain (1964)) which covers the area underlain by the Weardale Granite. The magnetic effects of the granite are almost completely obscured by secondary magnetic features and although some of these can be related to Tertiary dykes the distribution of the noise anomalies appears, to a first approximation, to be random.

To enhance the effects of the Weardale Granite an optimum Wiener filter was designed to suppress random noise relative to the magnetic effects of a prism with the dimensions deduced by Tanner (1967) from an interpretation of the gravity field over the Weardale Granite. The design of optimum filters was discussed in Chapter 6 and the computer program WIEN2D is capable of calculating and applying such filters. The filter was designed to provide an optimum separation

between the magnetic effects of a prism (depth 0.4 km., vertical thickness 10 km., north south width 20 km., and east west width 20 km. magnetized by induction) from white noise. White noise is completely random noise containing equal amounts of all frequencies. A unit spike has the same frequency spectrum as white noise (Hsu 1970, p.102) and it is thus possible to specify the noise to be removed as a unit spike.

It proved necessary to vary the noise reduction factor to achieve a visually optimum noise removal. The filtered map, shown in Fig. 8-5, reveals a low amplitude negative anomaly corresponding to the Weardale Granite and indicates that even though the model used for the noise is an approximation the method can provide useful results.

The contour map of Fig. 8-5 was automatically plotted using a modification of the computer program published by Holroyd and Bhattacharyya (1970).

### 8.5 Filtering Operations on the Magnetic and Gravity Fields Over a Postulated Tertiary Intrusion in Northern Ireland

The gravity and aeromagnetic maps of Northern Ireland (published by the Geological Survey of Northern Ireland, 1967, 1971) reveal large co-incident gravity and magnetic anomalies centred on Dromore, County Tyrone. Interpretation of these anomalies in 9.6 suggests they are caused by a buried Tertiary igneous centre. In the examples discussed below, gravity and magnetic profiles across the Dromore Intrusion have been used to demonstrate the application of Wiener filters to the resolution of anomalies.

The magnetic profile over the intrusion (Fig. 8-6) is dominated by the effects of a reversely magnetized Tertiary dyke swarm which obscure the anomaly due to the intrusion. Following the theory given in Chapter 6 it has been possible to design an optimum Wiener filter

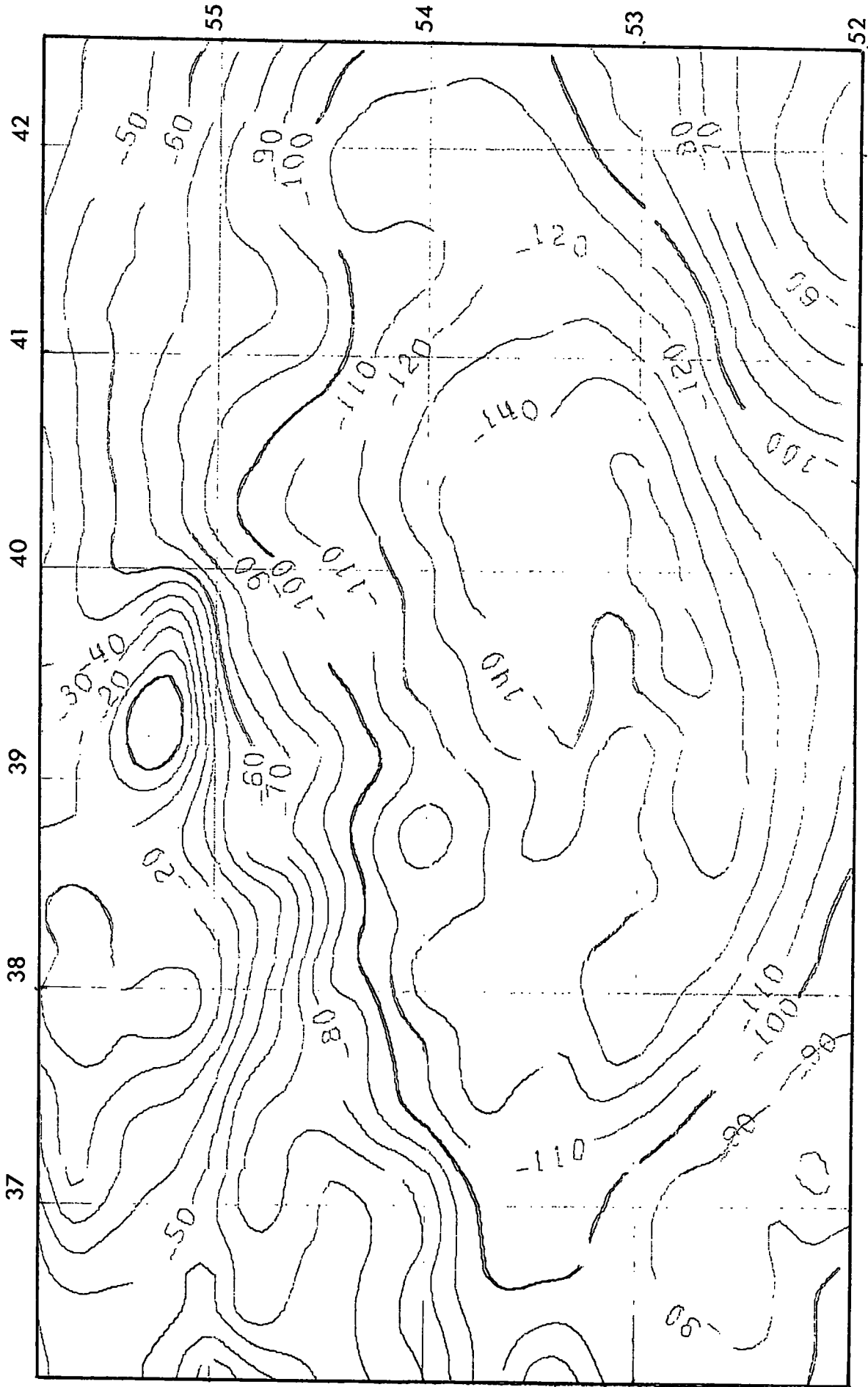


Fig. 3-5 Magnetic field over the Heavale Granite after the application of an optimum Wiener filter designed to remove the white noise from a prism, depth to top 0.4 km., depth to bottom 10.0 km., north-south width 30 km., and east-west width 40 km., magnetization 0.001 emu. in direction of the earth's field. The noise was modelled by a unit spike. The noise reduction factor used  $\gamma = 1,000,000$ .

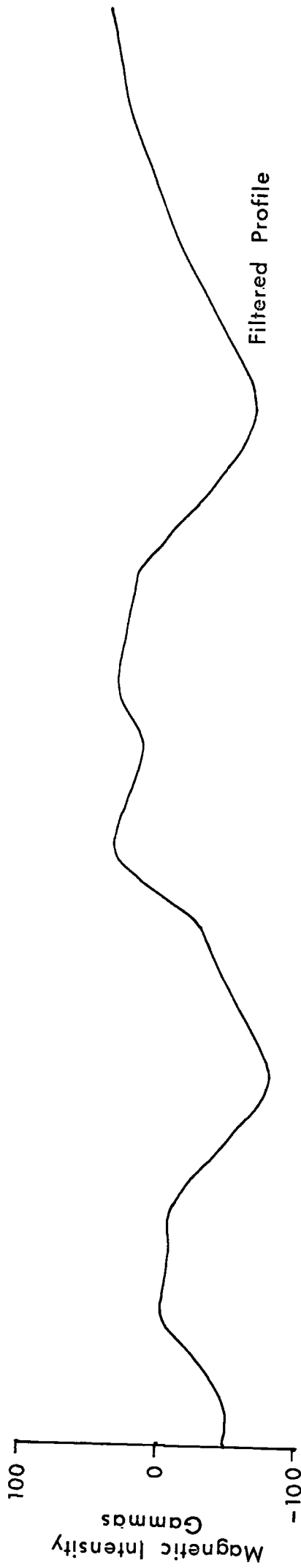


Fig. 8-6 Example of optimum filtering applied to a magnetic profile across the Drexmore Intrusion. The filter was designed to separate the effects of thin infinite (N<sub>0</sub>) of arbitrary dip and direction of magnetization, outcropping at ground surface, from the effects of a 20 x 20 km. width with top surface at 0.5 km. and bottom at 10 km., magnetized by induction in the earth's field. The magnetization of the dikes and the patterns was assumed to be the same.  $\theta = 0$ , inclination  $I = 49.6^\circ$  and  $M = 0.141946$ . Each data point is a mean of 100 observations.  $\sigma = 0.01$  and  $\sigma_{opt} = 0.005$ .

to suppress the effects of these dykes and to enhance the effects of the intrusion.

The signal to be enhanced was specified as the profile over a magnetic prism with depth 0.3 km., width 25 km. and vertical thickness 10 km. These parameters were estimated from the quantitative interpretation of the gravity anomaly in 9.6.

The noise was specified as the magnetic field over a 0.1 km. thick, vertical, vertically magnetized dyke with its top at ground surface. The shape of the autocorrelation function of such a dyke is the same as the average autocorrelation function of a random series of dykes such as cause the noise on the profile.

The filtered profile shown in Fig. 8-6, in which the effects of the dykes have been successfully removed, confirms the validity of the models used to calculate the optimum filter coefficients.

The remaining examples in this section demonstrate the high pass filtering effects of downward continuation and vertical gradient operators. The design of such filters was described in Chapter 4.

Fig. 8-7 shows a gravity profile over the intrusion along the same line as the magnetic profile. Several bulges on this profile suggest the presence of other bodies besides the intrusion. The gravity field continued down 1 km. (Fig. 8-7) effectively resolves these anomalies and allows a better appreciation of which effects are due to the intrusion and which are not. Although the continuation distance is greater than the depth to the top of the body interpreted in 9.6 the continued field has remained stable. This is because a profile across a body with finite lateral extent is being treated and the end effects effectively remove some of the sharpness (high frequency content) from the anomaly.

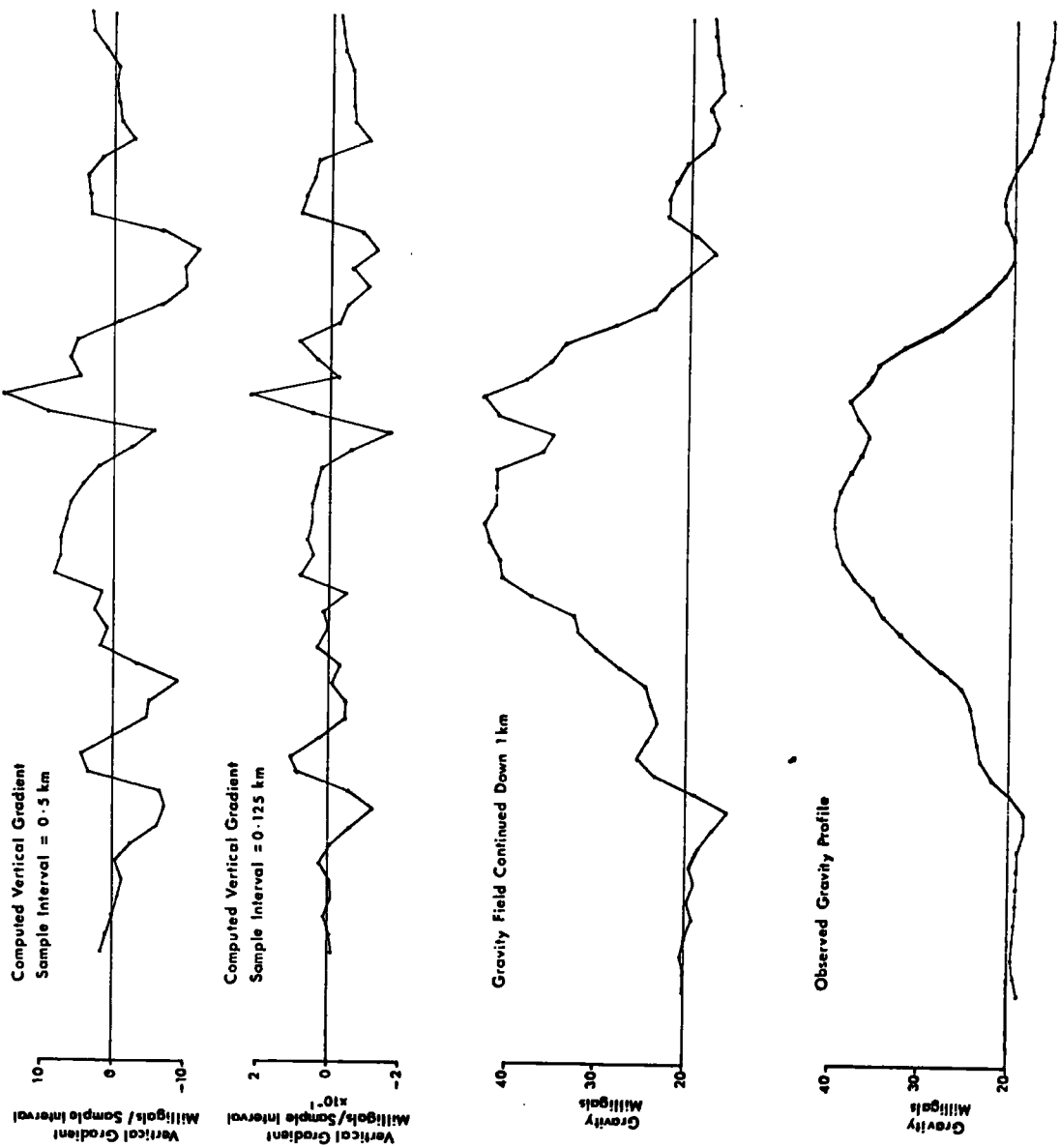


Fig. 8-7 Downward continuation and vertical gradient profiles computed from a gravity profile across the Denver intrusion. High C and coordinates of the profile are the same as in Fig. 8-6.

Also shown in Fig. 8-6 are calculated vertical gravity gradient profiles. Both vertical gradient profiles were computed using the same filter coefficients but with a different effective spacing of the digitized points on the profile. The results demonstrate a little appreciated feature of filter coefficients i.e. the values computed for the vertical gradient are not numerically equal even after the normalizing effect of the sample interval is compensated for. The results are similar however and the discrepancy can be attributed to numerical effects of approximating an integral expression with different sized finite elements. In terms of frequency response, altering the sample interval alters the effect of the filter operator on the different wavelengths because the frequency response of the operator is related to the size of the sample interval.

The vertical gradient profiles have isolated the smaller anomalies noticed on the downward continuation profile and have completely eliminated the effects of the intrusion.

### 8.6 Summary and Conclusions Concerning the use of Wiener Filters for Transforming Gravity and Magnetic Fields

The test examples demonstrated with model and real data show that the Wiener filter method is a simple and accurate method for performing any transformation of a gravity or magnetic field which involves a convolution type operation. Although Wiener filter theory was originally developed for the statistical processing of stationary signals the approximations which have been necessary to adapt the method to processing non stationary signals with finite length operators do not appear to be critical.

In the examples of applying optimum filtering to separate two types of anomalies it has been necessary to assume models for the average signal and noise waveforms. Even though only simple

representations of the true situations have been made the results, which may deviate from the output of an exact optimum filter, provide useful resolution of anomalies.

There are several other possible applications of Wiener filters to the processing of gravity and magnetic fields.

Gravity and magnetic terrain effects are the result of integrations of topographic effects and it would be possible to use the computer programs WIEN1D and WIEN2D to compute such effects by using the modelling principle to obtain suitable coefficients.

Wiener's (1949) original work included the design of interpolation and extrapolation methods and the programs developed could be applied to these uses, however the alternative interpolation and extrapolation routines which have been used in the examples demonstrated appear adequate for gravity and magnetic applications and are simpler to apply.

A separate study of the application of Wiener filters to the processing of electrical and electromagnetic survey results would be worthwhile because the theory is similar to gravity and magnetic field theory and similar transformations should be possible.

## CHAPTER 9

### REGIONAL GEOPHYSICAL INTERPRETATION OF THE MIDLAND VALLEY IN SCOTLAND AND NORTHERN IRELAND

#### 9.1 Introduction

##### 9.1.1 Previous Geological and Geophysical Studies

The Midland Valley of Scotland and Northern Ireland (Fig.9.1) is a graben-like tract approximately 80 km. wide separating the crystalline and metamorphic Caledonian rocks of the highlands from the relatively unmetamorphosed Lower Palaeozoic rocks of the Southern Uplands to the south. The rocks within the area have been subjected to complex phases of deformation and intense igneous activity, much of which is unique to the area.

The aim of this study has been to combine known geology with geophysical data to determine the subsurface distribution of rock types and to attempt to reconstruct the geological history of the region. The area considered in detail is confined to Scotland and Northern Ireland because this is the extent of the detailed geophysical coverage.

General accounts of the geology of the Midland Valley in Scotland are given by Macgregor and Macgregor (1948) and Craig (1965). Charlesworth (1963) describes the geology of the Midland Valley in Ireland. The geology of the relevant areas is shown in the 1:63,360 and 1:253,440 sheets published by the Geological Surveys of Scotland and Northern Ireland. The 1:625,000 and 1:584,000 sheets published by the Geological Survey of Great Britain allow an appreciation of the regional setting of the area.



A summary of the previous geophysical work in the area is given in Appendix 1.

Although the general area has been studied since the days of Hutton, it is only comparatively recently that comprehensive attempts have been made to deduce the regional structure and geological history of the zone. Kennedy (1958) was responsible for the first detailed attempt and mainly concentrated on deformational episodes. George (1960), using stratigraphic evidence, differs from Kennedy in several important conclusions. Anderson and Owen (1968) have produced a summary of previous work and have incorporated some ideas of their own.

Wilson (1966) postulated, using faunal, tectonic and stratigraphic evidence, that the northern and southern parts of the British Isles were once separated by an ocean (the proto-Atlantic Ocean) which has since been destroyed by a continental drifting process in which the British Isles resulted from the welding together of the land masses on different sides of the ocean. Several recent workers have combined Wilson's idea with the concepts of plate tectonics (summarized by Oxburgh, 1971) to produce models for the evolution of the Midland Valley and surrounding areas. These ideas are discussed in 9.3.

#### 9.1.2 Comments on Interpretation Methods Used

##### 9.1.2.1 Qualitative Interpretation

Although the geological history of the Midland Valley is complex, the emplacement of the various rocks and the tectonic events of the area tend to be confined to definite geological episodes. To attempt to simplify the interpretation of the area the data available has been used to produce a series of maps showing the known and postulated features which, in the author's opinion, correspond to these episodes.

These maps, which are discussed in detail in the following sections, show the positions of present day faults in instances where they are considered relevant to the distribution of the rock types. Also shown

on the maps are lines of "magnetic trend". These correspond to regions where there are sharp changes in magnetic gradient, places of maximum gradient, and also where there is a change in the character of the magnetic anomalies. Such effects can be generated by faults, geological contacts or changes in the geometry of the causative body. It has been necessary to use personal judgement in determining these trends. Automated methods for trend analysis of magnetic maps have been attempted by Hall (1964) and Agarwal and Kanasewich (1971) using correlation methods. However the anomalies of the Midland Valley are too small to be adequately digitized for such a method to be applied.

The features postulated on the following sheets are the result of an interpretation and must be regarded as such. The reasons for the interpretation are given and where possible, quantitative interpretation of the significant anomalies has been performed. Magnetic interpretation of this type cannot be automated and involves a knowledge of the type of magnetic anomalies to be expected for the magnetic latitude of the survey area. Magnetic fields over common geophysical models, such as dykes, thin slabs, and prisms, have been calculated by Vacquier et al. (1949), Reford (1964) and Andreasen and Zeitz (1969) for various angles of magnetization and are useful for gaining a feel for the anomalies to be expected in a particular area.

It is difficult to determine the boundary of a rock from a qualitative interpretation of magnetic data. The position of the maximum gradient (the zero second derivative contour position) is a good first approximation to the edge of a magnetic body and this has normally been used in the interpretation unless other evidence was available.

Transparent overlays of the geophysical maps were prepared at the same scale as the 1:253,440 geological maps and this enabled immediate identification of many of the gravity and magnetic features and in many instances subsurface extensions to the known distributions of rock types

could be made.

It is stressed that the interpretation is a regional study and for this reason it has been necessary to delete many of the smaller features.

#### 9.1.2.2 Quantitative Interpretation

The quantitative interpretation of gravity and magnetic profiles in this study were performed using non linear iterative techniques. Digitized field values were input to computer programs which iterated until the body shape (for a specified number of body corners), magnetization, and a constant background field level, were obtained such that the sum of the squares of the differences between the observed field values and the calculated field values was a minimum for a certain number of iterations. The application of such methods has been studied by Al-Chalabi (1970).

The programs used by the author, viz. OPIM2D, OPIMPR, OPTGPR combine subroutines to calculate the magnetic and gravity effect of arbitrary shaped two dimensional bodies and prisms with MINUIT, an optimization routine developed by CERN (1970).

The author has used the option which incorporates the Rosenbrock (1960) method of rotating co-ordinates and this is considered to give satisfactory results.

The interpretations obtained using such methods are not necessarily correct as it is possible that the convergence has been to a local minimum in the least square error hyperspace. The solutions presented however are geologically reasonable and give an idea of the dimensions of possible structures.

#### 9.1.3 Filtered Aeromagnetic Map of the Midland Valley

Fig. 9-2 shows the aeromagnetic map over the Midland Valley in Scotland and Northern Ireland. This map is characterized over a large part of its area by intense short wavelength anomalies which obscure

AEROMAGNETIC MAP OF  
PART OF GREAT BRITAIN & NORTHERN IRELAND

SHEET 11

200000 E  
GEOLOGICAL SURVEY  
OF  
GREAT BRITAIN

Scale 1:100,000 for actual Four Mile to One Inch

400000 E  
NATIONAL GRID  
DIAGRAM EDITION



800000 N

600000 N

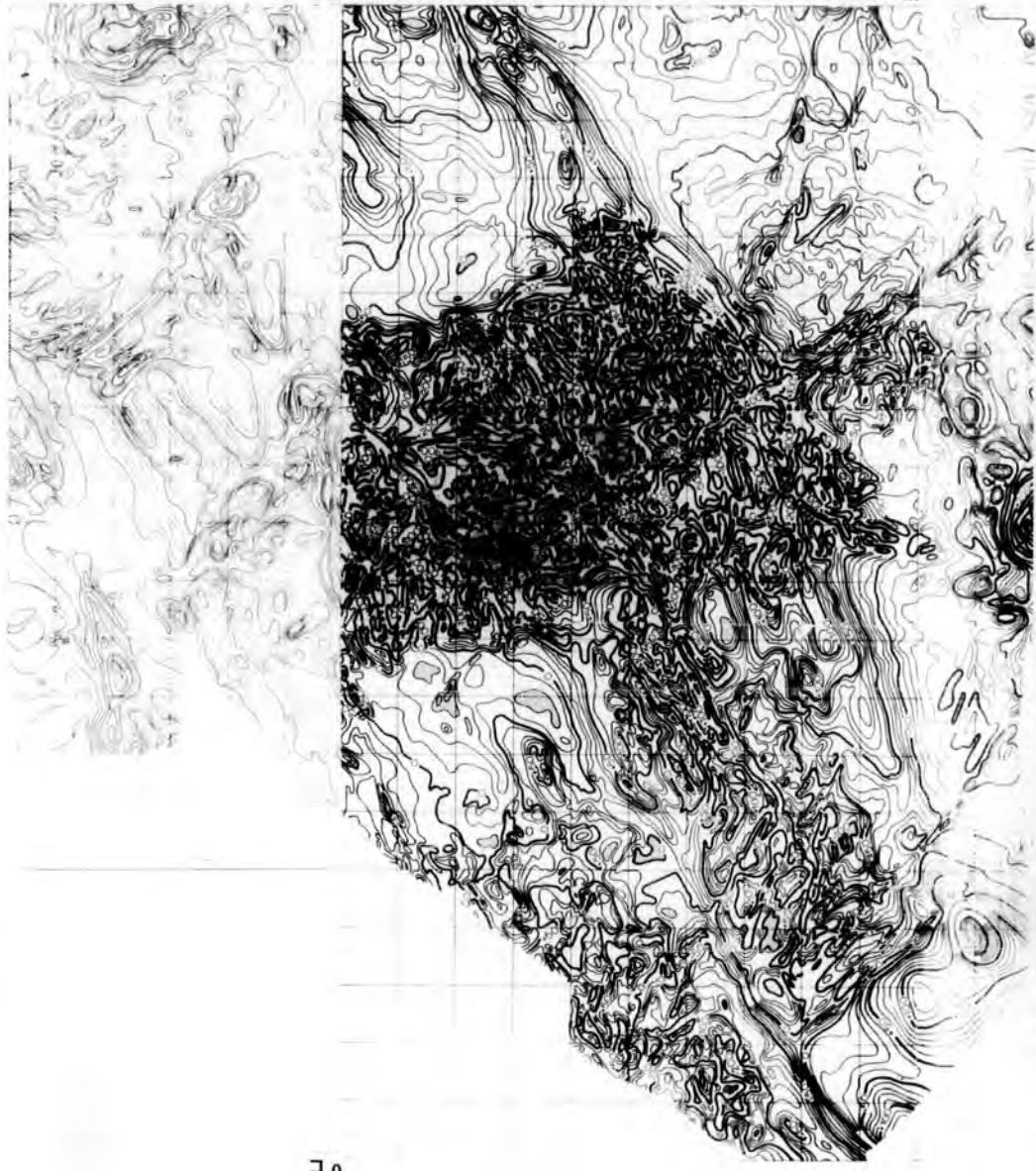
Fig. 9-2a Aeromagnetic map of Scotland

GEOLOGICAL SURVEY  
OF  
GREAT BRITAIN

AEROMAGNETIC MAP OF  
PART OF GREAT BRITAIN & NORTHERN IRELAND

NATIONAL GRID  
DIAGRAM EDITION

200000 E



0 E

600000 N

500000 N

Fig. 9-2b Aeromagnetic map of Northern Ireland



much of the significant detail of the area. These effects are mainly due to near surface lava flows, the most noticeable of which are the Tertiary Volcanics in Antrim, the Lower Carboniferous basalts of the Clyde Valley and the Lower Old Red Sandstone basalts and andesites.

To enable identification of the more important regional features of the aeromagnetic map an upward continuation filtering process was applied to the magnetic data and the resultant map is shown in Fig.9-3. Details of the production of this map are given in Appendix 2. The map approximates the magnetic field continued to a level 2 km. above the flight level of the original survey (which was 1000 feet above ground level). Many significant features have been revealed which will be referred to in the following sections.

Another filtered map of the area has been prepared by Hall and Dagley (1970) which successfully delineates large scale features. This map is considered to be complementary to the author's as the gridding interval and the filter coefficients used are such that the features detected are almost an order of magnitude larger than those in Fig. 9-3.

## 9.2 Lower Palaeozoic Features

The features considered relevant to the Ordovician and Silurian rock distribution in the Midland Valley are shown in Fig. 9-4.

### 9.2.1 Southern Uplands

The Southern Uplands is characterized by a marked linear magnetic high flanked by two magnetic lows. This anomaly was considered in detail in 8.2 and its most likely cause is a smooth rise in a magnetic basement rather than a fault or igneous feature. The nature of the magnetic basement and the sedimentary troughs occurring over the magnetic lows are relevant to the idea of the closing proto Atlantic Ocean and they will be discussed in 9.3.

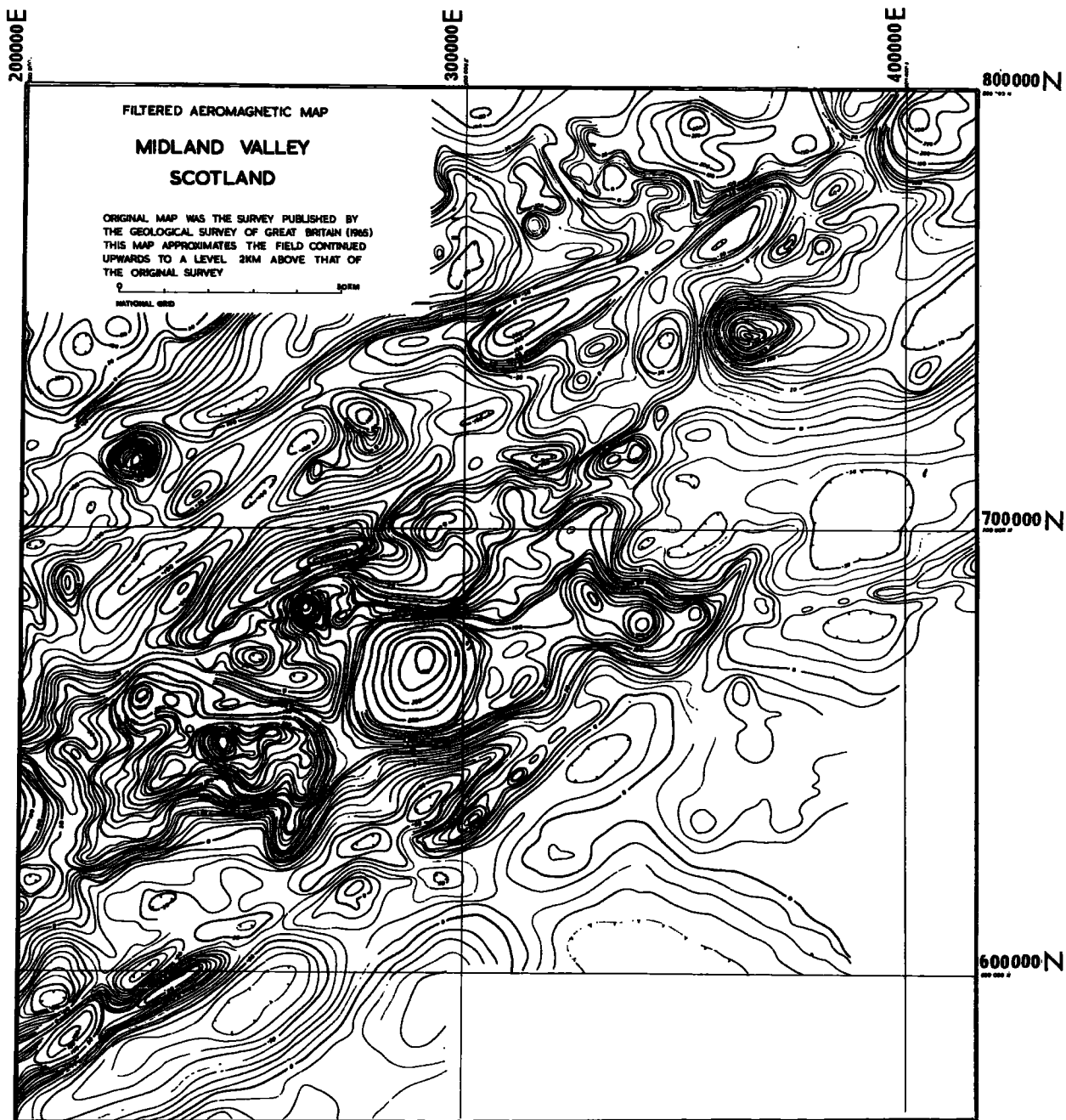
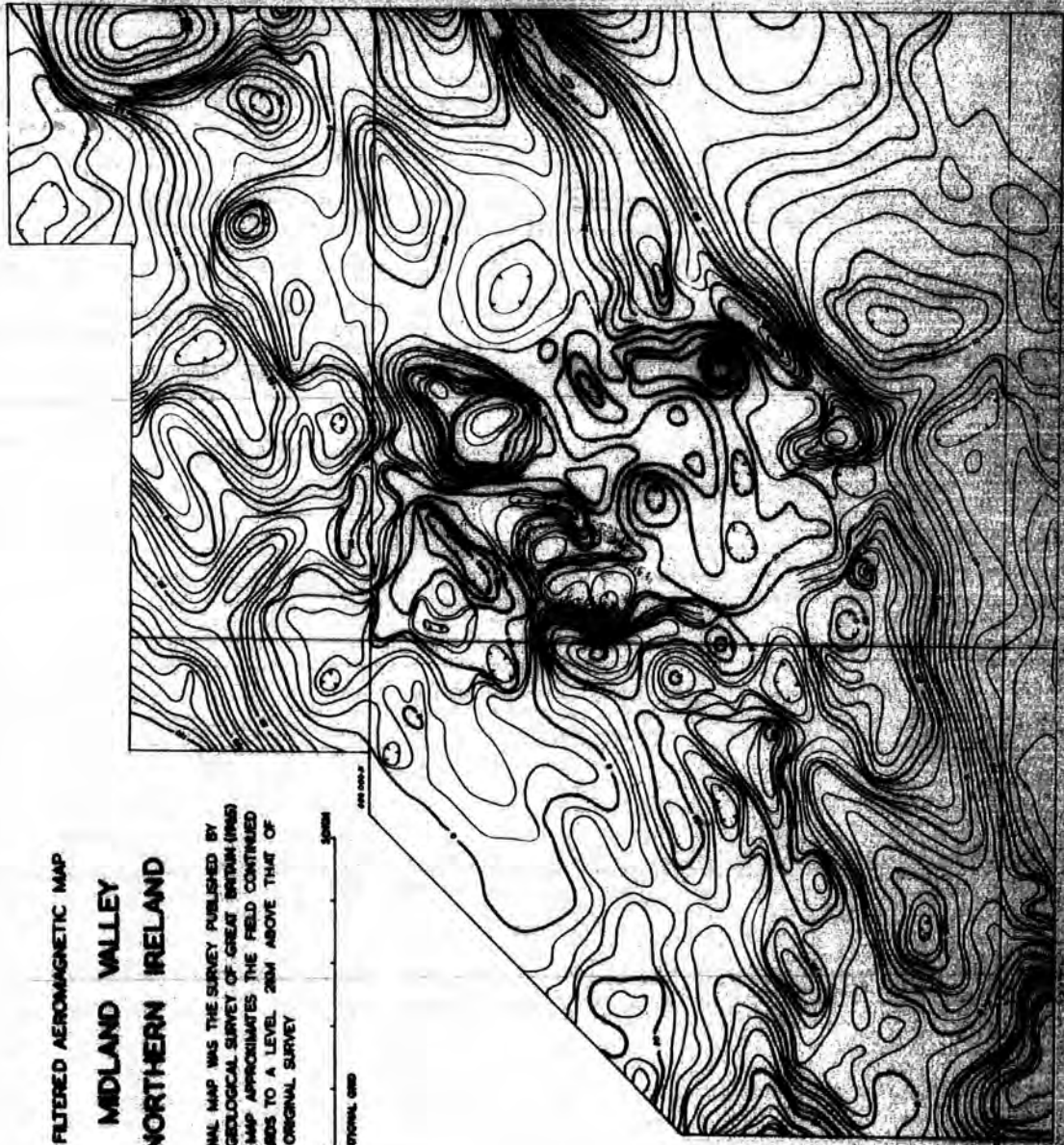


Fig. 9-3a Filtered aeromagnetic map of Scotland  
 (compare with Fig. 9-2a)

**FILTERED AEROMAGNETIC MAP  
MIDLAND VALLEY  
NORTHERN IRELAND**

ORIGINAL MAP WAS THE SURVEY PUBLISHED BY  
THE GEOLOGICAL SURVEY OF GREAT BRITAIN (1968)  
THIS MAP APPROXIMATES THE FIELD CONTINUED  
UPWARDS TO A LEVEL 200M ABOVE THAT OF  
THE ORIGINAL SURVEY





### 9.2.2 Southern Uplands Fault Zone

The Lower Ordovician (Arenig) Ballantrae Igneous Complex (Greig, 1971) consists of a sequence of black shales and cherts overlying spilitic lavas, layered gabbroic rocks and peridotites. This is the classic type-section of an ophiolite assemblage and as discussed by Dewey and Bird (1971) and Coleman (1971), such a sequence corresponds to the vertical section of oceanic crust deduced from geological and geophysical evidence. The current concept is that ophiolite complexes are wedges of oceanic crust, tectonically emplaced by thrusting, scraping or welding, at the positions where lithospheric plates were underthrust at continental margins.

The Ballantrae complex is considered to mark the position of a mobile continental margin which occurred in Lower Ordovician times and although the areal outcrop of these rocks is small they are extremely significant, especially as they appear to be part of a zone, which, from geophysical evidence, extends across Scotland and Northern Ireland.

The Ballantrae complex causes an intense magnetic high which Powell (1970), by ground measurements of susceptibility, has related mainly to the serpentized gabbros and in places to the spilitic lavas. The magnetic anomaly can be traced continuously south westwards into Ireland and this is considered to be a subsurface extension of the ophiolitic rocks.

The Ballantrae gabbros cause a gravity anomaly (5 milligals) which can be seen in the gravity map published by McLean and Qureshi (1966). There is no distinct line of gravity anomalies associated with the proposed ophiolitic rocks in Northern Ireland but consideration of the densities of the rock types occurring indicate that the obscuring effects of near surface low density rocks may be the reason. Fig. 9-5 shows gravity and magnetic profiles across Northern Ireland

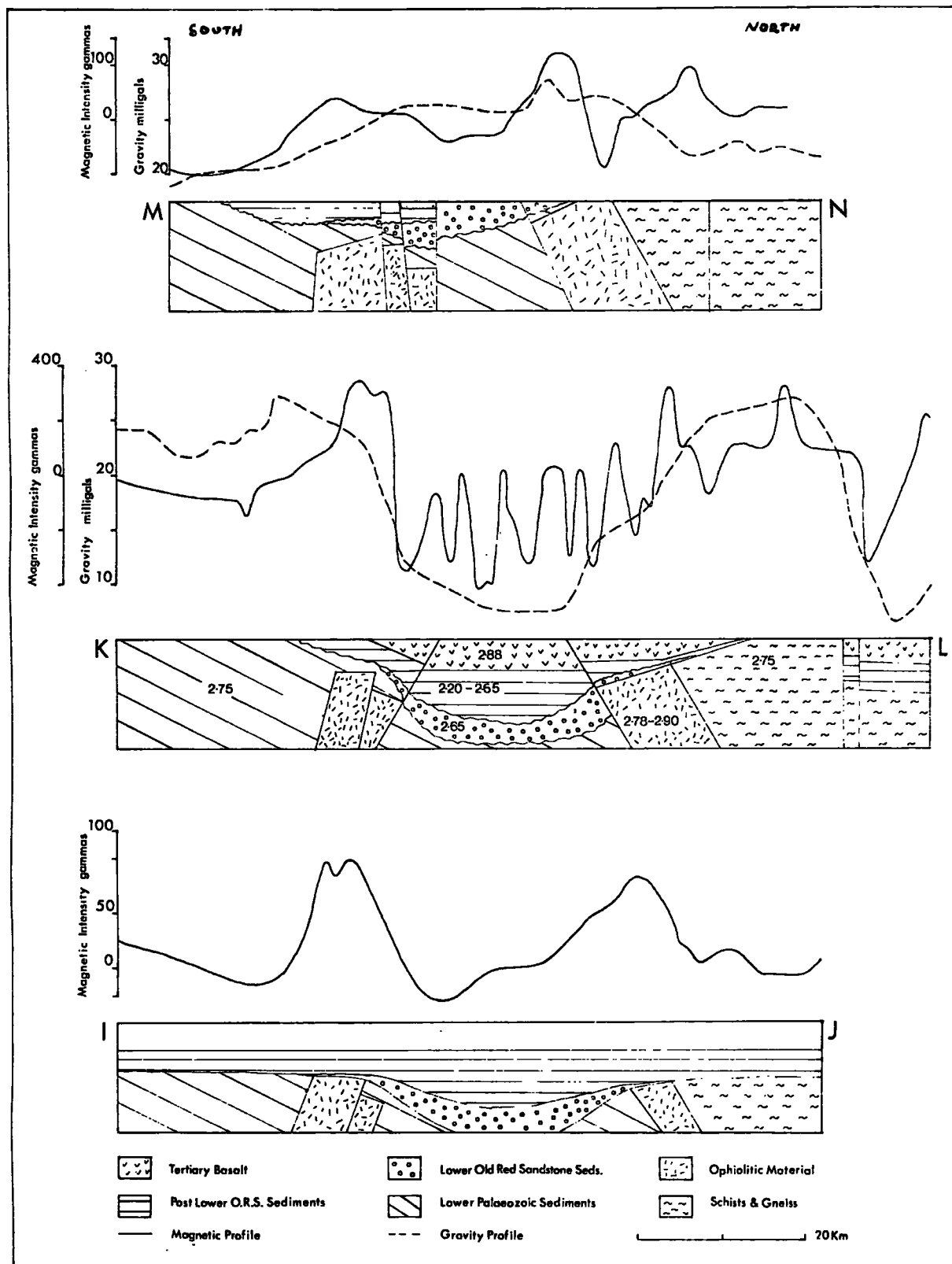


Fig. 9-5 Gravity and Magnetic profiles across Northern Ireland showing possible ranges of density of the rock types present and possible generalized geological cross sections. Approximately 5 km. of vertical section is shown. See Fig. 9-4 for locations of profiles.

and postulated geological cross sections. The density values have been taken from Cook and Murphy (1952) and Powell (1970).

The gravity profile across Antrim is dominated by the low density sediments and salt deposits which have been proved by drilling (Bullerwell, 1964). It is possible, and there is a slight suggestion on the profile, that there is a gravity high obscured by the steep regional gradient on the south side of this gravity low.

Further west in Fermanagh and Armagh there is a general rise in gravity along the postulated line of the ophiolites. The postulated geological section across this area shows how low density Carboniferous sediments may cancel any possible gravity high.

Several distinct trends in the gravity and magnetic map can be correlated with known faults. These are shown in Fig. 9-4.

A quantitative interpretation of the magnetic anomaly in the North Channel (Profile EF) is shown in Fig. 9-6. This interpretation is complicated by the presence of the magnetic low south of the Southern Uplands fault. As has been mentioned by Powell (1970) this low may be partly due to a polarity effect of the bottom of the magnetic rocks but it is also partly due to the effects of the structured low discussed in 8.2.

For the interpretation, the magnetization of the ophiolitic rocks has been assumed to be induced. It is well known (Vine and Mathews, 1963) that rocks of the sea floor acquire a significant permanent magnetization during their formation. There is however a decrease in amplitude of the magnetic anomalies away from the mid-oceanic ridges where they are formed. This suggests a temporal decay of the permanent magnetization of these rocks and Banerjee (1971) has suggested a possible viscous decay mechanism. For this reason it is considered that any permanent magnetization of the Ordovician ophiolites would now be negligible.

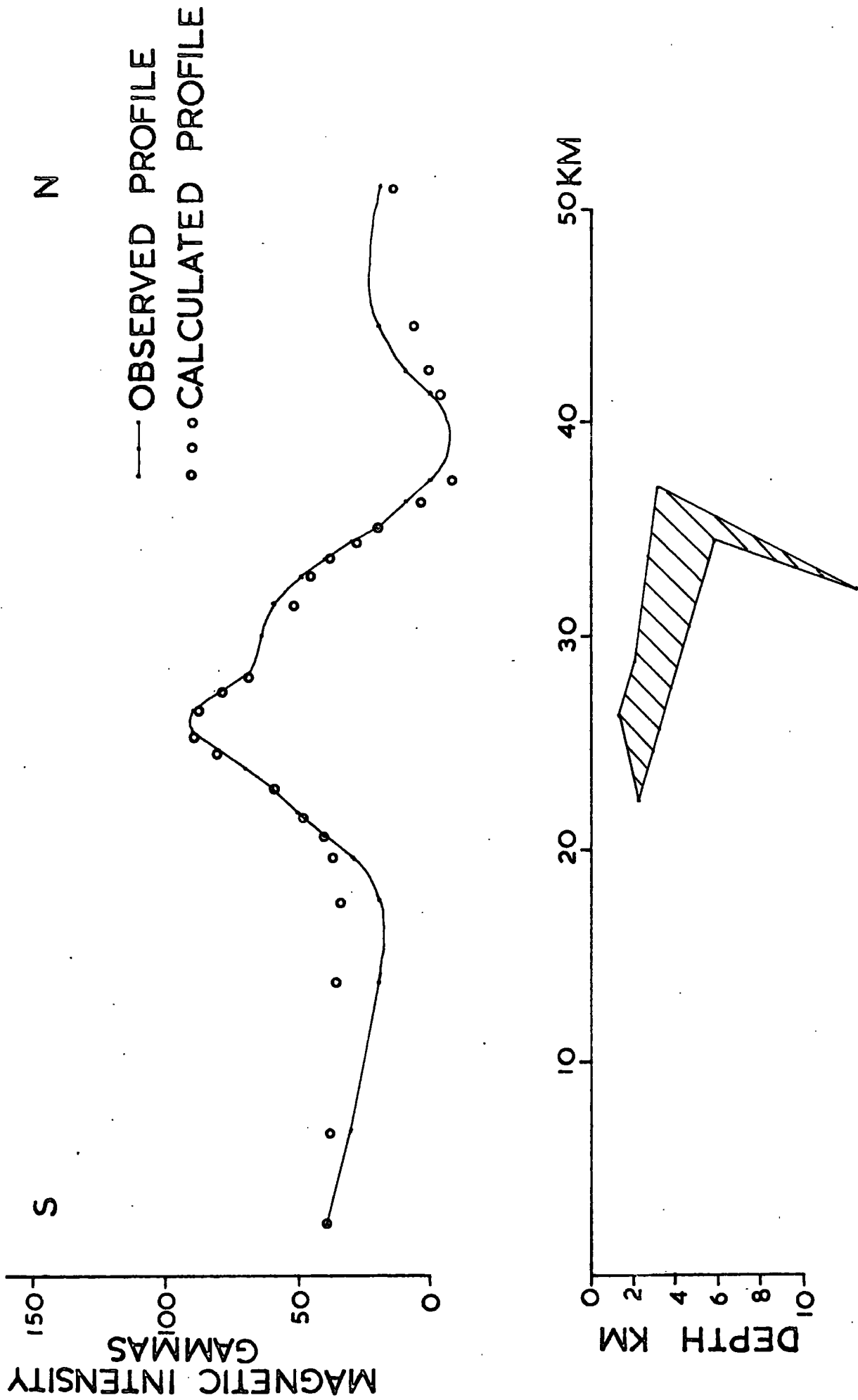


Fig. 9-6 Profile EF. A possible interpretation of the magnetic high along the line of the Southern Uplands fault in the North Channel. Magnetization of the body is 0.0003 emu. National Grid co-ordinates of the end points of the profile are NW580390 and NW500660.

The computer routine to calculate the 6 sided body whose profile fits best with the observed profile has produced a realistic slab type body dipping northwards. The spike on the bottom of the body is not considered significant. From the appearance of this model and the correlation of faults and trends in Ireland the body is considered to consist of two wedge like rock masses with the northern one faulted to a lower level than the southern one.

The abrupt lateral changes in intensity along this zone are thought to be due to the effects of later NS faulting causing relative displacement between sections of the ophiolitic material.

In several places along this zone intense local magnetic anomalies occur and over the land areas these generally coincide with slight gravity highs. None of these are well enough defined for a quantitative interpretation to be attempted and there are several possibilities for their origin. They may be fragments of gabbro faulted to a relatively higher level than in the surrounding ophiolites. This is what appears to have happened at Ballantrae. They may also be caused by localized thickening in the spilitic lavas originally deposited in depressions in the sea floor. Such thickenings of lava are known to account for many of the local magnetic anomalies of the ophiolitic Troodos Igneous Complex of Cyprus (Gass, 1972).

The magnetic anomalies in the zone which continues north eastwards along the Southern Uplands fault from the Ballantrae area can be closely correlated with outcrops of Old Red Sandstone lavas and these are considered to be the main cause although this does not preclude the presence of ophiolitic material at depth.

A narrow intense magnetic peak occurs along the line of the Southern Uplands fault extending north-westwards from Biggar. This anomaly is

similar in form and amplitude to the magnetic anomalies over known occurrences of serpentine intruded up the Highland Boundary Fault plane and it is thought probable that this anomaly is due to serpentine intruded up the plane of the Southern Uplands fault. A profile (shown in Fig. 9-7) has been taken in a N-S direction across this feature at a point where it is relatively isolated. Because of the complicated non-linear regional background a quantitative interpretation has not been attempted but it is obvious that if the magnetization is by induction then the general form of the anomaly corresponds, according to the model curves published by Reford (1964), to a south dipping dyke. Thus the Southern Uplands fault in this region appears to be a thrust from the south.

Continuation of the Southern Uplands fault eastwards from the end of the 'serpentine anomaly' is tenuous. There is no geophysical evidence for its continuation as the pair of faults reaching the sea near Dunbar. From the alignment of magnetic trend directions it seems to the author that the Southern Uplands fault flexes northwards and, obscured by the more recent volcanic rocks of the Garleton Hills, continues out into the North Sea in a north easterly direction. These trend directions are supported by marine sparker profiles conducted by Eden (1970). Also the large magnetic low of the Southern Uplands continues in this direction.

The elongate magnetic anomaly over the sea (crossed by Profile CD) could be due to another wedge of ophiolitic rocks. An interpretation of the anomaly is shown in Fig. 9-8.

To simplify the optimization process the cause of the anomaly was assumed to be an infinite dipping dyke. As Bruckshaw and Kunaratnam (1963) have shown, the dip of the angle of magnetization and the dip of the dyke are interchangeable in the mathematical expression for the field

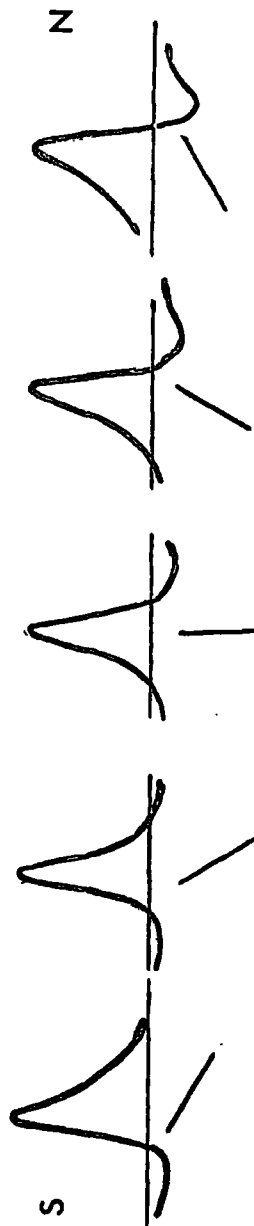
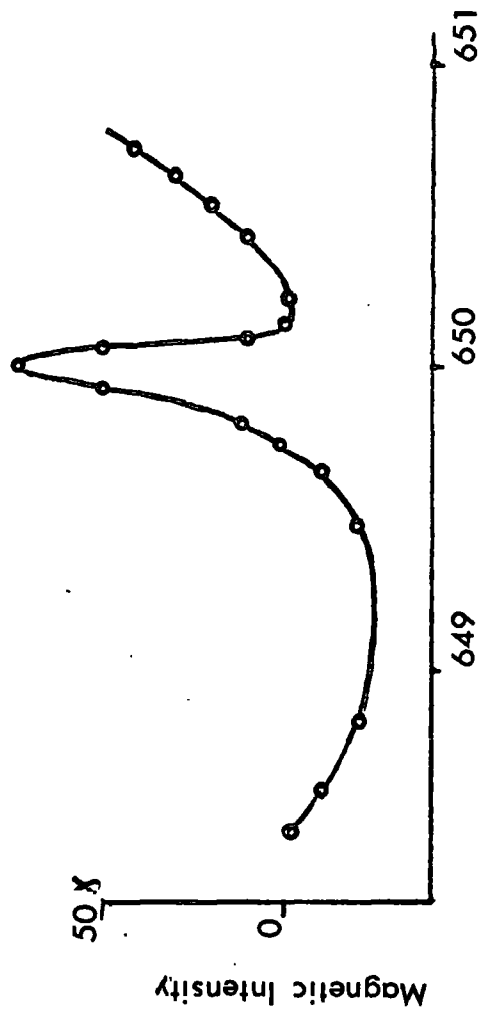


FIG. 9-7 Profile QR Shown below the profile are model profiles over dykes occurring at the same magnetic latitude. The dyke steeply dipping to the south appears to resemble the observed profile the closest. Profile is along National Grid line 320,000E.

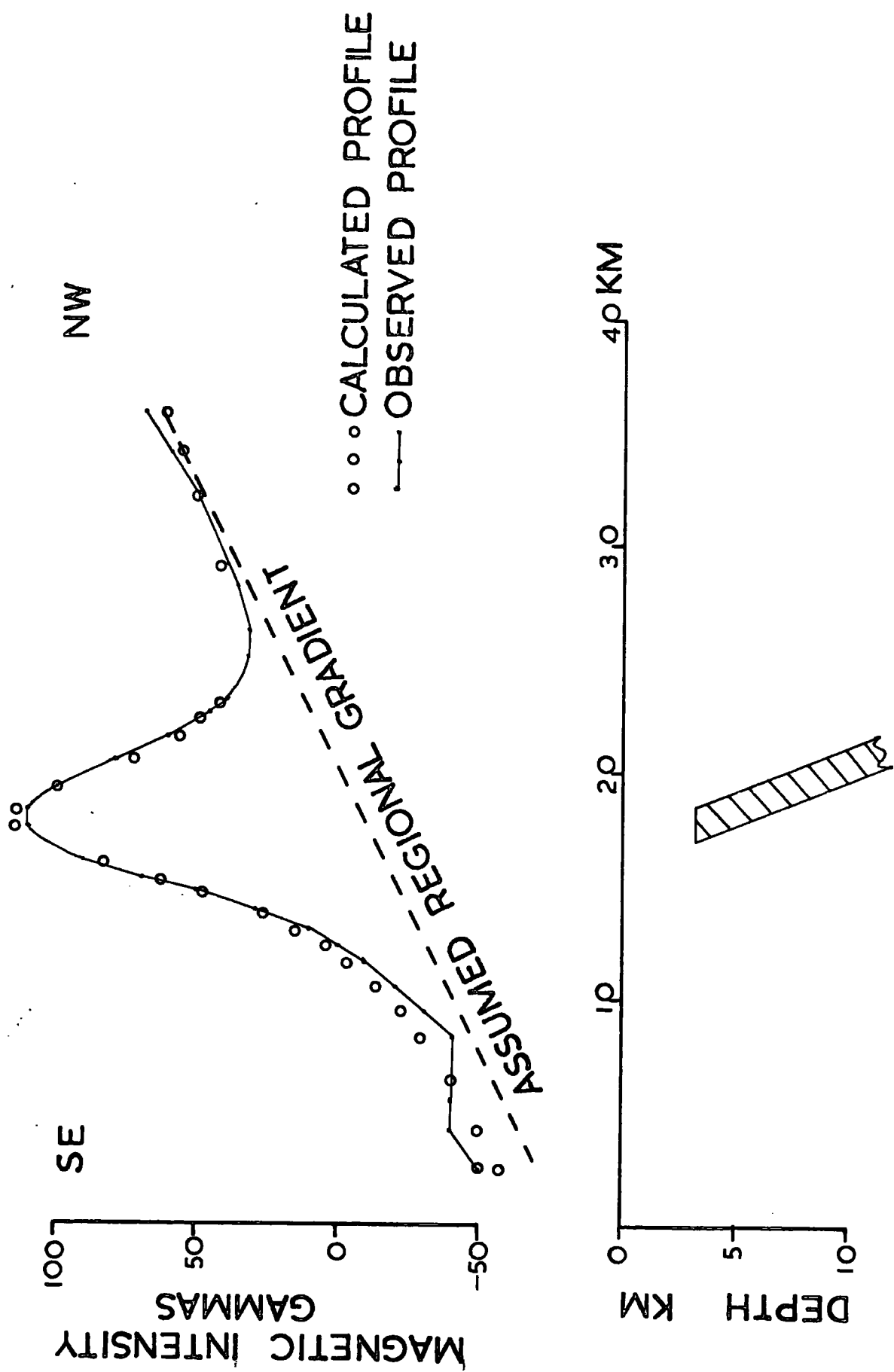


Fig. 9-8 Profile CD. A possible interpretation of the magnetic high along the line of the Southern Uplands fault in the North Sea. Magnetization of the body is 0.00074 emu. National grid co-ordinates of the end points of the profile are NE27540 and NP00035.

over such a dyke. If the dyke is assumed to be vertical with an unknown direction of magnetization then the depth and width of such a dyke can be determined unambiguously by curve fitting methods.

The regional field about the anomaly being interpreted is complicated due to the fact that the anomaly occurs at the junction of the regional magnetic low and the magnetic effects of rocks within the Midland Valley. Attempts were made to let the optimization routine select a regional background at the same time as it interpreted the anomaly. First a quadratic regional was tried and then a linear one. The method failed to converge to a reasonable answer in these situations and it was necessary to assume a regional gradient and to let the program calculate the optimum vertical dyke and constant background level of the field. By assuming induction in the earth's field the dip of the dyke was then calculated.

Thus the Southern Uplands fault appears to be the southern boundary of a zone of semi parallel faults bounding lenticular shaped wedges of ophiolitic material. Such a pattern is entirely consistent with what would be expected at a zone of underthrusting where ophiolitic material is tectonically emplaced.

It should be noted, as reviewed by Anderson (1965), the only firm evidence for the location of the Southern Uplands fault in Ireland is given by the geophysical data.

### 9.2.3 Highland Boundary Fault Zone

The Highland Boundary fracture zone in Scotland, described in detail by Anderson (1947), is marked along most of its course by serpentine intrusions which can be identified on the aeromagnetic map as sharp linear magnetic highs. The form of these anomalies in many places is consistent with that of a dyke dipping northwards and this implies that the present attitude of the Highland Boundary fault

corresponds to a thrust from the north. This conclusion agrees with the work of Ramsay (1964), who by studying deformed Lower Old Red Sandstone pebbles concluded that the main movement of the Highland Boundary Fault was a thrust in Middle Old Red Sandstone times. This thrust may well have been along the line of a thrust originally developed in Arenig times as suggested by Kennedy (1958).

The thin zone of rocks of the Highland Border, described by Anderson (1947) as spilites, black shales, and cherts, fit the description of ophiolitic material and suggest that this area may have once been a zone where oceanic material underthrust continental material.

Alternative explanations are possible for the position of these rocks. Shackleton (1958) suggests that the Arenig rocks of the Highland Border may have been thrust into their present position on an overturned limb of the Tay Nappe. Johnson and Harris (1967) have compared the folding style, orientation and direction of facing of the Dalradian and Arenig rocks and from similarities they conclude that both these rocks have undergone the same movements. This evidence supports the ideas of Shackleton. Borradaile (1972) has suggested that the Highland Border spilites may correlate with similar rocks he has mapped at Loch Avich within the Highlands. Nevertheless it is still possible that the Highland Border Arenig rocks were emplaced in an underthrusting process which caused the observed isoclinal folding.

The Highland Boundary Fault can be traced to the Isle of Bute but its extension further west is neither geologically nor geophysically obvious. The classical path of the fault, as drawn in most references to the area, is either through or around Arran and then between the Mull of Kintyre and Sanda Island, entering Northern Ireland at Cushendall. Recent unpublished marine gravity, magnetic and sparker work by McLean et al. of the Geology Department of the University of Glasgow has shown

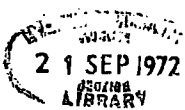
that there is no geophysical evidence for the Highland Boundary fault along this line. They conclude that the fault is stepped south along a series of north south faults. Suggestions of the existence of such faults can be seen on the aeromagnetic map. McLean et al.'s results are extremely significant and as an extension to their ideas the author proposes that, in keeping with the idea that the Highland Boundary marked a zone of underthrusting, the southwards offset of the fault line may be due to a tear in the lithospheric plate at this point. The Tertiary Igneous complex of Arran may have been intruded up this line of weakness.

Profile GH over the magnetic anomaly in the North Channel has been interpreted in Fig. 9-9. The interpretation of this anomaly has been complicated by surrounding anomalies but the general form of the shape obtained is consistent with a wedge of ophiolitic material. As this anomaly lines up with what is considered to be the Highland Boundary Fault in Ireland it is considered to be part of the same zone.

The Highland Boundary Fault is considered to enter Northern Ireland at Cushendall (Charlesworth, 1963, p.128) and its extension further west is thought to be marked by the fault between the Tyrone Igneous Complex and the Dalradian rocks to the north.

The rocks of the Tyrone Igneous Complex have been described by Hartley (1933) and more recently in greater detail by Cobbing, Manning and Griffith (1963) and Cobbing (1964). They consist of black shales and cherts overlying spilitic lavas and layered gabbros and thus appear to be ophiolitic. They also have small stocks of granite intruded into them, similar to the small granite intrusives of Ballantrae.

There is a definite zone of high magnetic and gravity values over this area and the south westwards continuation of the anomalies suggests a subsurface continuation of the Tyrone igneous rocks in this direction.



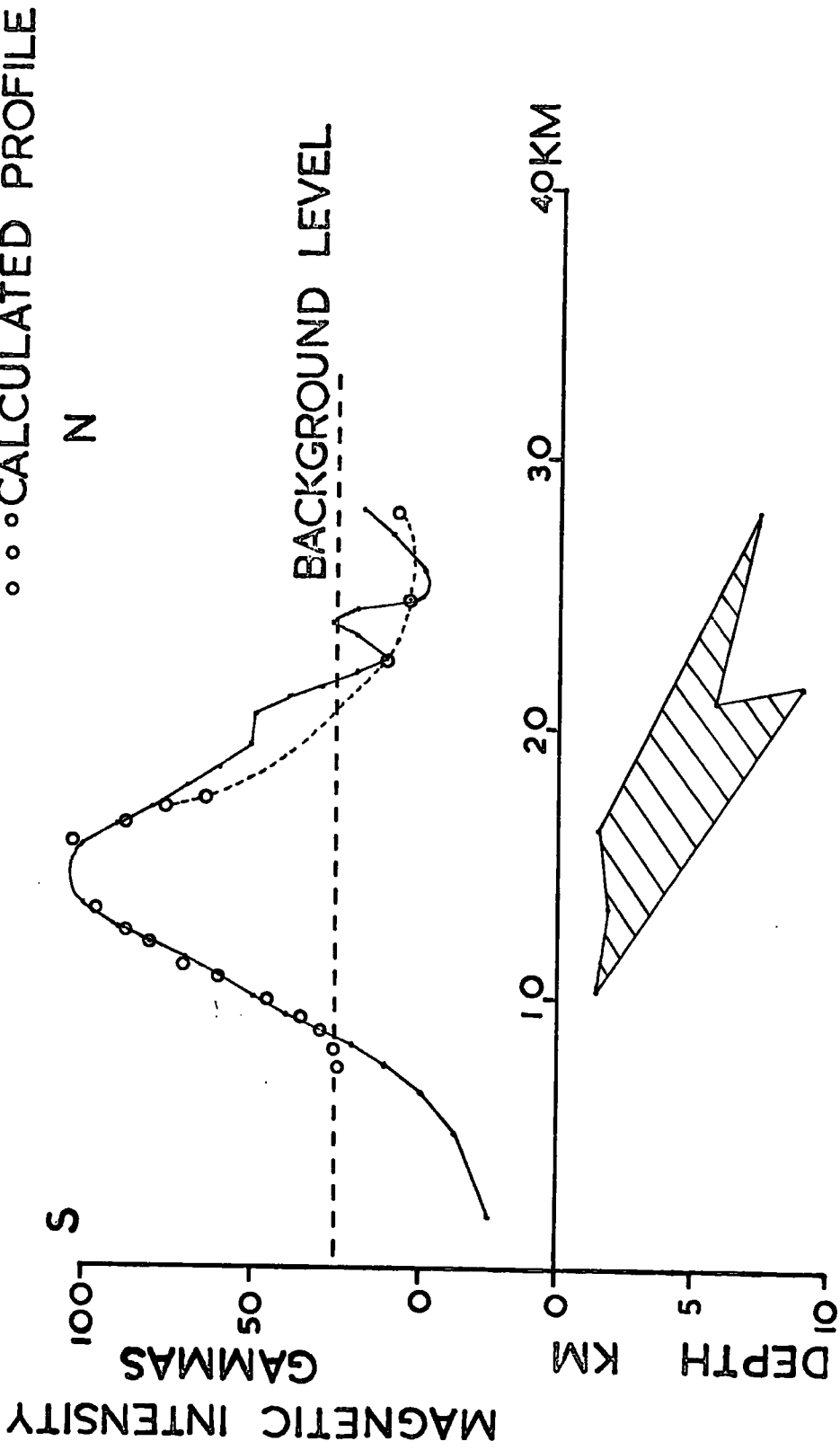


Fig. 5-9 Profile III. Possible interpretation of the magnetic high along the line of the Highland Boundary Fault in the North Channel. Magnetization of body is 0.0033 emu. National Grid co-ordinates of end points of profile are M650900 and NR690155.

Murphy (1952) has also made this suggestion. This continuation is obscured to some extent by the magnetic effects of a Tertiary dyke swarm and the gravity and magnetic effects of a large sub circular anomaly (the Dromore Intrusion) thought due to a Tertiary igneous centre which did not reach the surface (see 9-7).

Along the line marked by Upper and Lower Lough Erne the character of both the magnetic and gravity field changes abruptly and this probably corresponds to a fault line.

Along the southern boundary of the Tyrone Igneous complex is an intense magnetic high which appears too sharp to be a polarity effect of the southern margin of these rocks. As this zone corresponds with a linear belt of gravity highs the source rocks may be gabbro or peridotite. From the geology mapped by Cobbing (1964) the spilites, shales, and cherts occur to the north of the outcrop and the layered gabbros occur along the southern margin. Thus it seems that the ophiolite section has been tilted on its side with its top to the north. In such circumstances a band of gabbro or peridotite would be expected in the region of the linear anomalies.

The narrow intense anomaly can be traced beneath the Tertiary Antrim plateau basalts to the east. The continuation of the ophiolitic rocks of the Tyrone Igneous complex eastwards under the Antrim lavas is also suggested by a faint trend of gravity highs and the trend of other magnetic highs. The upward continuation map suggests a magnetic discontinuity along the southern margin of this zone. The map of the sub-Cretaceous basement published by Charlesworth (1963) p.353 also suggests a zone of faulting along this line.

It is reasonable, within the context of plate tectonics, to expect the ophiolitic rocks of the Highland Border to mark a zone of northwards underthrusting. Such a possibility raises the question of the 'Tyrone

Central Inlier' which is an area of Dalradian metamorphic rocks entirely surrounded by the ophiolitic rocks. The relationship between the two groups of rocks is uncertain (Cobbing et al., 1963, Cobbing, 1964). If this region is a zone of underthrusting then it is possible that this inlier has ophiolitic material beneath it. The grade of the metamorphism within the Dalradian rocks of the inlier is higher than in the Dalradian rocks to the north and this has been taken by Cobbing (1964) as proof that the Highland Boundary fault is a normal fault and that vertical movement on its southern side has brought the deeper, more metamorphosed basement to the surface. However even if some vertical movement has occurred this is not inconsistent with the idea of underthrusting along the Highland Border.

Fig. 9-5 shows gravity and magnetic profiles across both the northern and southern belts of postulated ophiolitic material and possible geological cross sections. It can be seen that in general comparable anomalies occur in the two regions. Because of the complicated shapes possible, the interfering effects of other rock types and the known irregular composition of ophiolitic rocks, detailed analysis of these profiles has not been attempted.

The Highland Border ophiolites appear to be of Arenig to Llanvirn age (Downie et al., 1971) although it is possible that some of the lower members have an Upper Cambrian age. The exact age of the Tyrone igneous rocks, which were shown above to be part of the same zone, is not definite either although a graptolite found by Hartley (1936) suggests a Llandeilo age for the shales. The underlying spilites could well be of Arenig age. If the shales and spilites originated on an oceanic sea floor in Arenig-Llandeilo times the pre Caradocian folding in these rocks (Kennedy, 1958) could have occurred during the underthrusting along the Highland Border.

An Arenig age for the Ballantrae ophiolites is well established (Greig, 1971) and the post Arenig, pre Caradocian folding in these rocks could also have occurred during underthrusting.

Thus, although there is some uncertainty in the exact dates it is likely that the northern and southern belts of ophiolitic material which flank the Midland Valley were formed contemporaneously.

### 9.3 Relationship of the Midland Valley to the Proto-Atlantic Ocean

#### 9.3.1 Introduction

Following the stimulus given by Wilson's (1966) idea of a proto-Atlantic Ocean and the possible mechanism for its closure suggested by plate tectonics, the geology of the central British Isles has been re-appraised by Dewey (1969), (1971), Dewey and Pankhurst (1970), Fitton and Hughes (1970), Ziegler (1970) and Bird, Dewey and Kidd (1971) who have related the igneous, stratigraphic and structural features of the area to the motion of lithospheric plates being thrust under continental land masses as the continents converged.

The case for a plate being thrust northwards under the Scottish Highlands has been convincingly postulated by Dewey and Pankhurst (1970) to explain some of the orogenic and igneous features of the area. Fitton and Hughes (1970) have shown from petrochemical analyses that the regional variation in magma type in the Ordovician volcanic rocks of England is consistent with that produced from a plate thrust southwards.

The author agrees with Wilson's (1966) hypothesis and with the ideas that oceanic crust was overridden from the north and south. None of the above authors however have considered any geophysical evidence nor the relationship of the Midland Valley to their models in any detail. This section critically examines their ideas in this context.

### 9.3.2 Dewey's Model and its Problems

Dewey (1971) describes a model for the Lower Palaeozoic evolution of the Highlands, the Midland Valley and the Southern Uplands in which, during the ocean closing process, oceanic crust was destroyed by underthrusting along two diverging Benioff zones; a northern one which occurred along the southern margin of the Midland Valley and a southern one which occurred just north of the Lake District (Fig. 2 of Dewey (1969)). The Southern Uplands according to this idea, overlies a remnant of oceanic crust.

Ziegler (1970) considers that an Ordovician geosyncline immediately south of the Southern Uplands fault (the Moffat Geosyncline) and a Silurian geosyncline just north of the Lake District locate the positions of the zones of underthrusting of Dewey's model.

There are severe objections to considering the Southern Uplands as an area underlain by oceanic crust in Ordovician times.

Powell (1971), reviewing a range of geophysical interpretations points out that the evidence indicates the Southern Uplands are underlain by a crust of normal continental thickness (30 km) and that thickening by compression from an oceanic crust (average thickness 7 km) is unreasonable. Powell (1971) omitted to mention the work of Agger and Carpenter (1965) who have analysed several crustal seismic refraction profiles (their locations are shown in Fig. 9-10). Their estimates of crustal thicknesses in the area however confirm the results mentioned by Powell (1971). Thus if the Southern Uplands were originally oceanic then this wide area (100 km) must have since been converted to continental material and there is no obvious reason, according to Dewey's model, why this should have happened.

Andesite volcanics (of Caradocian age) occur at Bail Hill near Sanquar within the Southern Uplands (Eyles in Pringle, 1948).

Andesites occur over regions where oceanic crust underthrusts continental

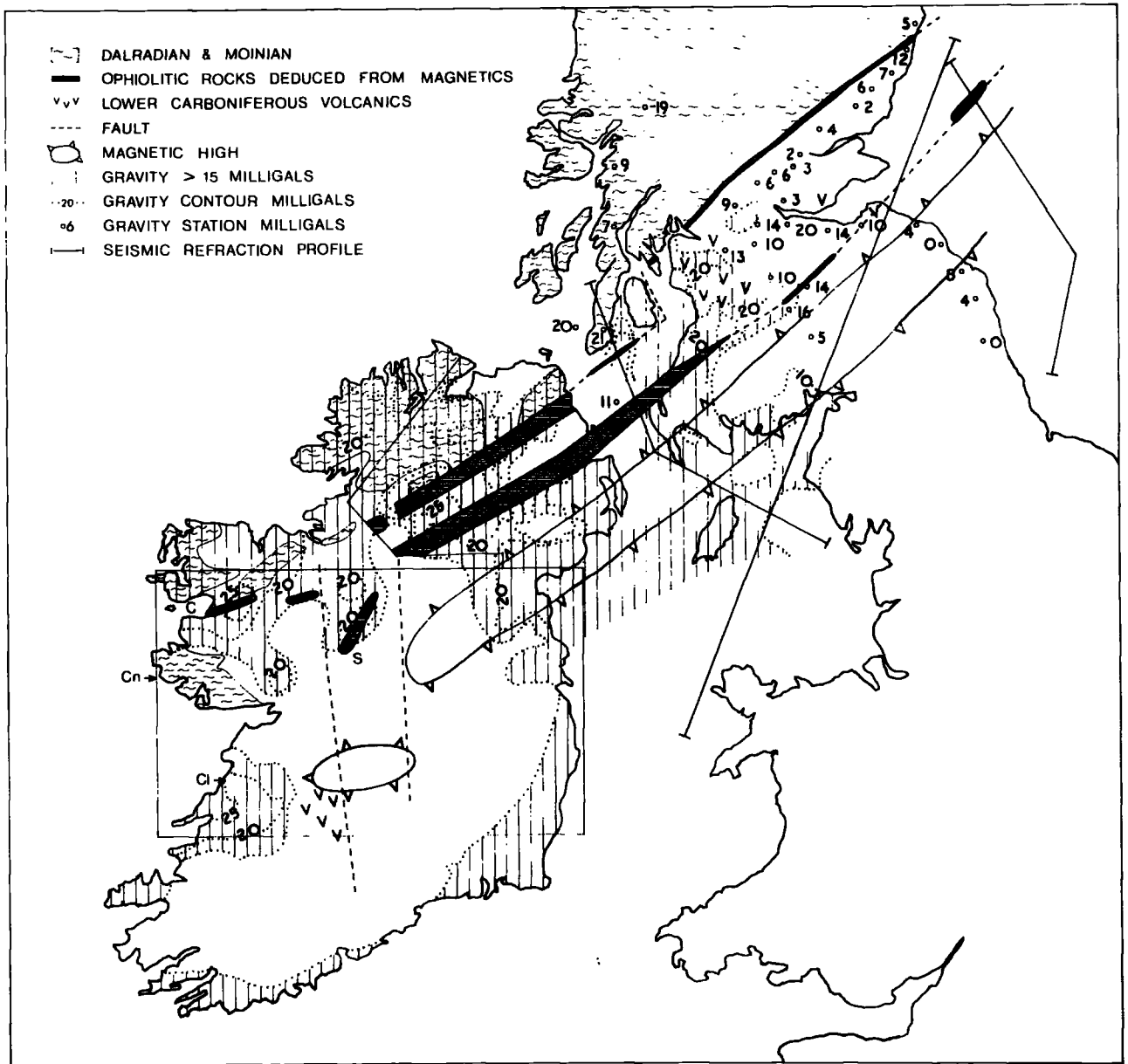


Fig. 9-10 Regional synthesis of data relevant to the location of the Midland Valley. Area outlined in Northern Ireland shows the extent of the aeromagnetic survey. Area outlined in Central Ireland shows the extent of ground magnetic surveys. All of Ireland has been covered by gravity surveys but for simplicity only the contours over 15 milligals are shown. C = Clew Bay, S = Stokestown Anomaly, Cn = Connemara, Cl = County Clare gravity high.

crust (Wright, 1971). Dewey (1971) admits that the Bail Hill rocks would not be expected over an area of oceanic crust and postulates their present position to be the result of a moving sea floor. It is difficult to imagine this happening with Dewey's model because the andesites occur between two plates being underthrust in different directions away from the andesites.

Dewey does not adequately explain the presence of the Highland Border ophiolite suite. The interpretation above has shown these to form an extensive zone with the Scottish belt being stepped south near Arran and then continuing underneath the Antrim lavas to the relatively complete ophiolitic sequence of Tyrone.

Dewey (1971) imagines the Midland Valley to form a shelf between the Highlands and the Southern Uplands. Seismic reflection studies over the Peru-Chile trench (Scholl, 1970) show a shelf type block occupying a position similar to Dewey's model of the Midland Valley so the basic idea appears reasonable. It is conceivable that the Highland Boundary serpentines were intruded up a major crustal fracture but it is difficult to account for the black shales, cherts, spilites and layered gabbros unless they are wedges of ophiolitic material emplaced at a zone of underthrusting.

The similar age of the two zones of ophiolitic rocks appears to preclude the possibility that the northern belt marked an earlier subduction zone which was later stepped south.

The Southern Uplands is characterized by extensive Lower Old Red Sandstone granite intrusions (Greig, 1971) which would be expected over an area of continental crust rather than oceanic crust.

The diagrammatic representation of the gravity field over the area of interest, shown in Fig. 9-10, has been prepared from previous compilations (De Bruyn (1955), Charlesworth (1963) p.175) and from more recent surveys by McLean and Qureshi (1966) and Bott (1968)).

There is no gravity high over the Southern Uplands such as would be expected over a thin oceanic crust or a crust formed from dense basic material. The Midland Valley however, as noted by McLean and Qureshi (1966), does coincide with a large regional gravity high which is much greater if the low density sediment infill of the Midland Valley is compensated for. Similarly there is a gravity high over the Midland Valley in western Northern Ireland. As mentioned previously low density sediments and salt are probably responsible for the gravity low over Antrim. The gravity high within, and on the flanks of the Irish Sea is probably caused by thin crust (Bott, 1968), possibly resulting from the present day continental drifting of Europe from America.

The objections to Dewey's model and the indications, from gravity, that a thin or dense crust occurs beneath the Midland Valley have induced the author to consider the possibility that the Midland Valley may mark the suture left during the ocean closing process.

### 9.3.3 The Midland Valley as an Oceanic Remnant

If the Midland Valley overlies the junction between the two continents, originally on either side of the proto-Atlantic Ocean, then the two belts of ophiolitic material are simply evidence for two zones of underthrusting of lithospheric plates, one to the north along the Highland Boundary and one to the south along the Southern Uplands fault. The evidence discussed above suggests that both the Highland Boundary fault and the Southern Uplands fault are reversed faults. A graben, flanked by reversed faults, pushed down by compression between two continental masses would act as a sediment trap in exactly the same way as the Midland Valley has done.

The gravity high over the Midland Valley does not necessarily mean that it is underlain by oceanic crust at the present day as it may indicate continental crust which has incorporated large amounts of basic material, possibly by a viscous spreading of the adjacent

continental crust into the space where the oceanic would occur. Such a spreading mechanism has been postulated by Bott (1971) in a different context.

The extremely active Lower Old Red Sandstone and Lower Carboniferous volcanism, which is largely confined to the Midland Valley area (Craig, 1965) could be the result of a thin crust or a largely basic crust. Squeezing or the viscous flow mechanism postulated above could have initiated the volcanism. Xenoliths of gabbro (Francis, 1965) and ultrabasic material (Chapman, 1971) found in Lower Carboniferous lavas may be fragments of the oceanic crust.

Kennedy (1958) has discussed a late Silurian phase of folding which does not effect rocks within the Midland Valley apart from the Hagshaw Hills, Pentland Hills region which can be regarded as part of a zone welded onto the Southern Uplands crustal plate. This late Silurian folding has effected the entire Southern Uplands region and the Lake District (Anderson and Owen, 1968). This evidence suggests that the Midland Valley formed one crustal block and that the Southern Uplands and the Lake District formed another.

Thus the features of the Midland Valley appear consistent with the idea that it, rather than the Southern Uplands, marks the remnant of the proto-Atlantic Ocean.

#### 9.3.4 Reinterpretation of Dewey's Evidence

If Dewey's hypothesis is incorrect then alternative explanations must be found for the features he cites as evidence.

The Ordovician sediments near the southern margin of the Midland Valley consist of shell beds and conglomerates interbedded with grey-wackes and this evidence and sediment transport directions indicate that the area was a rapidly subsiding trough with a shoreline to the north. The obvious interpretation of this shoreline with the Moffat

geosyncline to the south is to regard this as the position where a plate was thrust northwards. However, as Fitton and Hughes (1970) suggest, in the final stages of the closing of the proto-Atlantic Ocean flysch wedges from the rapidly eroding highlands could have completely covered a northern trench along the Highland Border and have formed a shoreline north of Ballantrae. Scholl (1970) mentions that in places the Peru-Chile trench has been completely filled with sediments from the Andes.

The author considers that the Southern Uplands may have formed a broad shelf between the Moffat geosyncline and the postulated island arc at the Lake District (Fitton and Hughes, 1970). A similar situation to that shown in the section across the Puerto Rico Trench, as determined by Talwani, Sutton and Worzel (1959), is envisaged. This would provide a suitable depositional environment for the Upper Ordovician black shales and cherts and occasional volcanism would explain the spilites.

A puzzling major feature is the elongate magnetic high (Fig. 9-10) over the Southern Uplands. The author has performed a quantitative interpretation of this feature (8.2) and considers it to be caused by undulations on a magnetic basement, between depths of 5 km. and 10 km., which has a magnetization of at least 0.001 emu. The deduced depth profile confirms the position of an axial rise and its two flanking depressions which have been deduced by Walton (1965). This structure may reflect broad warping of the crust caused by compression. The late Silurian folding (Anderson, 1965) which caused a series of faulted and folded monoclines was obviously a compressional effect. The Silurian geosyncline north of the Lake District could be the result of sediments deposited in a crustal downwarp rather than in a zone of plate consumption.

The cause of what appears to be a relatively uniform magnetic basement over such a large area is not obvious.

It is conceivable that this layer is a relic of an earlier ocean floor formed before the plate was stepped back to the Moffat trench. Possibly material rising from an underthrust plate could have converted the Southern Uplands to its present continental thickness.

#### 9.3.5 Continuation of the Midland Valley into Western Ireland

Although western Ireland is outside the area of this study, any model proposed for the Midland Valley in Scotland and Northern Ireland must be compatible with the geology further west.

George (1960), Charlesworth (1963) and others have considered that the Midland Valley continues to Clew Bay where Lower Palaeozoic rocks occur in a graben type structure flanked by ultrabasic material. However, an alternative explanation is required if this area is to fit with the closing ocean model, because immediately south of Clew Bay, at Connemara, is a large area of rocks which have been convincingly identified as Dalradian and correlate with those occurring north of Clew Bay (Shackleton, 1961). Dewey (1971) has postulated that the Clew Bay area may mark the position of a marginal basin where oceanic crust was generated behind a zone of plate consumption. The gravity high over the area (Fig. 9-10) is consistent with the idea that it overlies oceanic crust.

On the basis of the sparse geophysical evidence available, Dewey, following the ideas of Leake (1963), considers that the Southern Uplands fault, and hence the position where his plate began its northwards descent, continues from Upper Lough Erne to Galway Bay south of Connemara.

The author agrees with the marginal basin concept but prefers an alternative explanation for the position of the Midland Valley.

In Fig. 9-10 the area outlined in Northern Ireland shows the extent of the aeromagnetic coverage. The area outlined in Central Ireland has been covered by a ground vertical field magnetometer survey (Murphy, 1952).

There is an unfortunate gap in the magnetic coverage in the important area west of Northern Ireland.

The two large north-south faults in Central Ireland (Fig. 9-10) have been postulated by Russell (1968) after a study of the alignment of lead zinc mineralization in the area. Russell did not consider any geophysical evidence and several striking coincidences are apparent. The long magnetic high, after continuing across the British Isles for 300 km. terminates along the line of Russell's eastern fault. These faults also straddle a zone of high gravity and a magnetic anomaly which has become known as the Stokestown anomaly (Murphy, 1952). The faults also approximately straddle a large regional magnetic anomaly further south.

The zone of high gravity over the Midland Valley in Northern Ireland appears to be stepped southwards between the faults in the Stokestown area. There is also a zone of high gravity extending towards the sea in County Clare.

These features suggest to the author that the Midland Valley may have been stepped south around Connemara by transform faults.

Several other features are consistent with the idea that the Midland Valley, or its structural equivalent, occurs south of Connemara.

A change in the nature of the magnetic basement is evidenced by the transition from an irregular field north of an east west line from Galway Bay to Russell's western fault, to a smooth field south of this line.

Spilites of possible Arenig age have been found on islands south of Connemara (McKee and Burke, 1957).

There is intense Lower Carboniferous volcanism near Limerick on the eastern side of the County Clare gravity high (Charlesworth, 1963). This volcanism is similar to the Lower Carboniferous volcanism of the same age which occurs in the Midland Valley of Scotland (Francis, 1965).

Because of the quality of the data the transform fault idea must be regarded as a suggestion. The idea is feasible on geological grounds and a similar stepping of the zone of oceanic closing occurs in the junction between the Churchill and Superior provinces of the Canadian Shield (Gibb and Walcott, 1971). It will be difficult to prove or disprove these faults on geologic evidence because they presumably ceased moving in the Upper Ordovician and hence are covered by later sediments.

### 9.3.6 Conclusions

The author considers that the arguments given above indicate that the Midland Valley, and not the Southern Uplands, overlies a remnant of oceanic crust, compressed between two converging continental land masses.

Fig. 9-11 illustrates, in diagram form, the author's ideas of the geological history of the area. These events are summarized below.

#### Ordovician

Arenig: (A) Formation of proto-Atlantic Ocean by generation of oceanic crust at an oceanic ridge. Deposition of black shales and cherts on oceanic sea floor. Sediments deposited in a vast fan over the northern edge of the continental shelf. Process probably initiated during Cambrian.

Post Arenig-Pre Caradoc: (B) Initiation of closing of the proto-Atlantic Ocean. Underthrusting occurs at continental margins causing folding of shales scraped off sea floor. Ophiolitic mass detached from oceanic crust and welded onto southern continental mass.

Caradoc-Ashgill: (C) Final stages of closing of the proto-Atlantic Ocean. Orogeny in the Highlands causes mountain building, metamorphism and igneous intrusions. Flysch wedges from Highlands build out over oceanic crust to Ballantrae where greywackes are deposited in a trench. Volcanism due to south going plate causes the Bail Hill, Lake District and other volcanic rocks. The Highland Boundary serpentine may have

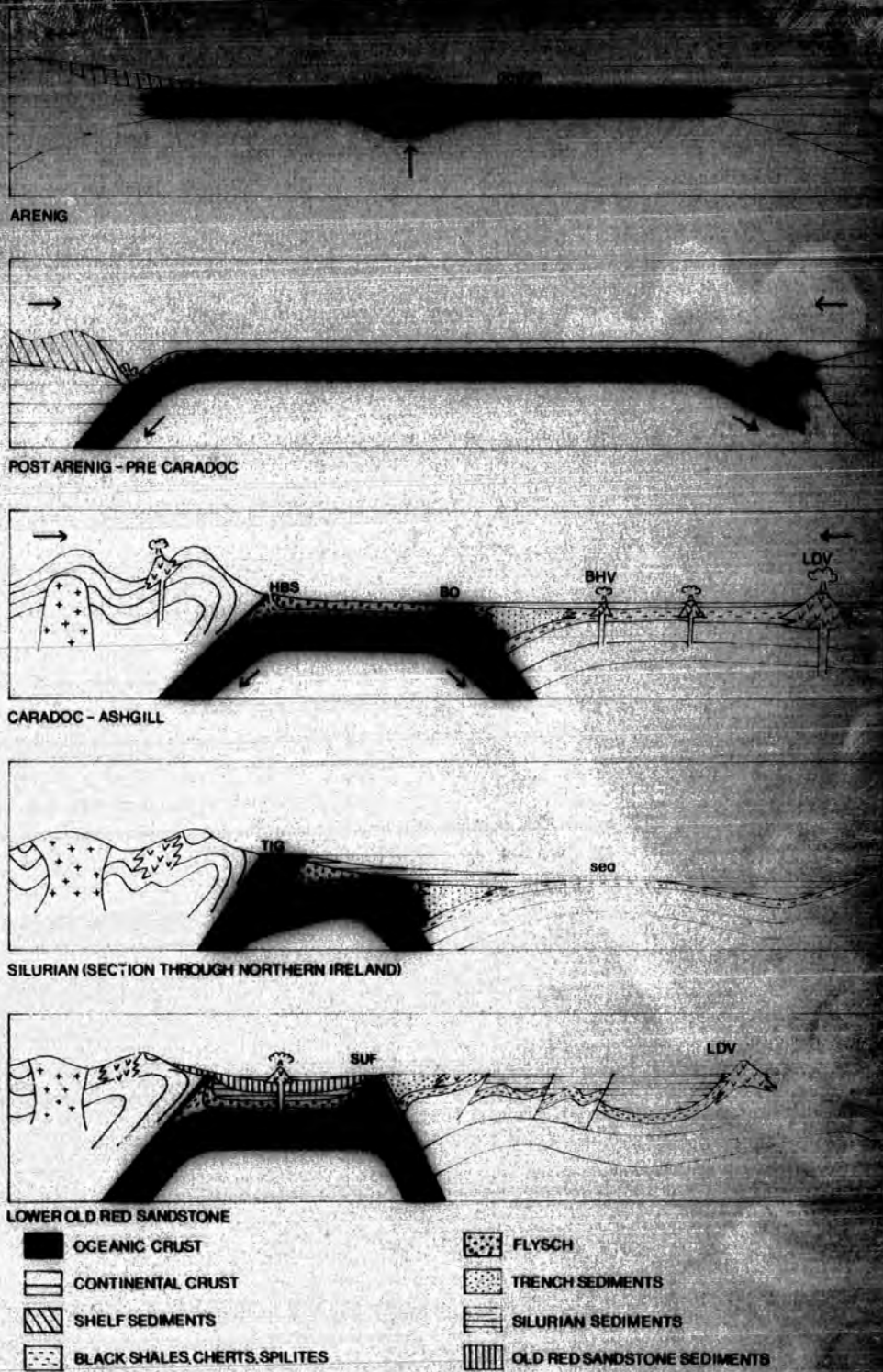


Fig. 9-11 Evolution of the Midland Valley  
 HBS = Highland Boundary serpentine  
 BO = Ballantrae ophiolites  
 BHV = Bail Hill volcanics  
 LDV = Lake District volcanics  
 TIG = Tyrone Igneous Group  
 SUF = Southern Uplands fault

been a result of plate movement at this stage.

Silurian: (D) Broad warping of the crust and deposition within the hollows. The figure illustrates the section in Northern Ireland.

Snapping of the oceanic crust occurs along the northern margin.

Lower Old Red Sandstone: (E) Late Silurian compression, folding and faulting with thrusting along the northern and southern boundaries of the Midland Valley causing a graben. Erosion from the Highlands and the Southern Uplands fills the depression.

#### 9.4 Lower Old Red Sandstone Features

The features, known from geology and deduced from geophysics which are considered relevant to the Lower Old Red Sandstone period are shown in Fig. 9-12.

The aeromagnetic map shows a line of magnetic highs in the north east corner of the Southern Uplands and as some of these correlate with outcrops of granite the remainder are probably also due to granite.

It is possible that other unknown granites occur within the Southern Uplands because the studies of Powell (1970) have shown that they do not always have a magnetic expression.

The filtered aeromagnetic map (Fig. 9-3) reveals a striking series of magnetic highs which tend to align along a known anticline (the Ochil-Sidlaw anticline) in the north of the Midland Valley and its south easterly extension as suggested by Anderson and Owen (1968). The evidence for the proposed flexure in the trend of the anticline in the centre of the Midland Valley is the abrupt difference in the overlying lower Carboniferous sediments on either side of a north south line which runs approximately through Lanark. To the west occur the Clyde Plateau lavas which thin rapidly eastwards and in the same stratigraphic horizon to the east oil shale formations occur.

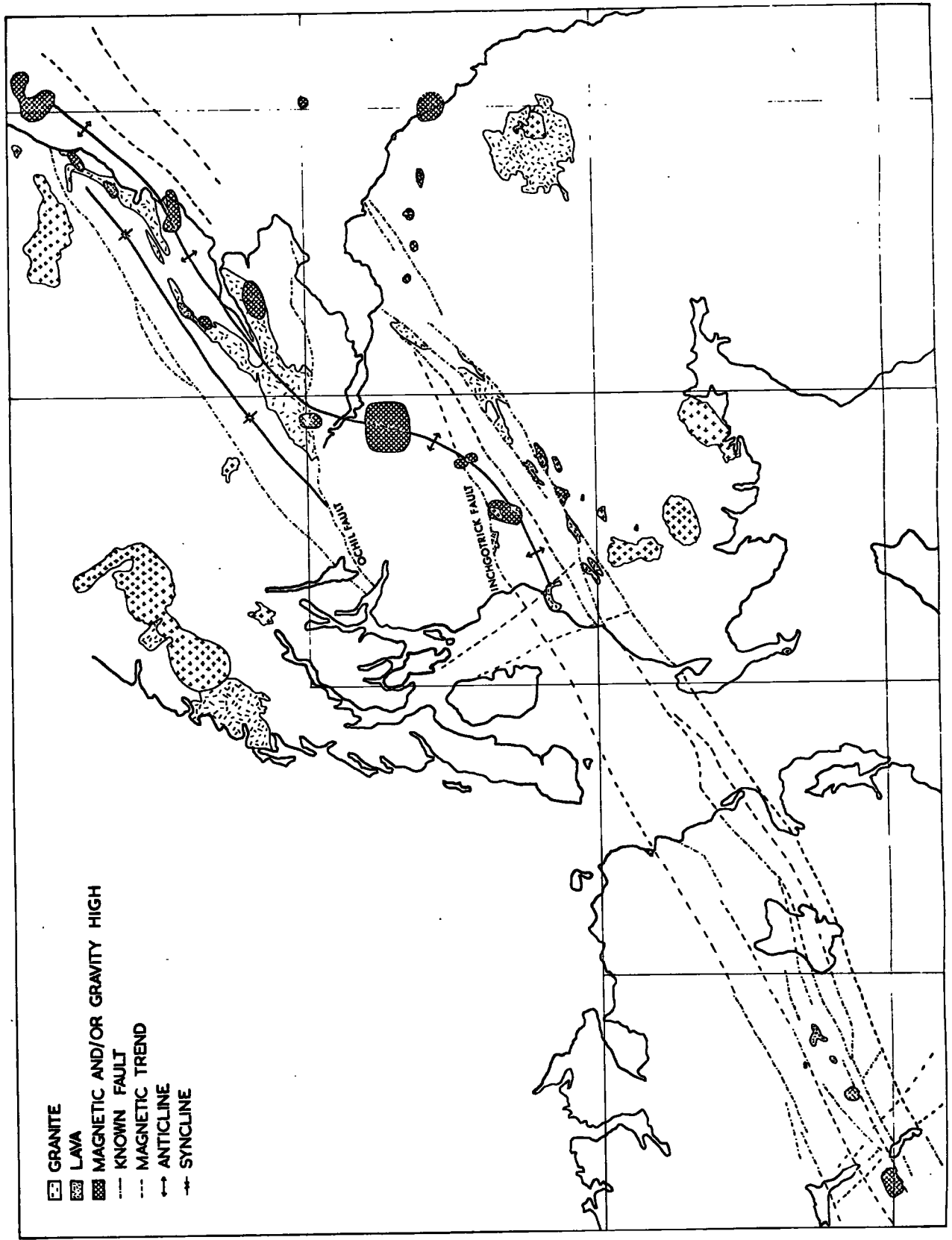


FIG. 9-12 Lower Old Red Sandstone features of the Midland Valley

This 'Lanark Line' has been investigated by Hall (1971) using seismic refraction methods which have confirmed the thinning of Lower Carboniferous sediments over this rise.

The D'Arcy No.1A drill at Salsburgh reported by Falcoln and Kent (1960) supposedly found Lower Old Red Sandstone lavas at a depth of 4000 feet. This indicates a rise in the level of these rocks compared with adjacent areas.

The southernmost magnetic high along this line is caused by the Middle Old Red Sandstone Distinkhorn Granite which has granodioritic affinities (Macgregor and Macgregor, 1948).

The magnetic high straddling the Ochil fault corresponds to Old Red Sandstone diorite intrusions and as noted by McQuillin (1970) the form of the anomaly suggests that the intrusion causing the anomaly has had its southern half downfaulted.

The anomaly on the Ochil fault, the one south of the Firth of Tay and the one near Montrose, correspond in position to localities where Giekie (1899), using local geological evidence, has postulated the presence of volcanic centres which gave rise to the extensive volcanics of the area. Thus it seems likely that these anomalies, and the others of the area, are caused by late stage granodioritic intrusions related to the source of the volcanic rocks. This is what appears to have happened in the Cheviot Hills and Glencoe (Mercy, 1965, p.256) and both of these volcanic centres give pronounced magnetic anomalies.

The most striking magnetic feature of the whole area is the large sub circular magnetic anomaly centred approximately on Armadale. The results of a qualitative interpretation of a north-south profile over this anomaly are shown in Fig. 9-13. The magnetic profile was calculated by using the spline subroutine (SPLINE) to interpolate between contour lines. The section shown with the profile incorporates known geology

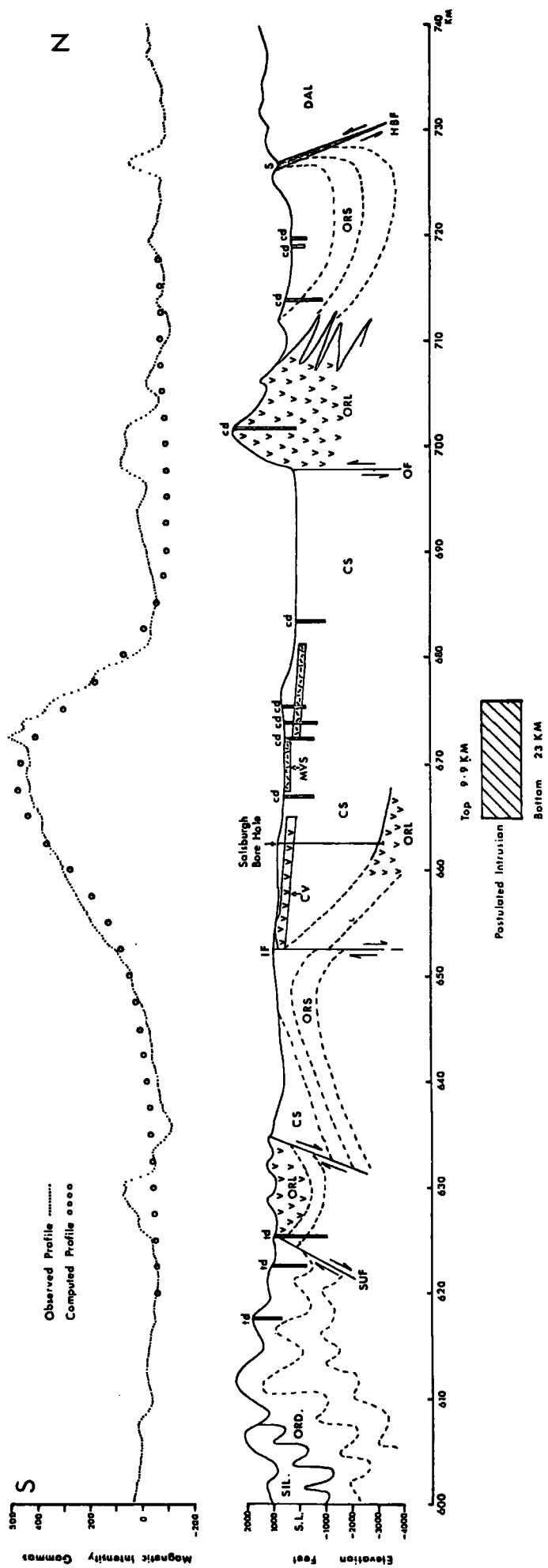


Fig. 9-13 Interpretation of Profile OP 990,000E on the National Grid). DAL = Dalradian, ORD = Ordovician, SIL = Silurian, ORS = Old Red Sandstone sediments, ORL = Old Red Sandstone lavas, CS = Carboniferous sediments, CV = Carboniferous volcanics, MVV = Midland Valley Sill, Cd = Carboniferous dyke, td = Tertiary dyke, S = serpentine, HBF = Highland Boundary Fault, SUL = Southern Uplands Fault. IF = Inchgotrick Fault, OF = Ochil Fault.

and results obtained from interpretations described elsewhere in this chapter.

The non linear optimization program OPIMPR was used to calculate a magnetic prism whose calculated effect gives the best least squares fit to the observed profile. Only field values which were considered to be relatively free from the effects of other bodies were selected to be used in the least squares interpretation.

Although only a profile has been analysed this is considered adequate because the form of the anomaly suggests that the causative body must have a roughly square plan and as the profile crosses the centre of the body, fitting a prism is considered to adequately compensate for end effects.

The magnetization of the body was assumed to be induced in the earth's field. This is suggested by the form of the anomaly and probable because, as Strangeway (1967) has discussed, large igneous intrusions cool relatively slowly forming larger mineral crystals which tend not to retain a strong remanent magnetization.

The agreement between the calculated and observed anomalies is considered reasonable and most discrepancies can be attributed to the effects of known or deduced rock occurrences, notably the Carboniferous dykes, the edges of the Midland Valley Sill and a possible Carboniferous lava flow (see 9.5). The anomaly over the Ochil Fault is partly due to the Old Red Sandstone lavas and partly due to the diorite intrusion mentioned above.

The calculated depth to the top of the intrusion (40,000 feet) is not unreasonable, especially as the most recent estimate of the thickness of the Lower Red Sandstone in the Strathmore region is 40,000 feet. (Armstrong and Paterson, 1970).

Unpublished gravity results collected by Dr. W. Bullerwell of the Institute of Geological Sciences indicate that there is a gravity high

corresponding to the magnetic anomaly and this suggests similarities with the Distinkhorn Granite which also causes a gravity and magnetic high. The gravity high over the Distinkhorn Granite can be seen on the map published by McLean and Qureshi (1966).

The only other large anomalies causing both gravity and magnetic anomalies in the area are the Tertiary igneous centres such as Arran (as shown on maps published by Powell (1970)). As the Armadale magnetic high is away from the line of the other Tertiary centres, and as it does not appear to be associated with any Tertiary dyke swarm as the other centres are, it is not considered to be of Tertiary age. In the opinion of the author the anomaly probably marks a volcanic centre similar to others on the line described above.

The four small magnetic highs to the north of the anticlinal axis may also be due to volcanic centres but could also be due to local thickenings or increases in magnetization of the lavas.

The Lower Old Red Sandstone lavas along the southern boundary of the Midland Valley give significant magnetic anomalies but this is not so noticeable along the northern boundary of the area although the magnetic field over the Ochil-Sidlaw lava fields does have a distinct character. Stubbs (1957) has studied the palaeomagnetism of these rocks and has found that the lower lavas are magnetized in a direction  $46^{\circ}$  west of south with a downwards inclination of  $54^{\circ}$  with approximately fifty per cent reversals. The higher lavas are more erratically magnetized. Possibly the relatively random magnetic effects may cancel and prevent definite anomalies over the lavas.

The sections of the lavas drawn by Armstrong and Paterson (1970) show the lavas fingering out towards the limbs of the Ochil-Sidlaw anticline and this suggests that the lavas, fed by the centres mentioned, built a ridge of volcanic material which during subsequent folding controlled the location of the anticline.

From the magnetic maps it is not obvious whether the change in magnetic character along the Angus and Kincardine coastline is due to lavas terminating or due to downfaulting.

In western Northern Ireland there are small outcrops of andesite which suggest there may be extensive subsurface lava beds similar to those occurring in Scotland. Although there is no obvious geophysical evidence for this, the gravity and magnetic maps show the locations of two centres which may be associated with the lavas. The locations of these features are shown in Fig. 9-12. The western one is indicated by a magnetic anomaly but no gravity anomaly whereas the reverse is true for the other.

The Middle Old Red Sandstone was climaxed by an orogeny which caused the folding in the Ochil-Sidlaw anticline and the adjacent Strathmore syncline. Ramsay (1964) has shown that this folding was predominantly the result of north-south compression within the Midland Valley.

The marked flexure in the line of volcanic centres appears to reflect the change in the width of the Midland Valley. They may follow a line of maximum bending of the oceanic crust compressed within the Midland Valley. Such a line would provide a zone of weakness for the intrusion of the igneous centres.

## 9.5 Carboniferous Igneous Activity

### 9.5.1 Introduction

The Carboniferous period was marked by two episodes of igneous activity within the Midland Valley. The first phase caused alkali basalt lavas and sills and occurred mainly in Lower Carboniferous times (the Calciferous Sandstone Series subdivision of the Geological Survey of Scotland), although there is evidence (Francis, 1965, p.359) that similar volcanism continued throughout the Carboniferous. The second

phase is evidenced by a series of east west trending quartz dolerite dykes and associated sills, of late Carboniferous, possibly early Permian age, which occur over a wide area in Scotland and Northern England.

Comprehensive accounts of these igneous periods are given by Macgregor (1948), Francis (1965), Francis (1967) and Francis (1968).

#### 9.5.2 Alkali Dolerite Phase

The alkali dolerite igneous features which are discernable on the aeromagnetic map are shown in Fig. 9-14. The Clyde Plateau lavas in the western Midland Valley appear to thin eastward against the north south rise postulated in the previous section. This rise, probably due to an Old Red Sandstone anticline appears to have influenced Carboniferous sedimentation and tectonism. Mapped fold axes in Carboniferous rocks east of this feature parallel the rise. Isopach maps published by Kennedy (1958) and Goodlet (1957) show the sedimentation also paralleling the fold. However as mentioned by Francis (1965) p.349 the figures used for these maps are not reliable.

The filtered aeromagnetic map shows three circular magnetic highs within the Clyde Plateau lavas which correlate with mapped outcrops of agglomerate. The northernmost anomaly, corresponding to Meikle Bin, also has a pronounced gravity high as can be seen on the maps published by McLean and Qureshi (1966). The remaining two magnetic highs do not appear to correlate with gravity highs. It is suggested that these three magnetic highs mark the positions of central type volcanoes whose lava flows fed the Clyde Plateau lava fields. The relative importance of these postulated igneous centres and the numerous volcanic necks which have been mapped in the area (Francis, 1965, p.374) is not known.

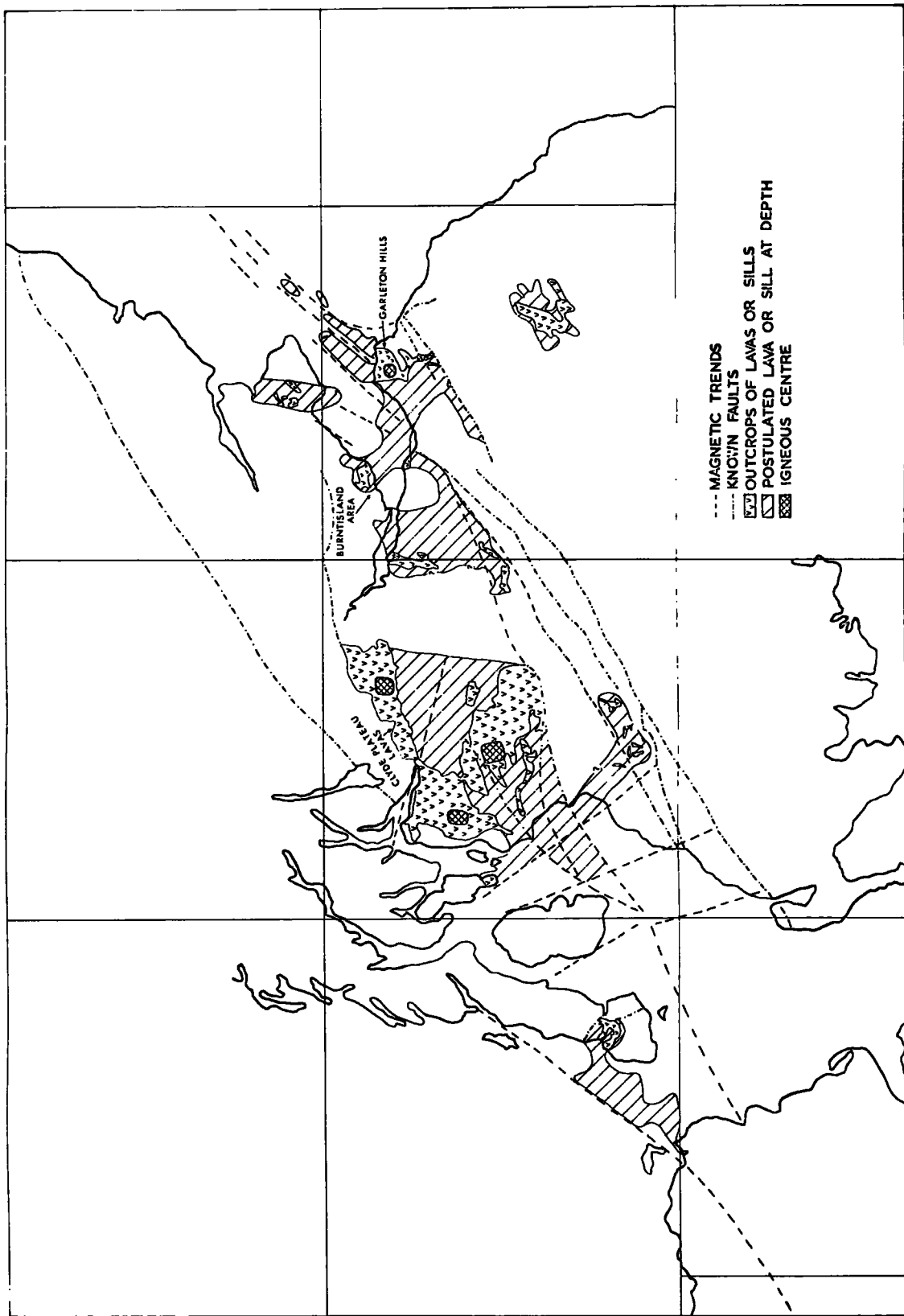


FIG. 9-14 Lower Carboniferous features of the Midland Valley

The Garleton Hills complex is another such volcanic centre and although it does not give such a pronounced magnetic high it can be related to several lava flows and sills (see Fig. 9-14). Two sills are postulated extending north east under the sea from the Garleton Hills. The northern one is confidently identified as a sill because its anomaly is surrounded by a magnetic low which indicates a relatively small vertical thickness. A small island at its northern end consists of quartz dolerite. The magnetic feature immediately to the south has also been identified as a sill or lava flow but confirmation of this is not so obvious and there is a slight possibility that it may be caused by ophiolitic material as it lies along the line of the Southern Uplands fault.

The magnetic data supports the suggestion of Francis (1961) that the Garleton Hills complex is connected at depth with the lavas of the Burntisland area. The continuation of these rocks further west is uncertain but is suggested by the general character of the magnetic field.

### 9.5.3 Quartz Dolerite Phase

As discussed by Anderson (1951) the Upper Carboniferous igneous activity is related to a north south tensional relief of pressure (Anderson's Borcovician stress system) which was responsible for a series of east west faults, east west quartz dolerite dykes and several large sills which have been fed by the dykes.

The igneous activity associated with this period is extremely widespread and extends at least from Aberdeenshire to Durham.

Anderson (1951) has demonstrated that the faulting and the dyke intrusion are contemporaneous and in many places the faults act as channelways for the dykes. The faults are extremely numerous in the central part of the Midland Valley and the northernmost of this suite,

and probably the largest, is the Ochil fault which has an estimated downthrow to the south of 10000 feet (Francis and Read, 1970) and is associated with quartz dolerite intrusions.

The aeromagnetic map and the filtered aeromagnetic map both suggest that the main structural control of the distribution of the Clyde Plateau lavas in the south west Midland Valley is the Inchgotrick Fault which appears to continue eastward almost to the Firth of Forth. The geological map of the area shows several faults of small lateral extent which correlate with the extended line of the Inchgotrick Fault as suggested by the aeromagnetic data but along large parts of this line no faults have been mapped. The northern side of the Inchgotrick Fault is the downthrown side and it is obviously a major fault.

A structural symmetry is suggested by the Ochil Fault and the Inchgotrick Fault and the area between the two appears to be a down-faulted graben which has been internally disturbed by numerous smaller east west faults.

Francis et al. (1970) have postulated that the Ochil Fault was moving continuously from the Upper Old Red Sandstone through the Carboniferous. It is difficult to date the Inchgotrick Fault precisely but a similar age is very likely and it may be a result of the same structural event as the Ochil Fault.

Fig. 9-15 shows the igneous features of the Upper Carboniferous period which have been deduced from the aeromagnetic data. The distribution of these rocks is largely as known from geological evidence but the geophysical data does indicate several seaward extensions.

The dykes within the Midland Valley tend to occur in swarms which suggest some local condition. There is one such swarm through the centre of the region between the Ochil Fault and the Inchgotrick Fault and these dykes feed the Midland Valley Sill. It is conceivable that

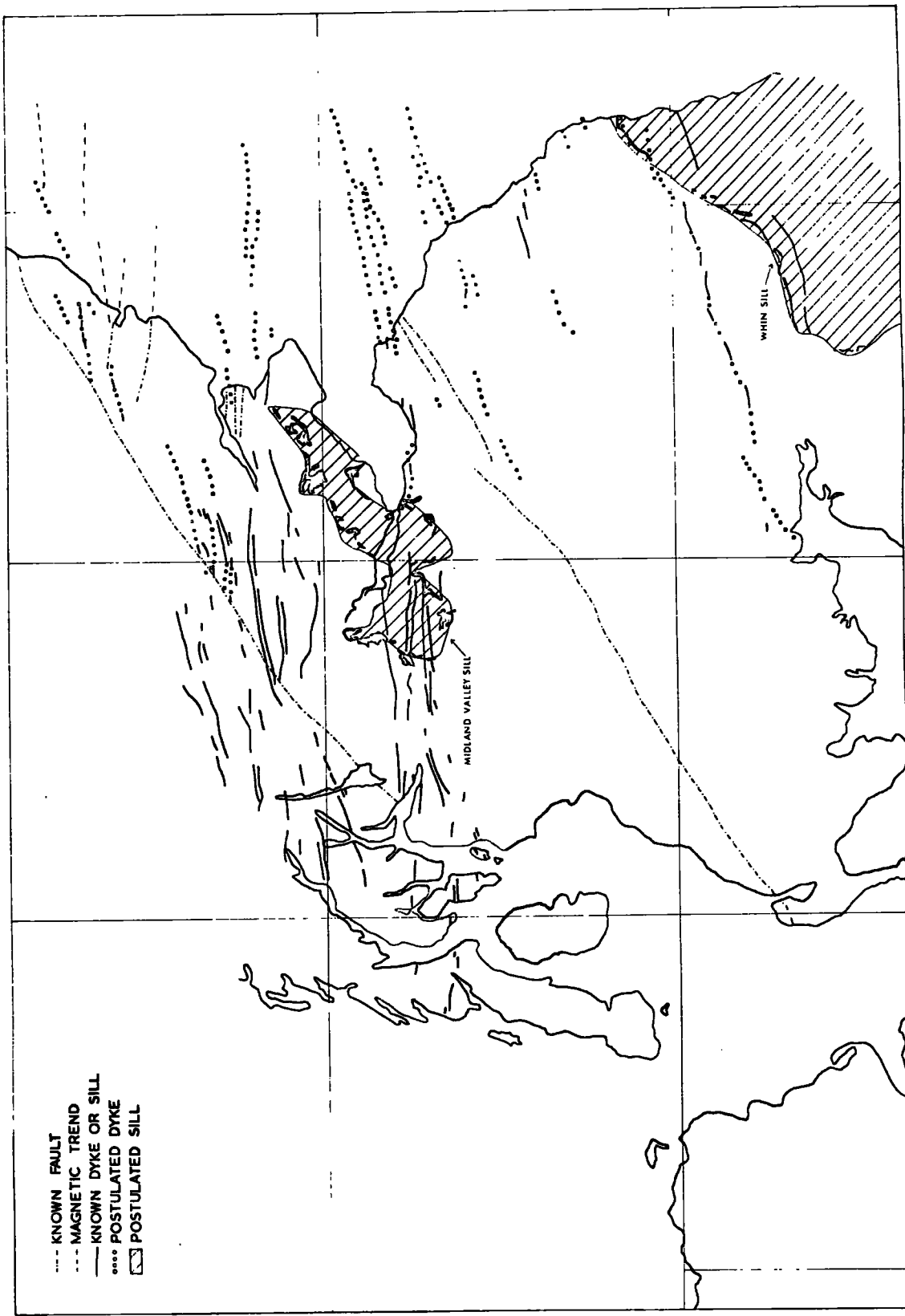


Fig. 9-15 Distribution of Upper Carboniferous quartz dolerite dykes and sills.

these dykes may be related to the large magnetic anomaly which underlies this area but the studies of 9.4 suggest that this feature is older.

The two dyke swarms in the north east corner of the Midland Valley coincide with the culminations in the Strathmore Syncline which have been mapped by Armstrong and Paterson (1970) and this suggests that they may be intruded up tensional cracks in local flexures.

#### 9.5.4 Origins of the Carboniferous Igneous Activity

The Carboniferous igneous features of the Midland Valley are anomalous because they cannot obviously be related to the initial formation of the Midland Valley as earlier igneous features can or to the opening of the North Atlantic as later features can. Stress relief has been a major controlling factor for the Upper Carboniferous activity and may have also initiated the Lower Carboniferous faulting and volcanism. Possible causes for these tensional effects are a slow doming of the crust as a late reaction to the closing of the Proto-Atlantic Ocean or the effects of Hercynian movements (Anderson and Owen, 1968).

#### 9.6 Post Carboniferous Features

Many of the post late Carboniferous features in the Midland Valley area have a north to north westerly alignment which is in marked contrast to the predominantly north easterly to easterly trend of the Caledonian and Hercynian features. These more recent trends can be ascribed to the effects of the continental drifting of Europe away from America. Russell (1972) elaborates on this hypothesis. The resulting tension and subsequent viscous spread of the continental crust towards the oceanic crust, as envisaged by Bott (1971), was probably responsible for the dykes, faults and sedimentary basins

with the north easterly alignment.

The Irish Sea may have been formed during this stretching process which may have thinned the crust and formed a hollow in which the sediments were deposited. It is likely that the North Channel is a similar feature although it may be partly fault bounded. A magnetic trend aligned with the east coast of Antrim suggests a possible fault. Charlesworth (1963) p.433 favours the faulting model and mentions several faults along the coastline which may be associated with the movement. The interpretation of magnetic anomalies in the North Channel (9.2) indicated downfaulting of the order of 2 km..

There are numerous other sedimentary basins which were probably formed in a similar way, for example the Upper Carboniferous Coal Measures basin around Falkirk, the Permian Mauchline Basin and the sedimentary basins indicated on either side of Arran by gravity data (McLean's results in Powell (1970)).

Cloos (1939) p.500, 512 has suggested that the Antrim lavas have been preserved by downfaulting between meridional faults. The linear boundaries and associated faults of these lavas (Charlesworth, 1963, p.318), and the gravity gradients paralleling the boundaries suggest that this is so.

The lateral changes in intensity along the magnetic anomaly marking the Southern Uplands ophiolite zone probably mark faults from this tectonic episode.

The Tertiary Period (Richey et al., 1961, Stewart, 1965) was marked by spectacular igneous activity in the form of intrusive centres, plateau basalts and dyke swarms. These features are probably also related to the effects of continental drift. The figures quoted by Allison (1936) for crustal stretching and dyke intrusion on the west coast of Scotland support the drift concept.

As mentioned previously (9.2) the igneous centre of Arran may be on the site of an older (Ordovician) tear in the lithospheric plate. There is magnetic evidence for the continuation of Arran into Ailsa Craig which is the small granite island to the south of Arran. The connection between the two is even more obvious in the gravity data collected by McLean (shown in Powell (1971)).

The extensive Tertiary dykes of the Midland Valley are related to the igneous centre of Mull. They give negative anomalies because, as Bruckshaw and Robertson (1949) have shown, they are reversely magnetized. These dykes are associated with a set of north westerly trending faults within the Midland Valley (Anderson, 1951).

The lavas of the Antrim Plateau are also reversely magnetized (Hospers and Charlesworth, 1954) and the magnetic highs around the edges of the lava field are merely polarity effects. Fowler and Robbie (1961) report finding ~~normal magnetization~~ and such <sup>polarity changes</sup>  $\wedge$  may account for the irregular nature of the field over the lava.

An anomalous feature of the aeromagnetic map is a linear positive anomaly trending from the Irish coast near Newcastle north westwards underneath the Antrim lavas. The form of the anomaly suggests that it is caused by a dyke and it has a Tertiary trend, but, in contrast to other Tertiary dykes, it is positively magnetized. This dyke which appears larger than most of the other Tertiary dykes may mark a fissure which acted as a feeder for the Antrim lavas.

Charlesworth (1963) p.411 has postulated the presence of a Tertiary igneous centre beneath the Tardree Rhyolite but although the magnetic map of Northern Ireland shows a positive magnetic anomaly over the rhyolite it is difficult to confirm the existence of an intrusion. The positive part of the anomaly appears confined to the region over the contact between the rhyolite and the basalt and this suggests

that the magnetization contrast at this contact causes the anomaly because an intrusion would cause an anomaly which is positive over a larger area. There is no definite gravity evidence to indicate an intrusion.

The most striking feature of the gravity field of western Northern Ireland is the large positive gravity anomaly centred on Dromore. This feature is not obvious on the aeromagnetic map because it is obscured by the magnetic effects of a Tertiary dyke swarm however filtering of a magnetic profile in 9.5 and the upward continuation map (Fig. 9.3) reveal the presence of a large magnetic anomaly coincident with the gravity anomaly.

Although the form of the gravity contours suggest that the anomaly may be the composite effect of the fields due to two separate bodies the vertical gradient and downward continuation filtering demonstrated in 9.5 show that the irregularities of the field are due to smaller additional masses and that the main anomaly is due to one large mass.

The only large intrusions in the area causing positive gravity and magnetic anomalies are the Tertiary igneous centres such as Slieve Gullion and Carlingford and as the Dromore Intrusion underlies a Tertiary dyke swarm trending north westwards from these centres to Barnesmore where Charlesworth (1963) p.411 has postulated another buried Tertiary centre, it seems reasonable to suppose the Dromore Intrusion is also a buried Tertiary centre. Fig. 105 of Charlesworth (1963) illustrates the distribution of known dykes and igneous centres in Northern Ireland. These features may all lie along a tensional fracture line resulting from crustal creep towards the Atlantic (c.f. Bott (1971)).

A large olivine dolerite sill of probable Tertiary age (Charlesworth,

1963, p.313) occurs in Carboniferous rocks to the west of the Dromore intrusion and may be related to it. The gravity contours suggest they may be related. There does not appear to be a magnetic anomaly associated with the sill.

Murphy (1952) considers the Dromore Intrusion to be caused by a buried mass of Ordovician age but part of the mass appears to occur north of the Highland Boundary fault and part occurs to the south of it. It is very difficult to explain such a body of Ordovician age if the Highland Boundary fault marks the position of a subduction zone as has been postulated in 9.3.

Fig. 9-16 shows the results of a quantitative interpretation of a gravity profile over the Dromore Intrusion using the computer program OPTGPR which applied the non linear optimization routine to obtain the prism whose gravity field gives the best least squares fit with the observed gravity field. By letting the depth to the bottom of the prism be an unconstrained parameter a good fit to the observed data was obtained after the computer program had iterated to a solution with depth to the top 0.1 km., depth to the bottom 25 km. and a density contrast 0.06 gm/cc.. By constraining the depth to the bottom of the prism to be 10 km. an equally acceptable visual fit of the observed and calculated data was obtained with an estimated depth to the top of 0.3 km. and a density contrast of 0.13 gm./cc.. This is the solution illustrated in Fig. 9-16. These examples illustrate the range of possible solutions for the Dromore gravity anomaly.

The geological section shown in Fig. 9-16 illustrates by showing the possible density values (taken from Murphy (1952)), that the gravity anomaly may be the combination of the effects of an intrusion, ophiolitic material and a dolerite sill. All these rock types may have the same density and all are expected to occur in the area. The boundaries illustrated between these three rock types in Fig. 9-16 are speculative.

— Observed Profile  
 ○ ○ ○ ○ ○ Calculated Profile

NW

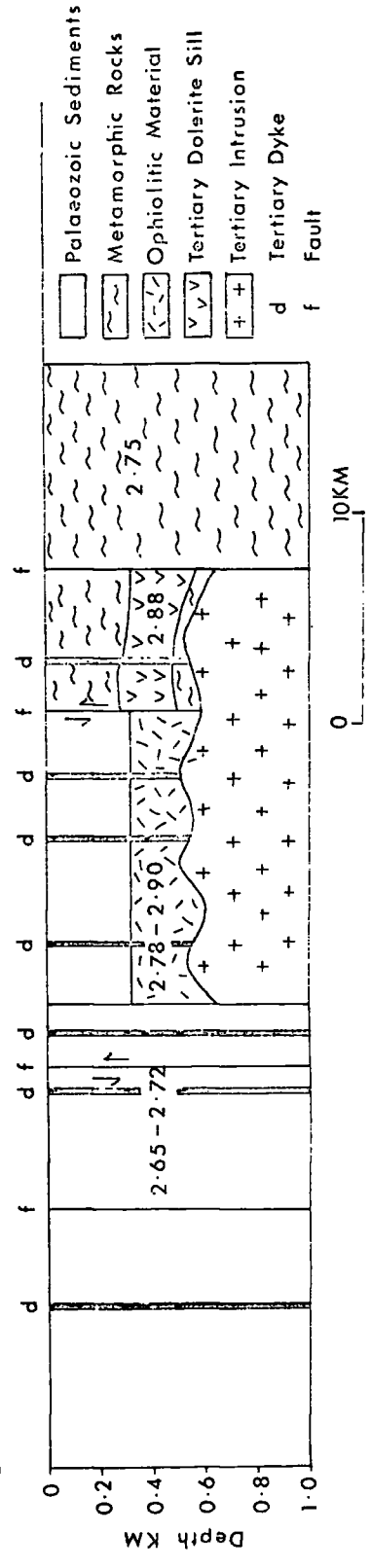
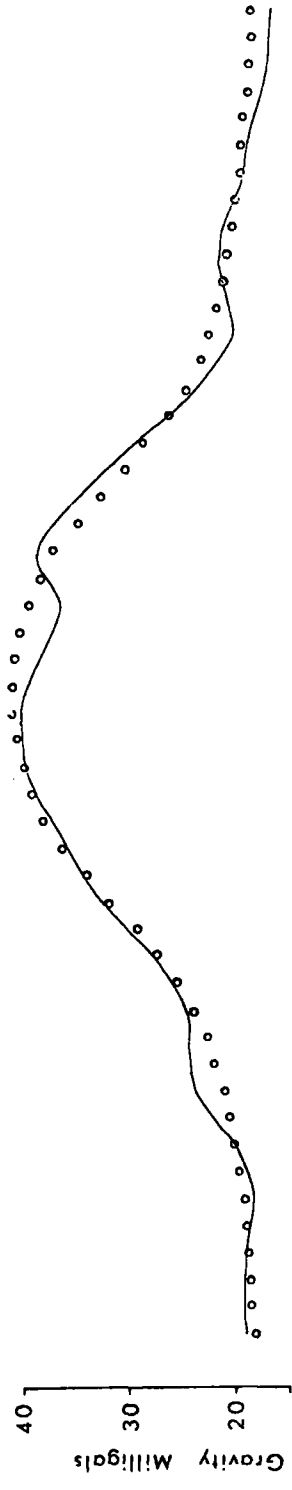
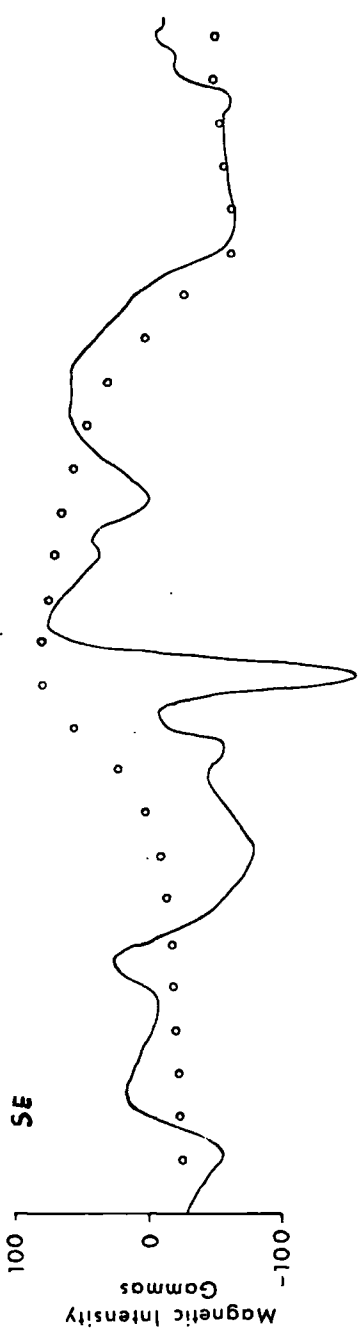


FIG. 9-16 Possible interpretation of the gravity profile across the Denovo Trench, with grid coordinates of the end points of the profile as in Figure 9-4, Profile ST - see Fig 9-4.

The magnetic anomaly calculated assuming the shape determined from the gravity interpretation is significantly wider than the observed magnetic anomaly and this suggests that the intrusion may have a central magnetic core rather than being uniformly magnetized. This is a plausible explanation because as Charlesworth (1963) p.411 has described, many of the Tertiary centres in the area have undergone successive injection of cone sheets.

Fig. 9-17 shows the location of the features described in this section.

#### 9.7 Concluding Comments Concerning the Structure and History of the Midland Valley

This study has related the major geological and geophysical features of the Midland Valley to three main tectonic episodes viz. the closing of the Proto-Atlantic Ocean, the effects of the Hercynian Orogeny and the opening of the present Atlantic Ocean.

The consistency of the interpreted structures with the postulated models suggests that these models are valid but further work is necessary to confirm them. In particular, a seismic study of the crustal structure beneath the Midland Valley could confirm the proposed oceanic origin of this crust. Seismic reflection profiles through the North Channel would probably locate the true paths of the Highland Boundary Fault and the Southern Uplands fault and determine the angles of their fault planes. An aeromagnetic survey of the Republic of Ireland would almost certainly reveal the position of the western extension of the Midland Valley.

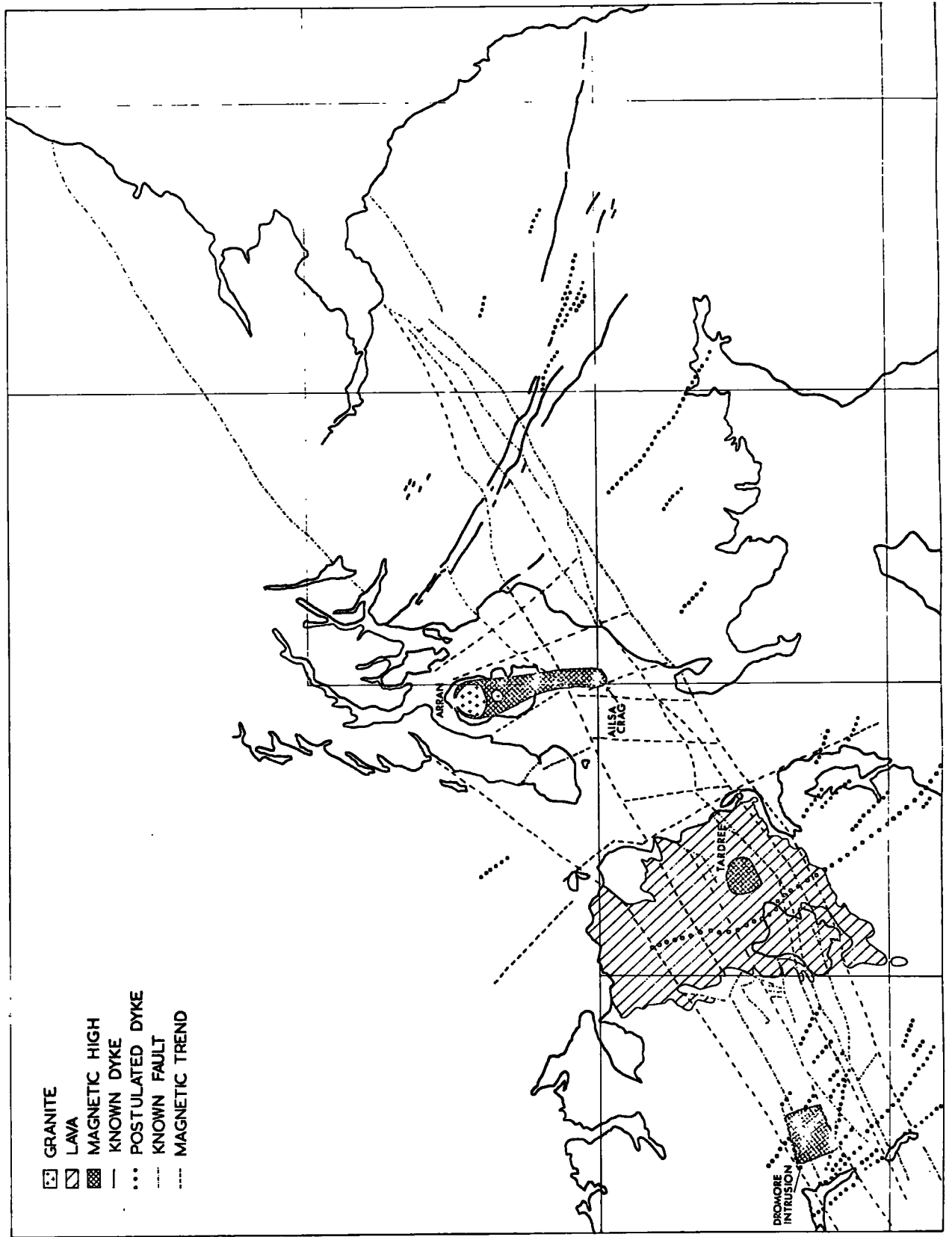


Fig. 9-17 Distribution of post Carboniferous igneous and structural features. Only major dykes are shown.

## APPENDIX 1

Summary of Previous Geophysical Surveys in the Midland Valley  
of Scotland and Northern Ireland

## Magnetic Surveys:

1. Ground magnetic surveys in Ayrshire (Park, 1961).
2. Study of magnetic profiles over Carboniferous dykes (Powell, 1963).
3. Aeromagnetic maps for Scotland and Northern Ireland published by the Geological Surveys of Great Britain and Northern Ireland.
4. Report on ground magnetometer surveys and a discussion of the aeromagnetic map for the Stirling area (McQuillin, 1970).
5. Report of ground magnetic surveys near Ballantrae and an interpretation of several features of the aeromagnetic map (Powell, 1970).
6. Marine magnetic profiles in the Firth of Forth (Eden, 1970).
7. Unpublished marine magnetic profiles in the Firth of Clyde and around Arran by Dr. A. McLean et al. of the University of Glasgow.

## Gravity Surveys:

1. Reconnaissance gravity survey of Northern Ireland (Cook and Murphy, 1952).
2. Unpublished regional gravity survey of the Midland Valley in Scotland by Dr. W. Bullerwell of the Institute of Geological Sciences.
3. Detailed gravity survey of Northern Ireland described by Bullerwell (1964).

4. Gravity surveys of the western Midland Valley in Scotland, described and interpreted by McLean (1966), McLean and Qureshi (1966) and Qureshi (1971).
5. Marine gravity surveys around Arran. The results are shown in Powell (1970).

Seismic Surveys:

1. Investigation of seismic velocities and seismic reflection profiles in the central Midland Valley by Hall (1970), (1971).
2. Sparker seismic survey of the Firth of Forth by Eden (1970).
3. Unpublished sparker surveys in the Firth of Clyde by Dr. A. McLean et al. of the University of Glasgow.

## APPENDIX 2

Filtering of Two Dimensional Data and Production of Contoured Maps

Various computer routines were written for the production processing of aeromagnetic data.

Initially it was intended to digitize aeromagnetic data along straight lines at the points where the contour lines crossed these straight lines and to use a spline interpolation method (c.f. Bhattacharyya, 1969) to convert this data to accurate data in gridded form. Although a computer routine was written to do this, the University of Durham d-mac digitizer was inconvenient to use for digitizing the data because of the extensive computer routines needed to correct digitizing mistakes. In practice it proved significantly faster to digitize manually on a regular grid. As only low pass filtering operations were attempted this was sufficiently accurate.

The aeromagnetic map of the Midland Valley in Scotland and Northern Ireland was digitized on a 2 km. grid and the digitized points stored on punched cards. As the flight line spacing of the data is 2 km. this is the minimum grid size which will avoid aliasing.

The computer program CONV2D was used to apply two dimensional filter coefficients to this data. Low pass and upward continuation coefficients published by Fuller (1967) were tried. It was found that the low pass filter, which had a very sharp frequency cut off, produced a smooth but unrealistic looking filtered field. The upward continued field (for a continuation of 2 km.) however showed realistic looking anomalies and the noise anomalies were sufficiently suppressed.

To contour the filtered data the computer contouring routine published by Holroyd and Bhattacharyya (1970) was adapted to the computer system at the University of Durham (Programs SPLINE 2 and

CONTOR). This necessitated modification of the plotting statements and the correction of several basic logic errors in the published program (such as a missing subroutine, BLINE). Although the contouring program worked it was impractical to use because the calculations had to be performed on the IBM 360 computer and the plotter pen movements had to be punched on cards, and subsequently fed into the IBM 1130 computer which controlled the plotter. The number of punched cards required was prohibitive.

For the production of contour maps of the filtered data a program was written to plot the numerical values of the filtered output on a regular grid (Program PLOTIT). This greatly simplified the manual contouring process.

Recently the IBM 360 computer has been adapted to allow on line plotting and the contouring program is now convenient to use.

Examples of the outputs of CONTOR and PLOTIT are given in Figs. 8-5 and 4-11b.

## APPENDIX 3

Summary of Computer Programs Used

Copies of programs listed below which are not included in this thesis are available in bound form, complete with instructions, in the Geology Department, University of Durham. The section numbers given with each program refer to the main reference to the program given in the thesis.

GRAV2D	computes gravity effect of arbitrary shaped two dimensional polygonal body. (4.2)
MAG2D	computes magnetic effect of arbitrary shaped two dimensional polygonal body. (4.2)
GRAVPR	computes gravity effect of a prism. (4.3)
MAGPR	computes magnetic effect of a prism. (4.3)
THIRDM	computes gravity effect of an arbitrary shaped three dimensional body. (5.1.2)
OPTM2D	non-linear optimization routine to find shape and magnetization of a two dimensional body causing a magnetic anomaly. (9.1.2.2)
OPTGPR	non-linear optimization routine to compute dimensions and density of a prism causing a gravity anomaly. (9.1.2.2)
OPTMPR	non-linear optimization routine to compute dimensions and magnetization of a prism causing a magnetic anomaly. (9.1.2.2)
SPLINE	converts irregularly spaced points along a profile to regularly spaced points. (8.1)

SPLIN2 calculates bicubic spline coefficients for regular grids of data. (Appendix 2)

CONTOR contours regularly gridded data. (Appendix 2)

PLOTT plots numerical values of regularly gridded data. (Appendix 2)

NLFILT performs non-linear filtering on profile data. (3.5)

CONV1D convolves one dimensional filter coefficients with profile data.

CONV2D convolves two dimensional filter coefficients with grid data. (Appendix 2)

WIEN1D calculates and applies one dimensional Wiener filter coefficients (listing enclosed). (4.1) and (6.2)

WIEN2D calculates and applies two dimensional Wiener filter coefficients (listing enclosed). (4.1) and (6.2)

MULTIW calculates and applies multichannel Wiener filter coefficients (listing enclosed). (7.1) and (7.3)

SHIFT calculates and applies one dimensional Wiener filter coefficients for optimum lag. (4.2.1.2)

MINIM non-linear optimization routine to compute depth and magnetization of a layer for which the relative relief is known. (8.2)

MATCH matched filter method to find the depth and width of a dyke. (5.2)

COEFF computes one dimensional filter coefficients using the Fourier transform method. (3.6)

SPECT1 computes phase and amplitude spectrum of profile data. (4.2.2.3)

SPECT2 computes amplitude spectrum of two dimensional gridded data using the Fourier transform method. (4.3)



REFERENCES

- Affleck, J. (1958). Interrelationship between magnetic anomaly components. Geophysics, 32, 738-748.
- Agarwal, R.G. and Kanasevich, E.R. (1971). Automatic trend analysis and interpretation of potential field data. Geophysics, 36, 339-348.
- Agarwal, B.N.P. and Lal, T. (1971). Coefficient sets for one dimensional gravity operators using filter theory. Geofis. pura. appl., 88, 6-11.
- Agger, H.E. and Carpenter, E.W. (1964). A crustal study in the vicinity of the Eskdalemuir seismological array station. Geophys. J.R. astr. Soc., 9, 69-83.
- Al-Chalabi, M. (1970). The application of non linear optimization techniques in geophysics. Ph.D. thesis, Univ. of Durham.
- Allison, A. (1936). The Tertiary dykes of the Craignish Area. Geol. Mag., 73, 73-87.
- Anderson, E.M. (1951). The dynamics of faulting and dyke formation with applications to Britain. Second edition. Oliver and Boyd, Edinburgh and London.
- Anderson, J.G.C. (1947). The geology of the Highland Border, Stonehaven to Arran. Trans. R. Soc. Edinb., 61, 419-515.
- Anderson, J.G.C. and Owen, T.R. (1968). The structure of the British Isles. Pergamon Press, London.
- Anderson, T.B. (1965). The evidence for the Southern Uplands Fault. In northeast Ireland. Geol. Mag., 102, 383-392.
- Andreasen, G.E. and Zeitz, I. (1969). Magnetic fields for a 4 x 6 prismatic model. U.S.G.S. Prof. Paper 666.
- Armstrong, M. and Paterson I.B. (1970). The Lower Old Red Sandstone of the Strathmore region. Rep. No.70/12 Inst. geol. Sci.
- Banerjee, S.K. (1971). Decay of marine magnetic anomalies by ferrous ion diffusion. Nature Phys. Sci., Lond., 229, 181-183.
- Baranov, V. (1953). Calcul du gradient vertical du champ de gravite ou du champ magnetique mesure a la surface du sol. Geophys. Prospect., 1, 171-191.
- Baranov, V. (1957). A new method for the interpretation of aeromagnetic maps: pseudo gravimetric anomalies. Geophysics, 22, 359-383.
- Baranov, V. and Naudy, H. (1964). Numerical calculation of the formula of reduction to the magnetic pole. Geophysics, 29, 67-79.

- Bhattacharyya, B.K. (1965). Two dimensional harmonic analysis as a tool for magnetic interpretation. Geophysics, 30, 829-857.
- Bhattacharyya, B.K. (1966). Continuous spectrum of the total magnetic field anomaly due to a rectangular prismatic body. Geophysics, 31, 97-121.
- Bhattacharyya, B.K. (1969). Bicubic spline interpolation as a method of treatment of potential field data. Geophysics, 34, 402-423.
- Bird, J.M., Dewey, J.F. and Kidd, W.S.F. (1971). Proto-Atlantic oceanic crust and mantle, Appalachian/Caledonian Ophiolites. Nature Phys. Sci. Lond., 231, 28-31.
- Black, D.I. and Scollar, I. (1969). Spatial filtering in the wave vector domain. Geophysics, 34, 916-923.
- Blackman, R.B. and Tukey, J.W. (1958). The measurement of power spectra. New York, Dover.
- Borradaile, G.J. (1972). Dalradian structure and stratigraphy of the northern Loch Awe District, Argyleshire. Trans. R. Soc. Edinb. (in press).
- Bott, M.H.P. (1960). The use of rapid digital computing methods for direct gravity interpretation of sedimentary basins. Geophys. J.R. astr. Soc., 3, 63-67.
- Bott, M.H.P. (1965). The deep structure of the northern Irish Sea - a problem in crustal dynamics. In Submarine Geology and Geophysics, 179-204, edited by Whittard, W.F. and Bradshaw, R., Colston Papers No.17, Butterworths, London.
- Bott, M.H.P. (1967a). Solution of the linear inverse problem in magnetic interpretation with application to oceanic magnetic anomalies. Geophys. J.R. astr. Soc., 13, 313-323.
- Bott, M.H.P. (1967b). Geophysical investigations of the northern Pennine basement rocks. Proc. Yorks. geol. Soc., 36, 139-168.
- Bott, M.H.P. (1968). The geological structure of the Irish Sea basin. In Geology of Shelf Seas, Donovan, D.T. (ed.), Oliver and Boyd, Edinburgh and London, 93-116.
- Bott, M.H.P. (1971). Evolution of young continental margins and formation of shelf basins. Tectonophysics, 11, 319-327.
- Bott, M.H.P., Smith, R.A. and Stacey, R.A. (1966). Estimation of the direction of magnetization of a body causing a magnetic anomaly using a pseudogravity transformation. Geophysics, 31, 803-811.
- Bruckshaw, J.M. and Robertson, E.I. (1949). The magnetic properties of the tholeiite dykes of North England. Mon. Not. R. astr. Soc., 5, 308-320.

- Bruckshaw, J.M. and Kunaratnam, K., (1963). The interpretation of magnetic anomalies due to dykes. Geophys. Prospect., 11, 509-522.
- Bullard, E.C. and Cooper, R.I.B. (1948). The determination of the masses necessary to produce a given gravitational field. Proc. R. Soc. Series A, 194, 332-347.
- Bullerwell, W. (1961). The gravity map of Northern Ireland. Ir. Nat. J., 13, 255-257.
- Bullerwell, W. (1964). Geophysical and drilling exploration in Northern Ireland. Report of the Government of Northern Ireland.
- Bush, M.D. (1971). A magnetic survey of the northern edge of the English Lake District. M.Sc. thesis, Univ. of Durham.
- Butler, P.F. (1968). The interpretation of magnetic field anomalies over dykes by optimization procedures. M.Sc. thesis Univ. of Durham.
- Byerly, P.E. (1965). Convolution filtering of gravity and magnetic maps. Geophysics, 30, 281-283.
- CERN (1970) Internal publication of instructions for Program MINUIT.
- Chapman, N. (1972) personal communication.
- Charlesworth, J.K. (1963). Historical geology of Ireland. Oliver and Boyd, Edinburgh and London.
- Clarke, G.K.C. (1969). Optimum second derivative and downward continuation filters. Geophysics, 34, 424-437.
- Gloos, H. (1939). Hebung-spaltung-vulkanismus. Geol. Rdsch., 30, 401-527.
- Cobbing, E.J. (1964). The Highland Boundary Fault in East Tyrone. Geol. Mag., 101, 496-501.
- Cobbing, E.J., Manning, P.I. and Griffith, A.E. (1965). Ordovician-Dalradian unconformity in Tyrone. Nature, Lond., 206, 1132-1135.
- Cochran, W.T. et al. (1967). What is the fast Fourier transform? I.E.E.E. Trans on Audio and Electronics, 55, 1664-1674.
- Coleman, R.G. (1971). Plate tectonic emplacement of upper mantle peridotites along continental edges. J. geophys. Res., 76, 1212-1222.
- Cook, A.H. and Murphy, T. (1952). Gravity survey of Ireland north of the line Sligo-Dundalk. Geophys. Mem., Dubl., 2, (4).

- Cooley, J.W. and Tukey, J.W. (1965). An algorithm for the machine computation of complex Fourier series. Maths. Comput., 19, 297-301.
- Craig, G.Y. (Ed.) (1965). The geology of Scotland, Oliver and Boyd, Edinburgh and London.
- Dampney, C.N.G. (1966). Three criteria for the judgement of vertical continuation and derivative methods of geophysical interpretation. Geoexploration, 4, 3-24.
- Danes, Z.F. (1962). Structure calculation from gravity data and density logs. Trans. Soc. Min. Eng., 223, 23-29.
- Danes, Z.F. and Oncley, L.A. (1962). An analysis of some second derivative methods. Geophysics, 27, 611-615.
- Darby, E.K. and Davies, E.B. (1967). The analysis and design of two dimensional filters for two dimensional data. Geophys. Prospect., 15, 383-406.
- Davies, E.B. and Mercado, E.J. (1968). Multichannel deconvolution filtering of field recorded seismic data. Geophysics, 33, 711-722.
- Dean, W.C. (1958). Frequency analysis for gravity and magnetic interpretation. Geophysics, 23, 97-127.
- De Bruyn, J.W. (1955). Isogam maps of Europe and North Africa. Geophys. Prospect., 3, 1-14.
- Dewey, J.F. (1969). Evolution of the Appalachian/Caledonian orogen. Nature, Lond., 222, 124-129.
- Dewey, J.F. (1971). A model for the Lower Palaeozoic evolution of the southern margin of the early Caledonides of Scotland and Ireland. Scott. J. Geol. 7, 219-240.
- Dewey, J.F. and Bird, J.M. (1970). Origin and emplacement of the ophiolite suite. J. geophys. Res., 76, 3179-3206.
- Dewey, J.F. and Pankhurst, R.J. (1970). Evolution of the Scottish Highlands and their radiometric age pattern. Trans. R. Soc. Edinb., 68, 361-389.
- Downie, C. et al. (1971). A palynological investigation of the Dalradian rocks of Scotland. Rep. No. 71/9, Inst. geol. Sci.
- Eastwood, T. et al. (1968). The geology of the country around Cockermouth and Calderbeck. Mem. Geol. Surv. Gt. Br.
- Eden, R.A. (1970). Report on geological and geophysical surveys in the Firth of Forth. Report of Inst. of Geol. Sci. (in preparation).

- Elkins, J.A. (1951). The second derivative method of gravity interpretation. Geophysics, 16, 29-50.
- Erdelyi, A. et al. (1954). Tables of integral transforms. McGraw Hill, New York.
- Evjen, H.M. (1936). The place of vertical gradient in gravitational interpretations. Geophysics, 1, 127-136.
- Falcoln, N.L. and Kent, P.E. (1960). Geological results of Petroleum exploration in Britain 1945-57. Mem. geol. Soc. Lond. No.2.
- Fitton, J.G. and Hughes, D.J. (1970). Volcanism and plate tectonics in the British Ordovician. Earth Planet. Sci. Letters, 8, 223-228.
- Folkman, Y. (1969). Gravity investigations in the Egremont area, West Cumberland. M.Sc. thesis Univ. of Durham.
- Fowler, A. and Robbie, J.A. (1961). The geology of the country around Dungannon. Mem. Geol. Surv. Gt. Br.
- Francis, E.H. (1967). Review of Carboniferous Permian volcanism in Scotland. Geol. Rdsch., 57, 219-246.
- Francis, E.H. (1968). Review of Carboniferous volcanism in England and Wales. J. Earth Sci. Leeds, 8, 41-56.
- Francis, E.H. et al. (1970). The Geology of the Stirling district. H.M.S.O., Edinburgh.
- Fuller, B.D. (1967). Two dimensional frequency analysis and design of grid operators. In Mining Geophysics v.2, SEG, Tulsa, 658-708.
- Galbraith, J.N. and Wiggins, R.A. (1968). Characteristics of optimum multichannel stacking filters. Geophysics, 33, 36-48.
- Gass, I.G. (1972). Talk presented at University of Durham.
- Gass, I.G. et al. (1971). Understanding the Earth. Artemis Press, Sussex.
- George, T.N. (1960). The stratigraphical evolution of the Midland Valley. Trans. geol. Soc. Glasg., 24, 32-107.
- Gibb, R.A. and Walcott, R.I. (1971). A Precambrian suture in the Canadian Shield. Earth Planet. Sci. Letters, 10, 417-422.
- Giekie, A. (1897). The ancient volcanoes of Great Britain. Macmillan and Co., London.
- Giletti, B.J. et al. (1961). A geochronological study of the metamorphic complexes of the Scottish Highlands. Q. Jl. geol. Soc. Lond., 117, 233-272.
- Goodacre, A.K. (1972). Ph.D. thesis, Univ. of Durham. (to be submitted).

- Goodlet, G.A. (1959). Mid Carboniferous sedimentation in the Midland Valley of Scotland. Trans. Edinb. geol. Soc., 19, 225-255.
- Grant, F. (1957). A problem in the analysis of geophysical data. Geophysics, 22, 309-344.
- Grant, F.S. and West, G.F. (1957). Interpretation theory in applied geophysics. McGraw Hill, New York.
- Greig, D.C. (1971). The South of Scotland, Third edition, HMSO, Edinburgh.
- Griffin, W.R. (1949). Residual gravity in theory and practice. Geophysics, 14, 39-56.
- Gudmundsson, G. (1966). Interpretation of one dimensional magnetic anomalies using the Fourier transform. Geophys. J.R. astr. Soc., 12, 87-97.
- Gunn, P.J. (1967). Gravitational and magnetic interpretation of the Middleback Range area, South Australia. M.Sc. thesis, Univ. of Melbourne.
- Hall, D.H. (1964). Magnetic and tectonic regionalization of Texada Island, British Columbia. Geophysics, 29, 565-581.
- Hall, D.H. (1968). Regional magnetic anomalies, magnetic units and crustal structure in the Kenora District of Ontario. Can. J. Earth Sci., 5, 1277-1296.
- Hall, D.H. and Dagley, P. Regional magnetic anomalies. Rep. No.70/10. Inst. geol. Sci.
- Hall, J. (1970). The correlation of seismic velocities with formations in South West Scotland. Geophys. Prospect., 18, 134-148.
- Hall, J. (1971). A preliminary seismic survey adjacent to the Rashie-hill borehole near Slamman, Stirlingshire. Scott. J. Geol., 7, 170-174.
- Hartley, J.J. (1933). Geology of North-eastern Tyrone. Proc. R. Ir. Acad., 41B, 184-285.
- Hartley, J.J. (1936). The age of the igneous series of Slieve Gallion. Geol. Mag., 73, 226-228.
- Heiland, C.A. (1963). Geophysical Exploration, Hafner Publishing Company, New York and London.
- Henderson, R.G. (1960). A comprehensive system of automatic computation in gravity and magnetic interpretation. Geophysics, 25, 569-585.
- Henderson, R.G. (1970). On the validity of the upward continuation integral for total magnetic intensity data Geophysics, 35, 916-919.

- Henderson, R.G. and Zeitz, I. (1949). The computation of second vertical derivatives of geomagnetic fields, Geophysics, 14, 508-516.
- Holroyd, M.T. and Bhattacharyya, B.K. (1970). Automatic contouring of geophysical data using bicubic spline interpolation. Geological survey of Canada, Paper 70-55.
- Hospers, J. and Charlesworth, H.A.K. (1954). The natural permanent magnetization of the lower basalts of Northern Ireland. Mon. Not. R. Astron. S. Geophys. Suppl., 7, 32-43.
- Hsu, H.P. (1970). Fourier Analysis. Simon and Schuster, New York.
- Hughes, D.S. (1942). The analytical basis of gravity interpretation, Geophysics, 7, 167-178.
- Hughes, D.S. and Pondron, W.L. (1947). Computation of vertical magnetic anomalies from total magnetic field measurements. Am. Geophys. Union Trans., 28, 193-197.
- IBM (1968). System/360, scientific subroutine package (360-CM-03X) Version III. IBM New York.
- Ingles, A.D. (1971). The interpretation of magnetic anomalies between Iceland and Scotland. Ph.D. thesis, Univ. of Durham.
- Jacobs, J.A. (1963). The earth's core and geomagnetism. Pergamon Press, London.
- Jenkins, G.M. and Watts, D.G. (1968). Spectral analysis and its applications. Holden Day series in time series analysis, San Francisco.
- Johnson, M.R.W. and Harris, A.L. (1967). Dalradian-?Arenig relations in parts of the Highland Border, Scotland, and their significance in the chronology of the Caledonian orogeny. Scott. J. Geol., 3, 1-16.
- Kanasewich, E.R. and Agarwal, R.G. (1970). Analysis of combined gravity and magnetic fields in the wave number domain. J. geophys. Res., 75, 5702-5712.
- Kennedy, W.Q. (1958). Tectonic evolution of the Midland Valley of Scotland. Trans. geol. Soc. Glasg. 23, 107-133.
- Lavin, P.M. and Devane, J.F. (1970). Direct design of two dimensional wavenumber filters, Geophysics, 35, 1073-1078.
- Laving, G.J. (1971). Automatic methods for the interpretation of gravity and magnetic field anomalies and their application to marine geophysical surveys. Ph.D. thesis, Univ. of Durham.
- Leake, B.E. (1963). The location of the Southern Uplands Fault in central Ireland. Geol. Mag., 100, 420-423.

- Levinson, N. (1947). The Wiener RMS (root mean square) error criterion in filter design and prediction. J. Math. Phys., 25, 261-278.
- Macgregor, A.G. (1948). Problems of Carboniferous-Permian Volcanicity in Scotland. Q. Jl. geol. Soc. London., 104, 133-153.
- Macgregor, M. and Macgregor, A.G. (1948). The Midland Valley of Scotland. H.M.S.O., Edinburgh.
- McQuillin, R. (1970). In Francis et al. (1970) 308-321.
- McKee, D. and Burke, K. (1957). Geology of the islands of South Connemara. Geol. Mag., 92, 487-498.
- McLean, A.C. (1966). A gravity survey in Ayrshire and its geological interpretation. Trans. R. Soc. Edinb., 66, 239-265.
- McLean, A.C. and Qureshi, I.R. (1966). Regional gravity anomalies in the western Midland Valley of Scotland. Trans. R. Soc. Edinb., 66, 267-283.
- Mercy, E.L.P. (1965). Caledonian igneous activity. In Craig (1965) 230-269.
- Mesko, A. (1965). Some notes concerning the frequency analysis for gravity interpretation. Geophys. Prospect., 13, 477-488.
- Meško, A. (1966). Two dimensional filtering and the second derivative method. Geophysics, 31, 606-617.
- Murphy, T. (1952). Gravity survey of central Ireland. Geophys. Mem. Dubl., 2, (3).
- Naidu, P.S. (1966). Extraction of potential field signal from a background of random noise by Strakhov's method. J. geophys. Res., 71, 5987-5995.
- Naidu, P.S. (1967). Statistical properties of potential fields over a random medium. Geophysics, 32, 88-98.
- Naidu, P.S. (1968). An example of linear filtering in aeromagnetic interpretation. Geophysics, 33, 602-612.
- Naudy, H. (1967). Essai de filtrage non-linéaire appliqué aux profils aeromagnetiques. Geophys. Prospect., 16, 171-178.
- Naudy, H. (1970). Automatic contouring of the total field and the vertical gradient. Boll. Geofis. teor. appl. 12, 123-136.
- Nesbitt, J.D. (1965). A preliminary statistical study of remanent intensities of magnetization and other palaeomagnetic investigations. Ph.D. thesis, Univ. of Newcastle.

- Oldham, C.H.G. (1967). The  $(\sin x)/x$ .  $(\sin y)/y$  method for continuation of potential fields. In Mining Geophysics v.2, SEG., Tulsa.
- Oxburgh, E.R. (1971). Plate tectonics. In Gass et al. (1971), 263-286.
- Park, R.G. (1961). A vertical force magnetic survey over part of the Dusk Water Fault in Ayrshire. Trans. geol. Soc. Glasg., 24, 154-168.
- Parker Gay, S. (1965). Standard curves for magnetic anomalies over long horizontal cylinders. Geophysics, 30, 818-828.
- Peach, B.N. and Horne, J. (1899). The Silurian rocks of Britain. 1, Scotland Mem. geol. Surv.
- Peters, L.J. (1949). The direct approach to magnetic interpretation and its practical application. Geophysics, 18, 894-912.
- Powell, D.W. (1963). Significance of differences in magnetization along certain dolerite dykes. Nature Lond., 199, 674-676.
- Powell, D.W. (1970). Magnetized rocks within the Lewisian of Western Scotland and under the Southern Uplands. Scott. J. Geol., 6, 335-369.
- Powell, D.W. (1971). A model for the Lower Palaeozoic evolution of the southern margin of the early Caledonides of Scotland and Ireland. Scott. J. Geol., 7, 369-372.
- Pringle, J. (1948). The South of Scotland. Second edition. H.M.S.O. Edinburgh.
- Qureshi, I.R. (1970). A gravity survey of a region of the Highland Boundary Fault in Scotland. Q. Jl. geol. Soc. Lond., 125, 481-502.
- Ramsay, D.M. (1964). Deformation of pebbles in the Lower Old Red Sandstone conglomerates adjacent to the Highland Boundary Fault. Geol. Mag., 101, 228-248.
- Reford, M.S. (1964). Magnetic anomalies over thin sheets. Geophysics, 29, 532-536.
- Richey, J.E. (1961). The Tertiary volcanic districts. Third edition, H.M.S.O., Edinburgh.
- Robinson, E.A. (1967). Multichannel time series analysis with digital computer programs. San Francisco. Holden Day.
- Robinson, E.A. and Treitel, S. (1967). Principles of Digital Wiener Filtering. Geophys. Prospect., 15, 311-333.
- Rosenbach, O. (1953). A contribution to the computation of the "second derivative" from gravity data. Geophysics, 18, 894-909.

- Rosenbrock, H.H. (1960). An automatic method for finding the greatest and least value of a function. Comp. J., 3, 175-184.
- Roy, A. (1962). Ambiguity in geophysical interpretation. Geophysics, 27, 90-99.
- Russell, M.J. (1968). Structural controls of base metal mineralization in Ireland in relation to continental drift. Trans. Instn. Min. Metall., B78, 127-131.
- Russell, M.J. (1972). North-south geofractures in Scotland and Ireland. Scott. J. Geol., 8, 75-84.
- Scholl, D.W. (1970). Peru Chile Trench, sediments and sea floor spreading. Bull. geol. Soc. Am., 81, 1339-1360.
- Serbulenko, M.G. (1965). Some applications of Wiener's filtration theory to the study of the earth's crust using gravitational data. Bull. (Izv.) Acad. Sci. USSR, Earth Phys. Ser., 8, 530-535.
- Shackleton, R.M. (1961) in Gilletti et al. (1961).
- Skeels, D.C. and Watson, R.J. (1949). Derivation of magnetic and gravitational quantities by surface integration. Geophysics, 14, 133-150.
- Slack, H.A., Lynch, V.M. and Langan, L. (1967). The geomagnetic gradiometer. Geophysics, 32, 877-892.
- Spector, A. (1968). Spectral analysis of aeromagnetic maps. Ph.D. thesis Univ. of Toronto.
- Spector, A. and Bhattacharyya, B.K. (1966). Energy density spectrum and autocorrelation function of anomalies due to simple magnetic models. Geophys. Prospect., 14, 242-272.
- Spector, A. and Grant, F.S. (1970). Statistical models for interpreting aeromagnetic data. Geophysics, 35, 293-302.
- Steenland, N.C. (1968). The geomagnetic gradiometer. Geophysics, 33, 680-686.
- Stewart, F.H. (1965). Tertiary igneous activity. In Craig (1965), 420-461.
- Strangeway, D.W. (1967). Mineral Magnetism in Mining Geophysics, v2, SEG, Tulsa.
- Strakhov, V.N. (1964a). The smoothing of observed strengths of potential fields I, Bull. (Izv) Acad. Sci. U.S.S.R., Geophys. Ser. (Eng. Trans.), 10, 897-904.
- Strakhov, V.N. (1964b). The smoothing of observed strengths of potential fields II, Bull. (Izv) Acad. Sci. U.S.S.R., Geophys. Ser. (Eng. Trans.), 11, 986-995.

- Stubbs, P.H.S. (1957). Continental drift and polar wandering: a palaeomagnetic study of the British and European Trias, and of the British Old Red Sandstone, Ph.D. thesis, Imperial College.
- Swartz, C.A. (1954). Some geometrical properties of regional maps. Geophysics, 19, 46-70.
- Talwani, M. (1964). Upward and downward continuation of gravity fields on a plane. In Computers in the Mineral Industries, Stanford University, 409-428.
- Talwani, M. and Ewing, M. (1960). Rapid computation of gravitational attraction of three dimensional bodies of arbitrary shape. Geophysics, 25, 203-225.
- Talwani, M. and Heirtzler, J.R. (1964). Computation of magnetic anomalies caused by two dimensional structures of arbitrary shape. In Computers in the Mineral Industries. Stanford University, 464-479.
- Talwani, M., Sutton, G.H. and Worzel, J.L. (1959). A crustal section across the Puerto Rico trench. J. geophys. Res., 64, 1545-1555.
- Talwani, M. Worzel, J.L. and Landisman, M. (1959). Rapid gravity computations for two dimensional bodies with application to the Mendocino submarine fracture zone. J. geophys. Res., 64, 49-59.
- Tanner, J.G. (1967). An automated method of gravity interpretation Geophys. J.R. astr. Soc., 13, 339-347.
- Tomoda, Y. and Aki, K. (1955). Use of the function  $(\sin x)/x$  in gravity problems. Proc. Japan. Acad., 31, 443-448.
- Treitel, S. (1970). Principles of digital multichannel filtering Geophysics, 35, 785-811.
- Treitel, S. and Robinson, E.A. (1966). The design of high resolution digital filters. IEEE Trans. on Geosci. Electronics, GE-4, 25-38.
- Treitel, S. and Robinson, E.A. (1969). Optimum digital filters for signal to noise ratio enhancement. Geophys. Prospect., 17, 248-293.
- Tsuboi, C. and Fuchida, T. (1938). Relation between gravity values and the corresponding subterranean mass distribution. Bull. Earthq. Res. Inst. Tokyo Univ., 15, 636-649.
- Tsuboi, C., Oldham, C.H.G. and Waithman, V.B. (1968). Numerical tables facilitating three dimensional gravity interpretations. J. Phys. Earth, 6, 7-13.
- Tsuboi, C. and Tomoda, Y. (1958). The relation between the Fourier series and the  $(\sin x)/x$  method for gravity interpretations. J. Phys. Earth, 6, 7-13.

- Vacquier, V. et al. (1949). Interpretation of aeromagnetic maps. Mem. Geol. Soc. Am. No.47.
- Vine, F.J. and Matthews, D.H. (1963). Magnetic anomalies over oceanic ridges. Nature, Lond., 199, 947-949.
- Walters, R.F. (1969). Contouring by machine: a users guide. Bull. Am. Ass. Petrol. Geol., 53, 2324-2340.
- Walton, E.K. (1963). Sedimentation and structure in the Southern Uplands, in British Caledonides, M.R.W. Johnson and F.H. Stewart (editors). Oliver and Boyd, Edinburgh.
- Walton, E.K. (1965). Lower palaeozoic rocks - palaeogeography and structure. In Craig (1965), 201-227.
- Wiener, N. (1949). Extrapolation, interpolation and smoothing of stationary time series. John Wiley and Sons, New York.
- Wiggins, R.A. and Robinson, E.A. (1965). Recursive solution to the multichannel filtering problem. J. geophys. Res., 70, 1885-1891.
- Wilson, J.T. (1966). Did the Atlantic close then re-open? Nature, Lond., 211, 676-681.
- Wright, J.B. (1971). Volcanism and the earth's crust, in Gass et al. (1971) 301-314.
- Ziegler, A.M. (1970). Geosynclinal development of the British Isles during the Silurian period. J. Geol., 78, 445-479.
- Zurflueh, E.G. (1967). Application of two dimensional linear wavelength filtering. Geophysics, 32, 1015-1035.



```

C ----- NC= NUMBER OF SIGNAL VALUES/CARD
C
C SPEC.CARD 4. (1GA4) XFO
C ----- XFO = FORMAT OF SIGNAL VALUES
C
C DATA CARDS. SIGNAL TO BE FILTERED IN FORMAT XFO. 999999. MUST BE
C ----- PUNCHED IN FIRST POSITION OF FOLLOWING CARD
C
C REPEAT SPEC.CARD 3 ETC. TO PROCESS MORE SIGNALS WITH THE
C CALCULATED FILTER COEFFICIENTS
C
C TERMINATION BLANK CARD
C -----
C OUTPUT SELF EXPLANATORY PRINTED OUTPUT. IF IPUNCH OPTION IS
C ***** USED THE FILTER COEFFICIENTS ARE PUNCHED ON CARDS IN
C ***** FORMAT (1CF8.5) *****
C ***** DOUBLE PRECISION B(1000),A(1000),C(1000),ERRORS(1000),SPACE(1000)
C ***** 1,D(1000),ASE,PI,XMID,WL,XI,THETA,Z,VAL(1000),BB(1000)
C B IS INPUT WAVELET LR IS THE LENGTH OF B
C D IS DESIRED OUTPUT LD IS THE LENGTH OF D
C A ARE SHAPING COEFFS LA IS THE LENGTH OF A
C C IS ACTUAL OUTPUT LC IS THE LENGTH OF C
C ***** WRITE(6,3C1)
C 301 FORMAT(1HC, ' CALCULATION AND APPLICATION OF A ONE DIMENSIONAL
C 1WIENER FILTER')
C 1 FORMAT(8I1C)
C 2 FORMAT(1CF8.2)
C READ(5,1) LB,LA,JUMP,IA,IB,IPUNCH,ISTAP,IDENTAP
C WRITE(6,3C2) LB,LA,JUMP,IA,IB,IPUNCH,ISTAP,IDENTAP
C 302 FORMAT(1HC, ' LB=',I4, ' LA=',I4, ' JUMP=',I4, ' IA=',I4, ' IB=',I4, ' IP
C 1UNCH=',I4, ' ISTAP=',I4, ' IDENTAP=',I4)
C LB=(IB-IA)/JUMP+1
C IT=C
C 11 I=IT+1
C IT=I+9
C READ(5,2) (VAL(J),J=I,IT)
C IF(VAL(I)-999999.) 11,10,11
C 10 NUM=I-1

```

```

K=0
DO 20 I=IA,IB,JUMP
K=K+1
20 B(K)=VAL(I)
IF(ISTAP.EQ.1) CALL TAPER(B,LB)
888 CONTINUE
IT=0
31 I=IT+1
IT=I+9
READ(5,2) (D(J),J=I,IT)
DO 900 L=I,IT
IF(D(L)-999999.) 900,30,30
900 CONTINUE
GO TO 31
30 CONTINUE
LD=LB
KS=LA/2
K=0
DO 220 I=IA,IB,JUMP
K=K+1
220 D(K)=D(I)
IF(IDTAP.EQ.1) CALL TAPER(D,LD)
CALL ZERO (KS,VAL)
K=KS
DO 221 I=1,LD
K=K+1
221 VAL(K)=D(I)
LD=KS+LB
CALL SHAPE(LB,B,LD,VAL,LA,A,LC,C,ASE,SPACE,D,IA,IB,JUMP,8B)
WRITE(6,101)
101 FORMAT(1H0,'INPUT WAVELET')
WRITE(6,102) (B(I),I=1,LB)
102 FORMAT(1X,10F12.4)
WRITE(6,103)
103 FORMAT(1H0,'DESIRED OUTPUT')
WRITE(6,102) (VAL(I),I=1,LD)
WRITE(6,104)
104 FORMAT(1H0,'ACTUAL OUTPUT')
WRITE(6,102) (C(I),I=1,LC)

```

```
WRITE(6,105)
105 FORMAT(1HC,'SHAPING COEFFS:')
WRITE(6,102) (A(I),I=1,LA)
IF(IPUNCH.EQ.1) WRITE(7,106) (A(I),I=1,LA)
106 FORMAT(10F8.5)
4 FORMAT(1X,10F12.2)
CALL CONV (LA,A,JUMP)
CALL EXIT
END
```

```
C
SUBROUTINE TAPER (B,LB)
DIMENSION B(1)
DOUBLE PRECISION PI,MWL,Z,XI,THETA,B
COSINE TAPER
PI=3.1415926536
MXMID=LB/2+1
XMID=DFLOAT(MXMID)
MWL=LB/2
WL=DFLOAT(MWL)
DO 200 L=1,LB
Z=DFLOAT(L)
XI=DABS(XMID-Z)
THETA=(PI*XI)/WL
200 B(L)=(3.5400+0.4600*DCOS(THETA))*B(L)
RETURN
END
```

```
SUBROUTINE CONV(LB,D,JUMP)
DIMENSION T(3000),B(1000),C(3000),VAL(3000)
DOUBLE PRECISION D(1)
DIMENSION XFO(10)
DO 1500 I=1,LB
1500 B(I)=D(I)
IGAP=1
LAG=((LB-1)*JUMP)/2+1
```

```

484 FORMAT(10X,10F7.1)
450 FORMAT(11C)
451 FORMAT(10A4)
401 FORMAT(411L)
C      JUMP ZEROES ARE INSERTED BETWEEN THE FILTER COEFFICIENTS
      JUL=LB#JUMP
      DO 300 I=1,JUL
300  C(I)=0
      J=0
      DO 301 I=1,JUL,JUMP
      J=J+1
301  C(I)=B(J)
      DO 302 I=1,JUL
302  B(I)=C(I)
      LB=JUL-1
      WRITE(6,201)
201  FORMAT(1X,'FILTER COEFFICIENTS')
      WRITE(6,3) (B(I),I=1,LB)
      4  FORMAT(10X,10F12.4)
4455 CONTINUE
      READ(5,450) NC
      IF(NC.EQ.0) GO TO 9999
      WRITE(6,202)
202  FORMAT(1HC,' INPUT FUNCTION')
      READ(5,451) XFO
      IT=0
      11 I=IT+1
      IT=IT+NC
      READ(5,XFO) (VAL(J),J=1,IT)
      3  FORMAT(1X,10F12.3)
      WRITE(6,3)(VAL(J),J=1,IT)
      DO 1501 J=1,IT
      IF(VAL(J)-999998.) 1501,10,10
1501 CONTINUE
      GO TO 11
      10 NP =I-1
      NS=LB
      NE=NP+LB-1
      DO 100 I=1,LB

```

```

100 T(NE+I)=2.*VAL(NP)-VAL(NP-I)
    T(NS-I)=2.*VAL(1)-VAL(1+I)
    IS=NS
    IE=NS+NP-1
    J=0
    DO 101 I=IS,IE
        J=J+1
101 T(I)=VAL(J)
    C   WRITE(6,203)
203 FORMAT(1X,'EXTRAPOLATED INPUT FUNCTION')
    LA=NP+LB-1
    LZ=NP+2*LB-2
    CALL FILD(LA,T,LB,B,LC,C,IGAP,LAG)
    ICS=1
    ICE=LA
    WRITE(6,204)
204 FORMAT(1HC,'OUTPUT FUNCTION')
    GO TO 4455
9999 CALL EXIT
      RETURN
      END

SUBROUTINE FILD(LA,A,LB,B,LC,C,IGAP,LAG)
DIMENSION A(1 ),B(1 ),C(1 ),XP(2000),CC(3000)
LC=LA+LB
DO 100 I=1,LC
100 C(I)=F.DC
    NP=0
    MP=-IGAP+1
    IZ1=LB+LAG-1
    IZ2=LA+LAG-1
    K=0
    DO 12 I=IZ1,IZ2,IGAP
        K=K+1
    NP=NP+1
    MP=MP+IGAP

```

```

XP(NP)=FLOAT(MP)
DO IC J=1,LS
10 C(K)=B(J)*A(I-J+1)+C(K)
12 CC(NP)=C(K)
LA=K
  IF(IGAP.EQ.1) GO TO 32
  CALL SPLINE(XP,CC,A,NP,NC,1)
L=LB-1
DO 31 I=1,NC
L=L+1
31 C(L)=A(I)
LC=NC
GO TO 33
32 LC=NP
33 RETURN
END

```

```

SUBROUTINE SHAPE(LB,B,LD,D,LA,A,LC,C,ASE,SPACE,VAL,IA,IB,JUMP,BR)
SHAPE IS SHAPING FILTER
INPUTS ARE LB,B,LD,D,LA
OUTPUTS ARE A,LC,C,ASE
SPACE(I),I=1,4#LA WORKING SPACE
MAY BE EQUIVALENCE (C,D)
DOUBLE PRECISION B(1),D(1),A(1),C(1),SPACE(1),VAL(1),BB(1)
1,DD,ASE,AG,GA
CALL CROSS(LB,B,LB,B,LA,SPACE)
READ(5,1) GA
1 FORMAT(F10.1)
  IF(GA.EQ.0) GO TO 200
WRITE(6,300) GA
300 FORMAT(1H0,' NOISE REDUCTION FACTOR = ',F10.3)
WRITE(6,301)
301 FORMAT(1H0,' NOISE WAVEFORM')
LB=(IB-IA)/JUMP+1
IT=0
11 I=IT+1
IT=I+9

```

```

READ(5,6) (VAL(J),J=1,IT)
6 FORMAT(1CF8.2)
IF(VAL(I)-9999999.) 11,10,11
10 NUM=I-1
K=0
DO 20 I=IA,IB,JUMP
K=K+1
20 BB(K)=VAL(I)
WRITE(6,4) (BB(J),J=1,LB)
4 FORMAT(1X,10F12.2)
CALL CROSS (LB, RB, LB, BR, LA, VAL)
DO 100 I=1,LA
100 SPACE(I)=SPACE(I)+GA*VAL(I)
200 CONTINUE
CALL CROSS(LD,D, LB,B, LA,SPACE(LA+1))
CALL EUREKA(LA,SPACE,SPACE(LA+1),A,SPACE(2*LA+1))
CALL DOT(LD,D,D,DD)
CALL DOT(LA,A,SPACE(LA+1),AG)
ASE=(DD-AG)/DD
CALL FOLD(LA,A, LB,B, LC,C)
RETURN
END

```

```

SUBROUTINE FOLD(LA,A, LB,B, LC,C)
FOLD IS FOLDING(CONVOLUTION)
DOUBLE PRECISION A(I),B(I),C(I)
LC=LA+LR-1
CALL ZERO(LC,C)
DO 10 I=1,LA
DO 10 J=1,LB
K=I+J-1
10 C(K)=A(I)*B(J)+C(K)
RETURN
END

```

C

```
SUBROUTINE IMPULS(LD,D,K)
DOUBLE PRECISION D(I)
DO 10 I=1,LD
10 D(I)=C.DC
D(K)=1.D0
RETURN
END
```

```
SUBROUTINE CROSS(LX,X,LY,Y,LC,C)
DOUBLE PRECISION X(I),Y(I),C(I)
DO 10 I=1,LC
10 CALL DOT
      ( MINE(LY+I-1,LX)-I+1,X(I),Y,C(I))
RETURN
END
```

```
SUBROUTINE DOT(L,X,Y,ANS)
DOT IS DOT PRODUCT
DOUBLE PRECISION X(I),Y(I),ANS
ANS=C.DC
IF(L) 30,30,10
10 DO 20 I=1,L
20 ANS=ANS+X(I)*Y(I)
30 RETURN
END
```

```
SUBROUTINE MINSN(LX,X,XMIN,INDEX)
DOUBLE PRECISION X(I),XMIN
XMIN=X(1)
DO 10 I=1,LX
10 XMIN=DMINI(XMIN,X(I))
DO 20 J=1,LX
INDEX=J
```

C

```
IF(X(J)-XMIN) 20,30,20
20 CONTINUE
30 RETURN
END
C ZERO IS TO STORE ZERO IN AN ARRAY
```

```
SUBROUTINE ZERO(LX,X)
DOUBLE PRECISION X(1)
IF(LX)30,30,10
10 DO 20 I=1,LX
20 X(I)=0.00
30 RETURN
END
C DOTR IS DOT PRODUCT REVERSE
```

```
SUBROUTINE DOTR(L,X,Y,ANS)
DOUBLE PRECISION X(1),Y(1),ANS
ANS=0.00
IF(L)30,30,10
10 DO 20 I=1,L
J=L-I+1
20 ANS=ANS+X(I)*Y(J)
30 RETURN
END
C EUREKA IS FILTER(LEAST SQUARES)
```

```
SUBROUTINE EUREKA(LR,R,G,A,C)
C(I) I=1,2*LR WORKING SPACE
DOUBLE PRECISION R(1),G(1),A(1),C(1)
A(1)=G(1)/R(1)
C(1)=-1.00
IF(LP-1)30,30,2
2 DO 20 LA=2,LR
```

```

CALL NEXTC(LA-1,R,C,C(LR+1))
DO 10 J=1,LA
I=LR+J
10 C(J)=C(I)
20 CALL NEXTA(G(LA),LA-1,A,C,R,A)
30 RETURN
END
C NEXTC IS CALLED BY EUREKA

```

```

SUBROUTINE NEXTC(LC,R,C,CP)
NON EQUIVALENCE (C,CP)
DOUBLE PRECISION R(1),C(1),CP(1),CONST1,CONST2
CALL DOT(LC,R(2),C,CONST1)
CALL DOTR(LC,R,C,CONST2)
CP(1)=CONST1/CONST2
IF(LC-1) 30,30,10
10 DO 20 I=2,LC
J=LC-I+1
20 CP(I)=C(I-1)-CP(1)*C(J)
30 CP(LC+1)=-1.00
RETURN
END
C NEXTA IS CALLED BY EUREKA

```

```

SUBROUTINE NEXTA(G,LA,A,C,R,AP)
MAY BE EQUIVALENCE(A,AP)
A(I) I=1,LA
C(I) I=1,LA+1
R(I) I=1,LA+1
AP(I) I=1,LA+1
DOUBLE PRECISION A(1),C(1),R(1),AP(1),T1,T2,G
CALL DOTR(LA,A,R(2),T1)
CALL DOTR(LA+1,C,R,T2)
AP(LA+1)=(T1-G)/T2
DO 10 I=1,LA

```

```
10 AP(I)=A(I)-AP(LA+1)*C(I)
   RETURN
   END
```





```

EQUIVALENCE(SIGE(1,1),A(1))
WRITE(6,8003)
8002 FORMAT(1H0,' CALCULATION AND APPLICATION OF TWO DIMENSIONAL WIENE
IR FILTERS')
READ(5,50) M,N,ITAP,IPUNCH
IF(ITAP.EQ.0) WRITE(6,8007)
IF(ITAP.EQ.1) WRITE(6,8008)
8007 FORMAT(1X,' INPUT AND DESIRED OUTPUT HAMMING WINDOW TAPERED')
8008 FORMAT(1X,' INPUT HAMMING WINDOW TAPERED DESIRED OUTPUT UNTAPERED')
MN=M*N
WRITE(6,51) M,N
50 FORMAT(4I10)
51 FORMAT(1H0,' WIDTHS OF DESIRED FILTER, M=',I3,' N=',I3)
GA=1.00
INDISE=0
ITWO=0
WRITE(6,8000)
8000 FORMAT(1H0,' INPUT SIGNAL')
5000 CALL IN (VAL,IMAX,JMAX)
IMID=IMAX/2+1
JMID=JMAX/2+1
WI=DFLOAT(IMAX)
WJ=DFLOAT(JMAX)
XIMID=DFLOAT(IMID)
XJMID=DFLOAT(JMID)
PI=3.141592653600
DEN=XIMID
DO 801 I=1,IMAX
DO 801 J=1,JMAX
ZI=DFLOAT(I)
ZJ=DFLOAT(J)
XI=DABS(XIMID-ZI)
XJ=DABS(XJMID-ZJ)
RAD=DSQRT(XI*XI+XJ*XJ)
THETA=(RAD#PI)/DEN
TAPERED INPUT SIGNAL
SIG(I,J)=(0.5400+0.4600#DCOS(THETA))*VAL(I,J)
801 IF(RAD.GT.XIMID) SIG(I,J)=0.00
IF(INDISE.GT.0) GO TO 5001

```

C

```

C FIND CROSSCORRELATION OF INPUT AND DESIRED OUTPUT
C READ DESIRED OUTPUT
C NOTE DESIRED OUTPUT MUST BE SAME SIZE AS INPUT
WRITE(6,800?)
800? FORMAT(:HO,' DESIRED OUTPUT')
CALL IN (VAL, IDMAX, JDMAX)
WI=DFLOAT(IDMAX)
WJ=DFLOAT(JDMAX)
IMID=IDMAX/?+1
JMID=JDMAX/?+1
XIMID=DFLOAT(IMID)
XJMID=DFLOAT(JMID)
DEN=XIMID
DO 802 I=1, IDMAX
DO 802 J=1, JDMAX
ZI=DFLOAT(I)
ZJ=DFLOAT(J)
XI=DABS(XIMID-ZI)
XJ=DABS(XJMID-ZJ)
RAD=DSQRT(XI*XI+XJ*XJ)
THETA=(RAD*PI)/DEN
C TAPERED DESIRED OUTPUT
C(I,J)=(0.54D0+0.46D0*DCOS(THETA))*VAL(I,J)
IF(RAD.GT.XIMID) C(I,J)=0.D0
802 IF(ITAP.F0.1) C(I,J)=VAL(I,J)
IEXT=IDMAX+M/2+M/2
JEXT=JDMAX+M/2+M/2
DO 550 I=1, IEXT
DO 550 J=1, JEXT
550 SIGE(I,J)=0.D0
JD=M/2
DO 551 J=1, JDMAX
JD=JD+1
ID=M/2
DO 551 I=1, IDMAX
ID=ID+1
C EXTRAPOLATED DESIRED OUTPUT
551 SIGE(ID,JD)=C(I,J)
CALL CONV(IEXT,JEXT,I*MAX,J*MAX,0,0)

```

C REVERSE CROSS CORRELATION

```
II=IMAX/2+M+1
IS=IMAX/2+1
IE=IS+M-1
DO 738 I=IS,IE
II=II-1
JJ=JMAX/2+N+1
JS=JMAX/2+1
JE=JS+N-1
DO 739 J=JS,JE
JJ=JJ-1
738 SIGE(I,J)=C(II,JJ)
LC=0
MS=IMAX/2
DO 600 LM=1,M
MS=MS+1
NS=JMAX/2
DO 600 LN=1,N
NS=NS+1
LC=LC+1
```

C CROSSCORRELATION OF DESIRED OUTPUT AND INPUT

```
600 R(LC)=SIGE(MS,NS)
500 ITEXT=IMAX+M-1
JEXT=JMAX+N-1+N-1
DO 100 I=1,ITEXT
DO 100 J=1,JEXT
100 SIGE(I,J)=0.00
NM=0
MS=M
NS=N
MF=MS+IMAX-1
NF=NS+JMAX-1
DO 101 J=NS,NE
NN=NN+1
MM=0
DO 101 I=MS,ME
MM=MM+1
```

101 SIGE(I,J)=SIG(MM,NN)

C NOW HAVE SIGE IN FORM FOR AUTOCORRELATION

```

CALL CONV (IEXT,JEXT,IMAX,JMAX,0,0)
JS=JMAX/2+1
IS=IMAX/2+1
JE=JS+2*N-2
IE=IS+M-1
JJ=0
DO 102 J=JS,JE
  JJ=JJ+1
  II=0
  DO 102 I=IS,IE
    II=II+1
  102 SIGE(II,JJ)=C(I,J)
  C
  NOW HAVE AUTOCORRELATION OF INPUT
  IS=II+1
  IE=IS+M-2
  DO 103 J=1,JJ
    IC=0
    DO 103 I=IS,IE
      IC=IC+1
      MI=II-IC
      MJ=JJ+1-J
    103 SIGE(I,J)=SIGE(MI,MJ)
    IF(ITWD.EQ.1) GO TO 4001
    DOUBLE PRECISION YY(28561)
    DO 5003 I=1,28561
      5003 YY(I)=0.000
    4001 CONTINUE
    ICCOUNT=0
    YAC=M
    NAC=N
    MM=-M/2-1
    DO 400 MP=1,MAC
      MM=MM+1
      NN=-N/2-1
      DO 400 NP=1,NAC
        NN=NN+1
        JJ=-M/2-1
        DO 400 JP=1,MAC
          JJ=JJ+1

```

```

KK=-N/2-1
DO 400 KP=1,NAC
KK=KK+1
C   INDICES OF PHI,II
   JPHI=JJ-MM
   KPHI=KK-NN
   JPHI=JPHI+M
   KPHI=KPHI+N
   ICCOUNT=ICCOUNT+1
   Y(ICCOUNT)=GA*SIGE(JPHI,KPHI)+YY(ICCOUNT)
400 YY(ICCOUNT)=Y(ICCOUNT)
402 FORMAT(1X,10F12.3)
   IF(ITWO.GT.0) GO TO 5004
   READ(5,5005) INOISE,GA
5005 FORMAT(110,F10.1)
5006 FORMAT(1H0,' WEIGHT OF NOISE REDUCTION = ',F10.2)
   WRITE(6,5006) GA
   ITWO=1
   IF(INOISE.GT.0) WRITE(6,8001)
8001 FORMAT(1H0,' NOISE SIGNAL')
   IF(INOISE.GT.0) GO TO 5000
5004 A(1)=Y(1)
   NA=1
   NROWS=N*N
   NCOLS=M*M
   IT=1
DO 403 J=2,NCOLS
IT=IT+NROWS
IB=IT+J-1
DO 405 I=IT,IB
NA=NA+1
405 A(NA)=Y(I)
403 CONTINUE
MN=M*N
DIMENSION AUX(200)
K=1
EPS=0.000000000001
CALL DGELS(R,A,MN,1,EPS,IER,AUX)
C   CALL SIMQ(A,P,MN,IER)

```

```

WRITE(6,730) IER
730 FORMAT(1X,' IER=',I10)
732 FORMAT(1X,10F12.6)
L=0
II=M+1
DO 734 I=1,M
II=II-1
II=I
JJ=N+1
DO 734 J=1,N
JJ=JJ-1
JJ=J
L=L+1
734 SIG(II,JJ)=R(L)
WRITE(6,731)
731 FORMAT(1X,' WIFNER SHAPING COEFFS')
DO 8005 J=1,JJ
8005 WRITE(6,732) (SIG(I,J),I=1,II)
1000 CONTINUE
READ(5,6401) I MAX,JMAX
IF(I MAX.EQ.0) GO TO 8006
WRITE(6,8004)
8004 FORMAT(1H0,' SIGNAL TO BE FILTERED')
6401 FORMAT(2I10)
DO 6402 J=1,JMAX
DO 6402 IS=1,I MAX,10
IE=IS+9
IF(IF.GT.I MAX) IE=I MAX
READ(5,200) (VAL(I,J),I=IS,IE)
WRITE(6,201) (VAL(I,J),I=IS,IE)
6402 CONTINUE
200 FORMAT(10X,10F5.0)
201 FORMAT(1X,10F12.2)
DO 803 II=1,I
DO 803 JJ=1,J
803 SIGE(II,JJ)=VAL(II,JJ)
WRITE(6,735)
735 FORMAT(1H0,' FILTERED OUTPUT')
CALL CONV(I,J,M,N,I PUNCH,I)

```

```
JS=N/2+1
IS=M/2+1
JE=J-N/2
IE=I-M/2
GO TO 1000
8006 CALL EXIT
END
```

```
      SUBROUTINE IN (VAL,IMAX,JMAX)
      DOUBLE PRECISION VAL
      DIMENSION VAL(81,81)
      C   I IS HORIZONTAL J IS VERTICAL
      C   READ INPUT
      READ(5,100) IMAX,JMAX
      100 FORMAT(2I10)
      WRITE(6,101) IMAX,JMAX
      101 FORMAT(1X,2I10)
      DO 500 J=1,JMAX
      DO 500 IS=1,IMAX,10
      IE=IS+9
      IF(IE.GT.IMAX) IE=IMAX
      READ(5,200) (VAL(I,J),I=IS,IE)
      WRITE(6,201) (VAL(I,J),I=IS,IE)
      200 FORMAT(10F8.1)
      201 FORMAT(1X,10F12.2)
      500 CONTINUE
      RETURN
      END
```

```
      SUBROUTINE CONV (IMAX,JMAX,LMAX,MMAX,IPUNCH,IWRITE)
      DOUBLE PRECISION VAL,C,SSUM
      DOUBLE PRECISION SUM
      COMMON VAL(169,169),C(80,80),SSUM(169,169)
      LI=LMAX/2+1
      MI=MMAX/2+1
```

```

C      CONVOLUTION BY A TWO DIMENSIONAL OPERATOR
C      LMAX AND JMAX ARE DIMENSIONS OF VALUE ARRAY
C      I IS HORIZONTAL J IS VERTICAL
C      LMAX AND MMAX ARE DIMENSIONS OF COEFF ARRAY
C      LIS HORIZONTAL MIS VERTICAL
C      LI AND MI ARE THE CENTRE OF THE COEFFICIENT ARRAY
C      VAL IS THE VALUE ARRAY      C IS THE COEFFICIENT ARRAY
100 FORMAT(4I10)
201 FORMAT(1X,10F12.5)
      LD=LI-1
      MD=MI-1
      IEND=I*MAX-LD
      JEND=J*MAX-MD
C
      DO 1 I=LI,IEND
      DO 1 J=MI,JEND
      SUM=0.0
      JJ=J-MI
      DO 1 M=1,MMAX
      JJ=JJ+1
      VI=I-LI
      DO 2 L=1,LMAX
      II=II+1
      ? SUM=C(L,M)*VAL(II,JJ)+SUM
      SSUM(I,J)=SUM
109 FORMAT(1X,4I,0)
      1 CONTINUE
      DO 500 J=MI,JEND
      DO 500 I=LI,IEND,10
      IK=I+9
      IF(IK.GT.IEND) IK=IEND
      IF(IWRIT.GT.0) WRITE(6,111) J,I,(SSUM(M,J),M=I,IK)
      IF(JPUNCH.EQ.1) WRITE(7,113) J,I,(SSUM(M,J),M=I,IK)
113 FORMAT(2I5,10F5.2)
112 FORMAT(12I5)
111 FORMAT(1X,2I5,10F10.2)
110 FORMAT(1X,2I5,10I5)
500 CONTINUE
      RETURN

```

END

```

C SUBROUTINE DGELS (P,A,M,N,EPS,IER,AUX)
C DOUBLE PRECISION TO SOLVE A SYSTEM OF SIMULTANEOUS LINEAR EQUATIONS
C WITH SYMMETRIC COEFFICIENT MATRIX UPPER TRIANGULAR PART OF WHICH IS
C ASSUMED TO BE STORED COLUMNWISE
C TAKEN FROM IRLM SSP 1968 P.185
C DIMENSION A(1),P(1),AUX(1)
C DOUBLE PRECISION R,A,AUX,PIV,TR,TOL,PIVI
IF(M) 24,24,1
1 IER=0
  PIV=0.00
  L=0
  DO 3 K=1,M
    L=L+K
    TR=DARS(A(L))
    IF(TB-PIV) 3,3,2
2 PIV=TR
  I=L
  J=K
3 CONTINUE
  TOL=EPS*PIV
  LST=0
  NM=N*M
  LEND=M-1
  DO 18 K=1,M
    IF(PIV) 24,24,4
4 IF(IER) 7,5,7
5 IF(PIV-TOL) 6,6,7
6 IER=K-1
7 LT=J-K
  LST=LST+K
  PIV=1.00/A(I)
  DO 8 L=K,NM,M
    LL=L+LT
    TR=PIV*TR(LL)
    R(LL)=P(LL)

```

```

8 P(L)=TR
  IF(K-M) 9,19,19
9 LR=LST+(LT*(K+J-1))/2
  LL=LR
  L=LST
  DO 14 II=K,LEND
  L=L+II
  LL=LI+1
  IF(L-LR) 12,10,11
10 A(LL)=A(LST)
  TB=A(L)
  GO TO 13
11 LL=L+LT
12 TB=A(LL)
  A(LL)=A(L)
13 AUX(II)=TR
14 A(L)=PIVI*TB
  A(LST)=LT
  PIV=0.00
  LLST=LST
  LT=0
  DO 18 II=K,LEND
  PIVI=-AUX(II)
  LL=LLST
  LT=LT+1
  DO 15 LLD=II,LEND
  LL=LL+LLD
  L=LL+LT
15 A(L)=A(L)+PIVI*A(LL)
  LLST=LLST+II
  LR=LLST+LT
  TB=DARS(A(LR))
  IF(TB-PIV)17,17,16
16 PIV=TB
  I=LR
  J=II+1
17 DO 18 LR=K,NM,M
  LL=LP+LT
18 P(LL)=R(LL)+PIVI*P(LP)

```

```
19 IF(LEND) 24,23,20
20 II=M
   07 22 I=2,M
   LST=LST-II
   II=II-1
   L=A(LST)+.5D0
   08 22 J=II,MM,M
   TB=R(J)
   LL=J
   K=LST
   DO 21 LT=II,LEND
   LL=LL+1
   K=K+LT
   21 TB=TB-A(K)*R(LL)
   K=J+L
   R(J)=R(K)
   22 R(K)=TB
   23 RETURN
   24 IER=-1
   RETURN
   END
```

\*\*\*\*\*

PROGRAM: MULTIM  
CALCULATES AND APPLIES MULTICHANNEL WIENER FILTERS  
HAS OPTION TO ALLOW FOR AUTOCORRELATED NOISE  
P. J. GUNN GEOLOGY DEPARTMENT UNIVERSITY OF DURHAM

\*\*\*\*\*

INPUT

SPEC.CARD 1 (4110) IS,IE,JS,JE  
IS=1

IE=NUMBER OF INPUT SIGNAL CHANNELS  
JS=NUMBER OF FIRST VALUE OF INPUT SIGNAL TO BE CONSIDERED  
JE=NUMBER OF LAST VALUE OF INPUT SIGNAL TO BE CONSIDERED

SPEC.CARD 2 (211, F1, .1) LR,LW,FLOOR  
LR=LENGTH OF DESIRED FILTER  
LW=1'  
FLOOR=LOWER SOUND FOR FILTER ERROR (NORMALLY = 0.1)

SPEC.CARD 3 (11) N  
N= NUMBER OF INPUT SIGNAL CHANNELS

DATA CARDS  
INPUT SIGNAL. THERE ARE N CHANNELS OF INPUT SIGNALS.  
THEY ARE FED IN ONE AFTER THE OTHER IN FORMAT(10F8.1)  
AND 999999. IS PUNCHED IN THE POSITION IMMEDIATELY  
FOLLOWING THE LAST VALUE FOR A CHANNEL. THE NEXT  
CHANNEL STARTS ON A NEW CARD

SPEC.CARD 4 (11) N  
N= NUMBER OF DESIRED OUTPUT CHANNELS

DATA CARDS  
DESIRED OUTPUT CHANNELS IN SAME FORMAT AS INPUT SIGNAL

SPEC CARD 5 (11) N





```

READ(5,3) GA
3 FORMAT(F11.01)
CALL ZFRO (IX,T)
LXN=LX
IF(GA,LE... ) GO TO 5
READ(5,1) N
WRITE(6,50(1)) GA
501 FORMAT(IX,'WEIGHT CF NOISE REDUCTION = ',F10.2)
K=
DO 310 I=1,N
CALL IN (P,LXN)
L=
DO 511 J=1,LXN
L=L+1
511 SSS(L)=P(J)
K=K+1
MS=
DO 411 J=1,LXN
MS=MS+1
411 SS(K,MS)=SSS(J)
31 CONTINUE
C NOTE THAT NOISE MUST HAVE SAME LENGTH AS SIGNAL
K=
DO 113 I=1,LX
DO 113 J=1,N
K=K+1
213 T(K)=SS(J,I)
WRITE(6,212)
212 FORMAT(IX,' NOISE IN MULTIPLEXED MODE')
IX=LX#N
WRITE(6,212) (T(I),I=1,IX)
WRITE(6,212) N,LX,M,LZ
CALL WIENER (N,LX,X,M,LZ,Z,LR,LW,FLOOR,
ILF,F,E,LY,Y,S,LXN,T,GA)
LFI=LE
WRITE(6,216) N,M,LX,LZ,LR,LW,LF,LY
216 FORMAT(IX,1111)
LE=LF
LE=LX#N

```

```

WRITE (6,2,4) LF
2 5 FORMAT(1X, '//', ACTUAL OUTPUT IN MULTIPLEXED MODE LENGTH =', I5)
WRITE (6,2,2) (F(I), I=1, LF)
LY=LY+M
WRITE (6,2,5) LY
2 4 FORMAT(1X, '//', COMPUTED MULTICHANNEL FILTER IN MULTIPLEXED MODE',
1:5)
WRITE (6,2,2) (Y(I), I=1, LY)
WRITE(6,2,7)
2 7 FORMAT(1X, ' NORMALIZED MEAN SQUARE FILTER ERRORS')
WRITE(6,2,2) (E(I), I=1, LE)
K=
6 DO 6 2 MM=1, N
CALL IN (P, LX)
LF=LE
NS=LF
NE=LX+LF-1
DO 6 3 I=1, LF
T(NE+I)=2.0D. *P(LX)-P(LX-I)
6 3 T(NS-I)=2.0D. *P(1)-P(I+1)
KK=LF-2
DO 6 11 I=1, LX
KK=KK+1
6 11 T(KK)=P(I)
LT=LX+2*LF-2
WRITE(6,6,7)
6 7 FORMAT(1X, 'SINGLE CHANNEL OF EXTRAPOLATED INPUT')
WRITE(6,2,2) (T(I), I=1, LT)
L=
DO 6 4 J=1, LT
L=L+1
6 4 XXX(L)=T(J)
K=K+1
M=
DO 6 5 J=1, LT
W=M+1
6 5 XX(K, M)=XXX(J)
6 2 CONTINUE

```

```

00 61 I=1,LT
00 61 J=1,N
K=K+1
61 X(K)=XX(J,I)
LX=N*LT
WRITE(6,62)
62 FORMAT(1X,' INPUT IN MULTICHANNEL MODE')
WRITE(6,202) (X(K),K=1,LX)
LY=LT+LF-I
M=1
CALL BRAINY (M,N,LF,F,N,I,LX,X,Y)
WRITE(6,605)
FORMAT(1X,' MULTICHANNEL OUTPUT')
6 6 WRITE(6,202) (Y(I),I=1,LY)
K=
GO TO 60
CALL EXIT
END
DOUBLE PRECISION FUNCTION SPUR(N,A)
DOUBLE PRECISION A(N,N)
SPUR=.0
DO 1 I=1,N
1 SPUR=SPUR+A(I,I)
RETURN
END

SUBROUTINE REMAY (LY,Y,AVERAG)
DOUBLE PRECISION Y(2)
S=.0
DO 1 I=1,LY
1 S=S+Y(I)
AVERAG=S/FLOAT(LY)
DO 2 I=1,LY
2 Y(I)=Y(I)-AVERAG
RETURN
END

```

```

SUBROUTINE IN(X,LX)
DOUBLE PRECISION X(1)
IT=1
1 IT=IT+1
IT=I+9
READ(5,7) (X(L),L=I,IT)
FORMAT(1,F8.1)
DO 2, L=I,IT
IF(X(L)-9999999.) 200,1,1
CONTINUE
GO TO 10
1 LX=L-1
RETURN
END

```

```

SUBROUTINE WIENER (N,LX,X,M,LZ,Z,LR,LW,FLOOR,
1E,F,E,LY,Y,S,LXN,XN,GA)
VERSION 1 OF SUBROUTINE WIENER
DIMENSION X(N,LX),Z(M,LZ),F(M,N,LR)
DIMENSION E(LR),Y(M,LY),S(NN*(5*LR+6)+MN*(LR+2)
1+2*M*M)
DOUBLE PRECISION FLOOR,P(S(NN*(5*LR+6)+MN*(LR+2)
1),GA)
DOUBLE PRECISION
X(1),Z(1),F(1),E(1),Y(1),S(1),XN(1)
1
NM=N*N
NNLR=NN*LR
MN=M*N

```

```

IR=1
IA=1+NNLR
IB=IA+NNLR
IAP=IB+NNLR
IBP=IAP+NNLR
IVA=IBP+NNLR
IVB=IVA+NN
ICA=IVB+NN

```

```

ICB=ICA+NN
IG=IC9+NN
ICF=IG+MN*LR
IGAM=ICF+MN
IH=IGAM+MN
IFGT=IH+M*M
CALL HEAT(N,1,LZ,Z,M,1,LZ,Z,1,S(IH))
IF(LW.LE.1) L=LR
IGZ=IG+MN*LR
IFZ=IR+NN*LR
IF(LW.GT.1.AND.LW.LT.LR) L=LW
IF(LW.GT.1.AND.LW.LT.LR) CALL ZERO (MN*(LR-LW),
1S(IGZ))
IF(LW.GT.1.AND.LW.LT.LR) CALL ZERO (NN*(LR-LW),
1S(IRZ))
IF(LW.GT.1.AND.LW.GE.LR) L=LR
CALL HEAT(M,1,LZ,Z,N,1,LX,X,L,S(IG))
CALL HEAT(N,1,LX,X,N,1,LX,X,L,S(IR))
WRITE(6,4) (S(J),J=1,L)
CALL HEAT (N,1,LXN,XN,N,1,LXN,XN,L,P)
DO 2: I=1,L
S(I)=S(I)+GA*P(I)
WRITE(6,4) (S(J),J=1,L)
4 FORMAT(IX,1.F10.1)
IF(LW.LE.1.OR.LE.1) GO TO 2
DO 1 K=2,L
IGK=IG+MN*(K-1)
IRK=IR+NN*(K-1)
DOUBLE PRECISION WINDOW
WINDOW=1.0D-DFLOAT(K-1)/DFLOAT(LW-1)
CALL SCALE (WINDOW,MN,S(IGK))
1 CALL SCALE (WINDOW,MN,S(IRK))
2 CALL RECUR (N,M,LR,S,IH),S(IG),FLOOR,LF,F,E,S(IA),
3S(IB),S(IAP),S(IBP),S(IVA),S(IVB),S(IDA),S(IDB),S(ICA),S(ICB),
2S(ICF),S(IGAM),S(IFGT))
LV=LX+LF-1
CALL BRAINY (M,N,LF,F,N,1,LX,X,Y)
RETURN
END

```

```

SUBROUTINE RECUR (N,M,LR,R,H,G,FLOOR,LF,F,E,
1  A,B,AP,BP,VA,VB,DA,DB,CA,CB,CF,GAM,FGT)
DOUBLE PRECISION
1 F(M,N,LR),R(N,N,LR),G(M,N,LR),H(M,M),
2 A(N,N,LR),AP(N,N,LR),B(N,N,LR),BP(N,N,LR),
3 VA(N,N),VB(N,N),DA(N,N),DB(N,N),
4 CA(N,N),CR(N,N),CF(M,N),GAM(M,N)
5 FGT(M,M),E(LR)
DCURLE PRECISION FLOOR
CALL ZERO (N*N*LR,A)
CALL ZERO (N*N*LR,B)
CALL ZERO (M*N*LR,F)
DO 2 I=1,N
DO 1 J=1,N
VA(I,J)=R(I,J,1)
VB(I,J)=R(I,J,1)
A(I,I,1)=1.D
R(I,I,1)=1.D
CALL SIMEQI(M,N,F,R,G)
LF=1
CALL HEAT (M,N,1,F,M,N,1,G,2,FGT)
E(I)=
1 1.D-SPUR(M,FGT)/SPUR(M,H)
IF(E(I).LE.FLOOR)RETURN
IF (LR.EQ.1) RETURN
DO 9 L=2,LR
CALL ZERO (N*N,DA)
CALL MOVE (M*N,G(I,1,L),GAM)
DO 5 I=1,N
DO 4 LI=1,L
LG=L-LI+1
DO 4 K=1,N
DO 2 J=1,N
3 DA(I,J)=DA(I,J)-A(I,K,LI)*R(K,J,LD)
DO 4 J=1,M
4 GAM(J,I)=GAM(J,I)-F(J,K,LI)*R(K,I,LD)
DO 5 J=1,N
5 DR(J,I)=DA(I,J)

```

```

CALL STMEQ1(N,N,CB,VA,DB)
CALL MOVE (N*N*L,A,AP)
CALL MOVE(N*N*L,B,BP)
DO 7 J=1,N
DO 7 K=1,N
DO 6 LI=1,L
LD=L-LI+1
DO 5 I=1,N
A(I,J,LI)=A(I,J,LI)+CA(I,K)*BP(K,J,LD)
B(I,J,LI)=B(I,J,LI)+CB(I,K)*AP(K,J,LD)
DO 7 I=1,N
VA(I,J)=VA(I,J)-CA(I,K)*DB(K,J)
VB(I,J)=VB(I,J)-CB(I,K)*DA(K,J)
CALL STMEQ1(M,N,CF,VB,GAM)
DO 8 LI=1,L
LD=L-LI+1
DO 3 J=1,N
DO 8 K=1,N
DO 9 I=1,M
9 F(I,J,LI)=F(I,J,LI)+CF(I,K)*B(K,J,LD)
CALL HEAT (M,N,L,F,M,N,L,G,I,FGT)
E(L)=
1 I.DI-SPUR(M,FGT)/SPUR(M,H)
WRITE(6,10) L,E(L)
FORMAT(IX,I1 ,F12.5)
LF=L
IF(E(L).LE.FLOOR) RETURN
9 CONTINUE
RETURN
END

```

```

SUBROUTINE HEAT(NRX,NCX,LX,X,NRY,NCY,LY,Y,LG,G)
DOUBLE PRECISION

```

```

2 X(NRX,NCX,LX),Y(NRY,NCY,LY),G(NRX,

```

```

NRY,LY)

```

```

CALL STMEQ1(N,N,CB,VA,DB)

```

```

00 I M=1,NPX
00 I N=1,NRY
00 I L=1,NCX
00 I J=1,MIN
LDOT=MIN(LY,LX-J+1)
00 I I=1,LDOT
K=I+J-1
1 G(M,N,J)=G(M,N,J)+X(W,L,K)*Y(N,L,I)
2 RETURN
END

```

```

SUBROUTINE ZERO (LX,X)
DOUBLE PRECISION X(LX)
Z=(LX*LE** ) RETURN
00 I I=1,LX
1 X(I)=Z
RETURN
END

```

```

SUBROUTINE SCALE (S,LX,X)
DOUBLE PRECISION X(LX),S
00 I J=1,LX
1 X(I)=S*X(I)
RETURN
END

```

```

SUBROUTINE BRAINY (NRA,NCA,LA,A,NRB,NCP,LR,B,C)
DOUBLE PRECISION
A(NRA,NCA,LA),R(NCA,NCB,LR),C(NPA,

```

```

DO 1 J=1, LB
  K=I+J-1
  DO 1 M=1, NPA
  DO 1 N=1, NCB
  DO 1 L=1, NCA
1 C(M,N,K)=C(M,N,K)+A(M,L,I)*B(L,N,J)
  RETURN
END

```

```

SUBROUTINE SIMEQ1(M,N,A,B,C)
DOUBLE PRECISION S(25,25)
DOUBLE PRECISION
1 A(M,N),B(N,N),C(M,N)
  CALL MOVE (N#N,B,S)
  CALL MAINE (N,S,B)
  DO 1 I=1,M
  DO 1 J=1,N
  A(I,J)=C(I,J)
  DO 1 K=1,N
2 A(I,J)=A(I,J)+C(I,K)*B(K,J)
  CALL MOVE (N#N,S,B)
  RETURN
END

```

```

C
C SUBROUTINE MAINE (M,A,B)
C VERSION 1 OF SUBROUTINE MAINE
C SYMMETRIC MATRIX INVERSION BY THE ESCALATOR METHOD
C DOUBLE PRECISION A(1),B(1),EK
  B(1)=1.0/A(1)
  IF(N.EQ.1) RETURN
  NN=N#N
  DO 5 I=2,NN

```

```

M=M+(M-1)*N
EK=A(M)
DO 1 I=1,K
DO 1 J=1,K
MI=M+(I-1)*N
IJ=I+(J-1)*N
JM=J+(M-1)*N
1 EK=EK-A(MI)*B(IJ)*A(JM)
  B(M)=1.0*/EK
DO 2 I=1,K
  IM=I+(M-1)*N
DO 2 J=1,K
  IJ=I+(J-1)*N
  JM=J+(M-1)*N
2 S(IM)=B(IM)-B(IJ)*A(JM)/EK
  NI=M+(I-1)*N
3 B(MI)=B(IM)
DO 4 I=1,K
  IM=I+(M-1)*N
DO 4 J=1,K
  MJ=M+(J-1)*N
  IJ=I+(J-1)*N
4 R(IJ)=S(IJ)+R(IM)*B(MJ)*EK
5 CONTINUE
  RETURN
END

```

```

SUBROUTINE MOVE (LX,X,Y)
DOUBLE PRECISION X(LX),Y(LX)
DO ? I=1,LX
1 Y(I)=X(I)
  RETURN
END

```

